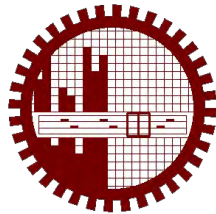


**CHARACTERIZATION OF COPPER OXIDE, TITANIUM
OXIDE AND COPPER DOPED TITANIUM OXIDE THIN
FILMS PREPARED BY SPRAY PYROLYSIS TECHNIQUE**

By

SONJIT SEN ROY
Roll No.: 1009144002F
Session: October, 2009



DEPARTMENT OF PHYSICS
BANGLADESH UNIVERSITY OF ENGINEERING AND TECHNOLOGY
DHAKA-1000, BANGLADESH

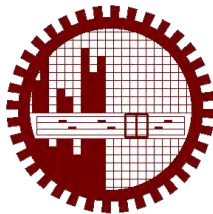
March, 2016

**CHARACTERIZATION OF COPPER OXIDE, TITANIUM
OXIDE AND COPPER DOPED TITANIUM OXIDE THIN
FILMS PREPARED BY SPRAY PYROLYSIS TECHNIQUE**

**A Dissertation Submitted to the Department of Physics, Bangladesh
University of Engineering and Technology (BUET), in Partial Fulfillment
for the Degree of Doctor of Philosophy (Ph. D.)**

By

**SONJIT SEN ROY
Roll No.: 1009144002F
Session: October, 2009**



**DEPARTMENT OF PHYSICS
BANGLADESH UNIVERSITY OF ENGINEERING AND TECHNOLOGY
DHAKA-1000, BANGLADESH**

March, 2016



CANDIDATE'S DECLARATION

It is hereby declared that this thesis or any part of it has not been submitted elsewhere for the award of any degree or diploma.

A handwritten signature in black ink, appearing to read "Sonjit Sen Roy", is positioned above a horizontal line.

Sonjit Sen Roy


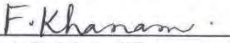
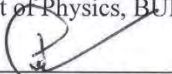


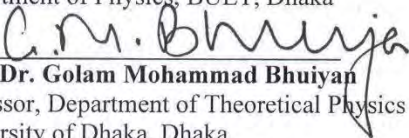
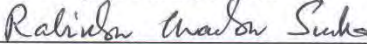
BANGLADESH UNIVERSITY OF ENGINEERING AND TECHNOLOGY
DEPARTMENT OF PHYSICS



Certification of Thesis

The thesis titled “CHARACTERIZATION OF COPPER OXIDE, TITANIUM OXIDE AND COPPER DOPED TITANIUM OXIDE THIN FILMS PREPARED BY SPRAY PYROLYSIS TECHNIQUE”, submitted by SONJIT SEN ROY, Roll No.: 1009144002 F, Registration No.: 1009144002, and Session: October, 2009, has been accepted as satisfactory in partial fulfillment of the requirement for the degree of **Doctor of Philosophy (Ph. D.)** on **March 01, 2016**.

BOARD OF EXAMINERS

1. 
Prof. Dr. Md. Abu Hashan Bhuiyan
Department of Physics, BUET, Dhaka
Chairman
(Supervisor)
2. 
Prof. Fahima Khanam
Head
Department of Physics, BUET, Dhaka
Member
(Ex-Officio)
3. 
Prof. Dr. Md. Feroz Alam Khan
Department of Physics, BUET, Dhaka
Member
4. 
Prof. Dr. Md. Mostak Hossain
Department of Physics, BUET, Dhaka
Member
5. 
Prof. Dr. Md. Forhad Mina
Department of Physics, BUET, Dhaka
Member
6. 
Prof. Dr. Golam Mohammad Bhuiyan
Professor, Department of Theoretical Physics
University of Dhaka, Dhaka
Member
7. 
Prof. Dr. Rabindra Chandra Sinha
Department of Physics
Jahangirnagar University, Savar, Dhaka
Member
(External)

*DEDICATED TO
"THE DEPARTED SOUL OF MY SISTER MINU
RANI ROY AND BROTHER SAJOL KUMAR ROY"*

ACKNOWLEDGEMENTS

At first I express my gratefulness to the **Almighty Eshwar**, Who gives me the strength and courage to complete this research work.

All of the freedom fighters who lost their lives and their fellow-soldiers, even supplied a spoon of salt with a green chilly during the liberation war, are acknowledged with love from the core of my heart.

It is a great pleasure for me to express my profound sense of gratitude, indebtedness and deep appreciation to my reverend and respectable supervisor **Prof. Dr. Md. Abu Hashan Bhuiyan**, Department of Physics and Dean, Faculty of Engineering, Bangladesh University of Engineering & Technology (BUET), Dhaka. I am most grateful to him for his constant supervision, inspiring guidance, gracious advice, active help, enthusiastic encouragements, co-operation and fruitful suggestions throughout the entire course of my research work. Due to his constant guidance and inspiring collaboration, I am very much benefited from his vast knowledge and experience.

I am deeply indebted to my respected teacher, **Prof. Fahima Khanam**, Head, Department of Physics, BUET, Dhaka for providing necessary facilities to carry out this research work and valuable suggestions on my thesis.

I am thankful to my respectable Members of the Doctoral Committee for their help and valuable suggestions, encouragements, insightful comments on this research work.

I express my deepest sense of gratitude, indebtedness and deep appreciation to my respected teacher **Prof. Dr. Jiban Podder**, Department of Physics, BUET, Dhaka for his encouragement and various help. I would like to express my gratitude to respected teachers **Prof. Dr. Md. Feroz Alam Khan, Prof. Dr. A. K. M. Akther Hossain, Prof. Dr. Md. Mostak Hossain, Prof. Dr. Afia Begum, Prof. Dr. Md. Forhad Mina**, for their inspirations. I would like to express my sincere thanks particularly to **Dr. Md. Abdul Basith, Dr. Md. Jellur Rahman, Dr. Md. Rakibul Islam, Mrs. Mehnaz Sharmin and Dr. Parvin Sultana**, Department of Physics, BUET, for their support and valuable discussion on various points.

I am also grateful to **Dr. Dilip Kumar Saha**, Director, Atomic Energy Center, Dhaka, for his kind help to take XRD patterns. I would like to thank **Prof. Dr. Md. Fakhru Islam**, Head, Department of Glass and Ceramics Engineering, BUET, Dhaka, for giving opportunity to perform SEM and EDX analysis. I am grateful to **Dr. Md. Abdul Gafur**, Senior Scientific Officer, PP & PDC, BCSIR Laboratories for help regarding UV-VIS analysis.

I would like to thank **Md. Idris Munsif, Md. Liakot Ali, Md. Abu Taher, Mr. Lutfur Rahaman Sarkar** and all other official staff of this Department for their sincere help and cooperation. I am also thankful to the technicians of the mechanical workshop of BUET for their technical support during this research work.

I am thankful to the authority of BUET for giving me necessary permission and providing financial support for this work and the Ph. D. fellowship granted to me. I acknowledge the Ph. D fellowship granted to me by the Ministry of Science and Technology, Government of the People's Republic of Bangladesh.

I am gratefully acknowledging the cooperation of my Ph. D fellow research and M. Phil. research colleagues and all other researchers for their constant support in many ways.

I am pleased to express my gratitude to the **Principal (Retrd.) Shams Uddin Ahamed, Principal Syed Monsural Haque** and all my colleagues and staff members of Dwarika Paul Mohila Degree College, Sreemongal for helping and supporting me in various ways and thanks to all of the members of the **Governing Body** of my College for allowing me to do Ph. D research work. I also wish to express heartfelt thanks to all my friends and students, who have always encouraged me to complete this work. I am grateful to **Joy Kumar Gope** and **Dr. Syed Abdul Mutakabbir Masud** for their continuous inspiration.

Finally, I would like to express my gratitude to my mother Mrs. **Jotika Roy**, brothers, sister and all other family members for their multifaceted support through all these years. Last, but not least, I am very much grateful to my wife Mrs. **Arpita Roy** for her constant support and encouragements during my research work and thanks to my loving children **Sajuti Roy Shraya** and **Sreejit Roy Argo**. Thanks are also due to all my relatives who are always appreciating me to do this work.

ABSTRACT

Copper oxide (CuO), titanium oxide (TiO₂) and copper (Cu) doped TiO₂ (Cu/TiO₂) thin films have been synthesized on to glass substrates for different molar concentrations (MC), different substrate temperatures (T_s) and various Cu doping by a spray pyrolysis technique (SPT) from aqueous solutions using cupric acetate Cu(CH₃COO)₂.H₂O for CuO, titanium chloride (TiCl₄) for TiO₂ and Cu(CH₃COO)₂.H₂O and TiCl₄ for Cu/TiO₂ thin films as a precursor.

All the CuO thin films, irrespective of T_s, show a monoclinic structure with the main CuO (111) orientation, and the crystallite size (D) is about 9.57 nm for the thin film synthesized with MC of 0.10 M at T_s of 350 °C. The optical transmission of the film is found to increase with the increase of MC from 0.05 to 0.10 M and then that decreases for the film with MC above 0.10 M. The optical band gap (E_g) is found to be 2.40 eV for MC of 0.05 M and then a minimum value 1.60 eV is observed for MC of 0.10 M. The room temperature electrical resistivities (ρ) are 31 and 24 Ω-cm for the films grown with MC of 0.05 and 0.15 M, respectively. The optical transmission of the film for MC of 0.10 M is found to increase with the increase of T_s. The E_g decreases from 1.90 to 1.60 eV and the room temperature ρ varies from 30 to 18 Ω-cm for the films grown at T_s from 250 to 350 °C for MC of 0.10M. The higher values of activation energy (E_a) of CuO thin films may suggest that the prepared sample is stoichiometric. The Figure of merit for the CuO thin films deposited with MC of 0.10 M and T_s of 350 °C is found to be 0.1424 Ω⁻¹.cm⁻¹.

MC has a significant effect on surface morphology, crystalline quality and crystallite size of the TiO₂ thin films. Energy dispersive analysis of X-ray (EDX) results clearly shows that the grains of TiO₂ thin films typically comprise both Ti and O. The XRD studies show the formation of tetragonal structure with anatase phase and the D value of the film is about 13 nm when films deposited at 400 °C from MC of 0.10M. The optical transmission of the films is found to increase from 60 to 80 % with the increases of MC. The value of E_g is decreased from 3.65 to 3.40 eV for the film of MC from 0.05 to 0.10 M whereas E_g increases for the films of MC above 0.10 M.

The ρ of the TiO₂ thin films are 55.67 and 27.50 Ω -cm for MC of 0.05 M and 0.10 M, respectively. Strong diffraction peaks (101) and (200) around at 25° and 48°, respectively, indicate TiO₂ of tetragonal structure with anatase phase at different T_s for MC of 0.10 M, except film deposited at T_s of 250 °C which shows amorphous nature. E_a is maximum, 0.028 eV for T_s of 400 °C and MC of 0.10 M of TiO₂ thin film. The peaks are found to shift a little from their standard positions at higher T_s, indicating a small deviation in the lattice parameters. The optical transmission of the films is found to increase from 73 to 89 % for the films grown at T_s of 250-400 °C and above these T_s, transmission decreases. E_g decreases with T_s up to 400 °C and above these T_s, E_g does not vary much. The room temperature ρ varies from 42 to 27.50 Ω -cm for T_s of 250 to 400 °C. It is observed that with increasing D of TiO₂ thin film, the E_g shifts from 3.64 eV to 3.40 eV. Moreover, other possible influences of microstructure of TiO₂ thin film, such as, surface roughness and thin film absorption on the modification of E_g may be present.

Cu/TiO₂ thin films have been prepared by SPT for MC of 0.10 M at T_s of 400 °C by variation of Cu doping (1-10 wt%). The XRD studies show that Cu/TiO₂ thin films have only tetragonal structure with anatase phase. The optical transmission of the thin films is found to increase from 88 to 94 % with the addition of Cu up to 8 wt% and then decreases for higher percentage of Cu doping. Due to Cu doping, the E_g is shifted to lower energies and increases further with increasing concentration of Cu. The refractive index (n) decreases up to 8 wt% Cu doping, above 8 wt% Cu doping, n increases. The room temperature ρ of the films decreases with increasing Cu doping and is found to be 27 -23 Ω -cm for Cu doping of 1-8 wt%. E_a increases with Cu doping and it is maximum, 0.0311 eV, for 8wt% Cu doped TiO₂ thin film. The Figure of merit of Cu/TiO₂ thin films varies from 0.2238 to 0.0.2328 Ω^{-1} -cm¹ for Cu doping from 0 to 10 wt% and it is maximum, 0.2334 Ω^{-1} -cm¹, for 8wt% Cu doped TiO₂ thin film.

It is evident from the present study that the Cu doping has modified the thin film morphology and so the effect on the structural, optical and electrical properties of the thin films.

Abbreviations and Symbols

A	Absorbance
AC	Alternating Current
AFM	Atomic Force Microscope
DC	Direct Current
EDX	Energy Dispersive X-ray
I	Current
IR	Infrared
J	Current Density
MHz	Mega Hertz
PVD	Physical Vapour Deposition
SPT	Spray Pyrolysis Technique
SEM	Scanning Electron Microscopy
UV	Ultra-Violet
Vis	Visible
n	Refractive index
T	Transmittance
t	Sample Thickness
α	Absorption Coefficient
k	Boltzmann Constant
k	Extinction coefficient
λ	Wavelength
μ	Mobility of Charge Carrier
θ	Diffraction angle
ρ	Electrical Resistivity
σ	Electrical Conductivity

CONTENTS

Candidate's Declaration	I
Dedication	II
Acknowledgements	III
Abstract	V
Abbreviations and Symbols	VII

CHAPTER –I: GENERAL INTRODUCTION 1

1.1 Introduction	2
1.2 Properties of Copper Oxide (CuO) and Titanium Oxide (TiO ₂)	4
1.3 Areas of Thin Films Application	5
1.4 Reviews of the Earlier Research Works on Thin Films	7
1.5 Objectives of the Present Work	22
1.6 Thesis Layout	24
References	25

CHAPTER –II: THEORETICAL BACKGROUND 34

2.1 Introduction	35
2.2 Formation of Thin Films	37
2.2.1 Introduction	37
2.2.2 Different Stages of Film Formation	38
2.2.3 Condensation	38
2.2.4 Nucleation	39
2.2.5 Growth	40
2.2.6 Polycrystalline and Amorphous Thin Films	42
2.2.7 The Incorporation of Defects during Growth	44
2.3 Theoretical Aspect of Different Preparation Methods of Thin Films	43
2.3.1 Introduction	43
2.3.2 Sol-gel Process	45
2.3.3 Pulsed ion-beam Evaporation (IBE) Method	46

2.3.4 Sputtering Method	48
2.3.5 Chemical Vapor Deposition	49
2.3.6 Plasma-enhanced Chemical Vapor Deposition (PECVD)	50
2.3.7 Molecular Beam Epitaxy	51
2.3.8 Thermal or Vacuum Evaporation Method	52
2.3.9 Spin Coating Process	53
2.3.10 Spray Pyrolysis Technique	54
2.4 Theoretical Aspect of Different Measurement Techniques Used for Study of Thin Films	57
2.4.1 Introduction	57
2.4.2 Measurement of Thin Film Thickness	57
2.4.2.1 Optical Interference Fringe Method	57
2.4.3 Surface Morphology and Compositional Analysis of Thin Films	59
2.4.3.1 Scanning Electron Microscopy (SEM)	60
2.4.3.2 Energy Dispersive Analysis of X-rays (EDX)	62
2.4.4 Structural Analysis of Thin Films	62
2.4.4.1 X-ray Diffraction (XRD)	63
2.4.5 Optical Analysis of Thin Films	65
2.4.5.1 Ultraviolet–visible Spectroscopy	65
2.4.5.2 Absorption	66
2.4.5.3 Absorption Coefficient	66
2.4.5.4 Extinction Coefficient	67
2.4.5.5 Band Gap	68
2.4.5.5.1 Direct and Indirect Optical Band Gap	69
2.4.5.6 Refractive Index	72
2.4.6 Electrical Analysis of Thin Film	73
2.4.6.1 Resistivity Measurement Techniques	73
2.4.6.1.1 Direct Method	73
2.4.6.1.2 van der Pauw’s Method	74
2.4.6.2 Factors Affecting Resistivity Measurement	75
2.4.6.3 Sheet Resistance	76

2.4.6.4 Activation Energy	76
2.4.6.5 Figure of Merit	77
References	78
CHAPTER –III: EXPERIMENTAL DETAILS	82
3.1 Thin Film Deposition	83
3.1.1 Introduction	83
3.1.2 The Design of the Spray Pyrolysis Deposition System	83
3.1.3 Thin Film Deposition Parameters	85
3.1.4 Experimental Equipments	85
3.1.4.1 Substrate and Substrate Cleaning	85
3.1.4.2 Preparation of Masks	86
3.1.4.3 Spray Nozzle	87
3.1.4.4 Heater	87
3.1.4.5 Air Compressor	87
3.1.4.6 The Fume Chamber	87
3.1.5 Optimization of the Deposition Process	88
3.1.6 Preparation of Thin Films	89
3.2 Summary of Spray Deposition Parameters of CuO, TiO₂, Cu/TiO₂...	91
3.3 Measurement Details	91
3.3.1 Thickness Measurement of the Thin Films	91
3.3.2 Surface Morphology and Elemental Analysis of the Thin Films	92
3.3.3 Structural Analysis of the Thin Films	93
3.3.4 Measurement of the Optical Properties of the Thin Films	94
3.3.5 Measurement of the Electrical Properties of the Thin Films	95
CHAPTER –IV: RESULTS AND DISCUSSION	96
4.1 Introduction	97
4.2 Results and Discussion on Prepared CuO Thin Films	98
4.2.1 CuO Thin Films Synthesized from Aqueous Solutions of Different Molar Concentrations at T _s of 350 °C	98

4.2.1.1 Surface Morphology and Elemental Analyses	98
4.2.1.2 Structural Analysis	100
4.2.1.3 Optical Properties	101
4.2.1.3.1 Transmittance and Optical Band Gap	101
4.2.1.3.2 Refractive Index and Extinction Coefficient	103
4.2.1.4 Electrical Properties	105
4.2.2 CuO Thin Films Synthesized Using Solution of 0.10M at Different T _s	108
4.2.2.1 Surface Morphology and Elemental Analyses	108
4.2.2.2 Structural Analyses	110
4.2.1.3 Optical Properties	112
4.2.2.3.1 Transmittance and Optical Band Gap	112
4.2.2.3.2 Refractive index and Extinction Coefficient	113
4.2.2.4 Electrical Properties	115
4.2. 3 Summary of Findings on CuO Thin Films	118
4.3 Results and Discussion of TiO ₂ Thin Films	119
4.3.1 TiO ₂ Thin Films Synthesized from Aqueous Solutions of 0.05 - 0.15 M Molar Concentration at T _s of 400 °C	119
4. 3.1.1 Surface Morphology and Elemental Analysis	119
4.3.1.2 Structural Analyses	120
4.3.1.3 Optical Properties	122
4.3.1.3.1 Transmittance and Optical Band Gap	122
4.3.1.3.2 Refractive Index and Extinction Coefficient	125
4.3.1.4 Electrical Properties	126
4.3.2 TiO ₂ Thin Films Synthesized Using MC of 0.10 M at Different T _s	129
4.3.2.1 Surface Morphology and Elemental Analyses	129
4.3.2.2 Structural Analyses	130
4.3.2.3 Optical Properties	132
4.3.2.3.1 Transmittance and Optical Band Gap	132
4.3.2.3.2 Refractive Index and Extinction Coefficient	134
4.3.2.4 Electrical Properties	135

4.3.3 Summary of Findings on TiO ₂ Thin Films	139
4.4 Results and Discussion on Cu/TiO ₂ Thin Films	140
4.4.1 Cu doped TiO ₂ Thin Films Synthesized from Aqueous Solutions of (0 -10%) (Cu(CH ₃ COO) ₂ .H ₂ O) Doped in TiCl ₄ of 0.10 M Molar Concentration at T _s of 400 °C	140
4.4. 1.1 Surface Morphological and Elemental Analysis	140
4.4. 1.2 Structural Analyses	142
4.4. 1.3 Optical Properties	144
4.4. 1.3.1 Transmittance and Optical Band Gap	144
4.4. 1.3.2 Refractive Index and Extinction Coefficient	147
4.4. 1.4 Electrical Properties	149
4.4.2 Summary of Findings on Cu/TiO ₂ Thin Films	153
4.5 Summary of Results for Prepared TiO ₂ in the Present Work and TiO ₂ Thin Films Reported by Others	154
References	155

CHAPTER –V: CONCLUSIONS 161

5.1 Conclusions	162
5.2 Suggestions for Further Research	165

APPENDIX 166

Publications	166
--------------	-----

List of Figures

1.1 XRD of copper oxide thin films: “as deposited”, annealed in vacuum at...	12
1.2 (a) Optical transmission spectra of 250 nm thick copper oxide thin films	12
(b) Tauc plots of copper oxide thin: as deposited, 623 K vacuum annealed and...	12
1.3 SEM images of the Sn:CuO films with different Sn concentrations:...	13
1.4 Effects of the Sn content of Sn:CuO films on the resistivity, carrier...	13
1.5 (a) SEM of TiO ₂ thin films grown by LPMOCVD at different deposition times	17

1.5 (b) Thickness of TiO₂ film as a function of deposition time	17
1.6 (a) XRD pattern of TiO₂/WO₃ multilayer thin film, target: TiO₂	19
1.6 (b) Transmittance of TiO₂/WO₃ multilayer thin film, Target: TiO₂	19
1.7 The UV-vis transmission spectrum of TiO₂ film under different heat...	19
2.1 Different stages of thin film growth	40
2.2 Generalized scheme of sol-gel synthesis	46
2.3 A schematic of the pulsed ion-beam evaporation (IBE) method	47
2.4 Schematic diagram of the magnetron sputtering system	48
2.5 Schematic diagram of a LPCVD system	49
2.6 Plasma polymerization chamber	50
2.7 Diagram of a molecular beam epitaxy	50
2.8 Thermal evaporation method	52
2.9 Schematic diagram of the spin coating process	53
2.10 Description of the deposition processes initiated with increasing T_s	55
2.11 Schematic diagram of a spray pyrolysis technique	56
2.12 Interferometer arrangements for producing Fizeau fringes of...	59
2.13 Schematic diagram of an SEM	61
2.14 Schematic diagram of a Bragg Spectrometer	64
2.15 Bragg condition	64
2.16 Schematic diagram of Ultraviolet-visible spectrophotometer	66
2.17 Energy-crystal momentum diagram of a direct band gap of semiconductor	71
2.18 Energy-crystal momentum diagram of an indirect band gap of...	72
2.19 Circuit arrangements for resistivity measurement	74
2.20 Schematic diagram of van der Pauw's method	74
3.1 Spray pyrolysis deposition system in Spray Pyrolysis Laboratory, BUET	84
3.2 Schematic diagram of SPT System in Spray Pyrolysis Laboratory, BUET	84
3.3 Mask for the sample	86
3.4 Flow diagram for CuO thin films prepared by SPT	90
3.5 Flow diagram for Cu/TiO₂ thin films prepared by SPT	90
3.6 Photograph of a multiple beam interferometer	92
3.7 Photograph of a scanning electron microscopy (SEM)	93

3.8 Photograph of an X-ray diffractometer	94
3.9 Photograph of a UV-1601 PC SHIMADZU VISIBLE spectrometer	95
3.10 Set up for resistivity measurement by van der Pauw's method	95
4.1 SEM images of CuO thin films for MC of (a) 0.05, (b) 0.10 M and...	99
4.2 EDX spectrum for CuO thin film MC of 0.10 M ($T_s = 350\text{ }^\circ\text{C}$)	99
4.3 XRD patterns of CuO thin films synthesized from solution of various MCs...	101
4.4 Optical transmittance vs. wavelength of CuO thin films for various MCs ...	102
4.5 Variation of $(\alpha h\nu)^2$ with $h\nu$ for CuO thin films for various MCs...	103
4.6 Band gap vs. MC of the solution for CuO thin films	103
4.7 Variation of n with MC for CuO thin films ($T_s = 350\text{ }^\circ\text{C}$)	104
4.8 Variation of k with $h\nu$ for various MCs of CuO thin films ($T_s = 350\text{ }^\circ\text{C}$)	104
4.9 Variation of resistivity with temperature of CuO thin films for various...	105
4.10 Variation of resistivity and conductivity at room temperature with MC...	106
4.11 Variation of $\ln\sigma$ with respect to inverse of absolute temperature of...	107
4.12 Variation of activation energy with MC for CuO thin films ($T_s = 350\text{ }^\circ\text{C}$)	108
4.13 Variation of Figure of merit versus MC for CuO thin films ($T_s = 350\text{ }^\circ\text{C}$)	108
4.14 SEM image of CuO thin films at T_s of (a) 250 (b) 300 (c) 350 (d) 400....	109
4.15 EDX spectra of CuO thin films at T_s of $400\text{ }^\circ\text{C}$ (MC = 0.10 M)	110
4.16 XRD patterns of CuO thin film synthesized at various T_s (MC = 0.10M)	111
4.17 Optical transmittance vs. wavelength for CuO thin films at various T_s...	112
4.18 Variation of $(\alpha h\nu)^2$ with $h\nu$ for CuO thin films at various T_s...	113
4.19 Variation of E_g with T_s for CuO thin films (MC = 0.10M)	113
4.20 Variation of refractive index with T_s (MC = 0.10M)	114
4.21 Variation of extinction coefficient with $h\nu$ at various T_s (MC = 0.10M)	114
4.22 Variation of DC electrical resistivity with temperature for various T_s...	115
4.23 Variation of DC electrical resistivity at room temperature with various...	116
4.24 Variation of $\ln\sigma$ with respect to inverse of temperature for at various T_s...	117
4.25 Variation of activation energy with T_s for CuO thin films (MC = 0.10M)	117
4.26 Variation of Figure of merit with T_s for CuO thin films (MC = 0.10M)	117
4.27 SEM image of TiO_2 thin films deposited at T_s of $400\text{ }^\circ\text{C}$ for MC of...	120
4.28 XRD patterns of TiO_2 thin film synthesized for various MCs...	122

4.29 Optical transmittance vs. wavelength TiO ₂ thin films for various of MCs...	123
4.30 Absorbance coefficient vs. wavelength of TiO ₂ thin films for various MCs...	124
4.31 Variation of $(\alpha h\nu)^2$ with $(h\nu)$ for various MCs of solution of TiO ₂ ...	124
4.32 Variation of E_g with MC of TiO ₂ thin film ($T_s = 400$ °C)	124
4.33 Variation of n with MC of TiO ₂ thin films ($T_s = 400$ °C)	125
4.34 Variation of k with wavelength for various MCs of the solution of TiO ₂ ...	126
4.35 Electrical resistivity vs. absolute temperature TiO ₂ thin films ($T_s = 400$ °C)	127
4.36 Room temperature electrical resistivity vs. MC of TiO ₂ thin...	127
4.37 Electrical conductivity ($\ln\sigma$) vs. inverse of absolute temperature for...	128
4.38 Variation of activation energy vs. MC of TiO ₂ thin films ($T_s = 400$ °C)	128
4.39 Variation of Figure of merit with MC the solution of TiO ₂ thin...	129
4.40 SEM images of TiO ₂ thin films at T_s of (a) 250 (b) 350 (c) 400 and...	130
4.41 XRD patterns of TiO ₂ thin film synthesized at various T_s (MC = 0.10 M)	132
4.42 Optical transmittance vs. wavelength for TiO ₂ thin films synthesized...	133
4.43 Variation of $(\alpha h\nu)^2$ with $h\nu$ for TiO ₂ thin films synthesized at various T_s ...	134
4.44 Variation of E_g with T_s of TiO ₂ thin films (MC = 0.10 M)	134
4.45 Variation of refractive index with T_s of TiO ₂ thin films (MC = 0.10 M)	135
4.46 Variation of extinction coefficient with $h\nu$ at various T_s TiO ₂ thin films...	135
4.47 Variation of resistivity with room temperature for various T_s ...	136
4.48 Variation of resistivity at room temperature at various T_s ...	136
4.49 Variation of $\ln\sigma$ with respect to inverse temperature T (K) of TiO ₂ ...	138
4.50 Variation of activation energy with T_s of TiO ₂ thin films (MC = 0.10 M)	138
4.51 Variation of Figure of merit with T_s of TiO ₂ thin films (MC = 0.10 M)	138
4.52 SEM images of Cu/TiO ₂ thin films ($T_s = 400$ °C, MC = 0.10 M)	141
4.53. XRD pattern of Cu/TiO ₂ thin films ($T_s = 400$ °C, MC = 0.10 M)	143
4.54 Optical transmittance vs. wavelength of Cu/TiO ₂ thin films...	145
4.55 α vs. wavelength of Cu/TiO ₂ thin films ($T_s = 400$ °C, MC = 0.10 M)	146
4.56 Variation of $(\alpha h\nu)^2$ with $h\nu$ for Cu/TiO ₂ thin films...	146
4.57 Variation of E_g with Cu for Cu/TiO ₂ thin films...	146
4.58 Variation of refractive index with Cu for Cu/TiO ₂ thin films...	148
4.59 Variation of extinction coefficient with wavelength for Cu/TiO ₂ thin...	148

4.60 Variation of resistivity with temperature for Cu/TiO₂ thin films...	150
4.61 Variation of resistivity with Cu for Cu/TiO₂ thin films...	150
4.62 Variation of $\ln\sigma$ with inverse of temperature T (K⁻¹) for Cu/TiO₂ thin...	151
4.63 Variation of activation energy with Cu for Cu/TiO₂ thin films...	152
4.64 Variation of Figure of merit with Cu for Cu/TiO₂ thin films...	152

List of Tables

1.1 Standard data for CuO and TiO₂	5
2.1 Classification of thin film deposition techniques	44
3.1 Summary of spray deposition parameters of CuO, TiO₂ and Cu/TiO₂...	91
4.1 Crystallite size for the CuO thin films for various MCs (T_s = 350 °C)	101
4.2 Crystallite size for the CuO thin films at various T_s (MC= 0.10 M)	111
4.3 Quantitative results of TiO₂ thin films for various MCs (T_s = 400 °C)	119
4.4 D and lattice constants of the TiO₂ thin films for various MCs...	121
4.5 Values of maximum T (λ), E_g, and n of the TiO₂ thin films for various...	126
4.6 Quantitative results of TiO₂ thin films from EDX analysis at various T_s...	129
4.7 Crystallite size and lattice parameters for the TiO₂ thin films synthesized...	132
4.8 Elemental analysis of Cu/TiO₂ thin films (T_s = 400 °C, MC = 0.10 M)	141
4.9 XRD data for Cu/TiO₂ thin films (T_s = 400 °C, MC = 0.10 M)	143
4.10 Comparison of results of all prepared TiO₂ thin films with the reported...	154

CHAPTER-I

GENERAL INTRODUCTION

1.1. Introduction

1.2. Properties of Copper Oxide (CuO) and Titanium Oxide (TiO₂)

1.3. Areas of Thin Films Application

1.4. Reviews of the Earlier Research Works on Thin Films

1.5. Objective of the Present Work

1.6. Thesis Layout

References

CHAPTER-I

GENERAL INTRODUCTION

1.1 Introduction

Thin films are thin material layers ranging from fractions of a nanometer to several micrometers in thickness. When a thin layer of solid material is formed on a solid substrate and if the layer thickness becomes comparable in magnitude to mean free path of the conduction electrons of solid material then this layer is termed as 'Thin Film'. Thin Film technology is an important branch of Physics in which the characteristics of different materials such as, semiconductors and insulators in thin film form are investigated. The properties of thin films are quite different from their bulk counterparts. 'Thin Solid Film', a new branch of science, has a great demand in microelectronics. Although a large number of experimental and theoretical works has been reported in the literature on these materials, still there is lack of understanding of the various physical chemical characteristics of these materials. So there has been a great interest to study transparent conducting oxide (TCO) thin films because these have important applications in thin film technology, particularly in solar cells, sensors, etc. These thin films are very efficient in reflecting broadband infrared heat radiation in a manner similar to highly conducting metal-like materials and in transmitting the light in the visible region as if they are insulators. Such spectrally selective coatings have wide applications in solar thermal energy conversion, solar photovoltaic conversion, solar heating, window insulation, and thermal insulation in lamps. The main requirement for thin film solar cells is the window material, which allows the visible region of solar spectrum to pass through but reflect the infrared (IR) radiation. This can be achieved by the development of TCO coatings such as copper oxide (CuO), zinc oxide (ZnO), tin oxide (SnO₂), nickel oxide (NiO), titanium oxide (TiO₂), indium oxide (In₂O₃), etc. [1-6].

From technological point of interest, I-VI, IV-VI and I- IV-VI group compound semiconductor thin films synthesized by various techniques have been investigated. These materials, show unique characteristics such as chemical inertness, stability to heat treatment, mechanical hardness, etc.

A large number of studies have been performed on the thin films, yet these materials need further study to find new materials for electronic and optical based applications. It is necessary to do both fundamental and applied research on these kinds of materials. For the development of fundamental and applied research and consequently to enrich knowledge in this field it is necessary to do research and analysis. Therefore it is very important to take this research programme to gather more knowledge in this field. The knowledge gained from research in the field of thin film science can be applied successfully for the technological development in the country. For all these applications, it is necessary to perform an accurate characterization of surface morphology, crystal structure, optical properties, electrical properties which include, surface structure, electrical conductivity, optical transmittance, energy band gap, refractive index, optical losses etc. Surface roughness, inhomogeneity and intrinsic defects, etc. are the causes of the optical losses. From practical point of view, these properties can severely degrade or modify the performances of a component. Overall, the structural, optical and electrical properties of the thin films depend on the method of the preparation. So highly conducting semiconductors have attracted the interest of many researchers because of their wide applications in technology,

CuO is a low energy band gap p-type semiconductor, and it is one of the hardest materials due to high melting and boiling points. CuO is abundant and relatively of low cost compound. TiO₂ is an n-type semiconductor, non toxic, soluble in water, high melting and boiling points and high optical transparency. CuO and TiO₂ are non toxic, so these are not harmful to the environment and living beings. Cu is cheap and nontoxic available material on earth. When Cu doped in TiO₂, concentration of charge carriers, chemical and physical properties of TiO₂ may change. A good homogeneous and stoichiometric thin film is expected to be grown by Cu doping in TiO₂.

A lot of works have been done on these materials but still new approach is coming up to find simple route and to synthesize quality films for better performance. Several methods have been used to synthesize TCOs thin films. These include physical vapour deposition [7], sol-gel deposition technique [8], spray pyrolysis technique (SPT) [9], electron beam evaporation deposition [10], reactive magnetron sputtering [11], pulsed laser deposition [12], chemical vapour deposition (CVD) [13]. SPT has emerged as one of the most

promising techniques as this method produces samples with good homogeneity at low cost. This simple and economical technique has attracted attention for commercial production and other reasons. SPT offers an extremely easy way to prepare films with dopants, virtually any element in any proportion by merely adding it in a spray solution [14]. It also offers an opportunity to have reactions at low temperatures (200-500 °C). The versatile nature of this technique lays in the way various parameters that include effect of precursors, deposition rate, thickness of the film, substrate temperature (T_s), dopants, in-situ annealing treatments, and solution concentrations, etc. can easily be controlled. Various types of metal oxide, metallic spinel oxide, binary and ternary chalcogenides and superconducting oxides can be prepared by SPT. The versatility of the homemade SPT unit has been demonstrated by way of preparing reasonably good quality thin films of CdO, SnO₂ etc. with Cu doping [15-16]. In considering the importance of these materials in the field of optoelectronic devices, particularly solar cells, high purity oxide thin films would be prepared using a homemade SPT system at different substrate temperature (T_s) (250-450 °C), different molar concentration (MC) (0.05-0.15 M), and different doping (Cu) concentration, so as to reduce the preparation cost and make it economically more viable. The present research work aimed at the production of uniform, conductive pure CuO, TiO₂ and Cu doped TiO₂ (Cu/TiO₂) thin films by a low cost technique which is particularly attractive because of its simplicity, fast, inexpensive, and suitable for mass production [17] using precursor solution of Cu(CH₃COO)₂.H₂O, TiCl₄, and mixture of Cu(CH₃COO)₂.H₂O and TiCl₄ respectively.

1.2 Properties of Copper Oxide (CuO) and Titanium Oxide (TiO₂)

CuO (I-VI compound) is a secondary copper mineral, a rare earth metal, and the most stable form of oxidized copper. TiO₂ also known as titanium oxide or titania (IV-VI compound), is the naturally occurring oxide of titanium. When deposited as a thin film, its refractive index and colour make it an excellent reflective optical coating for dielectric mirrors and some gemstones like "mystic fire topaz". Their properties are described in the Table 1.1 below.

Table 1.1 Standard data for CuO and TiO₂

Properties	Copper Oxide	Titanium Oxide
Molecular Formula	CuO	TiO₂
Molar Mass	79.55 g/mol	79.87 g/mol
Appearance	Black Powder	White
Density	6.31 g/cm³	4.23 g/cm³
Melting Point	1201 °C	1843 °C
Boiling Point	2000 °C	2972 °C
Solubility in Water	Insoluble	Soluble
Type of semiconductor	p type	n type
Energy Band Gap	1.35 eV	3.2 eV
Crystal Structure	Monoclinic	Tetragonal
Lattice Constants	a= 4.652 Å b= 3.410 Å c= 5.108 Å	a= 3.7300Å b= 3.7300Å c= 9.3700Å

1.3 Areas of Thin Films Application

Thin films have superior electrical conductivity, high transparency, and chemically inert, mechanically hard, uniform, stoichiometric and can withstand high temperature, so these films are to be used in different fields. Thin films are broadly used in today's technology, and their applications are expected to be even more widespread in future. Thin films are most commonly used for antireflection, achromatic beam splitters, color filters, narrow pass band filters, semitransparent mirrors, heat control filters, high reflectivity mirrors, polarizer's and reflection filters [18-28].

It is not possible to give an exhaustive survey over thin film application, but a list of them is given below.

a) Electrically Functional:

- (i) Conductors, Insulators (resistors, capacitors)
- (ii) Semiconductor, Super-conductors devices
- (iii) Contacts
- (iv) Micro electronic devices
- (v) Solar cells

b) Optically Functional:

- (i) Solar absorbing coatings
- (ii) Automotive windows
- (iii) Display devices
- (iv) Mirrors
- (v) Anti- reflection layers on optical components

c) Magnetically Functional:

- (i) Computer memories, Computer logic elements
- (ii) Radio-frequency and microwave

d) Mechanically Functional:

- (i) Adhesion, lubrication, micromechanics
- (ii) Hard coatings for cutting tools

e) Chemically Functional:

- (i) Barriers to diffusion or alloying
- (ii) Batteries
- (iii) Gas/liquid sensors

f) Decorative:

- (i) Eyeglass frames
- (ii) Watch bezels and bands
- (iii) Costume jewelry

CuO has been studied as a semiconductor material because of natural abundance of starting material (Cu); low cost production processing; non-toxic nature; and reasonably good electrical and optical properties [29]. CuO is attractive as a selective solar absorber since it has high solar absorbency and a low thermal emittance (Yoon et al 2000). Furthermore, it is a promising semiconductor for solar cell fabrication due to its suitable optical properties (Oral et al 2004) and its uses as gas sensor devices [30]. TiO₂ attracts much attention in recent years because of its unique physical and chemical properties, such as high refractive index, excellent optical transmittance in the visible and near-infrared regions, high dielectric constant and good insulating properties, photocatalytic activity and chemical stability [31-38]. As a result it is widely used as protective layer for very large scale integrated (VLSI) circuits and for manufacture of optical elements. Additionally TiO₂ films have potential uses for a number of electronic device applications such as dye-sensitized photovoltaic cells as well as antireflective (AR) coatings, gas sensors, electrochromic displays, and planar waveguides.

1.4 Reviews of the Earlier Research Works on Thin Films

Thin film science has grown world-wide into a major research area and hence transition metal-doped semiconducting thin films have attracted much attention due to their wide applications in areas such as photonic devices, transparent conductive oxide materials, photovoltaic cells, catalysts and gas sensors [39-44]. The importance of coatings and the synthesis of new materials for industry have resulted in a tremendous increase of innovative thin film processing technologies. Currently, this development goes hand-in-hand with the explosion of scientific and technological breakthroughs in microelectronics, optics and nanotechnology. A second major field comprises process technologies for films with thicknesses ranging from one to several microns. Presently, rapidly changing needs for thin film materials and devices are creating new opportunities for the development of new processes, materials and technologies.

Copper oxide-based materials are of interest on account of their potential uses in many technological fields. Copper oxide thin films were deposited on glass substrates at various growth temperatures by the reactive radio-frequency magnetron sputtering method [45]. The band gap energy, carrier concentration and Figure of merit of the CuO thin films were

found to depend significantly on the growth temperature. All of the CuO films, irrespective of growth temperature, showed a monoclinic structure with the main CuO (111) orientation, and the crystallite size, determined by using Debye-Scherrer's formula, was about 50 nm for the thin film deposited at 25 °C. The highest Figure of merit occurred for the film grown at 300 °C with an optical transmittance of 62.9% in the wavelength range of 800-1100 nm. The results suggest that the optimum growth temperature for growing high-quality CuO thin films is 300 °C.

Nanostructured CuO thin films were prepared on conducting glass support (SnO₂: F overlayer) via sol-gel starting from colloidal solution of copper (II) acetate in ethanol [46]. Films were obtained by dip coating under room conditions (temperature, 25–32°C) and were subsequently sintered in air at different temperatures (400–650°C). X-ray (XRD) diffraction patterns of CuO films obtained at different sintering temperatures and reveal formation of single phase CuO with tenorite structure. The peaks at 2θ angle 35.57, 38.76, 61.60, 65.88 and 67.99° with d_{hkl} 2.5, 2.3, 1.5, 1.4 and 1.4 Å correspond to diffraction from planes (111), (111), (113), (022) and (113), respectively, of CuO. The lattice parameters of films were calculated as $a = 4.67\text{--}4.72$ Å, $b = 3.42\text{--}3.49$ Å, $c = 5.12\text{--}5.20$ Å and $\beta = 99.20\text{--}99.60^\circ$, which are very close to the expected values from JCPDS 05-0661, for CuO. Microstructure of the films changes on varying film preparation conditions, particularly the sintering temperature. Optical band gap of the films, measured by employing a UV-vis scanning spectrophotometer, lies at 1.72–1.79 eV. Hence, the films of CuO obtained by this method may be exploited as cheap and efficient solar light absorber. However, their use for PEC splitting of water is possible only with an external bias. The films prepared at lower sintering temperature (=400–500 °C) yield higher photocurrent and are more efficient for photosplitting of water. Resistivity increases with thickness and thicker films are less effective in photoconversion.

Copper forms two well known oxides: cuprite (Cu₂O) and tenorite (CuO). CuO is attractive as a selective solar absorber since it has high solar absorbency and a low thermal emittance. CuO is a p-type semiconductor having a band gap of 1.21–1.51 eV and monoclinic crystal structure with lattice parameters $a = 4.6837$ Å, $b = 3.4226$ Å, $c = 5.1288$ Å and $\beta = 99.54^\circ$ [49-50] useful for fabrication of variety of devices. Furthermore, it is a promising semiconductor for solar cell fabrication due to its suitable optical properties. CuO is readily

available and nontoxic and this makes it even more attractive for different applications. CuO is attractive as a selective solar absorber since it has high solar absorbency and a low thermal emittance. Furthermore, it is a promising semiconductor for solar cell fabrication due to its suitable optical properties. CuO has been studied as a semiconductor material because of natural abundance of starting material (Cu); low cost production processing; non-toxic nature; and reasonably good electrical and optical properties high optical absorption coefficient in the visible range (0.4–0.7 μm) and reasonable good electrical properties make it suitable for fabrication of thin film solar cells with theoretically achievable efficiency up to 13% [29].

Single phase, epitaxial, transparent p-type CuAlO_2 films have been successfully grown on *c*-plane sapphire substrates by a polymer-assisted deposition (PAD) technique [51]. As can be seen from the SEM images of different magnifications, the film is dense and uniform with no detectable micro-cracks. The film is transparent, having an optical transmission of 60–80 % in the whole visible range. A sharp absorption edge was observed around the wavelength of 400 nm. The energy bandgap for the direct band transition is estimated to be 3.6 eV. The desired crystal structure and chemical stoichiometry of the films have been confirmed by XRD.

CuO thin films were deposited on glass substrates by reactive rf sputtering from a copper target in an argon-oxygen atmosphere [52]. The films were characterised by AFM, XPS, four point electrical resistivity probe measurements and spectrophotometry. The electrical sheet resistance of the films was found to vary from greater than 4×10^5 ohms/square for films prepared at 200W R.F. power to as low as 20 ohms/square for films prepared at 800W r.f. power. The variation in the electrical resistivity of the films with deposition conditions has been explained in terms of stoichiometric changes induced by copper or oxygen ion vacancies and neutral defects. The formation of these defects depends on the sticking coefficient, nucleation rates and the migration of impinging copper and oxygen species on the substrate during deposition. This information is expected to underlie the successful development of CuO thin films for solar windows and other semi-conductor applications including gas sensors.

Thin films of cuprous oxide have been deposited on glass substrates by sputtering of copper target at different substrate temperature in the range 303–523 K and at oxygen partial

pressure of 2×10^{-2} Pa using RF magnetron sputtering method [53]. The deposited films are characterised by studying crystallographic structure with XRD, surface morphology by atomic microscopy, and electrical and optical properties. The effect of substrate temperature on the physical properties of the deposited films has been systematically studied. The films deposited at 303 K are found amorphous while those formed at higher temperatures are polycrystalline with improved crystallinity. The electrical resistivity of the films decreases from 29 to 8 ohm and optical band gap increases from 2.15 to 2.32 eV with the increase of substrate temperature from 303 to 523 K. The AFM study revealed that grain size of the films increased from 20 to 130 nm with the increase of substrate temperature from 303 to 524 K.

CuO thin films have been synthesized by a sol-gel method using cupric acetate $\text{Cu}(\text{CH}_3\text{COO})_2$ as a precursor. XRD patterns of CuO thin films showed that all the films were nanocrystallized in the monoclinic structure. The crystallite size increased from 40 to 45 nm with increasing annealing temperature. The room temperature DC electrical conductivity was increased from 10^{-6} to 10^{-5} $(\Omega\text{-cm})^{-1}$ [54]. CuO thin films prepared by thermal preparation methods have resistivities in the range 10^2 - 10^4 $\Omega\text{-cm}$ [55]. Copper Oxide thin films were deposited by vacuum evaporation on silicon substrates in temperatures varying from 150 up to 450 °C. XRD patterns showed that in the copper oxide films two phases coexist: CuO and Cu_2O . Their proportions vary with oxidation temperature. Substrate temperatures up to 225 °C Cu and Cu_2O were formed while above this temperature CuO formed. Pure Cu_2O was obtained at 225 °C while pure CuO was found above 350 °C. Fourier transform infrared (FTIR) transmittance spectra confirmed the results from the XRD [56]. CuO thin films were deposited using a reactive DC sputtering method and the structure of the films determined by means of an XRD analysis indicated that the phase of copper oxide can be synthesized in the total pressure and temperature ranges of 6-8.5 mbar and 151-192 °C, respectively. The resistivity of the film synthesized at a T_s of 192 °C increases from 0.104 to 0.51 $\Omega\text{-m}$ after absorbing CO_2 gas at 135 °C. The gas sensitivity of the film synthesized at the T_s of 192 °C increased up to 5.1 in the presence of CO_2 gas at 160 °C. The gas sensitivity in the presence of N_2 gas reached only 1.43 even at 200 °C [30].

CuO thin films having different thicknesses (20,100,200) nm were deposited into glass substrates by a R.F. magnetron sputtering process using copper oxide target under (Ar) pressure and R.F. sputtering power of 130 W. XRD results suggested that the deposited CuO films were formed by nanoparticles with average particle size in the range of (4 - 11) nm. The results of these films have high absorbance in ultraviolet, visible regions and high transmittance in near infrared region. The optical properties concerning the absorption and transmission spectra were studied for the prepared thin films. The energy band gap were found to be in the range of (2.25 eV to 2.6 eV) When the film thickness varying from 20 nm to 200 nm [57].

CuO thin films were deposited on glass substrates by double dip method at various molar concentrations of copper sulphate salt. The structural studies revealed the deposited films exhibited polycrystalline nature with monoclinic structure. The change in the molar concentration of copper sulphate salt has pronounced effect on the microstructural properties of deposited thin films. XPS and EDS spectra confirmed the presence of Cu and O. Deposited films showed a high absorbance in the visible range with the band gap value of 1.3 eV making it a suitable material as semiconductor tandem absorber for solar cells. The prepared CuO thin films are identified as suitable candidates for optoelectronic devices and solar cell fabrication [58].

Hole conducting, optically transparent Cu_2O thin films on glass substrates have been synthesized by vacuum annealing (5×10^{-6} mbar at 700 K for 1 hour) of magnetron sputtered (at 300 K) CuO thin films. The Cu_2O thin films are p-type and showed enhanced properties: grain size (54.7 nm), optical transmission 72% (at 600 nm). The XRD pattern and optical transmittance is shown in Fig. 1.1 and Fig. 1.2 respectively [59].

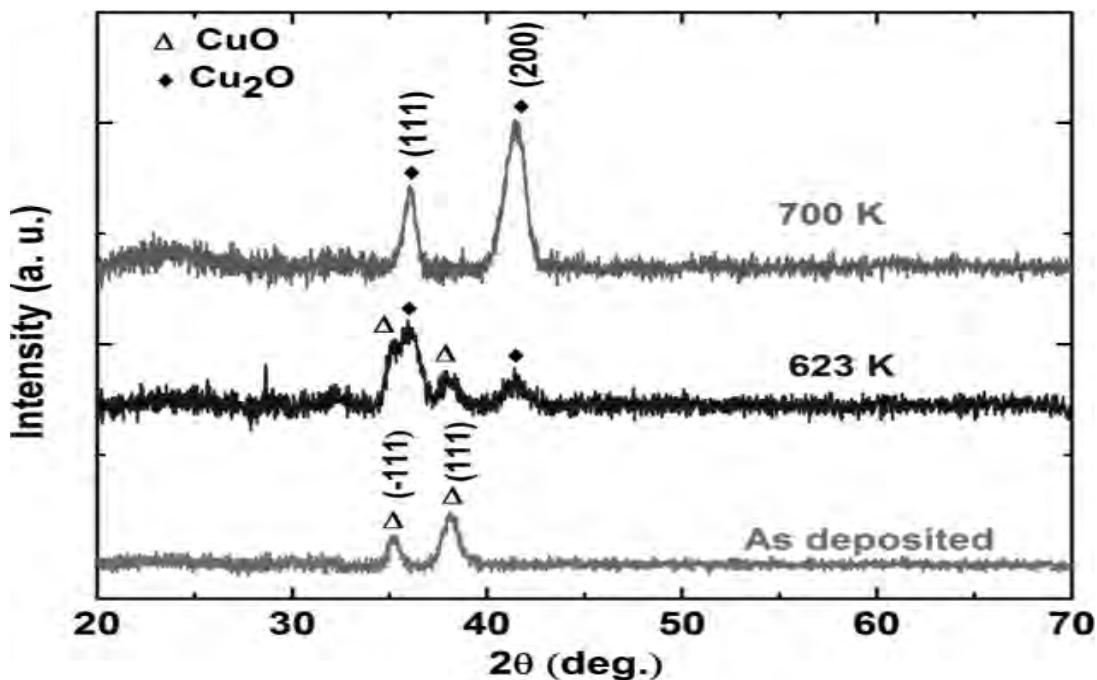


Fig. 1.1. XRD of copper oxide thin films: “as deposited”, annealed in vacuum at 623 K, and annealed in vacuum at 700 K

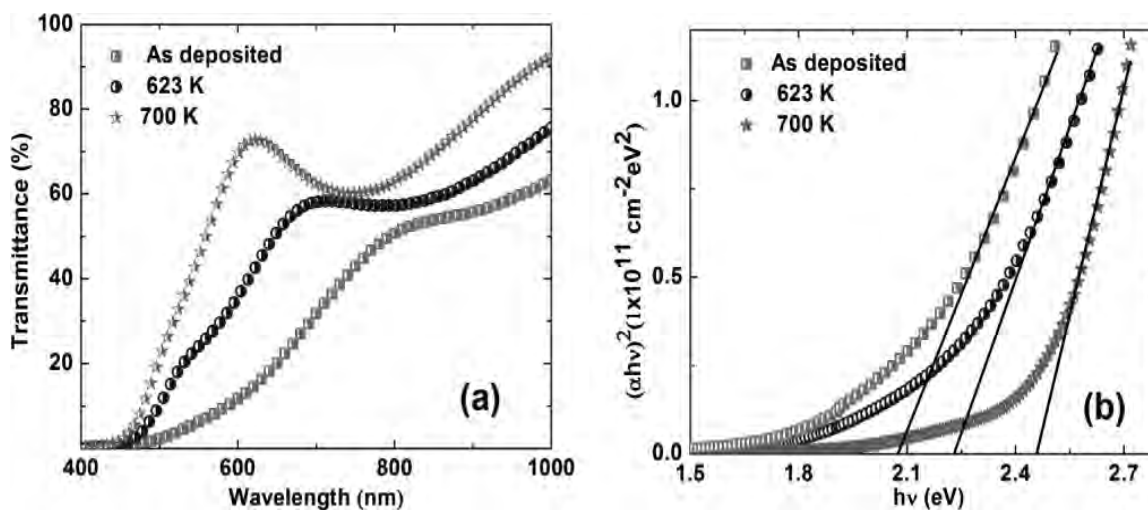


Fig. 1.2 (a) Optical transmission spectra of 250 nm thick copper oxide thin films (b) Tauc plots of copper oxide thin: as deposited, 623 K vacuum annealed and 700 K vacuum annealed

Sn:CuO films with different Sn concentrations from 0 to 2.0 mol% were prepared on glass substrates using a sol-gel method [60]. The obtained films showed good crystallinity and a smooth morphology. All the films exhibited a polycrystalline CuO phase with a monoclinic structure. No XRD peaks of SnO₂ were observed, which indicated that SnO₂ had entered the crystal lattice of CuO. The crystallite size decreased from approximately 84.1–61.8 nm with increasing Sn content. The Sn:CuO film with 1.5 mol% SnO₂ showed the lowest band gap 1.95 eV. All films showed a mean transmittance of more than 80 %, and the band gap was reduced from 2.00 to 1.96 eV with increasing Sn content. Overall, Sn doping has a great influence on the structural, electrical and optical properties of Sn:CuO films. Effects of the Sn content of Sn:CuO films on the surface (Fig. 1.3), resistivity, carrier concentration and mobility as shown in Fig. 1.4.

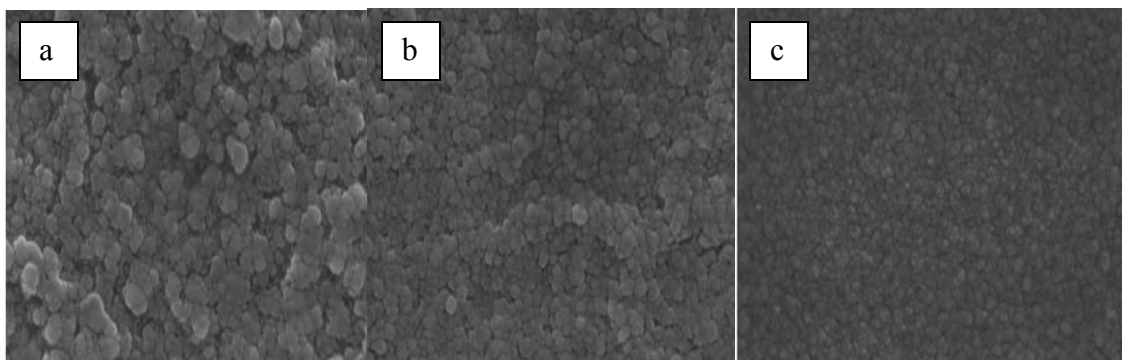


Fig. 1.3 SEM images of the Sn:CuO films with different Sn concentrations: (a) 0 mol%, (b) 1.0 mol%, (d) 1.5 mol%

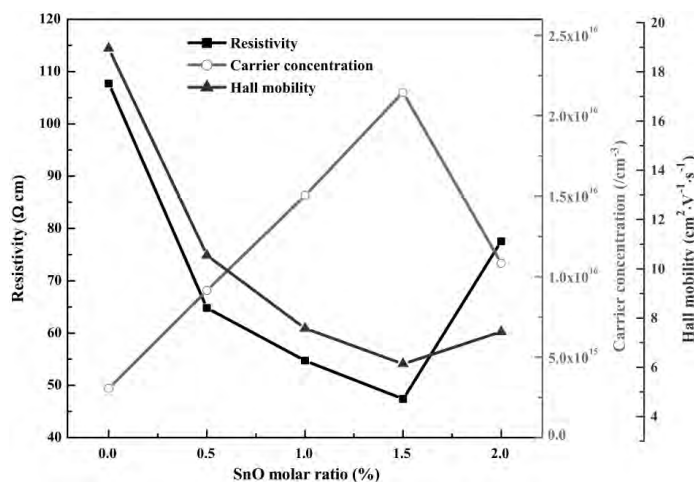


Fig. 1.4 Effects of the Sn content of Sn:CuO films on the resistivity, carrier concentration and mobility

CuO has been established as a number of applications like gas sensors, solar photovoltaic, lithium ion electrode, etc. prepared by different techniques [61-64].

The results of structural characterization of SnO₂ films doped by impurities such as Fe, Cu, Ni, and Co during spray pyrolysis deposition [65] from 0.2 M SnCl₄-water solutions were presented. The change of parameters such as film morphology, the grain size, texture, and the intensity of X-ray diffraction peaks were controlled. It was shown that the doping promoted the change of the film morphology and the decrease of the SnO₂ grain size; however, these changes were not great. The doping influence becomes apparent more obviously for thin films and the films deposited at low temperatures ($T_{\text{pyr}} = 350$ °C). At higher pyrolysis temperatures ($T_{\text{pyr}} = 450$ °C), the influence of the doping on both the grain size and the film morphology was weakened. We concluded that used additives had dominant influence on the structural properties of SnO₂ at the initial stages of the film growth, as well as at the stages of twinning and agglomeration of the SnO₂ crystallites. It was shown that the increase in the contents of the fine dispersion phase in as-deposited film is an important consequence of the SnO₂ doping.

Optical properties of pure and antimony (Sb) doped tin oxide (SnO₂) thin films, prepared from SnCl₂ precursor [66], have been studied as a function of Sb doping concentration. This paper investigates the variation of optical and electrical properties of the as-deposited films with Sb doping. The doping concentration was varied from 0-4 wt. % of Sb. All the films were deposited on microscope glass slides at the optimized substrate temperature of 400° C. The films are polycrystalline in nature with tetragonal crystal structure. The details on the optical properties along with the sheet resistance values are investigated. The sheet resistance of the undoped films is decreased with initial doping of antimony to attain a minimum value and increased for higher level of doping. The sheet resistance achieved for the films doped with 2 wt. % Sb is the lowest among the earlier reports for these films from SnCl₂ precursor. The change in the sheet resistance is explained in terms of different oxidation states of antimony. The sheet resistance of SnO₂ thin films was found to decrease from 38.22 Ω/square to 2.17 Ω/square for undoped and antimony doped films respectively. The transmittance increases initially with increase in doping concentration and then decreases for higher doping levels which is attributed to light absorption. The transmittance

of the films was observed to increase from 42 % to 55 % (at 800 nm) on initial addition of Sb and then it is decreased for higher level of Sb doping.

TiO₂ has been recently used to realize high-temperature ferromagnetic semiconductors. In fact, it has been widely used for a long time as white pigment and sunscreen because of its whiteness, high refractive index, and excellent optical properties [67]. Tran and Blaha's modified Becke-Johnson (TB-mBJ) exchange potential (plus a local density approximation correlation potential) within the density functional theory to investigate electronic structures and optical properties of rutile and anatase TiO₂. The energy gaps obtained from mBJ method agree better with the experimental results than that obtained from local density approximation (LDA) and generalized gradient approximation (GGA), in contrast with substantially overestimated values from many-body perturbation (GW) calculations. As for optical dielectric functions (both real and imaginary parts), refractive index, and extinction coefficients as functions of photon energy, mBJ calculated results are in excellent agreement with the experimental curves. This approach can be used as a standard to understand electronic structures and the related properties of such materials as TiO₂. Photocatalytic TiO₂ films on glass and quartz plates were obtained by the chemical vapour deposition using Ti(dpm)₂(Oprⁱ)₂ complex compound (CC-CVD method) in a standard vacuum apparatus at $1.2\text{--}2.0 \times 10^{-4}$ mbar [68]. The substrate temperature was stabilised in the range of 450–600 °C. The growth rate varied from several nanometres to several dozen of nanometres per minute. Two different crystalline forms, rutile and anatase, could be prepared using these precursors, as demonstrated by XRD. The photocatalytic activity of the TiO₂ thin films was studied using a photocatalytic reactor.

TiO₂ thin films have wide applications because of their useful electrical and optical properties, such as high refractive index, high dielectric constant, and excellent transmittance in the visible and near infrared range. TiO₂ films grown by RF magnetron sputtering without oxygen (O₂) addition showed considerable optical loss due to the optical absorption by an oxygen deficiency in the film and the scattering by large surface roughness. However, TiO₂ films grown with O₂ addition had a stoichiometric composition and a smooth surface morphology without optical loss. Substrate heating during deposition enhanced the packing density and crystallinity of the film, and as a result, TiO₂ films with higher refractive index (2.50) and better homogeneity could be obtained with substrate

heating between 200 °C and 400 °C [5]. TiO₂ and doped TiO₂ thin films were obtained by RF sputtering method and showed that structure of TiO₂ thin films was influenced by the substrate used and also by doping with cerium (Ce), niobium (Nb) and iron (Fe) impurities. Consequently, the transmittance was also modified [69]. Anatase TiO₂ thin films were successfully prepared on foam nickel (Ni) substrates by sol-gel technique using tetrabutyl titanate as precursor [28]. Ni²⁺ doping due to the foam (Ni) substrates resulted in the extension of absorption edges of TiO₂ films from ultraviolet (UV) region to visible (Vis) light region ($\lambda < 520$ nm). The photocatalytic activities of TiO₂ thin films were investigated by photocatalytic degradation reactions of gaseous acetaldehyde, an indoor pollutant, under UV light irradiation. TiO₂ thin films have been deposited on microscope glass substrate by SPT by varying T_s, molarity of solution and solution spray rate [70]. XRD patterns indicated that the films have amorphous and polycrystalline structure and the size of the crystallites have been changed from 9 to 48 nm. The optical band gap of the TiO₂ films was determined to be about 3.40 to 3.65 eV due to the change of deposition conditions. The electrical conductivity of the TiO₂ film prepared by spin coating method on indium tin oxide (ITO) coated glass substrate was found to be very high ($3.46 \times 10^5 \Omega^{-1}\cdot\text{cm}^{-1}$) and comparable to that of the bare ITO glass [71]. The hemin-doped TiO₂ thin films have been prepared by liquid phase deposition technique on soda lime glass [72]. The UV-vis spectrum shows the optical band gap of TiO₂ thin films to be 3.2 eV and XRD pattern of the thin films shows a single anatase phase at annealing temperature of 500 °C with some orientation effect in [101] peak. The rate of degradation increased with increasing concentration of hemin. Fluorine (F) doped TiO₂ (FTO) powders were synthesized by SPT from an aqueous solution of H₂TiF₆ [73]. The resulting FTO powders possessed spherical particles with a rough surface morphology and a strong surface acidity. The F concentrations in the FTO powders calculated from X-ray photoelectron spectroscopy (XPS) spectra significantly depended on T_s and ranged from 2.76 to 9.40 at.%. The FTO powder prepared at T_s of 1173 K demonstrated the highest photocatalytic activity for the decomposition of gas-phase acetaldehyde under both UV irradiations. It was interesting to point out that the Vis photocatalytic activity of FTO powders was achieved by the creation of surface oxygen vacancies rather than the improvement of optical absorption property of bulk TiO₂ in Vis region.

Fig.1.5(a, b) TiO₂ photocatalyst films having an anatase crystal structure with different thickness were prepared by the low-pressure metal organic chemical vapor deposition (LPMOCVD) to examine the effect of growth conditions on photocatalytic activity [74]. Film thickness was linearly proportional to the deposition time. Structure of the film was strongly dependent on the deposition time. In early stage of deposition, fine particles deposit on the substrate. As increasing the deposition time, crystal orientation is gradually selected following the Kolmogorov model and c-axis oriented columnar crystals become dominant. The photocatalytic activity strongly depends on the film deposition time (or film thickness) in nonlinear way. The optimum thickness of TiO₂ catalyst film grown by LPMOCVD may locate between 3 and 5 μm .

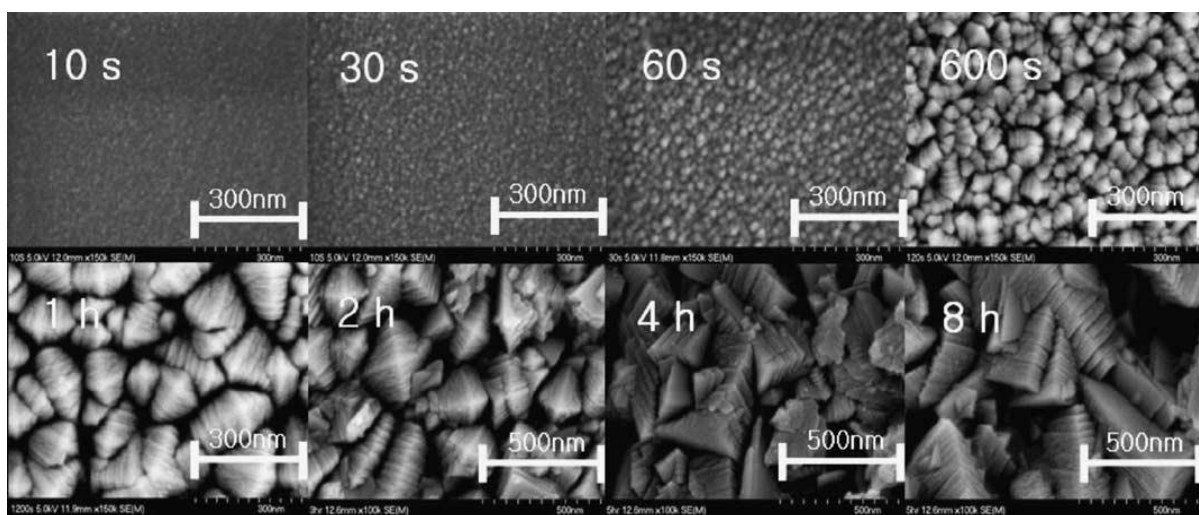


Fig. 1.5(a) SEM of TiO₂ thin films grown by LPMOCVD at different deposition times

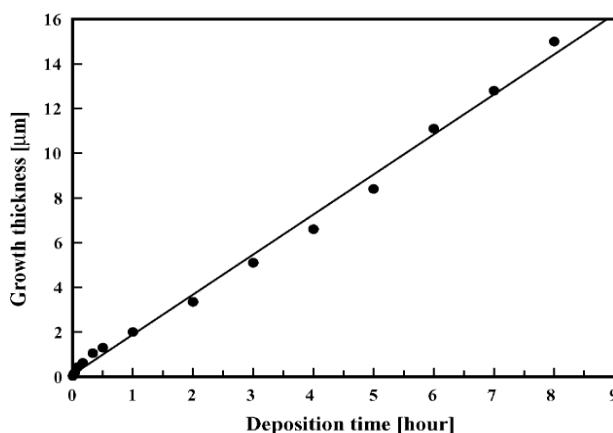


Fig. 1.5(b) Thickness of TiO₂ film as a function of deposition time

M/TiO₂ (M = Ag, Cu) thin films on quartz were prepared by RF magnetron co-sputtering process and the calcination effects on their optical and structural properties were

investigated [75]. These films were amorphous below 300 °C, and these were anatase phase at 300–700 °C. The crystallite size of the anatase phase and the agglomerates of primary particles of the M/TiO₂ thin films increase with increasing calcination temperature. TiO₂ thin films with higher refractive index and better homogeneity were obtained with substrate heating between 200 °C and 400 °C. TiO₂ thin films were prepared by chemical spray pyrolysis from aqueous solutions and it was shown that it had three different kinds of polymorphous crystalline forms: rutile, anatase, and brookite [76]. The rutile phase is always formed at higher temperatures, while the anatase phase is formed at lower temperatures and transformed into rutile phase above T_s of 800 °C. The refractive index lies in the range between 2.01 and 2.29.

TiO₂ thin films prepared with and without lithium (Li) and Nb were uniform, crack-free, stoichiometric, and amorphous when deposited at 300 °C and below; and were polycrystalline anatase when deposited at 400 °C. Films prepared around 200 °C were very porous, but the porosity was decreased as T_s increased [77]. Optical absorption spectra revealed an indirect band gap of 3.0 eV for amorphous and anatase films and a direct band gap of the same value in rutile. Dark dc conductivity of undoped films was lower than 10^{-10} (Ohm-cm)⁻¹. The presence of Nb and Li increased the conductivity by 2–3 orders of magnitude, similar to the effect of hydrogen annealing.

TiO₂ thin films were obtained using the metal-organic chemical vapor deposition (MOCVD) method [78], film thickness increased with deposition time as expected, while the transmittance varied from 72 to 91% and the refractive index remained close to 2.6.

Multilayer TiO₂/WO₃ thin films deposited on silicon and glass substrate by pulsed laser deposition (PLD) method [79]. The Multilayer film has higher photocatalytic activity than TiO₂ film under visible light irradiation. Clear diffraction peaks of anatase TiO₂ [(101), (105), (211)] are observed in both films. Weak and broad peaks from WO₃ [(002), (004)] may result from its thickness and low deposition temperature. The films of different WO₃ mixing ratio showed almost the same results. XRD and UV–VIS transmittance spectra are shown in Fig. 1.6 (a, b) of TiO₂/WO₃ multilayer film deposited using a TiO₂ target. In both cases, optical absorption edge increased from 300 nm to 350 nm with increasing WO₃ ratio in the film. This means that film of TiO₂/WO₃ multilayer structure can be activated by light of longer wavelength without decreasing transmittance in visible region.

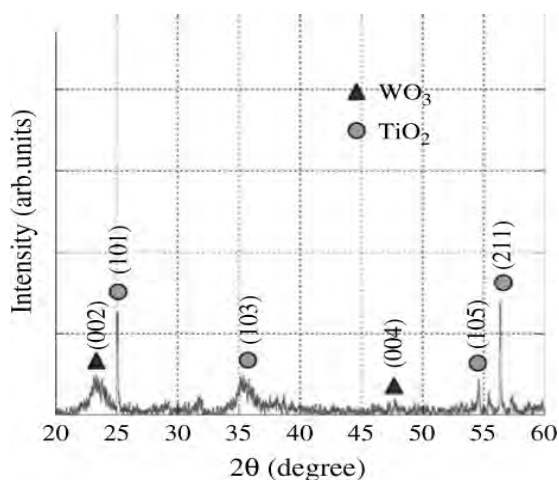


Fig. 1.6 (a) XRD pattern of TiO_2/WO_3 multilayer thin film, target: TiO_2

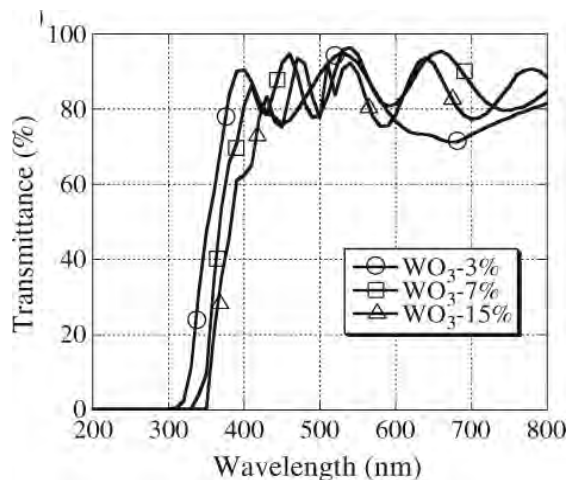


Fig.1.6 (b) Transmittance of TiO_2/WO_3 multilayer thin film, target: TiO_2

TiO_2 films were prepared by sol-gel methods with butyltitanate as main raw materials butyltitanate ($\text{Ti}(\text{OC}_4\text{H}_9)_4$) [80]. The results indicated that the TiO_2 films have better electrochromic properties when the films are amorphous with heat treatment temperature at 250°C and applied voltage of $\pm 2\text{V}$ with respect to the reference electrode. The UV-vis transmission spectrum of TiO_2 film under different heat treatment temperature is shown in Fig. 1.7.

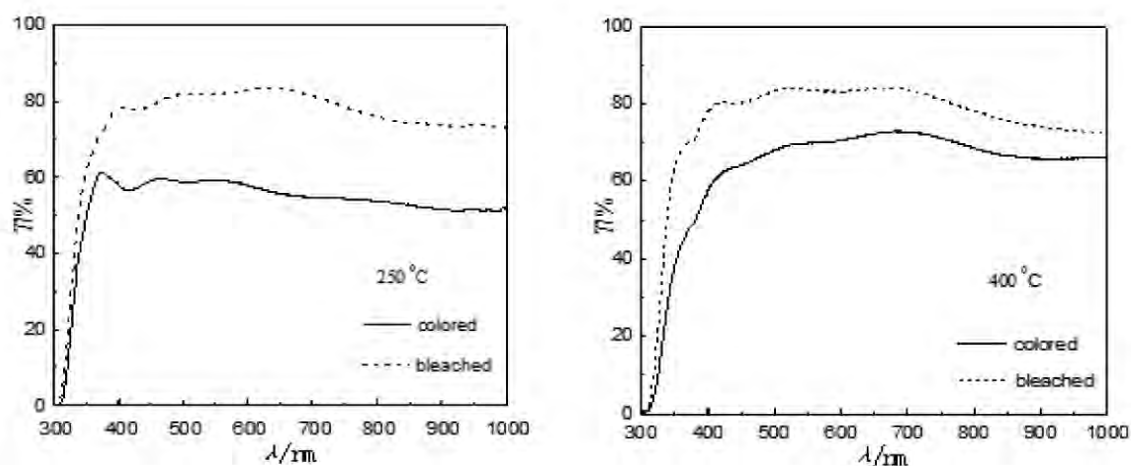


Fig. 1.7 The UV-vis transmission spectrum of TiO_2 film under different heat treatment temperature

TiO_2 thin films have been prepared from tetraisopropyl-orthotitanate solution and ethanol as a solvent by sol gel dip-coating technique [81]. The films and dry powder from the solgel solution were calcined at 500°C for 1 hour. It was found that the film consisted of fine

titanium dioxide grains homogeneously deposited on the indium tin oxide coated (ITO) glass.

Substrate dipping in a composite sol-gel solution was used to prepare smooth and rough thin films of TiO_2 on fiberglass from solution of titanium (IV) isopropoxide as sol-gel precursor and cetyltrimethyl-ammonium bromide as surfactant. [82]. In all samples, the gel films were converted to the anatase phase by calcining them at $500\text{ }^\circ\text{C}$. Both smooth and rough anatase thin films were obtained with a short immersion of fiberglass into the sol-gel with or without surfactant. All TiO_2 thin films deposited on fiberglass after a short immersion into the sol-gel were homogeneous and continuous. The gel film deposited on glass changes from a composite structure to TiO_2 when is calcined at $500\text{ }^\circ\text{C}$. The Raman study carried on the TiO_2 films showed that the films are formed predominantly of anatase phase. Nevertheless, this also could depend on the duration of the thermal treatment. Optical sensors or semiconductor wires are potential applications of these fibers with TiO_2 film. Moreover, this novel material could be used as a catalytic material in some oxidation processes or photo degradation reactions.

Amorphous TiO_2 thin films and $\text{TiO}_2/\text{ZnFe}_2\text{O}_4$ composite films were deposited by r.f. magnetron sputtering [83]. The influence of post deposition annealing on the structural and optical properties was studied. It was established that the anatase single phase exists between 250 and $800\text{ }^\circ\text{C}$ for the TiO_2 thin films, and between 450 and $650\text{ }^\circ\text{C}$ for the composite films. The optical band gap was determined for films annealed between 300 and $700\text{ }^\circ\text{C}$. The absorption edge of TiO_2 thin films and $\text{TiO}_2/\text{ZnFe}_2\text{O}_4$ composite films exhibits a blue shift with decreasing annealing temperature. The absorption edge of composite films has moved to visible spectrum range. A reduction of optical energy gap from 3.64 to 3.78 eV for TiO_2 thin films was noticed, which is considered mainly due to the change of the energy gap of the disorder crystal in TiO_2 films. And the reduction was from 3.14 to 3.56 eV for $\text{ZnFe}_2\text{O}_4/\text{TiO}_2$ composite films, which is believe caused by direct (Franck-Condon type) transition in an otherwise indirect band gap semiconductor. A very large red shift of the absorption edge of $\text{TiO}_2/\text{ZnFe}_2\text{O}_4$ composite films occurs in comparison with TiO_2 thin films. The red shift is considered mainly induced by the interface effect between ZnFe_2O_4 and TiO_2 particles.

Nanostructure TiO₂/Ag composite thin films were prepared by a sol-gel spin and dip coating technique while, by introducing methyl cellulose (MC) porous, TiO₂/Ag films were obtained after calcining at a temperature of 500 °C [84]. All the prepared composite films exhibited anatase-phase TiO₂ as determined by XRD. MC-TiO₂ films with Ag additions exhibited porous nanostructure but differed from that of porous TiO₂ film. The photocatalytic properties of the prepared thin films were evaluated by degrading methyl orange under UV. ANPSGF-MC-Ag, MPC500SGF-MC-Ag, and P25SGF-MC-Ag composite films exhibited 64%, 42%, and 69% degradation, respectively. By making the TiO₂ film porous and adding Ag element, the photocatalytic performance of the TiO₂ based composite films can be improved significantly.

NiO_x thin films were grown on quartz-glass substrates by two-step process: oxidation of metal Ni thin film which was obtained by vacuum evaporation method [85]. The structural, optical and electrical properties of NiO_x thin film were investigated by X-ray diffraction, absorption spectra and Hall measurement, respectively. The oxidation temperature could influence the structural, electrical and optical properties of NiO_x thin film. At lower oxidation temperature (623 K), the oxidation process was not finished completely. With the increase of oxidation temperature, Ni thin films were totally oxidized into p-type NiO thin films and the optical absorption edge became steeper. Furthermore, the conductivity and carrier concentration of p-type NiO thin film decreased with the increase of oxidation temperature.

The values of E_g for films are higher than that of bulk NiO (3.55 eV) and can be attributed to the reduced dimension of the crystallites. NiO/TiO₂ films with various NiO film thicknesses ranging from 10 to 320 nm were deposited on silicon and glass substrates by e-beam evaporation at 200 °C, and then annealed in H₂ atmosphere at 500 °C for 1 h in order to reduce the NiO film to Ni grains on the TiO₂ film [86]. The results showed that an amorphous TiO₂ was obtained as deposited at 200 °C and that the structure changes to the anatase phase after 500 °C annealing. As deposited, crystalline NiO films with XRD patterns similar to that of powder were obtained; however, diffraction peaks of (111) and (200) Ni appeared after annealing in H₂ atmosphere. Ni nanograins, coarsened grains, and films were obtained on the TiO₂ films when the NiO film with a thickness from 10 to 320 nm was reduced in H₂ atmosphere at 500 °C. The transmittance of the Ni/TiO₂ films

decreased with an increase in Ni particle size. The vis absorption measurement showed that the peak shifted toward a shorter wavelength with a decrease in Ni particle size.

There are different techniques to prepare oxide thin films under different deposition parameters: substrate temperature, time and flow rate of deposition, amount of base material, distance between the substrate and spray gun tip, and dopant concentration like as vapour deposition technique [3], electron beam evaporation deposition technique [10], spray pyrolysis technique (SPT) [15, 17], RF magnetron co-sputtering [75], MOCVD method [78], solgel [87], etc. The present research work aimed at to the production of uniform, transparent, and conductive CuO, TiO₂ and Cu doped TiO₂ (Cu/TiO₂) thin films by an inexpensive and locally fabricated spray pyrolysis system [88] using a precursor solution of Cu(CH₃COO)₂.H₂O, TiCl₄ and Cu(CH₃COO)₂.H₂O + TiCl₄ respectively and to study the effect of Cu doping of the precursor solution on the structural, optical and electrical properties of prepared thin films.

1.5 Objectives of the Present Work

On account of the numerous applications of oxide thin films, an attempt has been made to prepare such oxides thin films by locally fabricated SPT and to characterize these thin films, so as to reduce the preparation cost and make it economically feasible. From technological point of interest, I-IV-VI group compound semiconductor thin films would be deposited on to glass substrates by SPT. The plan of the present work is to carry out the investigation of structural, optical and electrical properties of CuO, TiO₂ and Cu/TiO₂ thin films synthesized by SPT. The study of these oxide thin films is motivated by their applications as a solid state gas sensor material, oxidation catalyst, transparent conductive coatings material, etc. Thin film processing techniques and research are strongly related to the basic research activities. A good homogenous and stoichiometric thin film with high efficiency is expected to be grown by taking the advantage of the low cost technique, SPT. Through careful control of the deposition parameters, it is possible to tailor the films with respect to specific chemical functionality, thickness and other chemical and physical properties. These deposition parameters include: T_s, substrate position, flow rate, distance between substrate and solution nozzle, and reactor type. Achievement of high optical transparency and electrical conductivity simultaneously in thin film is governed by the deposition

parameters, the dopants, and control of non-stoichiometry. Such good controllability of the thin films from aqueous solutions has great advantages on economy, convenience and capacity of large area deposition for production design.

From these points of view, SPT has been chosen to synthesize CuO, TiO₂ and Cu/TiO₂ thin film from aqueous solutions in the present research work. Recently researches have shown that simple (binary) metal oxides in many cases did not have a combination of properties, necessary for the fabrication of the gas sensors, satisfying the requirements such as high sensitivity and good selectivity at high temporal stability of operating characteristics. Those problems could be resolved by an optimization of the metal oxide matrix composition through doping by various additives. The additives, e.g., Cu doping can change parameters of the metal oxides such as the phase, composition, crystallite size, concentration of charge carriers, chemical and physical properties of the metal oxide matrix. Therefore, it is decided that optically transparent and low resistive, homogeneous and stoichiometric CuO, TiO₂ and Cu/TiO₂ thin films with high efficiency will be grown by using the low cost technique spraying the precursor solution onto a heated glass substrate. In this research work, three classes of samples would be synthesized by the followings three steps:

- (i) Copper oxide thin films would be prepared from aqueous solutions of Cu(CH₃COO)₂.H₂O of different MC (0.05-0.15M) at T_s of 350 °C and by variation of T_s (250-450 °C) for MC of 0.10 M.
- (ii) TiO₂ thin films would be prepared from aqueous solutions of TiCl₄ of different MC (0.05-0.15M) at T_s of 400 °C and by variation of T_s (250-450 °C) for MC of 0.10 M.
- (iii) Cu/TiO₂ thin films would be prepared at T_s of 400 °C from aqueous solutions (0.10 M) of Cu(CH₃COO)₂.H₂O (1 – 10 wt%) + TiCl₄ (99 – 90 wt%).

The following investigations would be carried out on the synthesized oxide thin films:

- (i) The thickness of the films would be measured by interferometric method (Fizeau fringes)
- (ii) The surface morphology and elemental analysis would be observed by Scanning electron microscopy (SEM) and Energy dispersive analysis of X-rays (EDX), respectively.
- (iii) The structural investigations would be performed by X-ray diffraction (XRD).
- (iv) The optical properties would be investigated by UV-visible spectroscopy.

(v) The electrical properties would be investigated by van-der Pauw method.

Finally, the findings would be discussed in relation to the MC, T_s and Cu doping. It is expected that this study would help to find better materials for application in electronic and optoelectronic devices.

1.6 Thesis Layout

This thesis is organized into five chapters as follows:

Chapter 1, the general introduction, begins with an introduction followed by standard data for copper oxide and titanium oxide, applications areas of thin films, brief review of oxide thin films, aim of the present work and thesis layout.

Chapter 2, the theoretical background chapter, discussing the different aspects of formation of thin films, surface morphology, elemental contamination, structural, optical and electrical properties. This chapter, also, provides the descriptions of various techniques for thin film deposition and theories on the different investigation methods.

Chapter 3 focuses experimental details with the description of film deposition and measurement in details.

Chapter 4 contains results and discussion on investigation of surface morphology, elemental analysis, structural analysis, optical properties, electrical properties, Figure of merit, etc.

Chapter 5 includes conclusions of the findings and suggestions for future work.

A complete list of references has been given at the end of each chapter.

References

- [1] Kumar S. K., Suresh S., Murugesan S., Raj S. P, “CuO thin films made of nanofibers for solar selective absorber applications”, *Solar Energy*, 94, pp. 299-304, 2013.
- [2] Islam M. R. and Podder J., “Optical properties of ZnO nano fiber thin films grown by spray pyrolysis of zinc acetate precursor”, *Cryst. Res. Technol* 44, 3, pp. 286–292, 2009.
- [3] Josph J., Mathew V., Mathew J., Abraham K. E., “Studies on physical properties and carrier conversion of SnO₂:Nd thin films”, *Turk J. Phys*, 32 , pp.1-10, 2008.
- [4] Han N., Tian Y., Wei L., Wang C., Chen Y., “NiO thin film fabricated by electrophoretic deposition and formaldehyde gas sensing property thereof”, *J. Nanosci. Nanotech.*, 9, 2, pp. 1346-1349, 2009.
- [5] Jeong S-H, Kim B-S, Lee B-T, “Structural and Optical Properties of TiO₂ Films Prepared Using Reactive RF Magnetron Sputtering”, *J. Korean Phys. Soci*. 41, 1, pp. 67-72, 2002.
- [6] Joseph J. P., Ramamurthy S., Subramanian B., Sanjeeviraja C., Jayachandran M., “Spray pyrolysis growth and material properties of In₂O₃ films”, *J. Cryst. Growth*, 240, pp. 142–151, 2002.
- [7] Akkari F. C., Kanzaria M., Rezig B., “Preparation and characterization of obliquely deposited copper oxide thin films”, *Eur. Phys. J. Appl. Phys.* 40, pp. 49–54, 2007.
- [8] Li Y., Zhao G., Su J., Shen E., Ren Y., “Top electrode effects on resistive switching behavior in CuO thin films”, *Appl Phys A*, 104, pp. 1069–1073, 2011.
- [9] Manohari A. G., Dhanapandian S., Kumar K. S., Mahalingam T., “Optimization of deposition parameters on the physical properties of TiO₂ thin films by spray pyrolysis technique” *Int. J. Thin Fil. Sci. Tec.*, 3,1, pp. 1-6, 2014.
- [10] Guang-Lei T., Hong-Bo H., Jian-Da S., “Effect of microstructure of TiO₂ thin film on optical band gap energy”, *Chinese Phys. Lett.*, 22, 1787, 2005.

- [11] Hou D. L., Meng H. J., Jia L. Y., Ye X. J., Zhou H J and Li X. L “Impurity concentration study on ferromagnetism in Cu-doped TiO₂ thin films”, EPL, 67001, pp.1- 5, 2007.
- [12] Duhalde S., Vignolo M. F., Chilotte C. , Torres C.E. R., Errico L. A., Cabrera A. F., Renteria M., Sanchez F. H., Weissmann M., “Appearance of room-temperature ferromagnetism in Cu-doped TiO_{2-δ} films”, Phys. Rev. B, 72, pp.1-4, 2005.
- [13] Besserguenev V. G., Pereira R. J. F., Mateus M. C., Khmelinskii I. V., Nicula R. C., Burkel E. “TiO₂ thin film synthesis from complex precursors by CVD, its physical and photocatalytic properties”, Inter. J. Photoenergy, 5, pp. 99-105, 2003.
- [14] Bhavana G., Nitu B., Shrivastav S.B., Ganesan V., “A simple chemical spray pyrolysis apparatus for thin film preparation”, J. Instrum. Soc. India, 39, 1, pp. 2-45, 2009.
- [15] Islam M. M., Islam M. R., Podder J., “Optical and electrical characteristics of CdO thin films deposited by spray pyrolysis method”, J. Bangladesh Acad. Sci., 32,1, pp. 97-105, 2008.
- [16] Podder J., Roy S. S. “An investigation of structural and electrical properties of nano crystalline SnO₂: Cu thin films deposited by spray pyrolysis”, Sensors & Transducers Journal, 134, 11, pp. 155-162, 2011.
- [17] Roy S. S., Podder J. “Synthesis and optical characterization of pure and Cu doped SnO₂ thin films deposited by spray pyrolysis”, JOAM, 12, 7, pp. 1479-1484, 2010.
- [18] Jachon J., Varghes M., Abraham K.E, “Studies on Cu, Fe, and Mn doped SnO₂ semi conducting transparent films prepared by a vapor deposition technique”, Chinese J. Phys. 45, 1, pp. 84-97, 2007.
- [19] Holzschuh H. Suhr H. , “Deposition of copper oxide (Cu₂O, CuO) thin films at high temperatures by plasma - enhanced CVD”, Applied Physics A: Materials Science & Processing, 51, 6, pp. 486-490, 1990.
- [20] Korosec R. C., Bukovec P., “Sol - Gel prepared NiO thin films for electrochromic applications”, Acta Chim. Slov., 53, pp. 136–147, 2006.

- [21] Benramache S., Benhaoua B. and Bentrach H., "Preparation of transparent, conductive ZnO:Co and ZnO:In thin films by ultrasonic spray method", *J. Nanostruct. Chemi.*, 3:54, 7 pages, 2013.
- [22] Kiriakidis G., Katsarakis N., Bender M., Gagaoudakis E., Cimalla V., "InO_x thin films, candidates for novel chemical and optoelectronics applications", *Mater. Phys. Mech.* 1, pp. 83-97, 2000.
- [23] Zakrzewska K., Redecka M., Rekas M., "Effect of Nb, Cr, Sn additions on gas sensing properties of TiO₂ thin films", *Thin Solid Films*, 310, pp. 161-166, 1997.
- [24] Manyala R., *Solar Collectors and Panels, Theory and Applications*, ISBN: 978-953-307-142-8, 2010.
- [25] Matsuzaki K., Nomura K., Yanagi H., Kamiya T., Hirano M., Hosono H., "Epitaxial growth of high mobility Cu₂O thin films and application to p-channel thin film transistor", *Appl. Phys. Lett.*, 93, 202107, 2008.
- [26] Nasr-Esfahani M., Habibi M. H., "Silver doped TiO₂ nanostructure composite photocatalyst film synthesized by sol-gel spin and dip coating technique on glass", *Int. J. Photo.*, 2008, 628713, 11 pages, 2008.
- [27] Ayele D. W., Su W-N., Hwang B-J., "A low-cost polytetrafluoroethylene-framed TiO₂ electrode decorated with oleic acid-capped CdSe quantum dots for solar cell", *J. Energy*, 2013, 394512, 2013.
- [28] Hai H., Wen-jun X., Jian Y., Jian-wei S., Ming-xia C., Wen-feng S. G., "Preparations of TiO₂ film coated on foam nickel substrate by sol-gel processes and its photocatalytic activity for degradation of acetaldehyde", *J. Environ. Sci.*, 19, pp. 80-85. 2007.
- [29] Rakhshani, A. E., "Preparation, Characteristics and photovoltaic properties of cuprous Oxide - A Review", *Solid State Electron.*, 29, pp. 7-17, 1986.
- [30] Samarasekara P., Kumara N. T. R. N., Yapa N. U. S., "Sputtered copper oxide (CuO) thin films for gas sensor devices", *J. Phys.: Condens. Matter*, 18, pp. 2417-2420, 2006.
- [31] Cahill D. G., Allen T. H., "Thermal conductivity of sputtered and evaporated SiO₂ and TiO₂ optical coatings", *Appl. Phys. Lett.* 65, pp. 309-311, 1994.

- [32] Amor S. B., Baud G., Besse J. P., Jacquet M., "Structural and optical properties of sputtered Titania films", *Mater. Sci. Eng: B*, 47, pp. 110-118, 1997.
- [33] Babelon P., Dequiedt A.S., Mostefa-Sba H., Bourgeois S., Sibillot P., Sacilotti M., "SEM and XPS studies of titanium dioxide thin films grown by MOCVD", *Thin Solid Films*, 322, pp. 63-67, 1998.
- [34] Fujishima A., Honda K., "Electrochemical Photolysis of Water at a semiconductor Electrode", *Nature*, 238, pp. 37-38, 1972.
- [35] Nishida S.Y., Fu X., Anderson M.A., Hori K., "Chlorinated byproducts from the photoassisted catalytic oxidation of trichloroethylene and tetrachloroethylene in the gas phase using porous TiO₂ pellets", *J. Photochem. Photobiol. A: Chem.*, 97, pp. 175-179, 1996.
- [36] Yamazaki S., Tanaka S., Tsukamoto H., "Kinetic studies of oxidation of ethylene over a TiO₂ photocatalyst", *J. Photochem. Photobiol. A: Chem.*, 121, pp. 55-61, 1999.
- [37] Tennakone K., Kottegoda I. R. M., "Photocatalytic mineralization of paraquat dissolved in water by TiO₂ supported on polythene and polypropylene films", *J. Photochem. Photobiol. A: Chem.* 93, pp. 79-81, 1996.
- [38] Kangarlou H., Rafizadeh S., "Structural and optical properties of titanium dioxide thin layers as a function of film thickness", *World Appl.Sci. J.*, 13, pp. 42-46, 2011.
- [39] Lee J. H., Jeong K. H., Cho W. H., Ho W. J., Yang H. J., Kim C. S., Lee J. G., "Deposition of copper oxide by reactive magnetron sputtering", *Met. Mater. Int.* 17, pp. 917-921, 2011.
- [40] Lv J., Liu C., Gong W., Zi Z., Chen X., Huang K., Liu F., Wang T., He G., Song X., Sun Z., "Facile synthesis of Zn_{1-x}Cu_xO nanorods with a very broad visible band", *Electron. Mater. Lett.*, 8, pp. 477-480, 2012.
- [41] Xiao X., Miao L., Xu G., Lu L., Su Z., Wang N., Tanemura S., "A facile process to prepare copper oxide thin films as solar selective absorbers", *Appl. Surf. Sci.*, 257, 24, pp. 10729-10736, 2011.
- [42] Barreca D., Comini E., Gasparotto A., Maccato C., Sada C., Sberveglieri G., Tondello E., "Chemical vapor deposition of copper oxide films and entangled quasi-

- 1D nanoarchitectures as innovative gas sensors”, *Sensor. Actuat. B: Chemical*, 141, pp. 270-275, 2009.
- [43] Lee E. J., Noh T., Jeon M. S., Jeong Y., Lee H., “Electrical degradation of Al doped ZnO thin films by a damp heat test”, *Korean J. Met. Mater.* 51, pp. 145-150, 2013.
- [44] Leng Y. X., Huang N., Yang P., Chen J.Y., Sun H., Wang J., Wan G.J., Tian X.B., Fu R.K.Y., Wang L.P., Chu P.K., “Structure and properties of biomedical TiO₂ films synthesized by dual 2 plasma deposition”, *Surf. Coat. Technol.*, 156, pp. 295–300, 2002.
- [45] Cho S., “Optical and electrical properties of CuO thin films deposited at several growth temperatures by reactive RF magnetron sputtering”, *Met. Mater. Int.*, 19, 6, pp. 1327-1331, 2013.
- [46] Chauhan D., Satsangi V. R., Dass S. Shrivastav R., “Preparation and characterization of nanostructured CuO thin films for photoelectrochemical splitting of water”, *Bull. Mater. Sci.*, 29, 7, pp. 709–716, 2006.
- [49] Marabelli F., Parraviciny G.B., Drioli F. S., “Optical gap of CuO”, *Phys. Rev. B*, 52, 3, pp. 1433-1436, 1995.
- [50] Ghijsen J., Tjeng L. H., Elp J.V., Eskes H., Westerink J., Sawatzky G.A., Czyzyk M. T., Electronic structure of Cu₂O and CuO”, *Phys. Rev. B* 38, pp. 11322-11330, 1988.
- [51] Luo H., Jain M., Mc Cleskey T. M., Bauer E, Burrell A. K., and Jia Q., “Optical and structural properties of single phase epitaxial p-type transparent oxide thin films”, *Adv. Mater.*, 2007, pp. 3604-3607, 2007.
- [52] Ogwu A. A., Darma T.H., Bouquerel E., “Electrical resistivity of copper oxide thin films prepared by reactive magnetron sputtering”, *JAMME*, 24, 1, pp. 172-177, 2007.
- [53] Reddy M. H. P., Narayana P., Uthanna S, “Structural, electrical and optical behaviour of rf magnetron sputtered cuprous oxide films”, *Indi. J. Pure Appl. Phys.*, 48, pp. 420-424, 2010.
- [54] Jundale D. M., Joshi P. B., Sen S., Patil V. B., “Nanocrystalline CuO thin films: synthesis, microstructural and optoelectronic properties”, *J Mater Sci: Mater Electron*, 23, pp. 1492-1499, 2012.

- [55] Drobny V.F., Pulfrey D.L., "Properties of reactively-sputtered copper oxide thin films", *Thin Solid Films*, 61, , pp. 89-98, 1979.
- [56] Papadimitropoulos G., Vourdas N, Vamvakas V. E. and Davazoglou D, "Deposition and characterization of copper oxide thin films" *J. Phys: Conf. Ser*, 10, pp. 182–185, 2005.
- [57] Riam A., Abdulhussain K. E. Ahmed K. A. A- Z., "Optical properties of (CuO) thin films prepared by (R.F.) plasma sputtering", *Wasit J. Sci. Medic.*, 7, 4, pp. 265-276, 2014.
- [58] Shrividhya T., Ravi G., Hayakawa Y., Mahalingam T., "Determination of structural and optical parameters of CuO thin films prepared by double dip technique", *J Mater Sci: Mater Electron*, 25, pp. 3885–389, 2014.
- [59] Dhanya S. Murali, Shailendra K., Choudhary R. J., Avinash D., Wadikar, Mahaveer K. J. , Subrahmanyam A., "Synthesis of Cu₂O from CuO thin films: Optical and electrical properties", *AIP Adv.*, 5, 047143-5, 2015.
- [60] Wu J., Hui K. S., Hui K. N., Li L., Chun H-H., Cho Y. R., "Characterization of Sn-doped CuO thin films prepared by a sol–gel method", *J Mater Sci: Mater Electron*, DOI 10.1007/s10854-015-3945-8, 2015.
- [61] Manish K. V., Vinay G., "A highly sensitive SnO₂–CuO multilayered sensor structure for detection of H₂S gas. Sensor", *Actuat B*, 166–167, pp. 378– 385, 2012.
- [62] Chandrasekaran, S., "A novel single step synthesis, high efficiency and cost effective photovoltaic applications of oxidized copper nano particles", *Sol. Energ. Mat. Sol. C*, 109, pp. 220-226, 2013.
- [63] Amun A., Xiao F. D., Chun-Yang Y., Zhong-Tao J., Mahbubur R. M. and Trevor P., "Solar absorptance of copper–cobalt oxide thin film coatings with nano-size, grain-like morphology: Optimization and synchrotron radiation XPS studies", *Appl. Surf. Sci.*, 275, pp. 127-135, 2013.
- [64] Jorg H., Claus-Dieter K., Bernd M. S., Tilman S., Jean-Mathieu T., Stefanie R., and Thorsten W., "CuO thin films for the detection of H₂S doses: Investigation and application", *Phys. Status Solidi A*, pp. 1-8, 2015.

- [65] Korotcenkov G., Brinzari V., Boris I., (Cu, Fe, Co, or Ni)-doped tin dioxide films deposited by spray pyrolysis: doping influence on film morphology, *J Mater Sci*, 43, pp. 2761–2770, 2008.
- [66] Elangovan E., Ramamurthi K., “Studies on optical properties of polycrystalline SnO₂:Sb thin films prepared using SnCl₂ precursor”, *Cryst. Res. Technol.* 38, No., pp. 779–784, 2003.
- [67] Sai G., Bang-Gui L., “Electronic structures and optical properties of TiO₂: Improved density-functional-theory investigation”, *Chin. Phys.B*, 21, 5, 2012.
- [68] Besserguenev V. G., Pereira R. J. F., Mateus M. C., Khmelinskii I. V., Nicula R. C., Burkel E. “TiO₂: (Fe, S) thin film synthesis from complex precursors by CVD, its physical and photocatalytic properties”, *Inter. J. Photoenergy*, 767054, 12 pages, 2012.
- [69] Mardare D., Tasca M., Delibas M., Rusu G. I., “On the structural properties and optical transmittance of TiO₂ R.F. sputtered thin films”, *Appl. Surf. Sci.*, 156, pp. 200–206, 2000.
- [70] Manohari A. G., Dhanapandian S., Santhosh K., Mahalingam T., “Optimization of deposition parameters on the physical properties of TiO₂ thin films by spray pyrolysis technique”, *Int. J. Thin Film Sci. Tec.*, 3, 1, pp. 1-6, 2014.
- [71] Daniyan A. A., Umoru L. E., Fasasi A. Y., Borode J. O., Oluwasegun K. M., Olusunle S. O. O., “Electrical properties of nano-TiO₂ thin film using spin coating method”, *JMMCE*, 2, pp. 15-20, 2014.
- [72] Begum N. S., Ahmed H. M. F., “Synthesis of nanocrystalline TiO₂ thin films by liquid phase deposition technique and its application for photocatalytic degradation studies”, *Bull. Mater. Sci.*, 31, 1, pp. 43–48, 2008.
- [73] Li D., Haneda H., Hishita S., Ohashi N., Labhsetwar N. K., “Fluorine-doped TiO₂ powders prepared by spray pyrolysis and their improved photocatalytic activity for decomposition of gas-phase acetaldehyde”, *J. Fluorine Chem.*, 126, pp. 69–77, 2005.
- [74] Jung S-C., Kim S-J., Imaishi N., Cho Y-I., “Effect of TiO₂ thin film thickness and specific surface area by low-pressure metal–organic chemical vapor deposition on photocatalytic activities”, *Appl. Catal. B: Environ.*, 55, pp. 53–257, 2005.

- [75] Ryu S. W., Kim E. J., Ko S. K., Hahn S. H., "Effect of calcination on the structural and optical properties of M/TiO₂ thin films by RF magnetron co-sputtering", *Mater. Lett.*, 58, pp. 582– 587, 2004.
- [76] Ayouchi R., Casteleiro C., Schwarz R., Barrado J. R., Martin F., "Optical properties of TiO₂ thin films prepared by chemical spray pyrolysis from aqueous solutions", *Phys. Status Solidi C*, 7, pp. 933– 936, 2010.
- [77] Golego N., Studenikin S. A., Cocivera M., "Spray pyrolysis preparation of porous polycrystalline thin films of titanium dioxide containing Li and Nb", *J. Mater. Res.*, 14, 3, pp. 698-707, 1999.
- [78] Bernardi M. I. B., Lee E. J. H., Lisboa-Filho P. N., Leite E. R., Longoa E., Varela J. A., "TiO₂ thin film growth using the MOCVD method", *Mater. Res.*, 4, 3, pp. 223-227, 2001.
- [79] Shinguu H., Bhuiyan M. M. H., Ikegami T., Ebihara K., "Preparation of TiO₂/WO₃ multilayer thin film by PLD method and its catalytic response to visible light", *Thin Solid Films*, 506–507, pp. 111 – 114, 2006.
- [80] Niu W., Wang G., Liu X – d., Tang J., Bi X – g., "Preparation and electrochromic performance of TiO₂ thin film", *Int. J. Electrochem. Sci.*, 10, pp. 2613-2620, 2015.
- [81] Hamid A. M., Rahaman I. A., "Preparation of titanium dioxide (TiO₂) thin films by sol gel dip-coating method" *Malaysian J. Chem.*, 5, 1, pp. 086-091, 2003.
- [82] Medina-Valtierra J., Sanchez-Cardenas M., Frausto-Reyes C., Calixto S., "Formation of smooth and rough TiO₂ thin films on fiberglass by sol-gel method", *J. Mex. Chem. Soc.*, 50, 1, pp. 8-13, 2006.
- [83] Li G.H., Yang L., Jin Y. X., Zhang L. .D. "Structural and optical properties of TiO₂ thin film and TiO₂ + 2 wt.% ZnFe₂O₄ composite film prepared by r.f. sputtering", *Thin Solid Films*, 368, pp. 163-167, 2000.
- [84] Nasr-Esfahani M., Habibi M. H., "Silver doped TiO₂ nanostructure composite photocatalyst film synthesized by sol-gel spin and dip coating technique on glass", *Int. J. Photo.*, 628713, 2008.
- [85] Wang X., Li Y., Wang G. Z., Xiang R., Jiang D. L., Fu S. C., Wu K., Yang X. Y., DuanMu Q. D., Tian J. Q., Fu L C, "Characterization of NiO thin film grown by two - step processes", *Physica B: Condensed Matter*, 404, 8-11, pp.1058-1060, 2009.

- [86] Hong - Hsin H., Hung-Peng C., Fang-Hsing W., Yuan-Shing L., Moo-Chin W., Ding - Fwu L., “Characteristics and optical properties of Ni nanograins reduced on TiO₂ film”, *Jpn. J. Appl. Phys.*, 47, pp.764-767, 2008.
- [87] Keshmiri M., Mohseni M., Troczynski T., “Development of novel TiO₂ sol-gel-derived composite and its photocatalytic activities for trichloroethylene oxidation”, *Appl. Catal., B*, 53, 4, pp. 209 – 219, 2004.
- [88] Das S. C., Green J. R., Podder J., Regier T. Z., Chang G. S., Moewes A., “Band gap tuning in ZnO through Ni doping via spray pyrolysis”, *J. Phys. Chem. C*, 117, pp. 12745–12753, 2013.

CHAPTER-II

THEORETICAL BACKGROUND

2.1 Introduction

2.2 Formation of Thin Films

2.2.1 Introduction

2.2.2 Different Stages of Thin Film Formation

2.2.3 Condensation

2.2.4 Nucleation

2.2.5 Growth

2.2.6 Polycrystalline and Amorphous Thin Films

2.2.7 The Incorporation of Defects during Growth

2.3 Theoretical Aspect of Different Preparation Methods of Thin Films

2.3.1 Introduction

2.3.2 Sol-gel Process

2.3.3 Pulsed ion-beam Evaporation (IBE) Method

2.3.4 Sputtering Method

2.3.5 Chemical Vapor Deposition

2.3.6 Plasma-enhanced Chemical Vapor Deposition

2.3.7 Molecular Beam Epitaxy

2.3.8 Thermal or Vacuum Evaporation Method

2.3.9 Spin Coating Process

2.3.10 Spray Pyrolysis Technique

2.4 Theoretical Aspect of Different Measurement Techniques Used for Study of Thin Films

2.4.1 Introduction

2.4.2 Measurement of Thin Film Thickness

2.4.3 Surface Morphology and Compositional Analysis of Thin Films

2.4.4 Structural Analysis of Thin Films

2.4.5 Optical Analysis of Thin Films

2.4.6 Electrical Analysis of Thin Film

References

CHAPTER-II

THEORETICAL BACKGROUND

2.1 Introduction

Thin film studies have directly or indirectly advanced many new areas of research in solid state physics and chemistry which are based on phenomena uniquely characteristic of the thickness, geometry, and structure of the film [1-2].

Each material surface is exposed to various environmental influences. The surface of a solid body is subjected to corrosion and wear and interacts with light and electromagnetic fields. From the technological point of view the miniaturization of mechanic, electronic, optical and optoelectronic components permanently increases the surface to volume ratio of the involved materials. In modern material science specific surface properties therefore gain increasing importance. The act of applying a thin film to a surface is known as thin-film deposition. Thin film deposition is a technique for depositing a thin film of material onto a substrate or onto previously deposited layers. "Thin" is a relative term, but most deposition techniques allow layer thickness to be controlled within a few tens of nanometers, and some (molecular beam epitaxy) allow single layers of atoms to be deposited at a time [3-5].

The properties of the film or coating have to differ significantly from the bulk. The limit between "thin" and "thick" films cannot generally be defined, although literature sometimes gives an arbitrary value of 1 μm . Basically, a film can be considered as "thin" when its properties are significantly different from the bulk. This can be due to:

1. The increasing surface to volume ratio as decreasing film thickness,
2. The microscopic structure which is dependent on the deposition parameters

In general the physical property of thin films depends on a number of factors, such as

I. The nature of substrates

It may be non-crystalline solids e.g., glass of vitreous silica or crystalline such as cleavage plates of rock salt or mica. To select a particular substrate one has to take into consideration of the lattice parameter of the substrate so that it matches to the lattice parameter of the

grown film, otherwise structural mismatch may create mechanical fracture of the film. It should be comparable with that of the substrate material. It should be comparable with that of the film material.

II. Substrate temperature

The temperature of substrate during deposition of film may affect the film properties. At low temperature polycrystalline films with high densities of structural imperfections are formed on both vitreous and crystalline substrate, but a high temperature oriented single crystal films are formed on crystalline substrates.

III. Pressure and nature of residual gas in deposition chamber

If the deposition chamber is not evacuated with the evaporated atoms can not reach the surface of the substrate. They interact with the gas molecules within the chamber and scattered inside the chamber. Sufficient low pressure is necessary for deposition of thin film on substrate.

IV. Temperature of evaporation source

If the temperature of the evaporation source is increased uniformly, then the film is likely to be uniform; otherwise it may not be uniform due to sudden increase in temperature.

V. Deposition rate and film thickness

The temperature at which epitaxy occurs is dependent on the deposition rate. Substrate temperature decreases with increasing deposition rate. Film thickness mainly depends on deposition rate and deposition time. If the deposition increases, the film thickness also increases having the same deposition time.

VI. Post deposition annealing of the films

Heating the deposited film below its melting point maintain a constant temperature a certain period, and then cooling it back to room temperature is known as annealing. Properties of deposited films are related to the annealing temperature. The post-annealing process removes some defects of the films. It plays an important role in the surface mobility of the atoms.

2.2 Formation of Thin Films

2.2.1 Introduction

The deposition process of a film can be divided into three basic phases:

1. Preparation of the film forming particles (atoms, molecules, cluster)
2. Transport of the particles from the source to the substrate
3. Adsorption of the particles on the substrate and film growth

These phases can - depending on the specific deposition process and/or on the choice of the deposition parameters - be considered as either independent or as influencing one another. The former is desirable since it allows controlling the basic steps independently and therefore yields a high flexibility in the deposition process.

The importance of coatings and the synthesis of new materials for industry have resulted in a tremendous increase of innovative thin film processing technologies. The properties of thin film strongly depend on their structure. So it is important to know the factors that govern the structure of the film. In thin film preparation, there are involved three steps:

- a) Creation of atomic or molecular species
- b) Transport of these species through a medium
- c) Condensation of the species on a substrate.

Thin film is prepared by deposition of the film materials (metals, semiconductors, insulators, dielectric etc.) atom by atom on a substrate through a phase transformation. Sufficient time interval between the two successive deposition of atoms and also layers are required so that these can occupy the minimum potential energy configuration. In thermodynamically stable films, all atoms (or molecules) will take up positions and orientations energetically compatible with the neighboring atoms of the substrate or to the previously deposited layers, and then the effect substrate or the initial layers will diminish gradually [6].

2.2.2 Different Stages of Film Formation

Basic steps of thin film growth are-

1. Thermal accommodation
2. Adsorption (physisorption) of atoms/molecules
3. Surface diffusion
4. Formation of molecule-molecule and substrate-molecule bondings (chemisorption)
5. Nucleation: aggregation of single atoms/molecules
6. Structure and microstructure formation (amorphous- polycrystalline - singlecrystalline, defects, roughness, etc.)
7. Changes within the bulk of the film, e.g. diffusion, grain growth etc

In thin film formation there are three mechanisms of thin film condensations which can be distinguished, depending on the strength of interaction between the atoms of the growing film and between the atoms of the film and substrate. These are:

- a) The layer by layer growth
- b) A three dimensional nucleation, forming, growth and coalescence of islands
- c) Absorption of monolayer and subsequent nucleation on the top of this layer.

In most cases, mechanism (b) takes place and we shall focus our attention on this mechanism in brief.

2.2.3 Condensation

Much research on the mechanism of thin film growth has been done with evaporated films; extensive information on initial growth has been published by D. W. Pashley and his co-workers [7]. The structural behavior and properties of films depend on the growth process. Thin film is most commonly prepared by the condensation of atoms from the vapor phase of a material means, the transformation of a gas into a liquid or solid. The condensation of vapor atom is determined by its interaction with the impinged surface in the following manner. The impinging atom is attracted to the surface by the instantaneous dipole and quadruple moments of the surface atoms. As a result, the atoms losses its velocity component normal to the surface in a short time, provided the incident kinetic energy is not too high. The vapor atoms is then physically absorbed (called adatom), but it may or may not be completely thermally equilibrium. It may move over the surface and its own

kinetic energy parallel to the surface. The adatom has a finite stay or residence time on the surface during which it may interact with other adatoms to form a stable cluster and be chemically absorbed, with the release of the heat of condensation. If not absorbed, the adatom evaporates or desorbs into the vapor phase. Therefore, thermodynamically, the only requirement for condensation to occur is that partial pressure of the film material in the gas phase be equal or larger than its vapor pressure in the condensed phase at that temperature [8].

The probability that an impinging atom will be incorporated into the substrate is called the “condensation” or “striking” coefficient. It is measured by the ratio of the amount material condensed on a surface to the total amount impinged. In fact, often the striking coefficient is so small that condensation is not observable by ordinary techniques. On the other hand, the striking coefficient is found to be strongly dependent on the total time during which the substrate was subjected to the impingement, and also on the substrate temperature. A non-unity striking coefficient is usually explained in terms of monomer re-evaporation from the areas on the substrate which are outside, the capture zones around each stable nucleus.

2.2.4 Nucleation

The stable clusters are called nuclei and the process of formation nuclei is called nucleation i.e. nucleation is the birth stage of a film. Condensation is initiated by the formation of small cluster through the combination of several absorbed atoms. These clusters are called nuclei and the process of formation is called nucleation.

There are two types of nucleation occur during the formation of a film;

I) Homogeneous nucleation: The total free energy is used in the formation of a cluster of adatoms.

II) Heterogeneous nucleation: Particular shapes of clusters are formed by collisions of atoms on the substrate surface, and in the vapor phase its super saturation is sufficiently high. [9]. They initially developed with an increase in free energy until a critical size is reached above which growth continues with a decrease in free energy. In atomistic theory, in low substrate temperature or very high super saturations, the critical nucleus may be a single atom which will form a pair with another atom by random occurrence to become a stable cluster and grow spontaneously.

2.2.5 Growth

The growth sequence of a film was originally deduced by Andrade from the observed optical transmission behavior of silver films. This deduction is in remarkable agreement with the electron microscope observations. The process of enlargement of the nuclei to final form a coherent is termed as growth. Different stages of film growth are shown in Fig. 2.1. There are four stages of the growth process based on the electron microscope observations are:

- i) The island stage
- ii) The coalescence stage
- iii) The channel stage
- iv) The continuous film stage

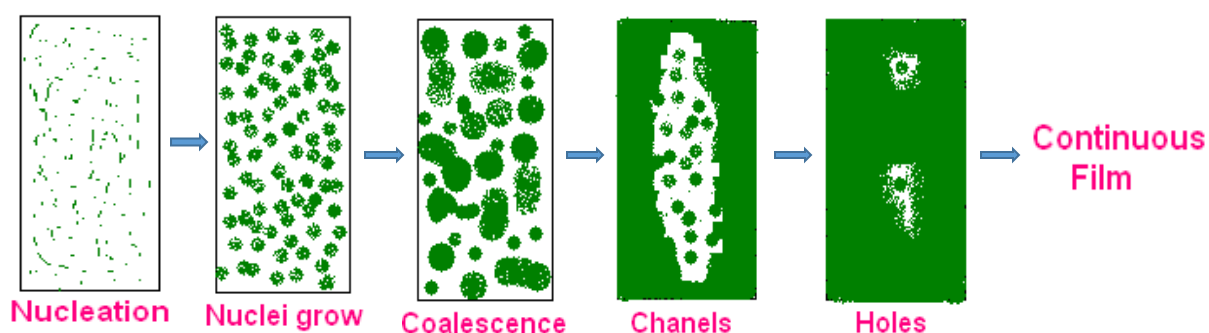


Fig. 2.1 Different stages of thin film growth

2.2.5 (i) The Island Stage

When a substrate under impingement of condenses monomers is observed in the electron microscope, the first evidence of condensation is a sudden burst of nuclei of fairly uniform size. The smallest nuclei detected have a size of 2.0 to 3.0 nm. Growth of nuclei is three dimensional, but the growth parallel to the substrate is greater than that normal to it. This is probably because growth occurs largely by the surface diffusion of monomers on the substrate, rather by direct impingement from the vapor phase. The tendency to form an island structure is increased by

- I) At high substrate temperature

- II) At low boiling point of film material
- III) At low deposition rate
- IV) At weak binding energy between film material and substrate
- V) At high surface energy of the film material and
- VI) At low surface energy of the substrate.

2.2.5 (ii) The Coalescence Stage

As island increases their size by further deposition and come closer to each other, the larger ones appear to grow by coalescence of the smaller ones. The coalescence occurs in less than 0.1s for the small nuclei. After coalescence has taken place, the island assumes a more hexagonal profile is often faulted. A sequence of micrographs illustrating the effects as shown in Fig.2.1 where island which eventually becomes crystallographically shaped.

2.2.5 (iii) The Channel Stage

When larger islands grow together they have channels of interconnected holes of exposed substrate in the form of a network structure on the substrate. As deposition continues, secondary nucleation occurs in these channels and forms the last stage of nucleation.

2.2.5 (iv) Continuous Film Stage

This is the final stage of the film growth. This process is slow and filling the empty channels which requires a considerable amount of deposits. These empty channels are filled by secondary nucleation, growth and coalescence and in this way a continuous film are formed.

2.2.6 Polycrystalline and Amorphous Thin Films

The film deposited by spray pyrolysis are generally polycrystalline or amorphous in structure. Lower temperature and higher gas phase concentration are actually favorable in forming polycrystalline film. In this situation the rate of arrival of the aerosol at the surface is high, but the surface mobility of absorbed atoms is low. A large number of differently oriented nuclei are formed, after coalesce between them the films that are obtained possess grains of different orientation. Further decrease in temperature and increase in super saturation result in even more nuclei and consequently in finer grained films are deposited. When crystalline is completely stopped formation of amorphous film is favored [10].

2.2.7 The Incorporation of Defects during Growth

When the islands during the initial stages of thin film growth are still quite small, they are observed to be perfect single crystal. A large number of defects are incorporated in the film during their recrystallization process at the early stage of film formation [11]. The defects that are usually encountered in spray deposited films are lattice vacancies, stoichiometric excess and grain boundary. Another type of defect namely surface roughness which stems from the quality of the sprayer is especially important in the use of spray deposited films. The properties of the film are strongly affected due to surface roughness if the film thickness is low. The most frequently encountered defects in evaporated films are dislocations, which are less important in chemical spray deposited films.

2.3 Theoretical Aspect of Different Preparation Methods of Thin Films

2.3.1 Introduction

The vast varieties of thin film materials, their deposition processing and fabrication techniques, spectroscopic characterization and optical characterization probes that are used to produce the devices. It is possible to classify these techniques in two ways [1-2].

1. Physical Process
2. Chemical Process.

Physical method covers the deposition techniques which depends on the evaporation or ejection of the material from a source, i.e. evaporation or sputtering, whereas chemical methods depend on physical properties. Structure-property relationships are the key features of such devices and basis of thin film technologies. Underlying the performance and economics of thin film components are the manufacturing techniques on a specific chemical reaction [3]. Thus chemical reactions may depend on thermal effects, as in vapour phase deposition and thermal growth. However, in all these cases a definite chemical reaction is required to obtain the final. The methods summarized in table 3.1 are often capable of producing films defined as thin films, i.e. 1 μm or less and films defined as thick films, i.e. 1 μm or more. However, there are certain techniques which are only capable of producing thick films and these include screen printing, glazing, electrophoretic deposition, flame spraying and painting.

1. Physical Process or Physical Vapour Deposition (PVD): PVD processes proceed along the following sequence of steps:
 - a) The solid material to be deposited is physically converted to vapour phase;
 - b) The vapour phase is transported across a region of reduced pressure from the source to the substrate;
 - c) The vapour condenses on the substrate to form the thin film.

The conversion from solid to vapour phase is done through physical dislodgement of surface atoms by addition of heat in evaporation deposition or by momentum transfer in sputter deposition. The third category of PVD technique is the group of so called augmented energy techniques including ion, plasma or laser assisted depositions.

2. Chemical Vapour Deposition (CVD): Chemical vapour deposition can be defined as a material synthesis method in which the constituents of vapour phase react together to form a solid film at surface. The chemical reaction is an essential characteristic of this method; therefore, besides the control of the usual deposition process variables, the reactions of the reactants must be well understood. Various types of chemical reactions are utilised in CVD for the formation of solids are pyrolysis, reduction, oxidation, hydrolysis, synthetic chemical transport reaction etc. Thin films can be deposited by number of physical and chemical techniques and can be classified as shown in Table 2.1.

Table:2.1 Classification of thin film deposition techniques

Physical Process (PVD)		Chemical Process (CVD)	
Sputtering Phase	Evaporation Gas	Gas Phase	Liquid Phase
Glow discharge DC sputtering	Vacuum Evaporation	Chemical vapour Deposition	Electro-deposition
Triode Sputtering	Resistive heating Evaporation	Laser Chemical vapour deposition	Chemical bath deposition (CBD)
Getter Sputtering	Flash Evaporation	Photo-chemical vapour deposition	Electro less deposition
Radio Frequency Sputtering	Electron beam Evaporation	Plasma enhanced vapour deposition	Anodisation
			Liquid phase Epitaxy
Magnetron Sputtering	Laser Evaporation	Metal-Organo Chemical Vapour Deposition (MOCVD)	Sol- gel
			Spin Coating
			Spray Pyrolysis Technique (SPT)
A.C. Sputtering	Arc		Ultrasonic SPT
	R. F. Heating		Polymer Assisted Deposition (PAD)

Among the methods mentioned in the Table 2.1, the chemical methods are economical and easier than that of the physical methods. Physical methods are expensive but give relatively more reliable and more reproducible results. Most of the chemical methods are cost effective, but their full potential for obtaining device quality films has not been fully explored [2]. But there is no ideal method to prepare thin films, which will satisfy all possible requirements. Among the chemical methods, probably the simplest method available for this purpose is spray pyrolysis technique (SPT) and it is the most popular technique today because large number of conducting and semiconducting thin films can be prepared by this technique.

Generally each method has its advantages and limitations. Here some of the commonly used techniques are described briefly. Among these techniques, the spray pyrolysis is well suited for the preparation of pure and doped oxide thin films. This technique has the advantage of simple and inexpensive experimental arrangement. In this case though, intrinsic advantages of SPT have been used to deposit CuO, TiO₂ and Cu/TiO₂ thin films.

2.3.2 Sol-gel Process

During sol-gel thin film formation via dipping, polymeric or particulate inorganic precursors are concentrated on the substrate surface by a complex process involving gravitational draining with concurrent drying and continued condensation reactions. The structure of films deposited from polymeric precursors depends on such factors as size and structure of the precursors, relative rates of condensation and evaporation, capillary pressure, and substrate withdrawal speed.

Sol-gel method is a wet chemical route for the synthesis of colloidal dispersions of oxides which can be altered to powders, fibers, thin films and monoliths [12]. In general, sol-gel method consists of hydrolysis and condensation reactions. Sol-gel coating as shown in Fig. 2.2 is a process of preparation of single or multicomponent oxide coating which may be glass, glass ceramic or crystalline ceramic depending on the process. Also, the nanomaterials used in modern ceramic and device technology require high purity and facilitate to control over composition and structure. The sol-gel coating is one of the interesting methods because it has many advantages. Examples are as the followings

1. The chemical reactants for sol-gel process can be conveniently purified by distillation and crystallization.
2. All starting materials are mixed at the molecular level in the solution so that a high degree of homogeneity of films can be expected.
3. Organic or inorganic salts can be added to adjust the microstructure or to improve the structural, optical and electrical properties of oxide films.
4. The sol-gel coating is almost exclusively applied for fabrication of transparent layers with a high degree of planarity and surface quality.

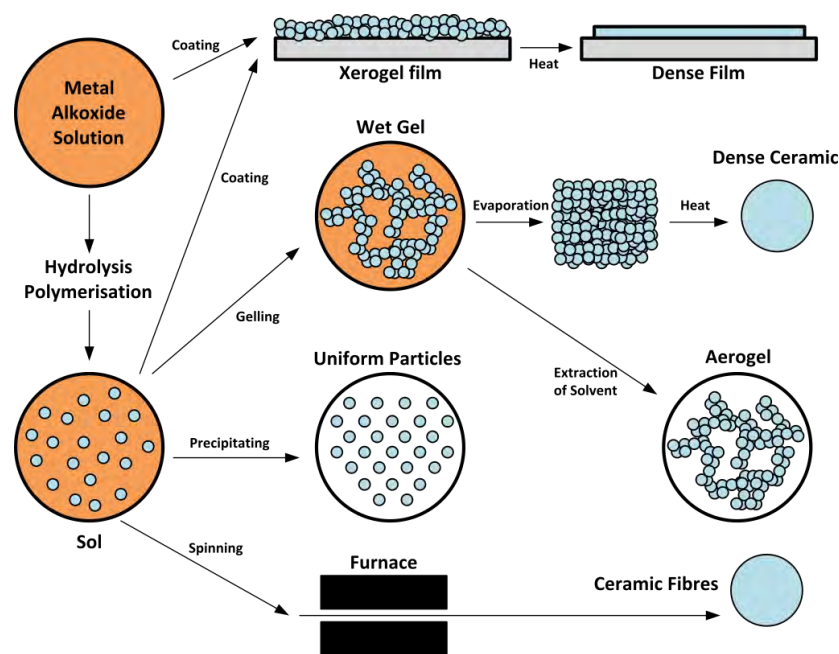


Fig. 2.2 Generalized scheme of sol-gel synthesis

2.3.3 Pulsed ion-beam Evaporation (IBE) Method

Evaporation or sublimation techniques are widely used for the preparation of thin layers. A very large number of materials can be evaporated and, if the evaporation is undertaken in vacuum system, the evaporation temperature will be very considerably reduced, the amount of impurities in the growing layer will be minimised. In order to evaporate materials in a vacuum, a vapour source is required that will support the evaporant and supply the heat of vaporisation while allowing the charge of evaporant to reach a temperature sufficiently high to produce the desired vapour pressure, and hence rate of

evaporation, without reacting chemically with the evaporant. To avoid contamination of the evaporant and hence of growing film, the support material itself must have a negligible vapour pressure and dissociation temperature of the operating temperature. Laser beam evaporation has also come in to use recently. The laser source is situated outside the evaporation system and the beam penetrates through a window and is focused on to the evaporate material, which is usually fine powder form [13].

A schematic of the experimental setup for thin film preparation by Pulsed ion-beam evaporation (IBE) method [14] is shown in Fig. 2.3. The Left-hand side represents an ion beam diode chamber, which produces a pulsed light ion beam (LIB), while the right-hand side represents the chamber to prepare thin films. The intense pulsed ion beam was extracted from the magnetically-insulated diode (MID) with a geometrically focused configuration. The MID consists of an aluminum anode, on which the flashboard (1.5 mm polyethylene) was attached as the ion source, and the cathode with slits to extracting the ion beam. The gap distance between the anode and the cathode is 10 mm. To achieve geometric focusing of the beam, the anode and the cathode were shaped as concave structures with curvature of 160 mm. The current supplied by the external slow capacitor bank produced a transverse magnetic field (~ 1 T) between the anode and the cathode, by which the electrons were magnetically insulated. The beams were mainly composed of protons ($>75\%$) and some carbon ions.

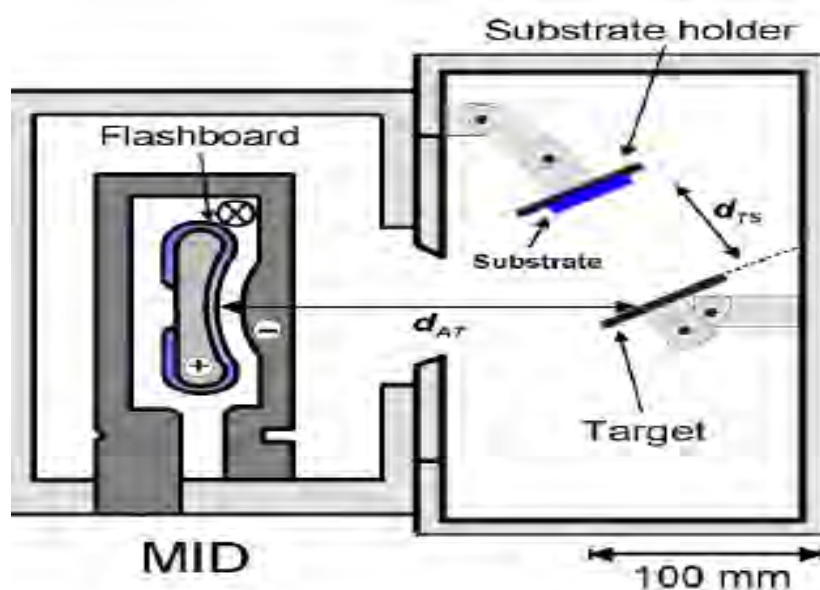


Fig. 2.3 A schematic of the pulsed ion-beam evaporation (IBE) method

2.3.4 Sputtering Method

If a surface of target material is bombarded with energetic particles, it is possible to cause ejection of the surface atom: this is the process known as sputtering (Fig. 2.4). The ejected atoms can be condensed on to a substrate to form a thin film. This method has various advantages over normal evaporation techniques in which no container contamination will occur. It is also possible to deposit alloy films which retain the composition of the parent target material. DC sputtering, radio frequency sputtering and magnetron sputtering methods are the oldest types of sputtering used [15-16]. High pressure oxygen sputtering and facing target sputtering are the two new methods introduced for deposition of thin films for applications in superconducting and magnetic films. Sputtering is a mechanism by which atoms are dislodged from the surface of a material as a result of collision with high-energy particles. Thus, PVD by Sputtering is a term used to refer to a physical vapor deposition (PVD) technique wherein atoms or molecules are ejected from a target material by high-energy particle bombardment so that the ejected atoms or molecules can condense on a substrate as a thin film. Sputtering has become one of the most widely used techniques for depositing various metallic films on wafers, including aluminum, aluminum alloys, platinum, gold, TiW, and tungsten [17]. This method can possibly be used to synthesize thin films of other oxide materials as well. All the films were deposited in a chamber with a base pressure of 10^{-7} Torr using rf Plasma Products RF-10. Ar was used as the sputtering gas.

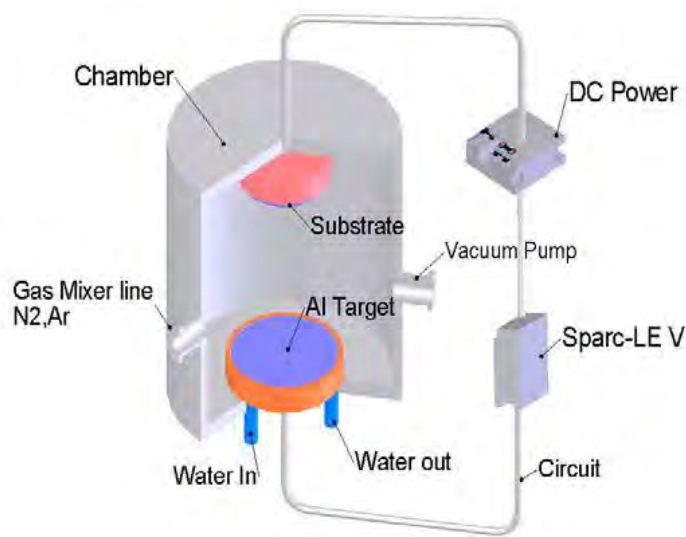


Fig. 2.4 Schematic diagram of the magnetron sputtering system

2.3.5 Chemical Vapor Deposition

In this process, the substrate is placed inside a reactor to which a number of gases are supplied. The fundamental principle of the process is that a chemical reaction takes place between the source gases. The product of that reaction is a solid material which condenses on all surfaces inside the reactor. The two most important CVD technologies in MEMS are the Low Pressure CVD (LPCVD) and Plasma Enhanced CVD (PECVD). The LPCVD process produces layers with excellent uniformity of thickness and material characteristics. The main problems with the process are the high deposition temperature (higher than 600°C) and the relatively slow deposition rate [18]. A schematic diagram of a typical LPCVD reactor is shown in the Fig. 2.5. CVD processes are ideal to use when we want a thin film with good step coverage. A variety of materials can be deposited with this technology; however, some of them are less popular with fabs because of hazardous byproducts formed during processing. The quality of the material varies from process to process, however a good rule of thumb is that higher process temperature yields a material with higher quality and less defects.

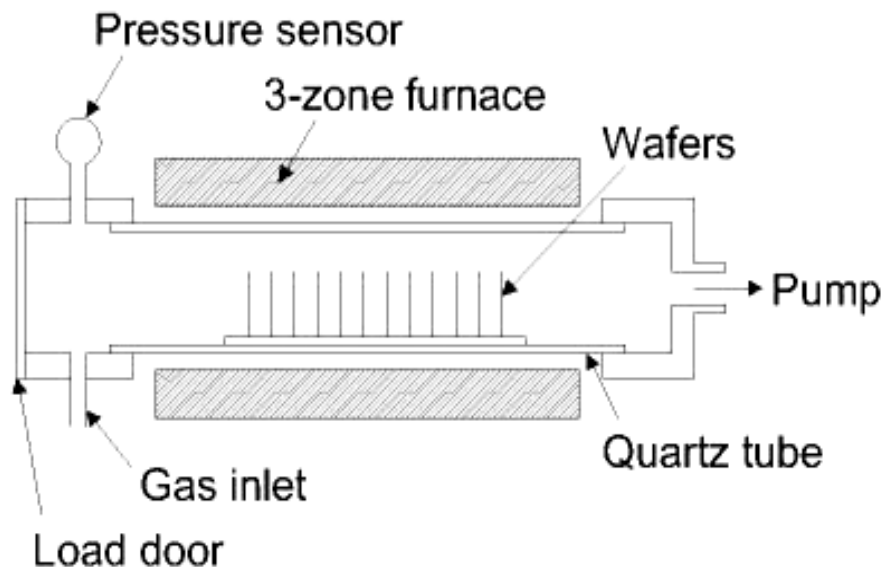


Fig. 2.5 Schematic diagram of a LPCVD system

2.3.6 Plasma-enhanced Chemical Vapor Deposition (PECVD)

PECVD [19] is a process used to deposit thin films from a gas state (vapor) to a solid state on some substrate. There are some chemical reactions involved in the process which occur after creation of plasma of the reacting gases. The important feature of glow discharge plasma is the non-equilibrium state of the overall system. In the plasmas considered for the purpose of plasma polymerization, most of the negative charges are electrons and most of the positive charges are ions. Due to large mass difference between electrons and ions, the electrons are very mobile as compared to the nearly stationary positive ions and carry most of the current. Energetic electrons as well as ions, free radicals, and vacuum ultraviolet light can possess energies well in excess of the energy sufficient to break the bonds of typical organic monomer molecules which range from approximately 3 to 10 eV. Some typical energy of plasma species available in glow discharge as well as bond energies encountered at pressure of approximately 0.01 mbar. A high-tension transformer along with a variac is connected to the feed-through attached to the lower flange. While increasing the applied voltage, the plasma is produced across the electrodes at around 0.15-mbar chamber pressure. Fig 2.6 shows the photograph of glow discharge plasma across the electrodes in the capacitively coupled parallel plate discharge chamber.



Fig. 2.6 Plasma polymerization Chamber

2.3.7 Molecular Beam Epitaxy

Epitaxy means growth of film with a crystallographic relationship between film and substrate. Molecular beam epitaxy is a technique for epitaxial growth via the interaction of one or several molecular or atomic beams that occurs on a surface of a heated crystalline substrate [20]. In Fig.2.7 a scheme of a typical MBE system is shown. The solid sources materials are placed in evaporation cells to provide an angular distribution of atoms or molecules in a beam. The substrate is heated to the necessary temperature and, when needed, continuously rotated to improve the growth homogeneity. Ultra high vacuum (UHV) is the essential environment for MBE. Therefore, the rate of gas evolution from the materials in the chamber has to be as low as possible. Focusing on the possibility that, despite the fact that MBE processes occur under strong nonequilibrium conditions, for the III/V elements, a thermodynamic approach can be used on the basis of equations for mass action in combination with the equations describing the conservation of the mass of the interacting elements.

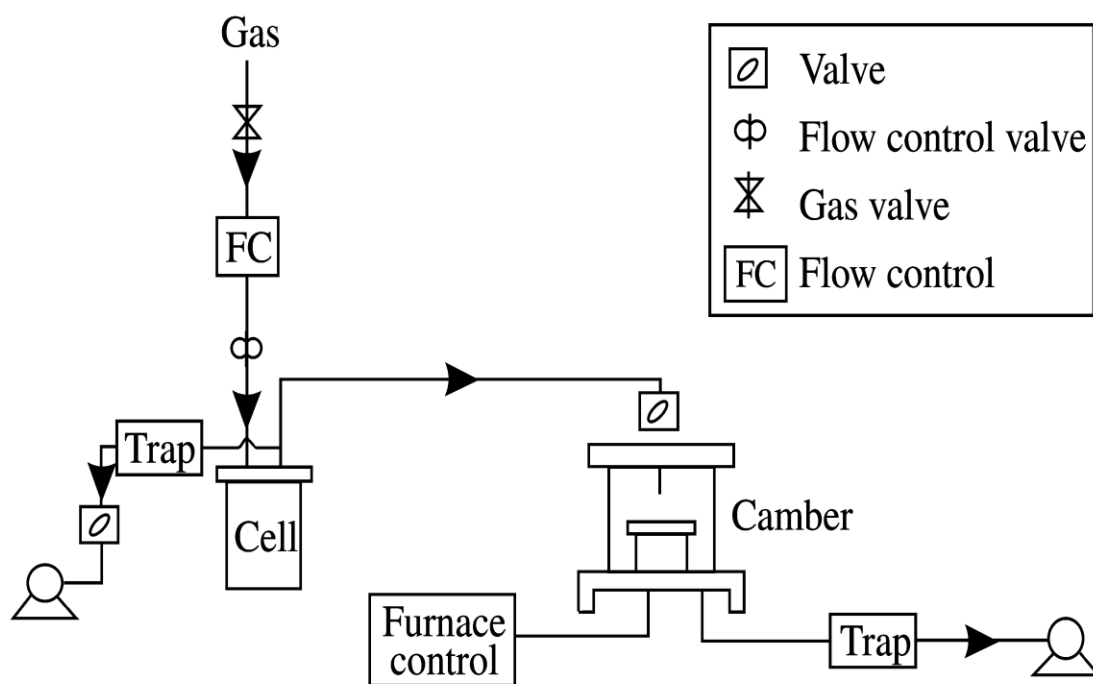


Fig. 2.7 Diagram of a molecular beam epitaxy

2.3.8 Thermal or Vacuum Evaporation Method

Among physical vapor deposition techniques thermal evaporation (TE) [21] is the one with the longest standing tradition. In intelligence, the story of high temperature superconductor (HTS) film deposition can serve as an example how this technique, sometimes regarded as old – fashioned, still bears a high potential for innovation and surprising efficiency. This technique is the simple, convenient and most widely used method for the preparation of the films. TE is the classical technique applied for metal - plating of glass or plastic surfaces, like e.g. aluminum coatings widely used for capacitors, plastic wrappings, and as barrier against water diffusion. It is evident that the deposition of quaternary metal – oxide compounds imposes quite different requirements to the technique and will go far beyond the rudimentary concept of evaporating a single metal in a vacuum chamber. The necessary features of a conventional HTS deposition system are depicted in Fig. 2.8. The metal species the superconductor is composed of are evaporated in high vacuum ambient. In this method materials are vaporized by heating to a sufficient high temperature and then condensation of the vapor into a relatively cooler substrate yielding thin solid films.

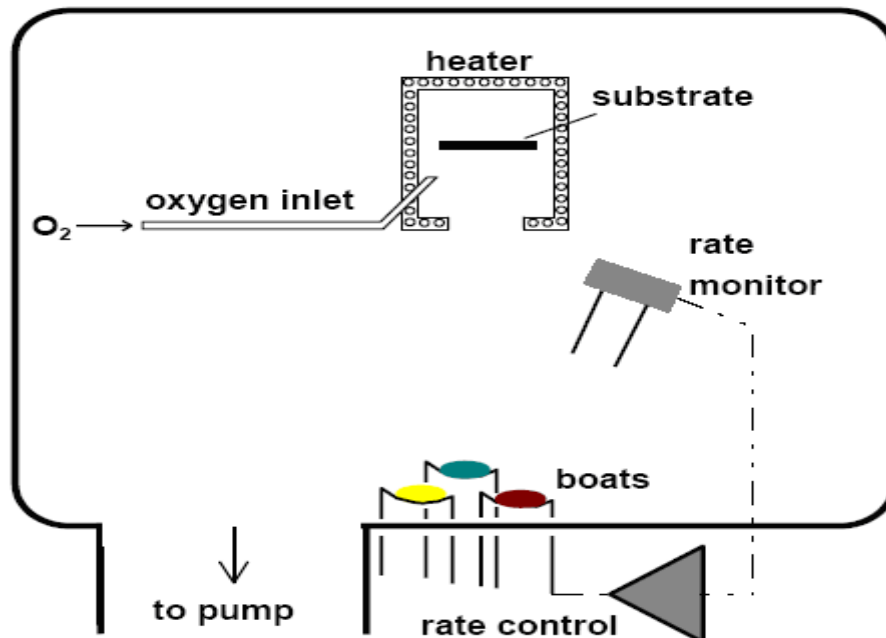


Fig. 2.8 Thermal evaporation method

2.3.9 Spin Coating Process

Spin coating (Fig. 2.9) has been used for several decades for the application of thin films. A typical process [22] involves depositing a small puddle of a liquid resin onto the center of a substrate and then spinning the substrate at high speed (typically around 3000 rpm). Centripetal acceleration will cause the resin to spread to, and eventually off, the edge of the substrate leaving a thin film of resin on the surface. Final film thickness and other properties will depend on the nature of the resin (viscosity, drying rate, percent solids, surface tension, etc.) and the parameters chosen for the spin process. Factors such as final rotational speed, acceleration, and fume exhaust contribute to how the properties of coated film are denned. One of the most important factors in spin coating is repeatability. Subtle variations in the parameters that define the spin process can result in drastic variations in the coated film.

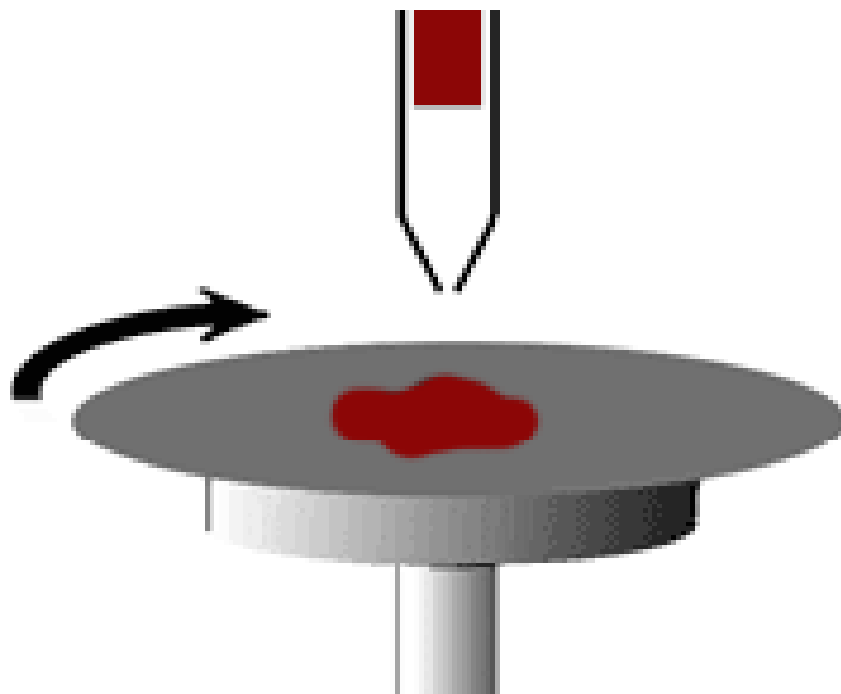
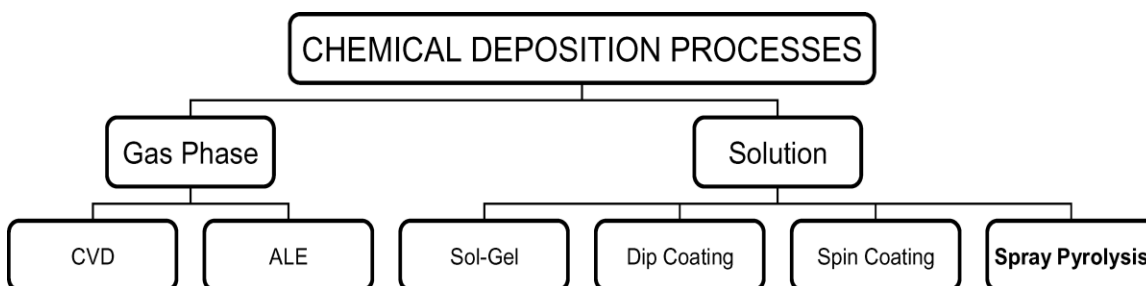


Fig. 2.9 Schematic diagram of the spin coating process

2.3.10 Spray Pyrolysis Technique

Spray pyrolysis technique (SPT) has been applied to deposit a wide variety of thin films [23-24]. These films were used in various devices such as solar cells, sensors, and solid oxide fuel cells. SPT is a convenient, low-cost, very simple and rapid method for the deposition of thin films, and is suitable for industrial applications and has been used for about 30 years for the manufacture of conductive glass. It is also an excellent method for preparing films of semiconductor alloys and complex compounds [25].

It is observed that often the properties of deposited thin films depend on the preparation conditions. An extensive review of the effects of spray parameters on film quality is given to demonstrate the importance of the process of optimization. The substrate surface temperature is the most critical parameter as it influences film roughness, cracking, crystallinity, etc. Processes involved in SPT are discussed in this review as well.



SPT is a process in which a thin film is deposited by spraying a solution on a heated surface, where the constituents react to form a chemical compound [26-27]. The chemical reactions are selected such that the products other than the desired compound are volatile at the temperature of deposition. We discuss here the method and its control; the properties of the films that have been deposited (particularly in relation to the conditions), some specific films, and device application. Because individual droplets evaporate and react very quickly, grain sizes are very small, usually less than 0.1 μ m. The small grains are a disadvantage for most semiconductor applications. The use of low concentration and slow spray rates to improve film quality tends to frustrate the low-cost processing objective, but post deposition heat treatment of small-grain. Films can improve stoichiometry and crystallinity. The process is sensitive to variables, particularly temperature, and the measurement at the surface is uncertain. Not only do the physical and electronic properties of the film vary with temperature, but the deposition efficiency decreases with increased temperature;

stoichiometry is also affected, particularly for alloys. In spite of these difficulties, spray pyrolysis is an excellent method for the deposition of large-area thin films.

Viguie and Spitz [28] classified chemical spray pyrolysis deposition process according to the type of reaction [28]. In chemical spray deposition processes classified according to the type of reaction. In process A, the droplet resides on the surface as the solvent evaporates, leaving behind a solid that may further react in the dry state. In process B, the solvent evaporates before the droplet reaches the surface and the dry solid impinges on the surface, where decomposition occurs. In process C, the solvent vaporizes as the droplet approaches the substrate; the solid then melts and vaporizes, and the vapor diffuses to the substrate, there to undergo a heterogeneous reaction. (They identify this process as true chemical vapor deposition.) In process D, the entire reaction takes place in the vapor state. In all processes, the significant variables are the ambient temperature, carrier gas flow rate, nozzle-to-substrate distance, droplet radius, solution concentration, solution flow rate, and--for continuous processes--substrate motion. To this list one should add the chemical composition of the carrier gas and/or environment, and, most importantly, substrate temperature. Most spray pyrolysis depositions are type A or B. In our experiment we have used a modified SPT and this will be discussed of the method and its control in some details later.

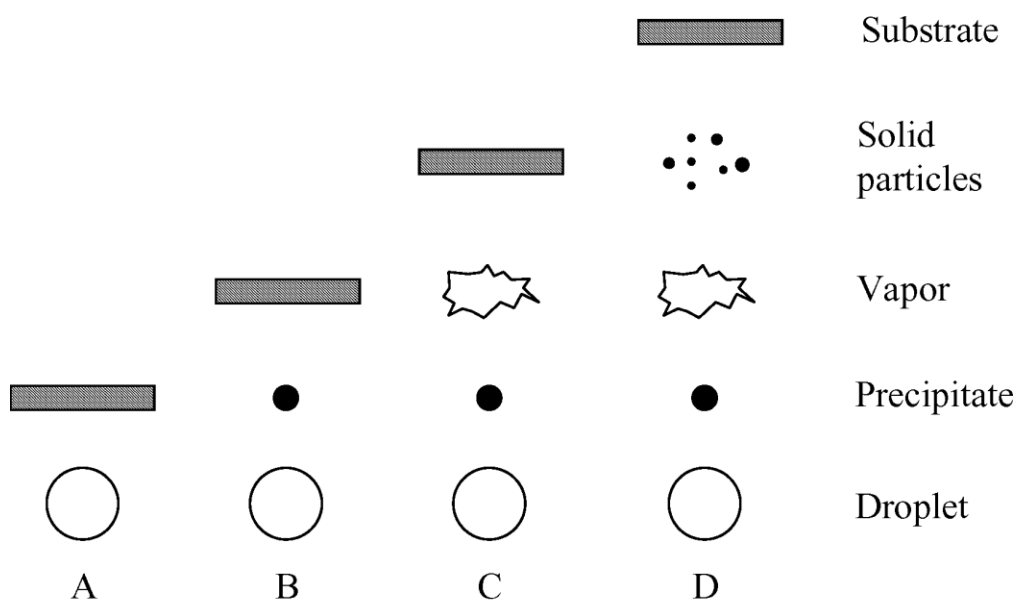


Fig. 2.10 Description of the deposition processes initiated with increasing T_s

The schematic diagram of a spray pyrolysis technique is shown in Fig. 2.11. This technique involves spraying of an ionic solution, usually aqueous containing soluble salts of the constituent atoms of the desired compound onto heated substrates. Hydrolysis and pyrolysis are the main chemical reactions involved in the process. SPT is a process in which a thin film is deposited by spraying a solution on a heated surface, where the constituents react to form a chemical compound. The chemical reactants are selected such that the products other than the desired compound are volatile at the temperature of deposition. The small grains are a disadvantage for most semiconductor applications. The process is sensitive to variables, particularly temperature, and the measurement at the surface is uncertain. Not only do the physical and electronic properties of the film vary with temperature, but the deposition efficiency decreases with increased temperature; stoichiometry is also affected, particularly for alloys. The process is particularly useful for the deposition of oxides and has long been a production method for applying a transparent electrical conductor. In spite of these difficulties, spray pyrolysis is an excellent method for the deposition of large-area thin films.

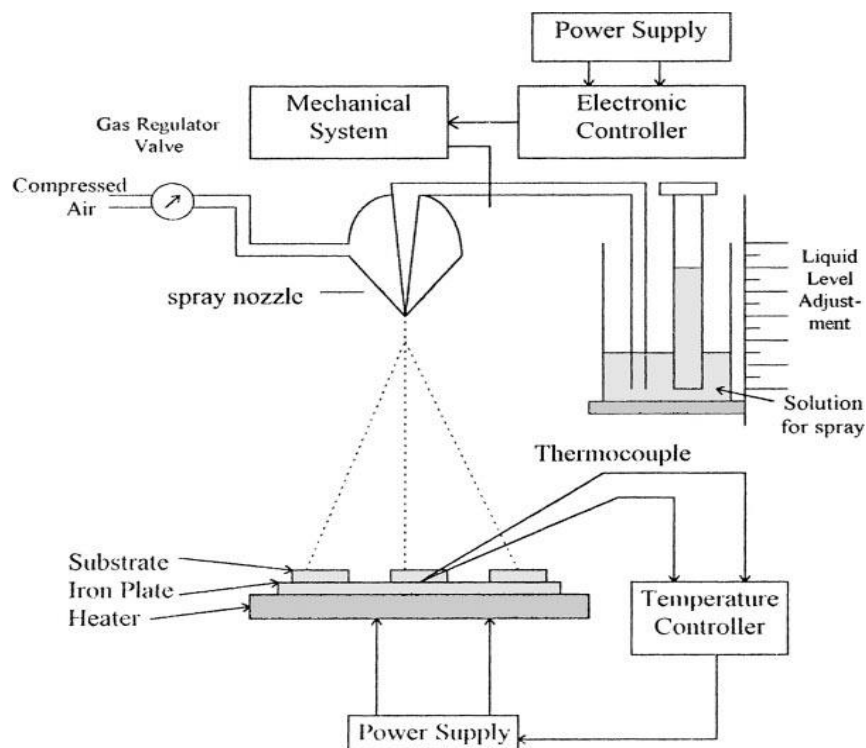


Fig. 2.11 Schematic diagram of a spray pyrolysis technique

Various thin films of pure and doped SnO_2 , In_2S_3 , ZnO , CdS , etc. have been deposited by a homemade and inexpensive spray pyrolysis set up which is established at the Spray Pyrolysis Laboratory, Dept. of Physics, BUET, Dhaka, Bangladesh [29-32]. So this thesis work has been undertaken to study the thin films of pure CuO , TiO_2 and Cu doped TiO_2 synthesized by SPT.

2.4 Theoretical Aspect of Different Measurement Techniques Used for Study of Thin Films

2.4.1 Introduction

The thin film thickness is one of the most significant film parameters and hence care should be taken to measure it. There are several methods for the measurement of film thickness and in the present work interference fringe method was used. There are several methods for surface morphology and structural characterization of thin films such as Scanning Electron Microscopy (SEM), Energy Dispersive Analysis of X-rays (EDAX) and X-ray Diffraction (XRD). For optical characterization measurement of thin films ultraviolet (UV) visible absorption spectroscopy is widely used. The electrical behavior of the films is characterized by van-der Pauw method. Here all these techniques are described from theoretical point of view.

2.4.2 Measurement of Thin Film Thickness

Thickness may be directly known by in-site monitoring the rate of deposition or it may be measured after the film is taken out of the deposition chamber. In the present work the later method was used known as optical interference fringe method and this is described below in briefly.

2.4.2.1 Optical Interference Fringe Method

The thickness of the film can be measurement accurately by optical interference method and it is one of the best method comparative others process. In this method two reflecting surfaces are brought into close proximity to produce interference fringes. Wiener was the first to use interference fringes for the measurement of film thickness. Latter on using

Fizeau fringes, Tolansky developed this method to a remarkable degree and is now accepted as a standard method [33]. When two reflecting surfaces are brought into close proximity, interference fringes are produced, the measurement of which makes possible a direct determination of film thickness and surface topography with high accuracy. In this method, two types of fringes are utilized for thickness measurement. The first produces Fizeu fringes of equal thickness, using a monochromatic light source. The second uses a white light source and produces fringes of equal chromatic order. The second method is prepared for thinner films.

The Fizeu fringes method was used in the present work for the measurement of film thickness. For the experimental set up a low power microscope, a monochromatic source of light, a glass plate and an interferometer are required. To make the Fizeau fringes of equal thickness visible in a multiple beam interferometer formed by a thin absorbing film on a glass substrate, generally an auxiliary reflecting coating on the film surface is required. But if the experimental sample is transparent with a very smooth surface no such auxiliary coating is necessary [34].

The film whose thickness is to be measured is required to form a step on a glass substrate and over it another plane glass plate (Fizeau plate) is placed. This illuminated with a parallel monochromatic beam of light a fringe system as shown in Fig. 2.12 is produced and is viewed with low power microscope. In this method, thickness from 3 nm to 2000 nm can be measured with an accuracy of ± 5 nm. The fringe spacing and fringe displacement across the step are measured and used to calculate the film thickness. The displacement 'h' of the fringe system across the film substrate step is then measured to calculate the film thickness 't' using the relation

$$t = \frac{h}{\text{fringes} - \text{spacing}} \times \frac{\lambda}{2} \dots\dots\dots (2.1)$$

Where λ is the wavelength of the monochromatic light (sodium light, $\lambda = 5893 \text{ \AA}$) employed.

If d is the fringe spacing then the film thickness t is given by,

$$t = \frac{h}{d} \times \frac{\lambda}{2} (\text{nm}) \dots\dots\dots (2.2)$$

The thickness of the film was calculated by using equation (2.2).

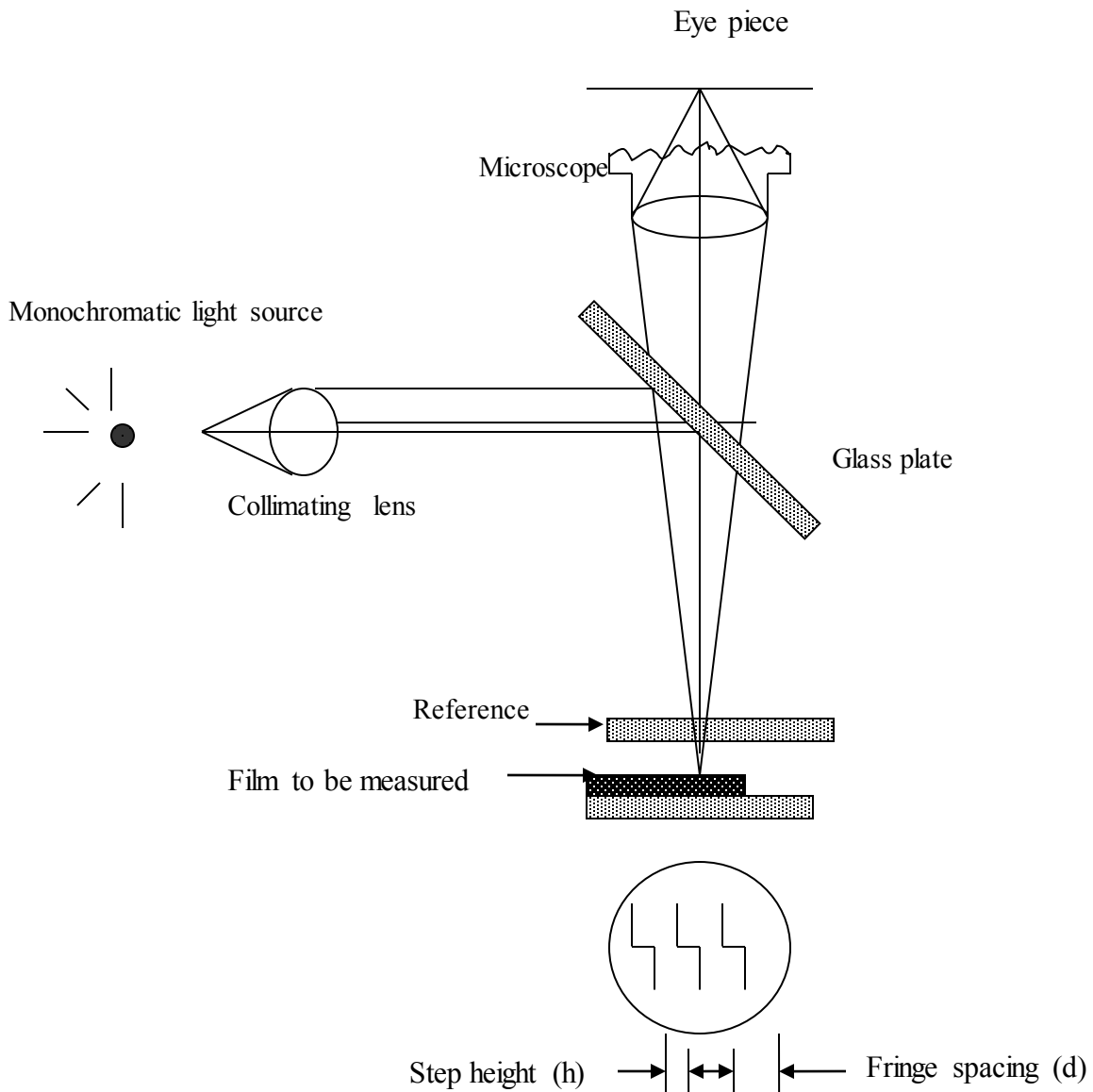


Fig. 2.12 Interferometer arrangements for producing Fizeau fringes of equal thickness

2.4.3 Surface Morphology and Compositional Analysis of Thin Films

The study of surface morphology and compositional analysis of thin films is essential and more significant where as these characteristic X-rays are used to identify the composition and measure the abundance of elements in the sample. In this thesis scanning electron microscopy (SEM) method is used to study the surface morphology and compositional analysis of prepared thin films.

2.4.3.1 Scanning Electron Microscopy (SEM)

A SEM is a type of electron microscope that images a sample by scanning it with a high-energy beam of electrons in a raster scan pattern. The electrons interact with the atoms that make up the sample producing signals that contain information about the sample's surface topography, composition, and other properties such as electrical conductivity. The types of signals produced by an SEM include secondary electrons, back-scattered electrons (BSE), characteristic X-rays, light (cathodoluminescence), specimen current and transmitted electrons. Secondary electron detectors are common in all SEMs, but it is rare that a single machine would have detectors for all possible signals. The signals result from interactions of the electron beam with atoms at or near the surface of the sample. In the most common or standard detection mode, secondary electron imaging or SEI, the SEM can produce very high-resolution images of a sample surface, revealing details less than 1 nm in size. Due to the very narrow electron beam, SEM micrographs have a large depth of field yielding a characteristic three-dimensional appearance useful for understanding the surface structure of a sample. This is exemplified by the micrograph of pollen shown to the right. A wide range of magnifications is possible, from about 10 times (about equivalent to that of a powerful hand-lens) to more than 500,000 times, about 250 times the magnification limit of the best light microscopes. Back-scattered electrons (BSE) are beam electrons that are reflected from the sample by elastic scattering. BSE are often used in analytical SEM along with the spectra made from the characteristic X-rays. Because the intensity of the BSE signal is strongly related to the atomic number (Z) of the specimen, BSE images can provide information about the distribution of different elements in the sample. For the same reason, BSE imaging can image colloidal gold immuno-labels of 5 or 10 nm diameter which would otherwise be difficult or impossible to detect in secondary electron images in biological specimens. Characteristic X-rays are emitted when the electron beam removes an inner shell electron from the sample, causing a higher energy electron to fill the shell and release energy. These characteristic X-rays are used to identify the composition and measure the abundance of elements in the sample. When the primary electron beam interacts with the sample, the electrons lose energy by repeated random scattering and absorption within a teardrop-shaped volume of the specimen known as the interaction volume, which extends from less than 100 nm to around 5 μm into the surface. The size of

the interaction volume depends on the electron's landing energy, the atomic number of the specimen and the specimen's density. The energy exchange between the electron beam and the sample results in the reflection of high-energy electrons by elastic scattering, emission of secondary electrons by inelastic scattering and the emission of electromagnetic radiation, each of which can be detected by specialized detectors. The beam current absorbed by the specimen can also be detected and used to create images of the distribution of specimen current. Electronic amplifiers of various types are used to amplify the signals which are displayed as variations in brightness on a cathode ray tube. The raster scanning of the CRT display is synchronised with that of the beam on the specimen in the microscope, and the resulting image is therefore a distribution map of the intensity of the signal being emitted from the scanned area of the specimen. The image may be captured by photography from a high resolution cathode ray tube, but in modern machines is digitally captured and displayed on a computer monitor and saved to a computer's hard disk. Schematic diagram of an SEM is shown in Fig. 2.13.

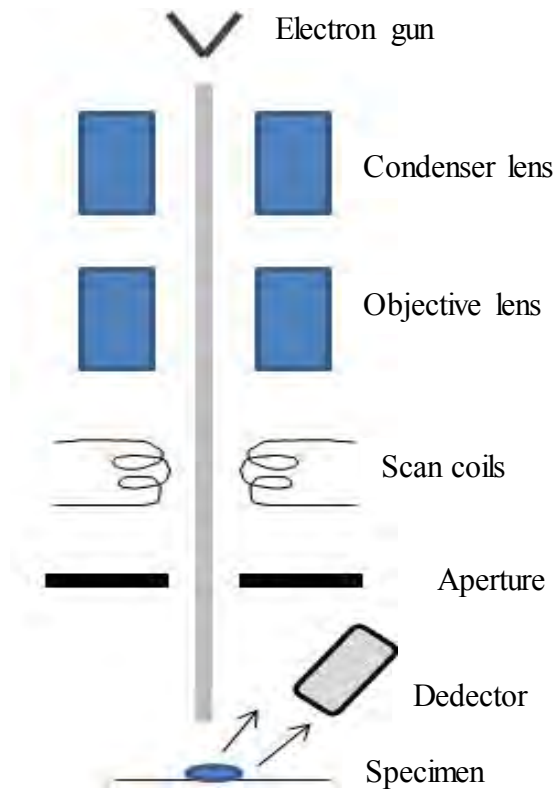


Fig. 2.13 Schematic diagram of an SEM

2.4.3.2 Energy Dispersive Analysis of X-rays (EDX)

Energy-dispersive X-ray spectroscopy (EDS or EDX) is an analytical technique used for the elemental analysis or chemical characterization of a sample. It is one of the variants of X-ray fluorescence spectroscopy which relies on the investigation of a sample through interactions between electromagnetic radiation and matter, analyzing X-rays emitted by the matter in response to being hit with charged particles. Its characterization capabilities are due in large part to the fundamental principle that each element has a unique atomic structure allowing X-rays that are characteristic of an element's atomic structure to be identified uniquely from one another. This is done by the SEM by focusing the X-ray beam on the full frame or a particular spot of the thin films. The analysis represents the individual weight (%) of the element that is present in the thin films.

2.4.4 Structural Analysis of Thin Films

X-ray diffraction is sensitive to thin films of atomic dimensions to thicknesses of many tens of microns, by virtue of the x-ray wavelengths employed and the very high diffraction space resolutions attainable. X-ray methods are generally non-destructive, in that sample preparation is not required, and they can provide a very appropriate route to obtain structural information on thin films and multilayers. Analysis can be performed across the whole spectrum of material types from perfect single crystals to amorphous materials. The choice of the x-ray diffraction analysis procedure depends on the quality of the structural form and therefore this review has been organized to reflect this. Following a description of the various material types, some typically important material parameters have been given arising from the application areas. These material parameters relating to the structure are then categorized into macroscopic and microscopic properties which can then be further subdivided and correlated to the most appropriate analysis method. It is clear from this that x-ray analysis covers the whole range and from this the recent developments will become clear. It is intended therefore that the reader is not compelled to read from beginning to end, but rather be able to find the structural parameter of interest to him/her in a simple way and from that discover the various approaches to its determination. Much of the technology available today arises from the specific physical properties of

materials, for example magnets, semiconductors and abrasive surfaces. Many of these materials exist in bulk form but additional physical properties can be accessed by reducing the dimensions of the material and also by combining many thin layers to create further properties. The physical properties of thin films must relate to their structure and it is the structure that can be studied by x-ray diffraction [35]. The diffraction effect in some cases is very clear whereas with others it can be very subtle. X-ray diffraction is sensitive to thin films of atomic dimensions to thicknesses of many tens of microns, by virtue of the x-ray wavelengths employed and the very high diffraction space resolutions attainable. X-ray methods are generally non-destructive, in that sample preparation is not required, and they can provide a very appropriate route to obtain structural information on thin films and multilayers. The X-ray diffraction (XRD) provides substantial information on the crystal structure.

2.4.4.1 X-ray Diffraction (XRD)

X-radiation (X-rays) is a form of electromagnetic radiation. X-rays have a wavelength in the range of 0.01 to 10 nanometers, corresponding to frequencies in the range 30 petahertz to 30 exahertz (3×10^{16} Hz to 3×10^{19} Hz) and energies in the range 120 eV to 120 keV. They are shorter in wavelength than UV rays and longer than gamma rays. In many languages, X-radiation is called Rontgen radiation, after Wilhelm Conrad Rontgen, who is usually credited as its discoverer, and who had named it X-radiation to signify an unknown type of radiation. XRAY is used as the phonetic pronunciation for the letter X. X-rays from about 0.12 to 12 keV (10 to 0.10 nm wavelength) are classified as "soft" X-rays, and from about 12 to 120 keV (0.10 to 0.01 nm wavelength) as "hard" X-rays, due to their penetrating abilities. Hard X-rays can penetrate solid objects, and their most common use is to take images of the inside of objects in diagnostic radiography and crystallography. As a result, the term X-ray is metonymically used to refer to a radiographic image produced using this method, in addition to the method itself. By contrast, soft X-rays hardly penetrate matter at all; the attenuation length of 600 eV (~2 nm) X-rays in water is less than 1 micrometer. Schematic diagram of Bragg Spectrometer is shown in Fig. 2.14.

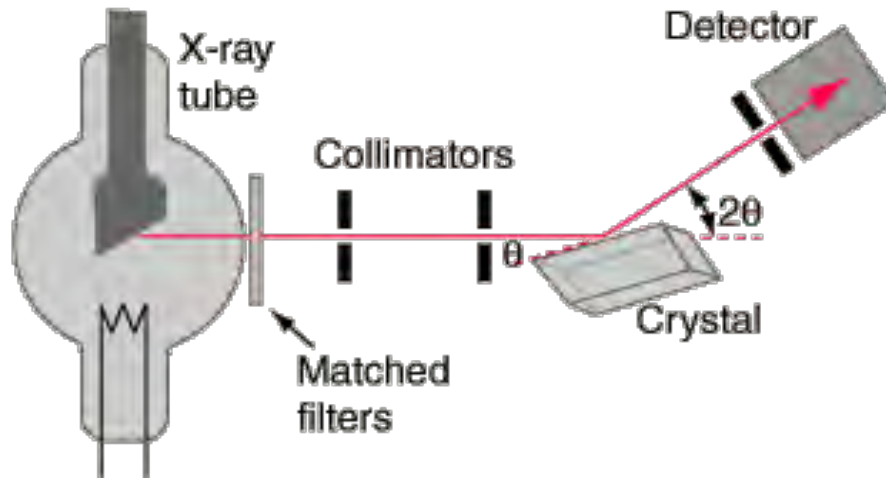


Fig. 2.14 Schematic diagram of a Bragg Spectrometer

When x-rays are scattered from a crystal lattice, peaks of scattered intensity are observed which correspond to the following conditions:

1. The angle of incidence = angle of scattering.
2. The pathlength difference is equal to an integer number of wavelengths.
3. When X-rays are incident on a crystal surface, they are reflected from it.

The reflection obeys the following Bragg's law

$$2d \sin \theta = n\lambda, \quad \dots\dots\dots (2.3)$$

Where, d is the distance between crystal planes; θ is the X-ray incident angle; λ is the wavelength of the X-ray and n is a positive integer. Bragg's law (Fig. 2.15) also suggests that the diffraction is only possible when $\lambda < 2d$. A diffraction pattern is obtained by measuring the intensity of scattered waves as a function of scattering angle.

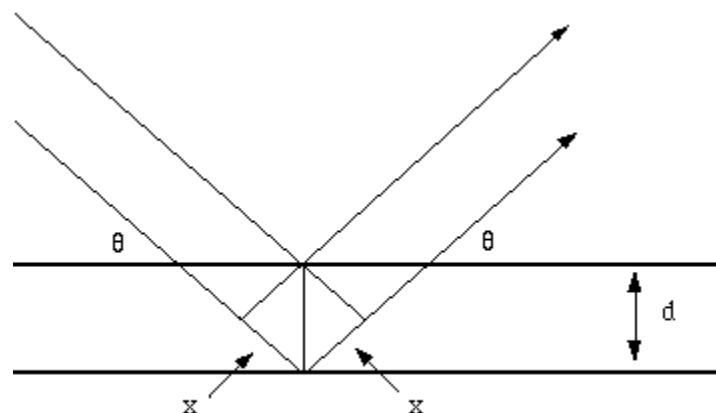


Fig. 2.15 Bragg condition

Crystallite size (D) of the prepared thin film can be by Debye-Scherrer formula given by equation,

$$D = K\lambda / (\beta \cos\theta) \dots\dots\dots (2.4)$$

where, λ is the wavelength of the X-ray radiation ($\lambda = 0.15406$ nm) for $\text{CuK}\alpha$; K is usually taken as 0.89; and β is the line width at half-maximum height.

The lattice constants (a, b, and c) for of crystal (thin films) can be determined by the equation,

$$\text{for monoclinic, } 1/d^2 = 1/\sin^2 \beta (1/h^2 a^2 + k^2 \sin^2 \beta / b^2 + l^2 c^2 - 2hlc \cos \beta / ac) \dots\dots\dots (2.5)$$

$$\text{and for tetragonal, } 1/d^2 = (h^2 + k^2) / a^2 + l^2 / c^2 \dots\dots\dots (2.6)$$

2.4.5 Optical Analysis of Thin Films

The optical behaviors of a semiconductor are investigated in term of the three phenomena namely transmission, reflection and absorption. When a semiconductor is illuminated by light, photon strikes the surface, a fraction of photons are reflected, some of these are absorbed within the semiconductor and the remainder transmitted into the semiconductor and some may be reflected. Here to calculate optical band gap of thin films and then other optical parameters from observation of transmission and absorption property of prepared samples by Ultraviolet-visible spectroscopy meter.

2.4.5.1 Ultraviolet-visible Spectroscopy

Schematic diagram of Ultraviolet-visible spectrophotometer is shown in Fig.2.16. Ultraviolet-visible spectrophotometer (UV-Vis or UV/Vis) refers to absorption spectroscopy or reflectance spectroscopy in the ultraviolet-visible spectral region. This means it uses light in the visible and adjacent (near-UV and near-infrared (NIR)) ranges. The absorption or reflectance in the visible range directly affects the perceived color of the chemicals involved. In this region of the electromagnetic spectrum, molecules undergo electronic transitions. This technique is complementary to fluorescence spectroscopy, in that fluorescence deals with transitions from the excited state to the ground state, while absorption measures transitions from the ground state to the excited state.

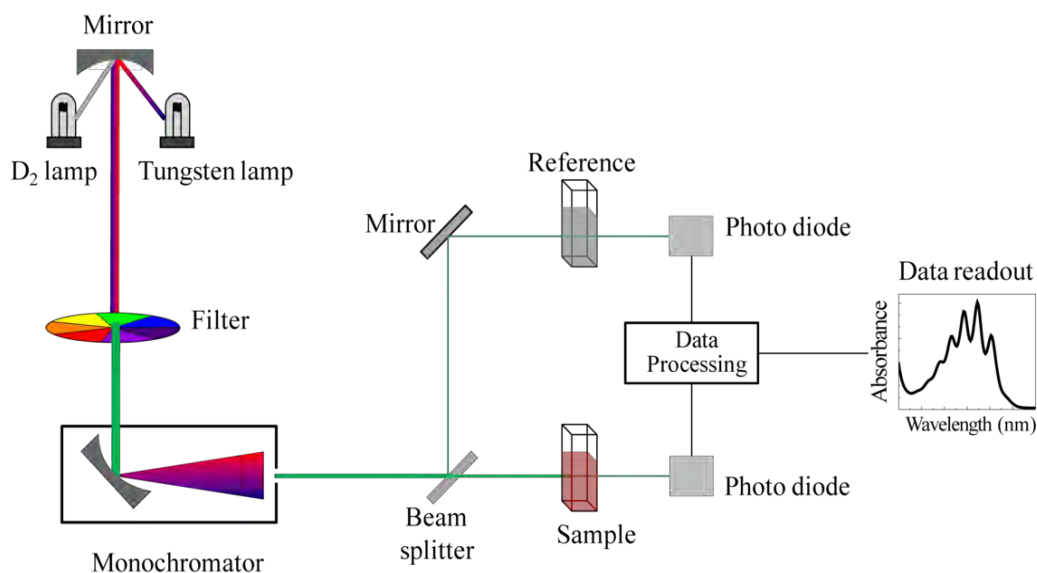


Fig. 2.16 Schematic diagram of Ultraviolet-visible spectrophotometer

2.4.5.2 Absorption

In physics, absorption of electromagnetic radiation is the way by which the energy of a photon is taken up by matter, typically the electrons of an atom. Thus, the electromagnetic energy is transformed to other forms of energy, for example, to heat. The absorption of light during wave propagation is often called attenuation. Usually, the absorption of waves does not depend on their intensity (linear absorption), although in certain conditions (usually, in optics), the medium changes its transparency dependently on the intensity of waves going through, and the saturable (or nonlinear absorption) occurs [36].

2.4.5.3 Absorption Coefficient

When a semiconductor is illuminated by light, photon strikes the surface, a fraction of photons are reflected, some of these are absorbed within the semiconductor and the remainder transmitted into the semiconductor. The absorption of radiation by any medium occurs through the excitation of electrons and photons.

For semiconductor, it is convenient to consider several types of absorption arising from

- i) Electronic transitions between different energy bands.
- ii) Electronic transitions within energy band.
- iii) Electronic transitions to localized states of impurity atoms.

- iv) Lattice vibrations.
- v) Vibrations of impurity atoms.

In the fundamental absorption region the transmission T is given by

$$T = A \exp\left(-\frac{4\pi kt}{\lambda}\right) \dots\dots\dots (2.7)$$

Where A is a constant, k is the extinction co-efficient and t is the thickness. For $k^2 \ll n^2$, the principle variation of T occurs in the exponential term and pre-exponential term A .

Therefore, $T \sim \exp(-\alpha t) \dots\dots\dots (2.8)$

Where $\alpha = \frac{4\pi k}{\lambda}$ is the absorption co-efficient of the films. Thus the value of absorption co-efficient may be calculated from the relation

$$\alpha = -\frac{\ln T}{t} \dots\dots\dots (2.9)$$

Otherwise from equation (2.4). Plotting Eqn. (2.4) as $\ln(1/T)$ vs t curve at a fixed wavelength, a straight line will be obtained. The slope of the straight line will give α and intercept will give A .

2.4.5.4 Extinction Coefficient

The absorption coefficient, α is a quantity that characterizes how easily a material or a medium can be penetrated by a beam of light. The absorption coefficient, α can be

calculated from observed absorbance data using Beer Lambert's formula $\alpha = 2.303 \left(\frac{A}{d}\right)$,

where A is the optical absorbance and d is the thickness of the film. The extinction coefficient is the imaginary part of the complex index of refraction, which also relates to light absorption [37]. The extinction coefficient can be obtained from the relation,

$$k = \frac{\alpha \lambda}{4\pi} \text{, where } \lambda \text{ is the wavelength.}$$

Since the extinction coefficient describes the attenuation of light in a medium and increase of k with the increase of $h\nu$ indicates the probability of raising the electron transfers across the mobility gap with photon energy. Therefore the higher values of k are the representation of greater attenuation of light in a thin film and also the higher probability of raising the electron transfer across the mobility gap with the photon energy.

2.4.5.5 Band Gap

In solid state physics, a band gap, also called an energy gap or band gap, is an energy range in a solid where no electron states exist. For insulators and semiconductors, the band gap generally refers to the energy difference (in electron volts) between the top of the valence band and the bottom of the conduction band. It is the amount of energy required to free an outer shell electron from its orbit about the nucleus to become a mobile charge carrier, able to move freely within the solid material. In semiconductor physics, the band gap of a semiconductor is always one of two types, a direct band gap or an indirect band gap. The minimal-energy state in the conduction band, and the maximal-energy state in the valence band, are each characterized by a certain k -vector in the Brillouin zone. If the k -vectors are the same, it is called a "direct gap". If they are different, it is called an "indirect gap". Interactions among electrons, holes, phonons, photons, and other particles are required to satisfy conservation of energy and crystal momentum (i.e., conservation of total k -vector). A photon with energy near a semiconductor band gap has almost zero momentum. An important process is called radiative recombination, where an electron in the conduction band annihilates a hole in the valence band, releasing the excess energy as a photon. If the electron is near the bottom of the conduction band and the hole is near the top of the valence band (as is usually the case), this process is possible in a direct band gap semiconductor, but impossible in an indirect band gap one, because conservation of crystal momentum would be violated. For radiative recombination to occur in an indirect band gap material, the process must also involve the absorption or emission of a phonon, where the phonon momentum equals the difference between the electron and hole momentum. (It can also, instead, involve a crystallographic defect, which performs essentially the same role.) The involvement of the phonon makes this process much less likely to occur in a given span of time, which is why radiative recombination is far slower in indirect band gap materials than direct band gap ones [38]. This is why light-emitting and laser diodes are almost always made of direct band gap materials, and not indirect band gap ones like silicon. The fact that radiative recombination is slow in indirect band gap materials also means that, under most circumstances, radiative recombinations will be a small proportion of total recombinations, with most recombinations being non-radiative, taking place at point defects or at grain boundaries. However, if the excited electrons are prevented from

reaching these recombination places, they have no choice but to eventually fall back into the valence band by radiative recombination. This can be done by creating a dislocation loop in the material. At the edge of the loop, the planes above and beneath the "dislocation disk" are pulled apart, creating a negative pressure, which raises the energy of the conduction band substantially, with the result that the electrons cannot pass this edge. Provided that the area directly above the dislocation loop is defect-free (no non-radiative recombination possible), the electrons will fall back into the valence shell by radiative recombination and thus emitting light. This is the principle on which "DELEDs" (Dislocation Engineered LEDs) are based.

2.4.5.5.1 Direct and Indirect Optical Band Gap

The band gap generally refers to the energy difference between the top of the valence band and the bottom of the conduction band. Fundamental absorption refers to the annihilation or absorption of photons by the excitation of an electron from the valence band up into the conduction band, leaving a hole in the valence band. Both energy and momentum must be conserved in such a transition.

In the case of an indirect-band gap semiconductor, the minimum energy in the conduction band and the maximum energy in the valence band occur at different values of crystal momentum. Photon energies much larger than the forbidden gap are required to give direct transitions of electrons from the valence to the conduction band. However, transitions can occur at lower energies by a two-step process involving not only photons and electrons but also a third particle, a phonon.

To estimate the nature of absorption a random phase model is used where the k momentum selection rule is completely relaxed. The integrated density of states $N(E)$ has been used and defined by

$$N(E) = \int_{-\infty}^{+\infty} g(E) dE \quad \dots\dots\dots (2.10)$$

The density of states per unit energy interval may be represented by

$$g(E) = \frac{1}{V} \sum \delta(E - E_n) \quad \dots\dots\dots (2.11)$$

where V is the volume, E is the energy at which $g(E)$ is to be evaluated and E_n is the energy of the n th state.

If $g_v \propto E^p$ and $g_c \propto (E-E_{opt})$, where energies are measured from the valance band mobility edge in the conduction band (mobility gap), and substituting these values into an expression for the random phase approximation, the relationship obtained

$\alpha^2 I_2(\nu) \propto (h\nu - E_0)^{p+q+1}$, where $I_2(\nu)$ is the imaginary part of the complex permittivity. If the density of states of both band edges is parabolic, then the photon energy dependence of the absorption becomes

$$\alpha h\nu \propto \nu^2 I_2(\nu) \propto (h\nu - E_{opt})^2 \quad \dots\dots\dots (2.12)$$

So for higher photon energies the simplified general equation which is known as Tauc relation is,

$$\alpha h\nu = B(h\nu - E_{opt})^n \quad \dots\dots\dots (2.13)$$

where $h\nu$ is the energy of absorbed light, n is the parameter connected with distribution of the density of states and B , a constant or Tauc parameter and here $n = 1/2$ for direct and $n = 2$ for indirect transitions [39].

The above equation can be written as

$$\frac{d[\ln(\alpha h\nu)]}{d[h\nu]} = \frac{n}{h\nu - E_{opt}} \quad \dots\dots\dots (2.14)$$

When finding the n , type of transition can be obtained from the absorption spectrum.

A discontinuity in the $d[\ln(\alpha h\nu)]/d(h\nu)$ versus $h\nu$ plot at the band gap energy (E_{opt} or E_g), i.e. at $h\nu = E_g$ can be observed. The discontinuity at a particular energy value gives the band gap E_g . Thus from the straight-line plots of $(\alpha h\nu)^2$ versus $h\nu$ and $(\alpha h\nu)^{1/2}$ versus $h\nu$ the direct and indirect energy gaps of thin films can be determined.

If the maximum of the valance band and the minimum of the conduction band energy exist for the same value of crystal momentum p in a semiconductor, then this type of semiconductor is called direct band gap semiconductor. The form of the absorption process for a direct band gap semiconductor is shown in the energy momentum sketch of (Fig. 2.17) Since the momentum of photons is small compared to the crystal momentum, the latter essentially is conserved in the transition. The energy difference between the initial and final state is equal to the energy of the original photon, i.e,

$$E_f - E_i = h\nu \quad \dots\dots\dots (2.15)$$

Where, $E_f - E_i = h\nu = \text{Photon energy}$

The band gap represents in Fig. 2.17 the minimum energy difference between the top of the valence band and the bottom of the conduction band, however, the top of the valence band and the bottom of the conduction band are not generally at the same value of the electron momentum. In a direct band gap semiconductor, the top of the valence band and the bottom of the conduction band occur at the same value of momentum, as in the schematic below.

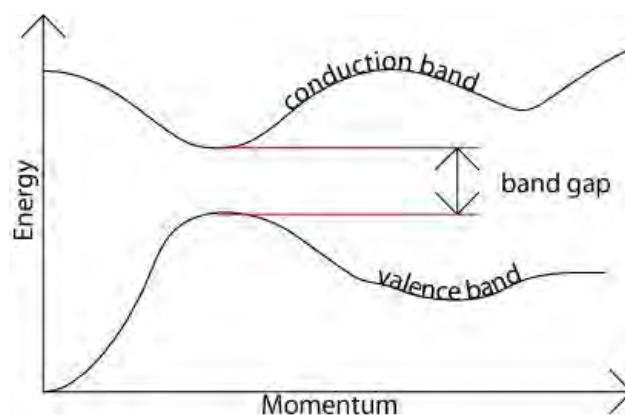


Fig. 2.17 Energy-crystal momentum diagram of a direct band gap of semiconductor

In the case of indirect band gap semiconductor, the minimum energy in the valence band occurs at different values of crystal momentum (Fig. 2.18) Photon energies much larger than the forbidden gap is required to give transition of electrons from the valence band to conduction band. As indicated in the energy momentum sketch of Fig. 2.18 an electron can make a transition from the maximum energy in the valence band to the minimum energy in the conduction band in the presence of photons of suitable energy by the emission or absorption of photon. Hence the minimum photon energy required to excite an electron from the valence to conduction band is

$$h\nu = E_g - E_p \quad \dots\dots\dots (2.16)$$

Where E_p is the energy of an absorbed photon with the required momentum.

An analysis of the theoretical value of the absorption co-efficient for the transition involving photon absorption gives the result in an indirect band gap semiconductor, the

maximum energy of the valence band occurs at a different value of momentum to the minimum in the conduction band energy:

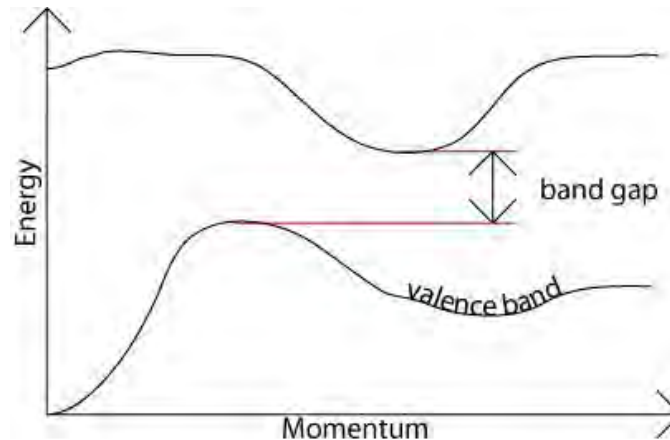


Fig. 2.18 Energy-crystal momentum diagram of an indirect band gap of Semiconductor

Figure shows energy vs. crystal momentum for a semiconductor with an indirect band gap, showing that an electron cannot shift from the lowest-energy state in the conduction band to the highest-energy state in the valence band without a change in momentum.

2.4.5.7 Refractive Index

The refractive index (n) of the films has been calculated from the transmission spectra using the relation as equation (2.17) and considered highest transmission (T_{\max}) at wavelength 740 nm and lowest transmission (T_{\min}) at wavelength 380 nm [39-40].

$$n^2 = \left(\frac{n_a^2 + n_g^2}{2} + 2n_a n_g T_0 \right) + \left\{ \left(\frac{n_a^2 + n_g^2}{2} + 2n_a n_g T_0 \right)^2 - n_a^2 n_g^2 \right\}^{1/2} \dots \dots \dots (2.17)$$

where,

$$T_0 = \left(\frac{T_{\max} - T_{\min}}{T_{\max} \times T_{\min}} \right),$$

n_a = Refractive index of air, and n_g = Refractive index of glass.

2.4.6 Electrical Analysis of Thin Film

Electrical parameters like resistivity (ρ), conductivity (σ), sheet resistance (R_s), activation energy (E_a) etc. of thin film recognize electrical property of the prepared sample. The property of a material to resist the flow of electrical current is called the resistance and the resistance per unit length of cross-section is called resistivity. It is denoted by ρ and mathematically defined as

$$\rho = \frac{RA}{L} \quad \dots\dots\dots (2.18)$$

Where, A is the cross-sectional area, R is the resistance and L is the length of the material along the direction of current flow. Resistivity is an intrinsic property of a material and depends only on the crystal structure of the material. Electrical conductivity of a material is reciprocal of resistivity of the material. Conductivity is denoted by σ and defined as

$$\sigma = \frac{1}{\rho} \quad \dots\dots\dots (2.19)$$

Conductivity depends only on the structural and physical property of the material.

2.4.6.1 Resistivity Measurement Techniques

A number of methods are used to measure the resistivity of a material. Only two of them are discussed below.

2.4.6.1.1 Direct Method

The resistivity of a thin film can be measured easily by using direct method. The experimental arrangement is shown in Fig.2.19. If the current I is flowing along L and voltage drop across L is V, then $R=V/I$ and then by using the following equation, one can easily determine the resistivity if the thickness of the film t is known

$$\rho = \frac{RWt}{L} \quad \dots\dots\dots (2.20)$$

If $W = L$ i.e. film having square shape, then resistivity equation becomes

$$\rho = Rt \quad \dots\dots\dots (2.21)$$

and corresponding conductivity is defined as

$$\sigma = 1/\rho \quad \dots\dots\dots (2.22)$$

Thus one can easily determine the resistivity as well conductivity by measuring R_s and film thickness (t).

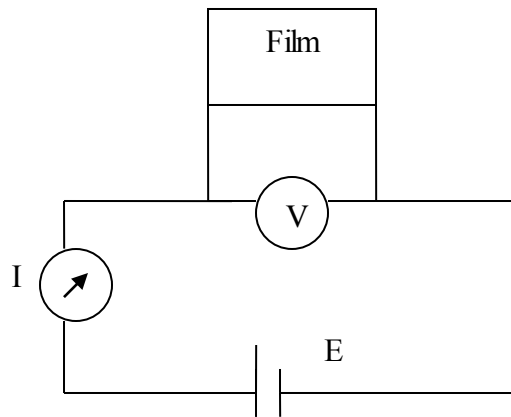


Fig.2.19 Circuit arrangements for resistivity measurement

2.4.6.1.2 van der Pauw's Method

Electrical resistivity of metal and semiconductor film of any shape may be measured by using van der Pauw's method [41]. This method is shown in Fig. 2.20. The resistivity of film having any arbitrary shape can be uniquely determined by using this method. To explain this method, let us consider the Fig.2.20, if A, B, C, and D are any four sufficiently small, Ohmic contacts arranged successively on the circumference of a film of any arbitrary shape.

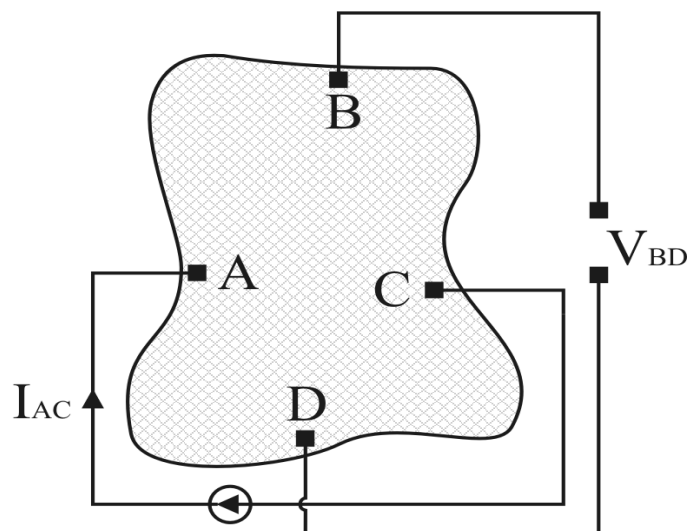


Fig.2.20 Schematic diagram of van der Pauw's method

If a current I_{AB} entering into the film through the contact A and leaving it from the contact B and produces a potential difference V_{DC} between points D and C then

$$R_{AB,CD} = \frac{V_{DC}}{I_{AB}} \quad \dots\dots\dots (2.23)$$

Similarly, we can write

$$R_{CD,AB} = \frac{V_{BA}}{I_{CD}} \quad \dots\dots\dots (2.24)$$

$$R_{BC,DA} = \frac{V_{AD}}{I_{BC}} \quad \dots\dots\dots (2.25)$$

$$R_{DA,BC} = \frac{V_{CB}}{I_{DA}} \quad \dots\dots\dots (2.26)$$

Using reciprocal theorem van der Pauw (1958) showed that

$$\rho = 4.543t \left(\frac{R_{AB,CD} + R_{BC,DA}}{2} \right) f \left(\frac{R_{AB,CD}}{R_{BC,AD}} \right) \quad (\Omega\text{-cm}) \quad \dots\dots\dots (2.27)$$

The correction factor f has been calculated by van der pauw and is equal to unity when $R_{AB,CD} \cong R_{BC,AD}$ and then equation (2.27) becomes

$$\rho = 2.266t(R_{AB,CD} + R_{BC,DA}) \quad (\Omega\text{-cm}) \quad \dots\dots\dots (2.28)$$

where, t is the film thickness in cm. and corresponding conductivity is defined as

$$\sigma = \frac{1}{\rho} (\Omega\text{-cm})^{-1} \quad \dots\dots\dots (2.29)$$

2.4.6.2 Factors Affecting Resistivity Measurement

The effects of the following factors are remarkable in the measurement of resistivity:

- a) Length to breadth ratio, L/b of the film
- b) Current electrodes
- c) Current density
- d) Microscopic inhomogeneity of the film
- e) Sensitivity of the measuring devices
- f) Electrical contact resistivity

2.4.6.3 Sheet Resistance

The resistance of a thin film directly proportional to the ρ and inversely proportional to the t and we can write for a rectangular film of length L and width W .

$$R = \left(\frac{\rho}{t}\right) \times \left(\frac{L}{W}\right) = R_s \left(\frac{L}{W}\right) \quad \dots\dots\dots (2.30)$$

where, R_s is known as the sheet resistance and expressed in ohms per square.

$$R_s = \frac{\rho}{t} \text{ ohm per square} \quad \dots\dots\dots (2.31)$$

The ratio (L/W) is called the number of squares.

The number of “squares” is a pure number have no dimensions. It is very useful quantity that is widely used for comparing films, particularly those of the same material deposited under similar conditions.

2.4.6.4 Activation Energy

Activation energy (E_a) is a term introduced in 1889 by the Swedish scientist Svante Arrhenius to describe the minimum energy which must be available to a chemical system with potential reactants to result in a chemical reaction. Activation energy may also be defined as the minimum energy required starting a chemical reaction. The activation energy of a reaction is usually denoted by E_a . The energy required to transfer charge from one initially neutral island to another is known as activation energy and denoted by E_a . This is equivalent to the electrostatic binding energy of the charge to the island. When these charge carriers are excited to at least this energy from the Fermi-level, there will be tunneling from one island to another. These islands or small particles are called crystallites. The activation energy is related with film conductivity and given by the relation

$$\sigma = \sigma_0 \exp\left(-\frac{E_a}{2kT}\right) \quad \dots\dots\dots (2.32)$$

where σ_0 is the conductivity at 0 °C and k is the Boltzmann constant and T is the absolute temperature. Equation (2.32) can be written as

$$\ln \sigma = -\frac{E_a}{2kT} + \ln \sigma_0 \quad \dots\dots\dots (2.33)$$

Equation (2.33) is equivalent to a straight line equation, $y = mx+c$. So that ΔE can be determined from the slope of the straight line $\ln \sigma = -\frac{E_a}{2kT} + \ln \sigma_0$. From the graph of $\ln \sigma$ vs. $1/T$, ΔE can be calculated by using the relation

$$E_a = -\left(\frac{\ln \sigma}{\frac{1}{T}}\right) \times 2k \text{ (eV)} \quad \dots\dots\dots (2.34)$$

2.4.6.5 Figure of Merit

Figure of merit is a quantity used to characterize the performance of a device, system or method, relative to its alternatives. In engineering, figures of merit are used as a marketing tool to convince consumers to choose a particular brand.

1. Aeronautics, a measure of the efficiency of a helicopter in hover.
2. Electrical engineering, a measure of the efficiency of a component, such as a circuit.

A numerical quantity based on one or more characteristics of a system or device that represents a measure of efficiency or effectiveness.

The Figure of merit is well-known as an index for evaluating the performance of transparent conducting film. The increase in the Figure of merit of the thin films is mainly due to the increase in the optical transmittance. The Figure of merit is related with film conductivity and transmittance corresponding wavelength [42] and given by the relation

$$F = (-\rho \ln T)^{-1} \quad \dots\dots\dots (2.35)$$

References

- [1] West A. R., 'Solid State Chemistry' John Willey & Sons, Singapore, 2003.
- [2] Chopra K. L., 'Thin Film Phenomena', McGraw Hill, New York, 1969.
- [3] Shakti N., Gupta P. S., "Structural and optical properties of sol-gel prepares ZnO thin film", *Appli. Phys. Res.*, 2, 1, pp. 19-28, 2010.
- [4] Marisol T. R., Barbara G. R., Rio, R. D., Cabello G., "Investigation and optical evaluation of precursors for the photodeposition of nanosized ZnS amorphous thin films" *J. Chil. Chem. Soc*, 52, 3, pp 1257, 2000.
- [5] Papadimitropoulos G, Vourdas N, Vamvakas V E., Davazoglou D., "Deposition and characterization of copper oxide thin films", *Journal of Physics: Conference series*, 10, pp. 182–185, 2005.
- [6] Lampkin, Curt M., "Aerodynamics of nozzles used in spray pyrolysis", *Prog. Crystal Growth Chaact.* 1, pp. 406-416, 1979.
- [7] Pashley, D. W., Stowell M. J., Jacobs M. H. Law T. J., "The growth and structure of gold and silver deposits formed by evaporation inside an electron microscope", *Phil. Mag.*, 10, pp.127-158, 1964.
- [8] Jeson R. B, Wang A , Metz W A, Endleman N. L, Matthew V. M, Lane A. M, Kannewurf C. R, and Marks T. J, "Transparent conducting CdO thin film growth using a highly volatile, thermally and airstable cadmium precursor", *Chem. Vap. Depos.*, 7, pp. 239-242, 2001.
- [9] Ahtiokka B, Aksay S, "Optical properties of CuInS₂ films produced by spray pyrolysis method", *J. Arts Sci.*, 31, pp. 27-34, 2005.
- [10] Ambia M.G., Islam M.N., Hakim M.O, "Temperature-dependent studies on the electrical properties of pyrolytic ZnO thin film prepared from Zn(C₂H₃O₂)₂", *J. Meter. Sci.*, 28, pp. 2659-2663, 1993.
- [11] Basset G.A, Menter J. W., Pashley D.W, "Structure and Properties of Thin Films", 11, edit. by Neugebauer et al. (Wiley and Sons, New York), 1959.
- [12] Kajitvichyanukul P., Ananpattarachai J., Pongpom S., "Sol-gel preparation and properties study of TiO₂ thin film for photocatalytic reduction of chromium (VI) in photocatalysis process", *Sci. Technol. Adv. Mater.*, 6, pp. 352–358, 2005.

- [13] Acosta R.E., Romankiw L.T., Von Gutfeld R. J., "Laser-enhanced plating: A review of its mechanisms and applications", *Thin Solid Films*, 95, 2, pp. 131-132, 1982.
- [14] Suematsu H, Saikusa T, Suzuki T, Jiang W and Yatsui K, "Preparation of TiFe thin films by pulsed ion beam evaporation", *Mat. Res. Soc. Symp. Proc.*, 697, pp. 107-120, 2002.
- [15] Behrisch R. 'Sputtering by Particle Bombardment', Springer, Berlin, 1981.
- [16] Samarasekara P., Yapa N. U. S., "Effect of sputtering conditions on the gas sensitivity of copper oxide thin Films", *Sri Lankan J. Phys.*, 8, pp. 21-27, 2007.
- [17] Samarasekara P." A Pulsed RF Sputtering Method for Obtaining Higher Deposition Rates", *Chinese J. Physics*, 41, 1, pp. 70-74, 2003.
- [18] Bessergenev V. G., Mateus M. C., Vasconcelos D. A., Mariano J. F. M. L., Botelho do Rego A. M., Lange R., and Burkel E., "TiO₂:(Fe, S) Thin Films Prepared from Complex Precursors by CVD, Physical Chemical Properties, and Photocatalysis", *Int. J. Photo.*, 2012, 767054, 12 pages, 2011.
- [19] Matin R., Bhuiyan A. H., "Heat treatment and aging effect on the structural and optical properties of plasma polymerized 2, 6-diethylaniline thin films", *Thin Solid Films*, 520, pp. 6463-6470, 2012.
- [20] Bernardi M.I.B., Lee E.J.H., Lisboa-Filho P.N., Leite E.R., Longo E., Varela J.A. "TiO₂ Thin Film Growth Using the MOCVD Method", *Mater. Res.*, 4, 3, pp. 223-227, 2001.
- [21] Tripathy S. K, Nagarjun B., Jahnvy V. S., "Optical and structural characteristics of copper doped tin oxide thin film prepared by thermal evaporation method", *IJEIT*, 3, 1, pp. 296-300, 2013.
- [22] Diaz-Urbe C. E., Lozada W. A.V., Ortega F. M., "Synthesis and characterization of TiO₂ thin films doped with copper to be used in photocatalysis", *ITECKNE*, 10, 1, pp. 16-20, 2013.
- [23] Ayieko C. O., Musembi R. J., Waita S. M., Aduda B. O., Jain P. K., "Structural and optical characterization of nitrogen-doped TiO₂ thin films deposited by spray pyrolysis on fluorine doped tin oxide (FTO) coated glass slides", *Int. J. Energy Eng.*, 2, 3, pp. 67-72, 2012.

- [24] Castaneda, L., Alonso J. C., Ortiz A., Andrade E., Saniger J. M., Banuelos J. G. "Spray pyrolysis deposition and characterization of titanium dioxide thin films", *Mater. Chem. Phys.*, 77, 3, pp. 938-944, 2002.
- [25] Zayed M. K., Mostafa M. A., Ebaid M. "Preparation and structural properties of sprayed lanthanum oxide films from an aqueous precursor", *J. Mater. Sci. Eng. A*, 1, pp. 1-8, 2011.
- [26] Pramod S. P., "Versatility of chemical spray pyrolysis technique", *Mater. Chem. Phys.*, 59, pp. 185-198, 1999.
- [27] Perednis D., Gauckler L. J., "Thin film deposition using spray pyrolysis", *J. Electroceram.*, 14, pp. 103–111, 2005.
- [28] Viguie J. C., Spitz J., "Chemical vapor deposition at low temperatures" *J. Electrochem. Soc.*, 122, 4, pp. 585-588, 1975.
- [29] Roy S. S., Podder J., "Synthesis and optical characterization of pure and Cu doped SnO₂ thin films deposited by spray pyrolysis", *JOAM*, 12, 7, pp. 1479 – 1484. 2010.
- [30] Rahman F. Podder J., "Structural, optical, and electrical characterization of spray pyrolysed indium sulfide thin films", *Surf. Rev. Lett.*, 20, 02, 1350014, 7 pages, 2013.
- [31] Taskin M., Podder J. "Structural, optical and electrical properties of pure and Co-doped ZnO Nano fiber thin films prepared by spray pyrolysis", *Appl. Sci. Report*. 2 (3), pp. 107-113, 2014.
- [32] Rubel A. H. Podder J., "Optical properties of spray pyrolysis deposited Cd:Al Thin Films", *J. Bangladesh Acad. Sci.*, 39, 1, pp. 25-30, 2015.
- [33] Tolansky S. "Multiple beam interferometry of surface and films", Oxford University Press, 1948.
- [34] Gottling J. G., Nikol W.S., "Double-layer interference in Air-CdS films", *J. Opt. Soc. Am.*, 56, 9, pp. 1227-1231, 1966.
- [35] Paul F., "X-ray analysis of thin films and multilayers", *Rep. Prog. Phys.*, 59, pp. 1339–1407, 1996.
- [36] Morales-Acevedo A., Vigil-Galan O., Contreras-Puente G., Vidal-Larramendi J., Arriaga-Mejia G., Chavarria-Castaheda M., Escamilla-Esquivel A., Hernandez-Contreras H., Arias-Carbajal A., Cruz-Gandarilla F., "Physical properties of CdS

- thin films grown by different techniques: a comparative study”, Photovoltaic Specialists Conference, ISSN 1060-8371, pp. 624- 627, 2002.
- [37] Xiao, H., Xianogyan, Z., Uddin, A., Leu, C. B., “Preparation and characterization of electronic and optical properties of plasma polymerized nitrites”, Thin Solid Films, 477, pp 81-87, 2005.
- [38] Prince J. J., Ramamurthy S., Subramanian B., Sanjeeviraja C., Jayachandran M. M., “Spray pyrolysis growth and material properties of In_2O_3 films”, J. Cryst. Growth, 240, pp. 142-151, 2002.
- [39] Davies E. A., Mott N. F., “Conduction in non-crystalline system, optical absorption and photoconductivity in amorphous semiconductors”, Philos. Mag. 22, pp 3, 1970.
- [40] Elangovan E., Ramamurthi K., “Optoelectronic properties of spray deposited $\text{SnO}_2\text{:F}$ thin films for window materials in solar cells ”, JOAM, 5, 1, p. 45 – 54, 2003.
- [41] Pauw L. J. van der, “A method of measuring specific resistivity and Hall Effect of discs of arbitrary shapes,” Philips Res. Repts., 13, pp. 1-9, 1958.
- [42] Shinho Cho, “Optical and electrical properties of CuO thin films deposited at several growth temperatures by reactive RF magnetron sputtering”, Met. Mater. Int., 19, 6, pp. 1327-1331, 2013.

CHAPTER-III

EXPERIMENTAL DETAILS

3.1 Thin Film Deposition

3.1.1 Introduction

3.1.2 The Design of the Spray Pyrolysis Deposition System

3.1.3 Thin Film Deposition Parameters

3.1.4 Experimental Equipment

3.1.5 Optimization of the Deposition Process

3.1.6 Preparation of Thin Films

3.2 Summary of Spray Deposition Parameters of CuO, TiO₂ and Cu/TiO₂ thin films

3.3 Measurement Details

3.2.1 Thickness Measurement of Thin Films

3.2.2 Surface Morphology and Elemental Analysis of the Thin Films

3.2.3 Structural Analysis of the Thin Films

3.2.4 Measurement of the Optical Properties of the Thin Films

3.2.5 Measurement of the Electrical Properties of the Thin Films

CHAPTER-III

EXPERIMENTAL DETAILS

3.1 Thin Film Deposition

3.1.1 Introduction

This chapter deals mainly with the description of the apparatus and the preparation of the thin films. Thin films can be prepared from a variety of materials such as metals, semiconductors, insulators or dielectrics etc., and for this purpose various preparation techniques has also been developed. SPT is the most commonly used technique adopted for the deposition of metals, alloys and many compounds. Hydrolysis and pyrolysis are the main chemical reactions involved in the process. In this technique, the chemicals vaporized and react on the substrate surface after reaching on it. SPT is particularly attractive because of its simplicity. It is fast, inexpensive, vacuum less and is suitable for thin film production. The SPT is used basically a chemical deposition method in which fine droplets of the desired material are sprayed onto a heated substrate. A continuous film is formed on the hot substrate by thermal decomposition of the material droplets. The system is equipped with an electric heater and thermo couple. An air compressor pipe is attached within and an exhaust fan is fitted in order to remove the gas which is produced during the film deposition. Various steps of the preparation of CuO, TiO₂ and Cu/ TiO₂ thin films on glass substrate by SPT and characterization is discussed below.

3.1.2 The Design of the Spray Pyrolysis Deposition System

The general simplified system for SPT is shown in Fig. 3.1, where three processing steps can be viewed and analyzed. The three processing steps for spray pyrolysis deposition are

1. Atomization of the precursor solution.
2. Aerosol transport of the droplet.
3. Droplet evaporation, spreading on the substrate, and drying and decomposition of the precursor salt to initiate film growth.

The Schematic diagram of SPT System in Spray Pyrolysis Laboratory, BUET, Dhaka is shown in Fig. 3.2.



Fig. 3.1 Spray pyrolysis deposition system in Spray Pyrolysis Laboratory, BUET

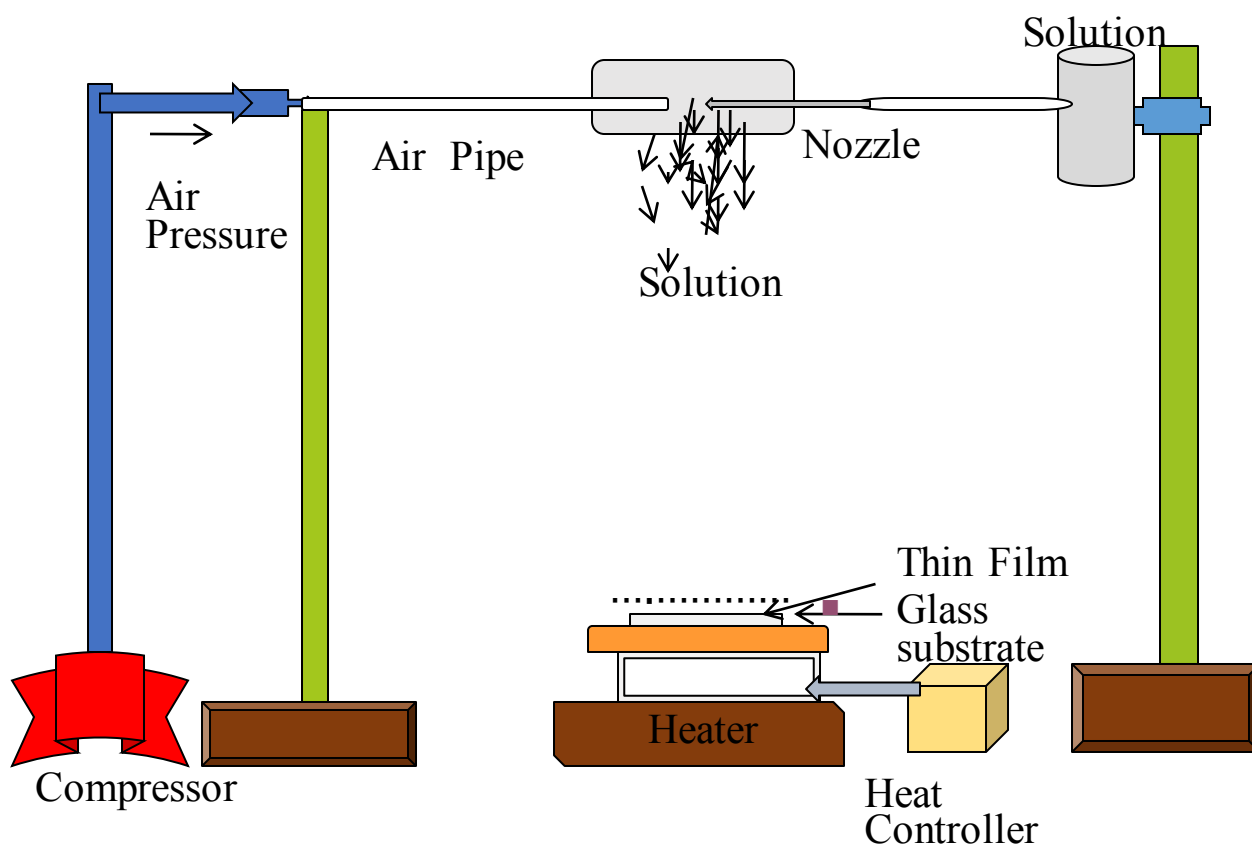


Fig. 3.2 Schematic diagram of SPT System in Spray Pyrolysis Laboratory, BUET

3.1.3 Thin Film Deposition Parameters

In the chemical spray deposition technique the structure, composition and other characteristics of the deposited films depend on a number of process variables [deposition parameters]. The variable quantities such the substrate temperature, solution and gas flow rate, deposition time, quality of the substrate material, size of atomized particles, solution concentration, and substrate to spray outlet distance, etc. are affected on the film properties. It is obvious that the substrate temperature is the most important deposition parameter and it is controlled with great care.

For the deposition of thin film, all the above mentioned parameters except

- (i) Substrate temperature (T_s)
- (ii) Deposition time (t_d)
- (iii) Solution concentration (C)
- (iv) Spray rate (S_r)
- (v) Spray outlet to substrate distance (d_s) and
- (vi) Carrier air pressure (P_a),

were kept at their optimum values. To study the effect of any one of these six parameters on the film properties the remaining other were kept constant. Air current disturbances become another parameter, which creates problem to get uniformity of thickness and homogeneity of the film.

3.1.4 Experimental Equipment

3.1.4.1 Substrate and Substrate Cleaning

For thin film deposition, several types of substrates are used. Generally, glass, quartz, plastic and ceramic substrates are used for polycrystalline films. However, in the present work, thin films were deposited on glass substrates. The most commonly microscope glass slides having 5 cm long, 2 cm wide and 0.1 cm thickness were used. These were fine smooth high quality microscope glass slides.

The cleaning of substrate has a major influence on the properties of the thin film deposited onto them. Surface contaminations manifest it in pinholes, which can cause open resistor or localized high resistance. The following procedures were used for substrate cleaning. The gross contamination of each of the substrates were first removed by ethanol and then

washed with distilled water. After washing in distilled water, the substrates were dipped at first into nitric acid for some time. Again washed in distilled water and thoroughly rinsed with deionized water for several times. Finally, these were dried in hot air and preserved for use. During the whole process the substrates were always held by slide holding forceps.

3.1.4.2 Preparation of Masks

The mask (Fig. 3.3) was prepared in such a way that the edge of the mask is smooth so that it is helpful for determining the film thickness accurately. The direct deposition of thin film pattern requires a suitably shaped aperture, commonly referred to as a mask. For the purpose of various experimental studies, film of specific size and shape are required. Mask was made from stainless steel plate with the desired pattern cut into it. The aperture was made in a bath machine.

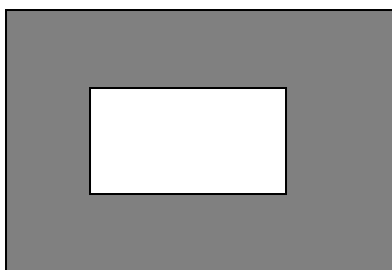


Fig. 3.3 Mask for the sample

The mask is placed in proximity to the substrate, thereby allowing condensation of the evaporate only in the exposed substrate areas. The mask was prepared in such a way that the edge of the mask is smooth so that it is helpful for determining the film thickness accurately. Regardless of mask material and fabrication process all masks should be thoroughly cleaned and inspected before use. Surface contaminants, particularly oil, grease or other organic materials may become volatile when the mask is heated and then be absorbed by the substrate and this may be a cause of weak film adhesion. The mask is placed in proximity to the substrate, thereby allowing condensation of evaporate only in the exposed substrate areas.

3.1.4.3 Spray Nozzle

The single spray nozzle (0.10 mm diameters) consists of capillary tubes (stainless steels) fitted perpendicular to the other tube as shown in Fig. 3.2. When compressed air is passed rapidly through the upper tube in direction tangential to the mouth of the lower tube, a partial vacuum is created at the front part of the tube whose other end is kept immersed in the spray liquid. Due to this partial vacuum the liquid rises up through the tube and the compressed air drives it away in the form of fine spray particles. The thinner spray nozzle would give the finer spray particles. A very fine needle shaped capillary tube was used for the spray nozzle and it may vary from nozzle to nozzle.

3.1.4.4 Heater

The heater is an ordinary hot plate 5k-watt nichrome wire heater connected with voltage variac which is put in spherical shape holder. An electronic power supply (voltage variance) unit is connected with the heater power line to supply proper heat to the substrate. A thick stainless steel plate is placed on heater. Substrate with mica sheet is placed on this suspected plate.

3.1.4.5 Air Compressor

It is reservoir type electrical air compressor. A rotary pump in this section mode draws atmospheric air and keeps it reserved in a large capacity air tank. At the outlet of the tank a pressure gauge is attached which records the pressure of the air at the time of supplying it from the tank. There is a bypass control valve which can keep the output pressure constant.

3.1.4.6 The Fume Chamber

It is a large type chamber with a slanting top and is provided with a chimney. There is an exhaust fan fitted at the mouth of the chimney to remove the unused gases from the chamber. The slanting top and the sidewalls are made of glass and wood. There air tight doors in the front side. The chamber has purging facilities. The whole spray system and the reactor are kept inside this fume chamber at the time of film deposition because of the safety grounds and to check air current disturbances at the deposition site. These two points just stated are very important for the spray process when deposition is carried out in open-air atmosphere.

3.1.5 Optimization of the Deposition Process

To obtain the optimum condition of the film deposition process, it is essential to select at first the requirements with respect to which the process should be optimized. The basic requirement was to get a film of high transparency as well as high transparency and electrical conductivity. Since the spray system used in the present experiment operates via a partial vacuum path as the mouth of the spray nozzle, the concentration of the solution prepared by the solvent was made in such a way that it could be at least be drawn by the nozzle.

For the process of optimization following set of films have been deposited:

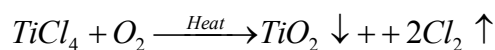
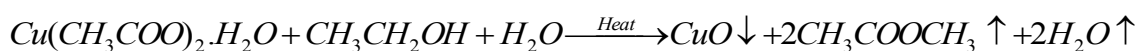
- (i) The first set of films was deposited at various substrate temperatures, keeping all other deposition parameters constant at an arbitrary level. From the set of films the optimum substrate T_s was selected with respect to the best conducting and transparent film.
- (ii) After obtaining the optimum value of T_s , second set of films were deposited by varying the substrate to spray outlet distance, d_s using the optimized T_s and other parameters were kept constant to the arbitrary level as they were in the first set. From this second set of films the optimum distance d_s was selected corresponding to the best film.
- (iii) Fixing d_s and T_s , the carrier gas (air) P_a a third set of films were deposited by varying the molar concentration (MC) of solution. From this set, optimum molar concentration was selected.
- (iv) Keeping T_s , d_s , P_a and MC as fixed fourth set of films (pure films) were deposited by taking constant spray rate, S_r for 5 or 6 minutes deposition.
- (v) The fifth set of films (Cu doped) were deposited keeping T_s , d_s , P_a , S_r , MC, deposition time fixed at their optimum values. In this case, the concentration of Cu was varied for Cu doped TiO_2 thin films.

Thus in all cases the optimum values of the parameters (T_s , d_s , P_a , and S_r) were selected for deposition of films that exhibit good conductivity and high transparency. The flow rate of the solution during spraying is to be adjusted to be about 1 ml/min and kept constant throughout the experiment. The distance between the spray nozzle and the substrate is to be maintained about 25 cm, air pressure is 1 bar, different T_s (250-450 °C) to be measured by Copper-Constantan thermocouple and MC (0.05-0.15M) of solution and wt% of Cu doped varying from 1 to 10.

3.1.6 Preparation of Thin Films

A considerable amount of (about 50 ml) solution taken in the container fitted with the spray nozzle. The clean substrate with a suitable mask was put on the susceptor of the heater. Before supplying the compressed air T_s was to be kept at a level slightly higher than the required substrate temperature because at the onset of spraying a slight fall of temperature is likely. T_s were controlled by controlling the heater power using a variance. T_s was measured by placing a copper constantan thermocouple on the substrate. Deposition rate and time was kept constant for every film such that the thickness of the film may same. When compressed air is passed through at constant pressure (1 bar), a fine thin film was produced and was automatically carried to the reactor zone where film was deposited on the heated substrate. We have adjusted a situation such that 5 to 6 minutes of spray produces thin film, thickness of the range 180 nm to 220 nm. The rate of flow of the working solution can be controlled by a suitable nozzle and adjusting the airflow rate.

CuO thin films have been synthesized by SPT at T_s of 350 °C using (0.05-0.15) mole of cupric acetate ($\text{Cu}(\text{CH}_3\text{COO})_2 \cdot \text{H}_2\text{O}$) which was dissolved in de-ionized 90 ml water and 10 ml ethanol. To enhance the solubility of prepared solution, a few drops of HCl were added. Again another set of CuO thin films have been synthesized for MC of 0.10 M at at five different T_s , namely 250, 300, 350, 400 and 450 °C. The T_s was recorded using a Chromel-alumel thermocouple. The solution was sprayed onto the ultrasonically cleaned glass substrates heated. Similar step was used for TiO_2 thin films using titanium chloride (TiCl_4) as a precursor. The Fig. 3.4 shows the preparation steps of the CuO thin films. The possible chemical reaction that takes place on the heated substrate to produce thin film of CuO and TiO_2 when the droplets of $\text{Cu}(\text{CH}_3\text{COO})_2 \cdot \text{H}_2\text{O}$ water solution and TiCl_4 solution respectively reached the heated substrate, chemical reaction takes place under stimulated temperature as shown below .



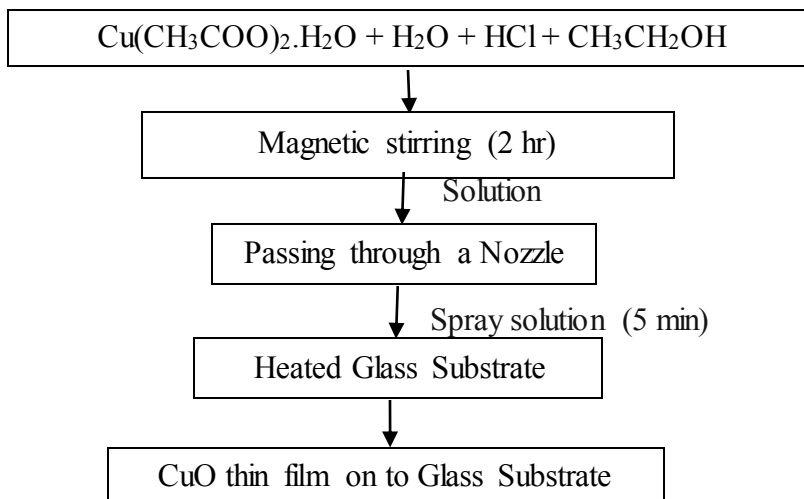


Fig. 3.4 Flow diagram for CuO thin films prepared by SPT

(1-10) wt % of $\text{Cu}(\text{CH}_3\text{COO})_2 \cdot \text{H}_2\text{O}$ was added with (99-90 wt%) of TiCl_4 for solution for Cu/TiO thin films deposited onto glass substrate for 0.10 M at T_s of 400 °C. Solution was stirred by magnetic stirrer for enhance the solubility of prepared solution. For each concentration the reproducibility of the films were verified by repeating the experiments several times. Diagram of Cu/TiO₂ thin film preparation steps is shown in Fig. 3.5.

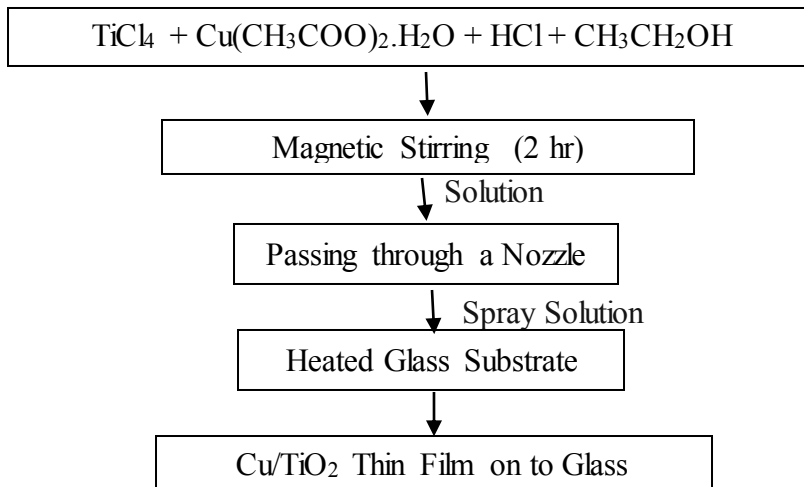
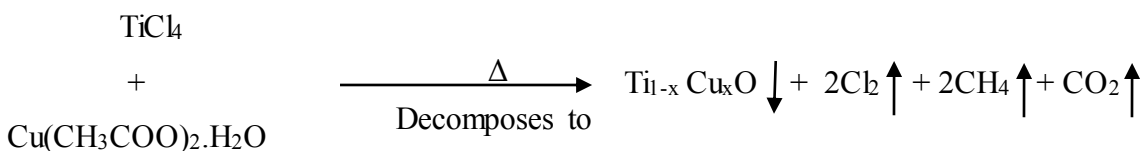


Fig. 3.5 Flow diagram for Cu/TiO₂ thin films prepared by SPT

3.2 Summary of Spray Deposition Parameters of CuO, TiO₂, and Cu/TiO₂ Thin Films

Table 3.1 Summary of Spray Deposition Parameters of CuO, TiO₂, and Cu/TiO₂ Thin Films

Sample Parameters	CuO Thin film	TiO₂ Thin film	Cu/TiO₂ Thin film
Starting chemicals	Cu(CH ₃ COO) ₂ .H ₂ O + H ₂ O + CH ₃ CH ₂ OH + HCl	TiCl ₄ + H ₂ O + CH ₃ CH ₂ OH + HCl	TiCl ₄ + Cu(CH ₃ COO) ₂ .H ₂ O + H ₂ O + CH ₃ CH ₂ OH + HCl
Volume of sprayed (ml)	5	5	5
Sprayed time (min)	5	5	5
Carrier gas pressure (bar)	1	1	1
Nozzle to substrate distance (cm)	25	25	25
MC (M)	0.05, 0.075, 0.10, 0.125, 0.15	0.05, 0.075, 0.10, 0.125, 0.15	0.10
T _s (°C)	250, 300, 350, 400, 450	250, 300, 350, 400, 450	400
Cu doping (wt%)	-	-	1-10

3.3 Measurement Details

3.3.1 Thickness Measurement of the Thin Films

Film thickness plays an important role on the properties of thin film and those it is one of the most significant film parameter and thickness measurement is a most essential job. Therefore, the thickness should be measured with great care as far as possible to have an accurate value. In the present work, the film thickness is measured after taking out the film from the chamber. There are several methods for the measurement of film thickness and in the present work optical interference fringe method (Fizeu fringes method) was used which is shown as Fig. 3.6. For film thickness measurement separate glass slide has been used in addition to the sample substrates. The step generated on the surface of the glass slide was used to measure the film thickness.



Fig. 3.6 Photograph of a multiple beam interferometer

3.3.2 Surface Morphology and Elemental Analysis of the Thin Films

The scanning electron microscope (SEM) (Fig. 3.7) is a type of electron microscope that creates various images (surface morphology) by focusing a high energy beam of electrons onto the surface of a sample and detecting signals from the interaction of the incident electron with the sample's surface. SEM measurement was performed at the Department of Glass and Ceramics, BUET, Dhaka S-3400N HITACHI, JAPAN, apparatus is used to carry out the SEM measurement. This apparatus operates in the range of 300 V to 30 KV. It has 5 to 300 thousand times magnification capacity. This apparatus has two imaging system, secondary electron imaging (SE imaging) and back scattered imaging (BS imaging). EDAX describes the compositional analysis of the thin films. This is done by the scanning electron microscopy (SEM) by focusing the X-ray beam on the full frame or a particular spot of the thin films. The analysis represents the individual weight (%) of the element that is present in the thin films. All the SEM images were recorded with a magnification of $\times 5000$.



Fig. 3.7 Photograph of a scanning electron microscopy (SEM)

3.3.3 Structural Analysis of the Thin Films

Attempts were made to study the structure of the films by XRD. XRD provides substantial information on the crystal structure. XRD is one of the oldest and effective tools for the determination of the atomic arrangement in a crystal; X-rays are the electromagnetic waves and its wavelength $\approx 0.1\text{nm}$. The wavelength of an X-ray is thus of the same order of magnitude as the lattice constant of crystals. When X-rays are incident on a crystal surface, they are reflected from it. The reflection obeys the following Bragg's law $2d \sin\theta = n\lambda$, where d is the distance between crystal planes; θ is the X-ray incident angle; λ is the wavelength of the X-ray and n is a positive integer. Bragg's law also suggests that the diffraction is only possible when $\lambda < 2d$. X-ray diffractometer system PW3040 X'Pert PRO X-ray Philips Company was used at Magnetic Material Division (MMD) of Atomic Energy Center, Dhaka (AECD) (Fig 3.8). The monochromatic (using Ni filter) $\text{CuK}\alpha$ radiation was used and the accelerating potential was 40 KV constituting a current of 30 mA. The scanning speed was 2 θ degree and the measurement was done in the range 20 $^\circ$ to 60 $^\circ$, respectively to obtain the X-ray diffraction pattern of the thin films. All the data of the samples were analyzed by using computer software "X'PERT HIGHSCORE" from which structural parameters was determined.



Fig. 3.8 Photograph of an X-ray diffractometer

3.3.4 Measurement of the Optical Properties of the Thin Films

The optical behaviors of a semiconductor are investigated in term of the three phenomena namely transmission, reflection and absorption. When a semiconductor is illuminated by light, photon strikes the surface, a fraction of photons are reflected, some of these are absorbed within the semiconductor and the remainder transmitted into the semiconductor and some may be reflected. For optical property studies of thin films were measured transmittance and absorbance by using a double beam UV spectrophotometer. Measurements were made by placing the sample in the incident beam and another empty glass substrate in the reference beam of the instrument. The optical transmission and reflection spectra of the film with respect to glass substrate were than taken for wavelength range 290 to 1100 nm using UV-1601 PC SHIMADZU VISIBLE SPECTROMETER (Fig 3.9). The spectral transmittance and absorbance of SnO₂ films was considerer in two wavelength regions, namely, visible and infrared regions. The optical spectra of transmittance, T (%) and absorbance, A (%) have been measured with respect to plain glass substrate were taken using the spectrophotometer.



Fig. 3.9 Photograph of a UV-1601 PC SHIMADZU VISIBLE spectrometer

3.3.5 Measurement of the Electrical Properties of the Thin Films

Electrical resistivity of thin film may be measured by different methods. In the present work, the resistivity of thin films was measured by using van der Pauw's technique shown in Fig.3.10. The van der Pauw method is one of the standard and widely used techniques for the measurement of resistivity of thin film. The van der Pauw method is a technique for doing 4-probe resistivity and Hall effect measurements. The advantages of this method include low cost and simplicity. The van der Pauw technique can be used on any thin sample of material and the four contacts can be placed anywhere on the perimeter/boundary, provided certain conditions.

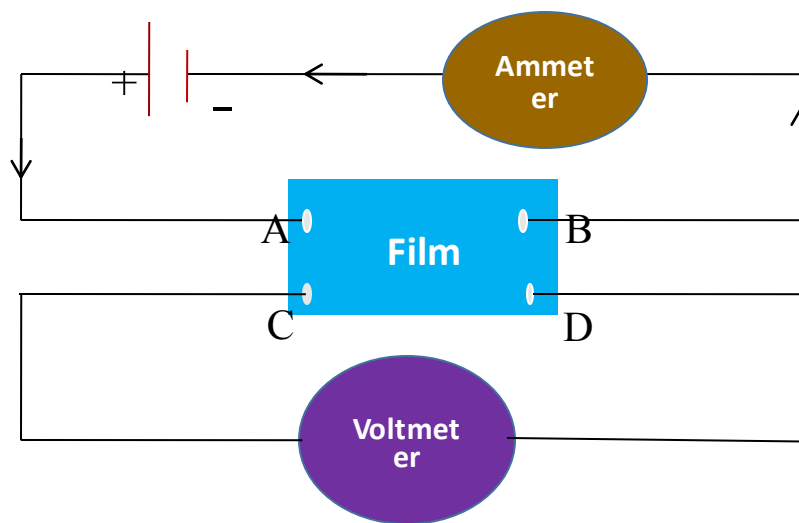


Fig. 3.10 Set up for resistivity measurement by van der Pauw's method

CHAPTER-IV

RESULTS AND DISCUSSION

4.1 Introduction

4.2 Results and Discussion on CuO Thin Films

4.2.1 CuO Thin Films Synthesized from Aqueous Solutions of Different Molar Concentrations at T_s of 350 °C

4.2.1.1 Surface Morphological and Elemental Analyses

4.2.1.2 Structural Analysis

4.2.1.3 Optical Properties

4.2.1.3.1 Transmittance and Optical Band Gap

4.2.1.3.2 Refractive index and Extinction Coefficient

4.2.1.1 Electrical Properties

4.2.2 CuO Thin Films synthesized using 0.10M at Different T_s (250 – 450 °C)

4.2.2.1 Surface Morphological and Elemental Analyses

4.2.2.2 Structural Analysis

4.2.2.3 Optical Properties

4.2.2.3.1 Transmittance and Optical Band Gap

4.2.2.3.2 Refractive index and Extinction Coefficient

4.2.2.4 Electrical Properties

4.2.3 Summary of Findings on CuO Thin Films

4.3 Result and Discussion on TiO₂ Thin Films

4.3.1 TiO₂ Thin Films Synthesized from Aqueous Solutions of Different Molar Concentrations at T_s of 300 °C

4.3.1.1 Surface Morphological and Elemental Analyses

4.3.1.2 Structural Analysis

4.3.1.3 Optical Properties

4.3.1.3.1 Transmittance and Optical Band Gap

4.3.1.3.2 Refractive index and Extinction Coefficient

4.3.1.1 Electrical Properties

4.3.2 TiO₂ Thin Films Synthesized Using 0.10M at Different T_s (250 – 450 °C)

4.3.2.1 Surface Morphological and Elemental Analyses

4.3.2.2 Structural Analysis

4.3.2.3 Optical Properties

4.3.2.3.1 Transmittance and Optical Band Gap

4.3.2.3.2 Refractive index and Extinction Coefficient

4.3.2.4 Electrical Properties

4.3.3 Summary of Findings on TiO₂ Thin Films

4.4 Results and Discussion on Cu/TiO₂ Thin Films

4.4.1 Cu doped TiO₂ Thin Films Synthesized from Aqueous Solutions of (0 – 10%) (Cu(CH₃COO)₂.H₂O) Doped in TiCl₄ of 0.10 M Molar Concentration at T_s of 400 °C

4.4.1.1 Surface Morphological and Elemental Analyses

4.4.1.2 Structural Analysis

4.4.1.3 Optical Properties

4.4.1.3.1 Transmittance and Optical Band Gap

4.4.1.3.2 Refractive index and Extinction Coefficient

4.4.1.4 Electrical Properties

4.4.2 Summary of Findings on Cu/TiO₂ Thin Films

4.5 Summary of Results of the Prepared Thin Films and the Reported TiO₂ Thin Films

4.1 Introduction

The objective of this study is to synthesis and characterize CuO, TiO₂ and Cu doped TiO₂ thin films by SPT. Thickness of the films is about 200±10 nm. In this chapter the results and discussion of the various experimental studies viz. surface morphology structural, optical and electrical properties of CuO, TiO₂ and Cu doped TiO₂ thin films are presented and are discussed step by step.

4.2 Results and Discussion on Prepared CuO Thin Films

4.2.1 CuO Thin Films Synthesized from Aqueous Solutions of Different MCs at T_s of 350 °C

CuO thin films were synthesized from solutions of molar concentrations (MCs) of 0.05, 0.075, 0.10, 0.125 and 0.15 M at T_s of 350 °C by SPT. Surface morphology, structural, optical and electrical properties of the synthesized samples are presented and discussed in the following sections.

4.2.1.1 Surface Morphology and Elemental Analyses

The surface morphology of CuO thin films observed by SEM is shown in Fig. 4.1. It is seen that the surface of the thin film with 0.10 M is comparatively well aggregated and less rough. This could be the result of the chemical reaction of the sprayed solution on the hot substrate during the deposition. SEM micrographs reveal the formation of particles with different shapes and sizes. It seems appropriate to consider that the particles which appear in the SEM images are, in fact, grain agglomerates. The EDX spectrum of Fig. 4.2 reveals the presence of copper (Cu) and oxygen (O) and other elements from the glass substrates confirming that the CuO thin films prepared through the chemical oxidation route are free from impurities. The atomic ratio between Cu and O was found to be 1:1. Hence, it is confirmed that CuO is formed through chemical oxidation route by SPT.

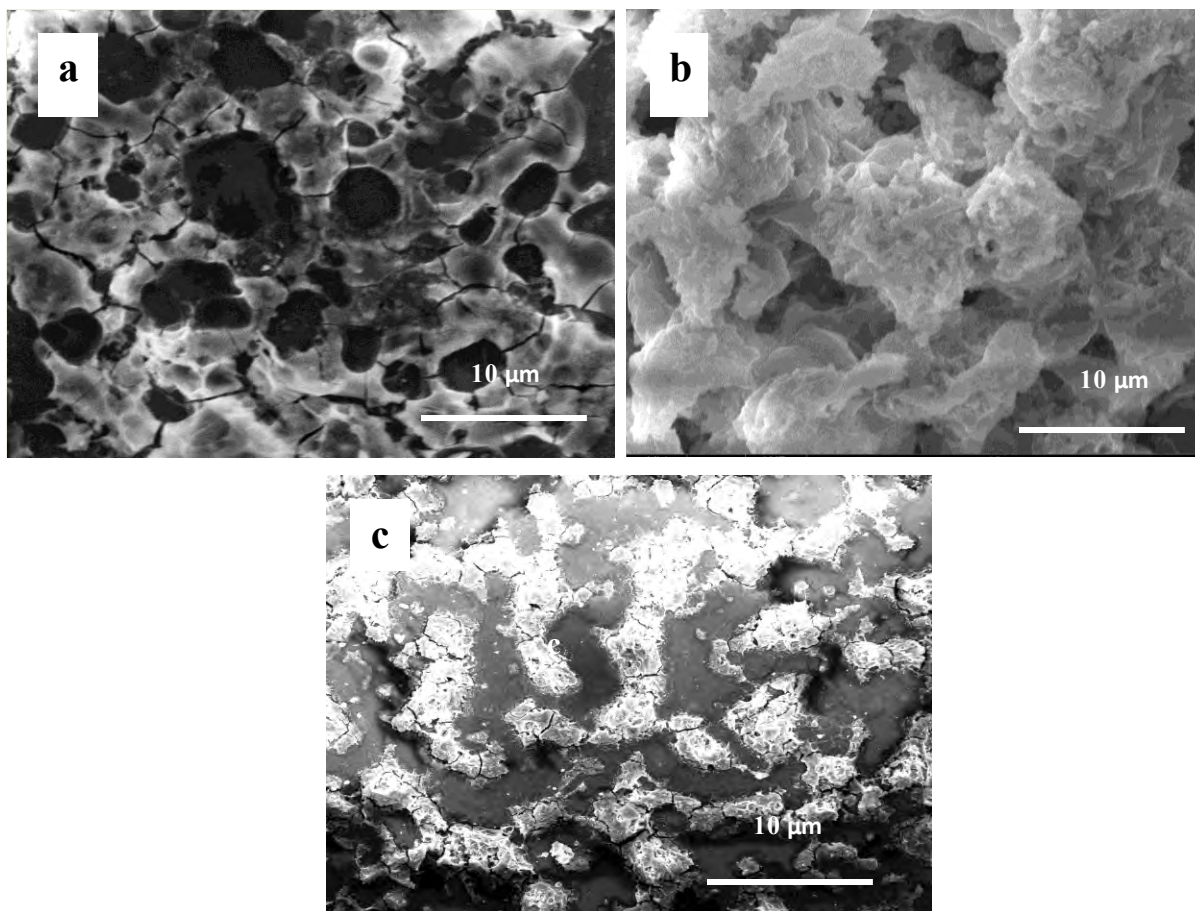


Fig. 4.1 SEM images of CuO thin films for MC of (a) 0.05, (b) 0.10 M and (c) 0.15M ($T_s = 350\text{ }^\circ\text{C}$)

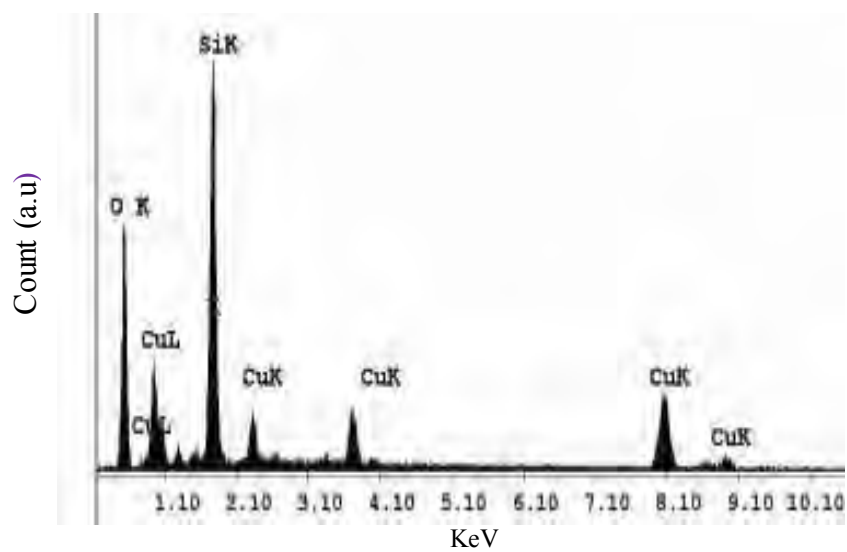


Fig. 4.2 EDX spectrum for CuO thin film MC of 0.10 M ($T_s = 350\text{ }^\circ\text{C}$)

4.2.1.2 Structural Analyses

XRD patterns for CuO thin films synthesized from solution of different MCs are shown in Fig. 4.3. XRD analysis shows that the CuO thin films have monoclinic crystal structure with some shifts in the position of characteristic peaks. The diffraction peaks observed at different 2θ values correspond to the diffraction lines produced by (110), (002), (111), (200), (202), and (020) planes of the end-centered monoclinic structured CuO (JCPDS card No. 89-5895). Crystallite size (D) of the prepared CuO thin film was determined from the strongest peak of (111) for every XRD pattern using Debye-Scherrer formula given by equation $D = K\lambda/(\beta\cos\theta)$ where, λ is the wavelength of the X-ray radiation ($\lambda = 0.15406$ nm) for $\text{CuK}\alpha$; K is usually taken as 0.89; and β is the line width at half-maximum height [1]. The (111) surface of CuO is energetically the most stable and the predominant crystal face found in the polycrystalline CuO thin films. Although (111) and (200) reflections are present, no other planes are present for Cu_2O . The lattice constants of the CuO thin films are found to be: $a = 4.6623$ Å, $b = 3.4431$ Å and $c = 5.1345$ Å for solution of 0.10M and are in good agreement with the standard JCPDS data for monoclinic structure of CuO. It is observed in the XRD patterns that the intensity of the peaks slightly increases as MC increases. For peak (111) the calculated values of the D for the CuO thin films are presented in Table 4.1. It is seen that D increases with MC of solution up to 0.125 M and then decreases, above 0.125 M. Similar results were observed for CuO thin films prepared by SPT using copper (II) chlorite precursor solution on the glass substrate at 350 °C [2]. It implies that the crystallinity of the CuO thin films is improved at higher MC. For the spray solution with low MC of 0.05 M, the net heat absorbed by the droplet, may not sufficient enough to vaporize the entire droplet due to fast travel of droplet to the substrate. As a result precipitation and sublimation has taken place on the substrate. So, the reaction appears to be a homogeneous one and the film has low crystallinity. When the molar concentration was increased to 0.125 M, the intensities of the peaks of CuO get enhanced which indicates that the crystallinity of crystallites has been improved. The peak positions of the diffraction peaks and 'D' values for CuO thin films are in good agreement with the earlier reports of the spray deposited CuO thin films using $\text{CuCl}_2 \cdot 2\text{H}_2\text{O}$ [3].

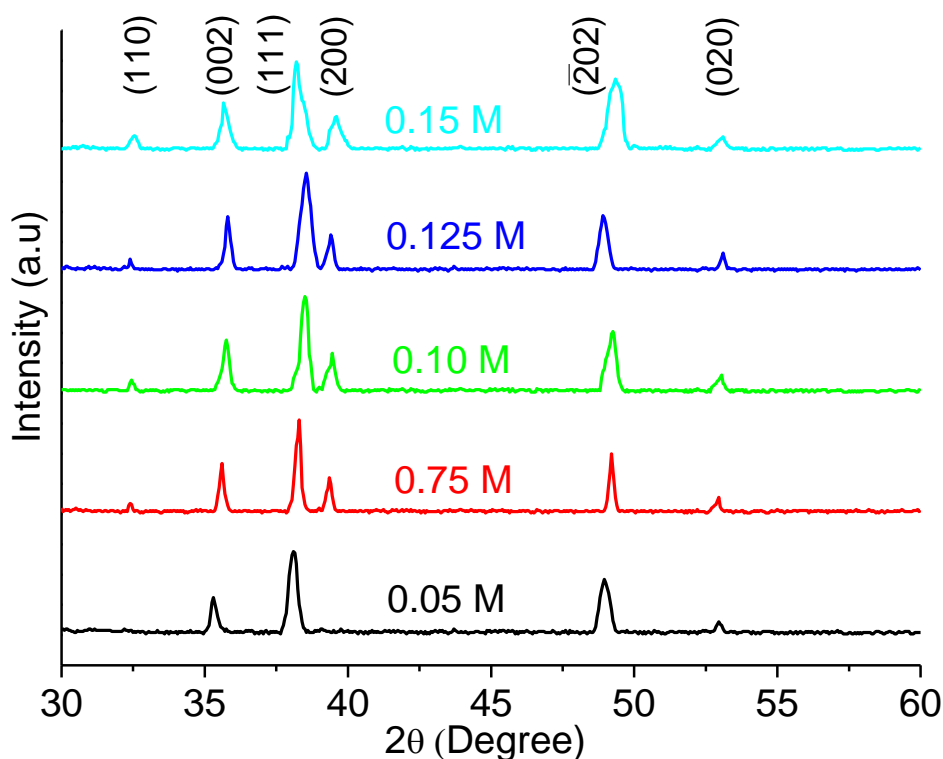


Fig. 4.3 XRD patterns of CuO thin films synthesized from solution of various MCs ($T_s = 350\text{ }^\circ\text{C}$)

Table 4.1 Crystallite size for the CuO thin films for various MCs ($T_s = 350\text{ }^\circ\text{C}$)

MC (M)	0.05	0.075	0.10	0.125	0.15
D (nm)	8.0257	8.9341	9.5743	9.6232	9.0532

4.2.1.3 Optical Properties

4.2.1.3.1 Transmittance and Optical Band Gap

The variation of transmittance, T of CuO thin films for MC of 0.05 - 0.15 M with wavelength is shown in Fig. 4.4. It is seen that T is high in the near infrared region and minimum at wavelength $\sim 300\text{ nm}$ 60 to 80% transmittances are observed in the wavelength range of 800-1100 nm and below 800 nm transmittance decreases gradually. The transmittance is high about 80% for CuO thin films grown with MC of 0.10 M at T_s of 350 $^\circ\text{C}$. The increase in transmittance may be due to the transition of the CuO films from

amorphous to polycrystalline structure. A relatively high transmittance value for the thin film deposited at T_s of 350 °C for MC of 0.10 M, may be attributed to less scattering due to the decrease in the degree of irregularity in the grain size distribution [4]. The transmittance values are decreased for the next MC of 0.15 M. This suggests that the decrease in the transmittance of CuO thin films with increasing in MC may lead to increase in the degenerate nature of the films, which results in light absorption. The optical band gap (E_g) for the direct band gap semiconductors is determined using the Tauc model and parabolic bands [5], $(\alpha h\nu)^2 = A(h\nu - E_g)$, where A is a proportionality constant, $h\nu$ is the incident photon energy ($h\nu$), α is the absorption coefficient, and E_g is the optical band gap. Fig. 4.5 shows $(\alpha h\nu)^2$ as a function of, $h\nu$ for the CuO thin films deposited at various MCs. The α was found in the order of 10^6 m^{-1} which may be suitable for a transparent conducting film. The E_g of the CuO thin films against MC is plotted in Fig. 4.6. The E_g is found to be 2.40 eV for MC of 0.05 M and a minimum value of E_g of 1.60 eV for MC of 0.10 M. It can be seen that a band gap tuning of 0.80 eV results when the MC is changed by about 0.05 M. The value of the α and E_g decrease as the MC increases gradually up to 0.10 M whereas it starts to increase with further increase of MC. It may be due to the removal of defects and disorderness in the film with increasing MC.

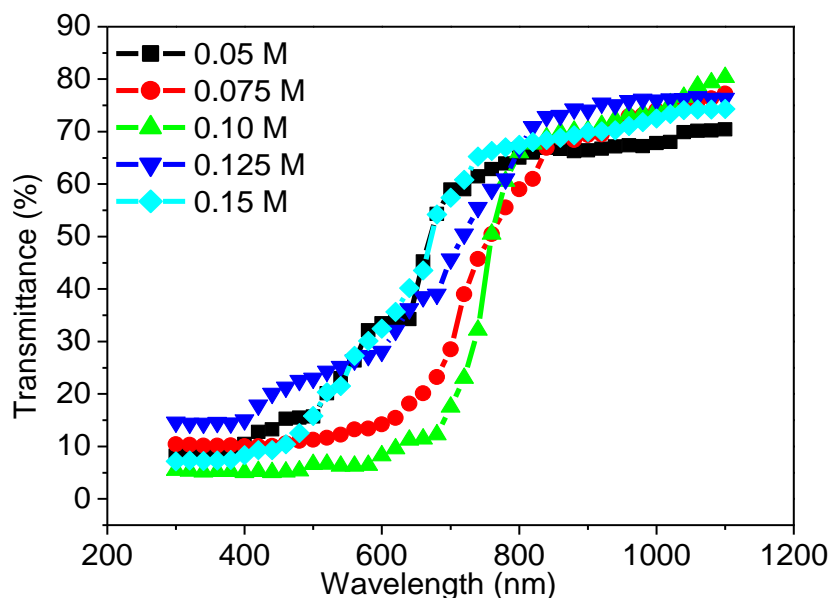


Fig. 4.4 Optical transmittance vs. wavelength of CuO thin films for various MCs ($T_s = 350 \text{ }^\circ\text{C}$)

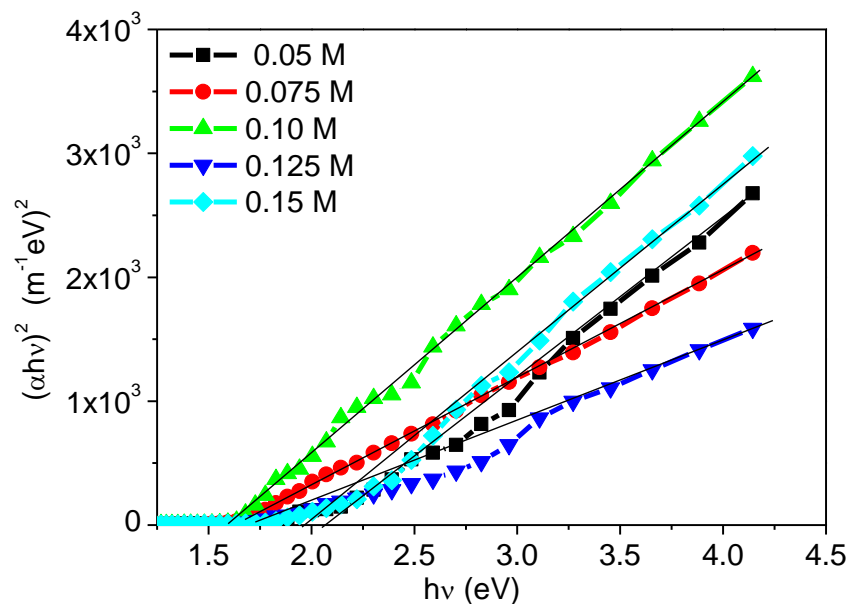


Fig. 4.5 Variation of $(\alpha hv)^2$ with $h\nu$ for CuO thin films for various MCs ($T_s = 350\text{ }^\circ\text{C}$)

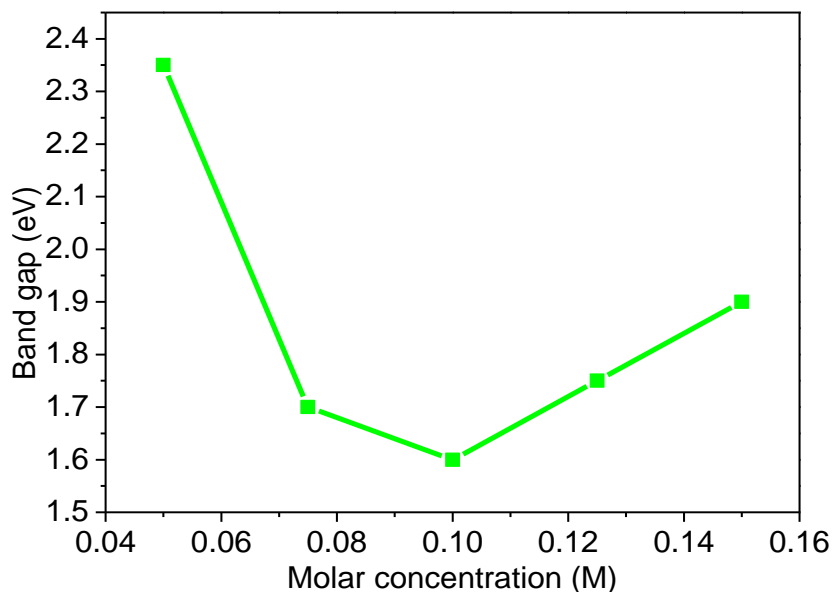


Fig. 4.6 Band gap vs. MC of the solution for CuO thin films ($T_s = 350\text{ }^\circ\text{C}$)

4.2.1.3.2 Refractive Index and Extinction Coefficient

The variation of refractive index, n with MC of solution for CuO thin films is presented in Fig. 4.7. The n of CuO thin film is obtained to be 2.82 for MC of 0.05 M and it becomes lowest, 2.68 for MC of 0.10 M. This lowest value is very close to the reported value 2.65 of CuO thin film prepared by reactive RF magnetron sputtering [6] and it is lower than that of bulk CuO and this low value of n may probably due to the smaller density of the films.

The variation of extinction coefficient, k with $h\nu$ is shown in Fig. 4.8. It is observed that the k increases with the increase of MC. In the variation of k with energy, the k values for all the films behave a linear increase upto 2.2 eV after that there is a gradual decrease in the k value. The blue shift in the k value denotes that the films are stronger absorbing medium in this range and is very close to the reported value of CuO thin films prepared on to glass substrates from different aqueous solution of copper (II) chlorite [2]. The k of CuO thin films increases rapidly for photon energies above 1.6 eV for better crystallization and tends to decrease above 2.3 eV for scattering of phonons dominant with electrons.

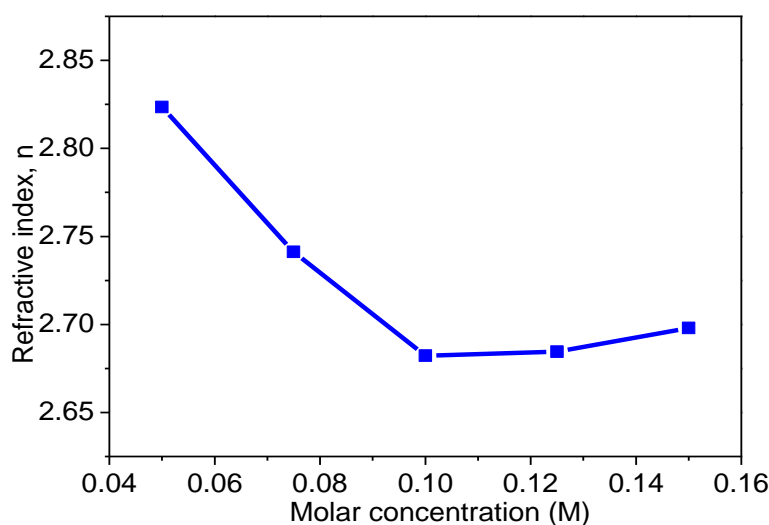


Fig. 4.7 Variation of n with MC for CuO thin films ($T_s = 350^\circ\text{C}$)

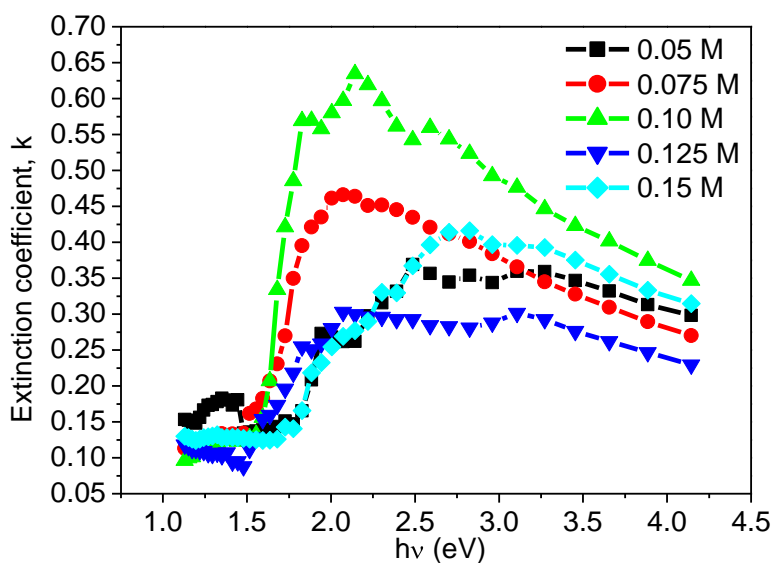


Fig. 4.8 Variation of k with $h\nu$ for various MCs of CuO thin films ($T_s = 350^\circ\text{C}$)

4.2.1.4 Electrical Properties

The variation of electrical resistivity (ρ) of CuO thin films with temperature is shown in Fig. 4.9. The ρ of CuO thin films with temperature is decreased, indicating that these films are semiconducting nature. Room temperature electrical conductivity (σ) and ρ of CuO thin films with MC are presented in Fig. 4.10. The room temperature ρ of the prepared CuO thin films decreases as MC increases and the minimum value of ρ is found for 0.10 M. This variation in the ρ of the films with MC has been explained in terms of stoichiometric changes induced by copper (Cu) or oxygen O ion vacancies and neutral defects. The reduction in ρ with the increase in MC is due to the increase of carrier concentration of Cu and lower scattering of excess conduction electrons. Further increase in oxygen during deposition is observed to result in a high airing of the film resistivity, which was explained as resulting from the MC of the films with excess oxygen i.e. effectively producing more copper ion vacancies and a p-type semiconductor CuO. It may be due to increase in the free path of carrier concentration. The formation of these defects depends on the sticking coefficient, nucleation rates and the migration of impinging Cu and oxygen species on the substrate during deposition. Generally, the σ in semiconductor is caused by thermal excitation of electron, impurities and lattice defects such as dislocation, stacking faults and micro twines [7]. This study reveals that MC increase has a considerable effect on the electrical properties of CuO thin films.

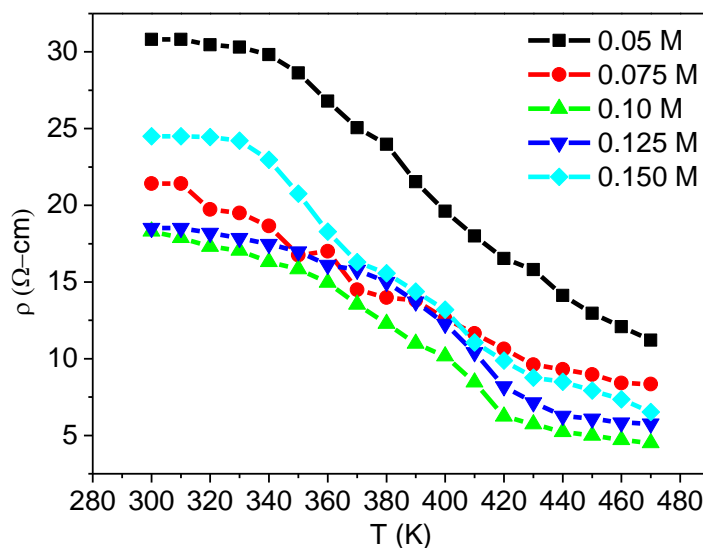


Fig. 4.9 Variation of ρ with temperature of CuO thin films for various MCs ($T_s = 350^\circ\text{C}$)

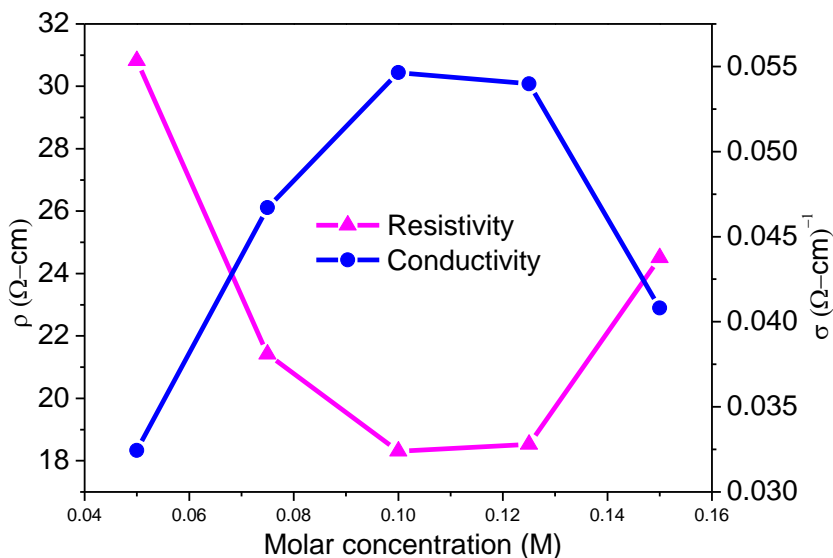


Fig. 4.10 Variation of resistivity and conductivity at room temperature with MC of CuO thin films ($T_s = 350\text{ }^\circ\text{C}$)

The activation energy (E_a) is calculated from the slope of a curve $\ln\sigma$ vs. $(1/T)$ using the equation (2.31) given in chapter II. A plot of $\ln\sigma$ vs $1000/T$ is shown in Fig. 4.11 and variation of E_a with MC of solution is shown in Fig.4.12. The nonlinear nature of the plots exhibit two types of conductivity mechanism. The E_a values in two temperature regions are calculated from the graphs. The σ (Fig. 4.10) as well as the E_a (4.12) was increased as of MC increases up to 0.10 M and above 0.10 M both parameters decreases. The activation energy E_1 , 0.30 eV for 0.10 M in the high temperature region to the impurity scattering and E_2 , 0.12 eV for 0.10 M in the low temperature region is related to the intrinsic generation process [8-9]. The conduction mechanism at lower temperatures can be explained in terms of hopping through a band of localized states and at the higher temperatures in terms of thermal excitation of carriers to the band edges. The low value of E_a may be associated with the localized levels hopping due to the excitation of carriers from donor band to the conduction band. A low activation energy of 0.14 eV was reported for sputtered CuO thin films [10]. This low value of E_a was assumed due to the nonstoichiometry of the CuO thin film but in the present case the higher values of E_a in the higher temperature region may suggest that the prepared sample is stoichiometric. For SEM and EDX observations, it is also found that CuO thin films are stoichiometric. The Figure

of merit is well-known as an index for evaluating the performance of transparent conducting films, and it is given by the equation $F = (-\rho \ln T)^{-1}$ where ρ is the electrical resistivity and T is the average transmittance in the wavelength range of 800-1100 nm [11]. Fig. 4.13 shows the Figure of merit values of CuO thin films deposited for various MCs. The Figure of merit for the CuO thin films deposited with MC of 0.05, 0.10 and 0.15 M were found to be 0.1278, 0.1424 and 0.1418 $\Omega^{-1} \cdot \text{cm}^{-1}$, respectively. The increase in the figure of merit of the CuO thin films is mainly due to the increase in the optical transmittance with increasing MC.

It is observed that transmittance of the prepared sample is maximum, E_g is minimum and D is maximum for CuO thin films prepared with MC of 0.10 M due to better crystal structure and surface morphology. Thus it is observed from these studies that CuO thin films synthesized at T_s of 350 °C with 0.10 M of MC of solution have optimum properties. So, the detail investigations on the CuO thin films synthesized with 0.10 M at various T_s have been performed. The findings from these observations are discussed in the following sections.

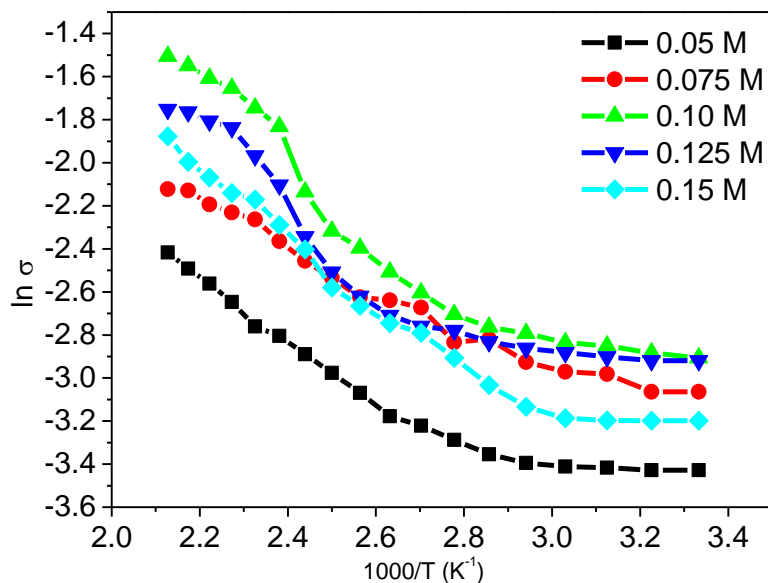


Fig. 4.11 Variation of $\ln \sigma$ with respect to inverse of absolute temperature of CuO thin films for various MCs ($T_s = 350$ °C)

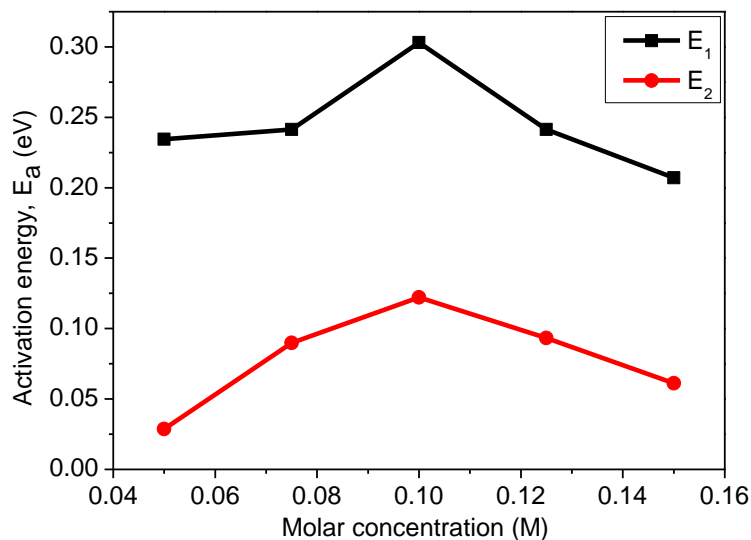


Fig. 4.12 Variation of activation energy with MC for CuO thin films ($T_s = 350\text{ }^\circ\text{C}$)

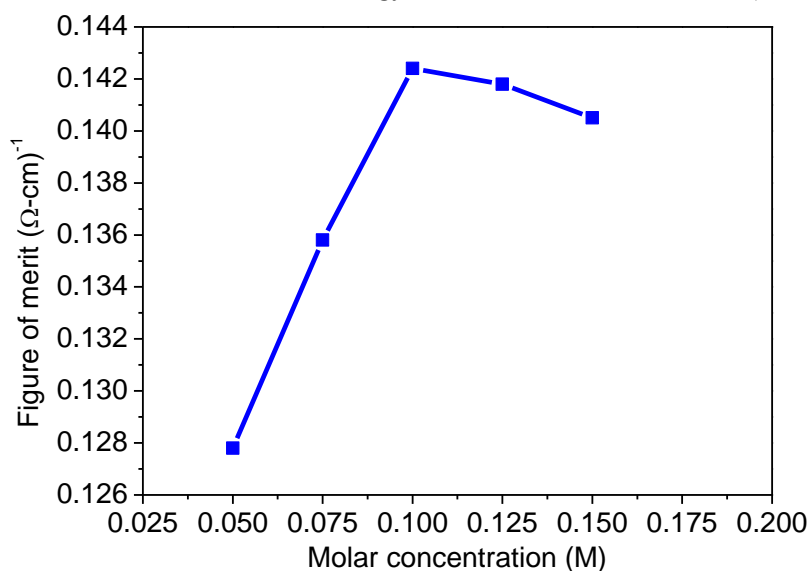


Fig. 4.13 Variation of Figure of merit versus MC for CuO thin films ($T_s = 350\text{ }^\circ\text{C}$)

4.2.2 CuO Thin Films Synthesized Using Solution of 0.10M at Different T_s

4.2.2.1 Surface Morphology and Elemental Analyses

SEM images were recorded to examine the surface morphology of the CuO thin films synthesized at five different T_s for MC of 0.10M and the images are shown in Fig. 4.14. The CuO thin films have grain agglomerates of different sizes and shapes formed during deposition, and their distribution on the surface is not homogeneous. From SEM micrographs, it is seen that agglomerates become larger as T_s increases up to $400\text{ }^\circ\text{C}$ and

above T_s of 400 °C crystallite size decreases. This change corresponds to the change in crystallite size presented in Table 4.2.

Fig.4.15 shows EDX spectrum of CuO thin films prepared at T_s of 400 °C. Cu and O are identified with atomic ratio 1:1, which confirm that the CuO thin films prepared through the chemical oxidation route. Other elements may arise from the substrate.

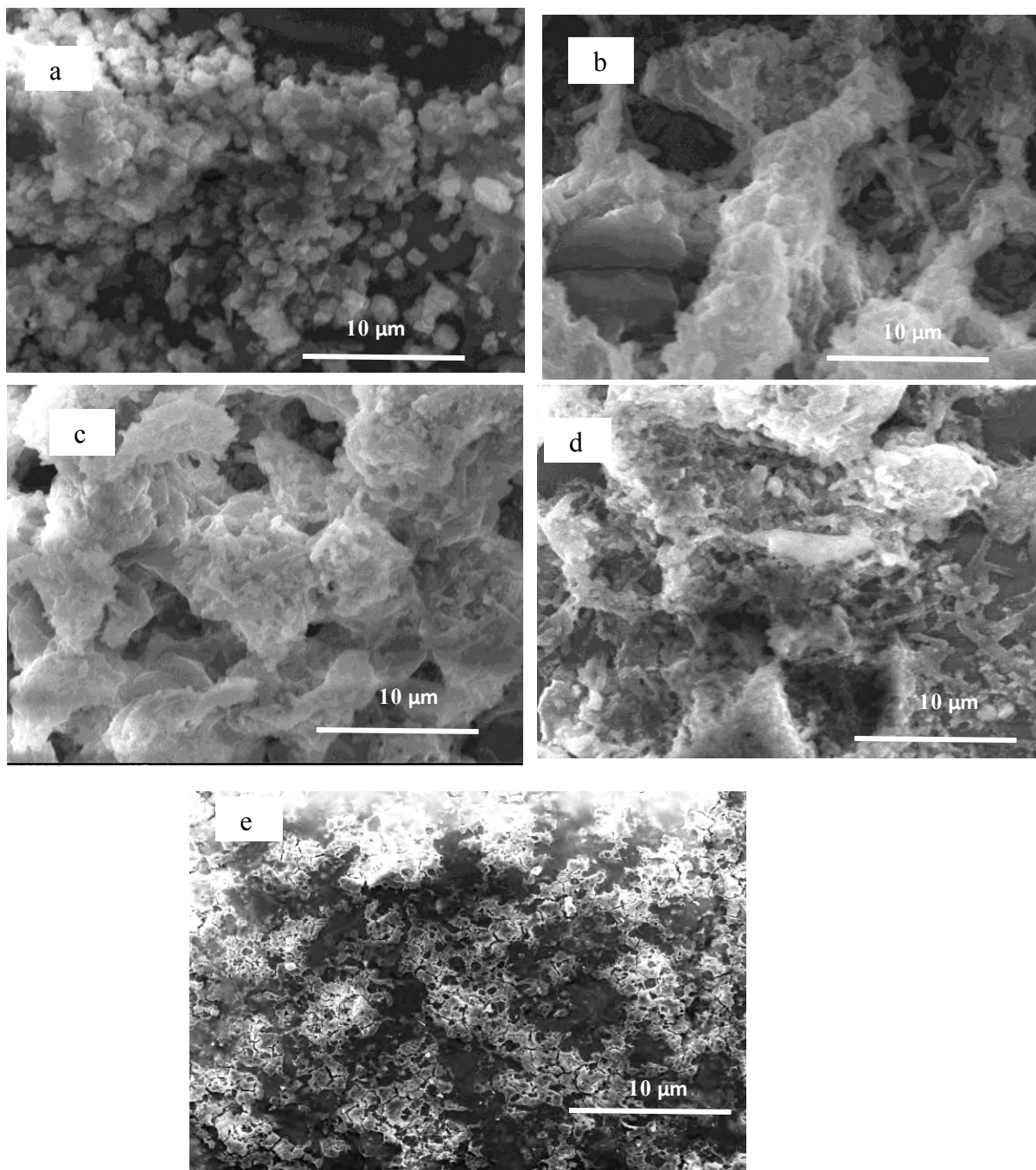


Fig. 4.14 SEM image of CuO thin films at T_s of (a) 250 (b) 300 (c) 350 (d) 400 and (e) 450 °C (MC = 0.10M)

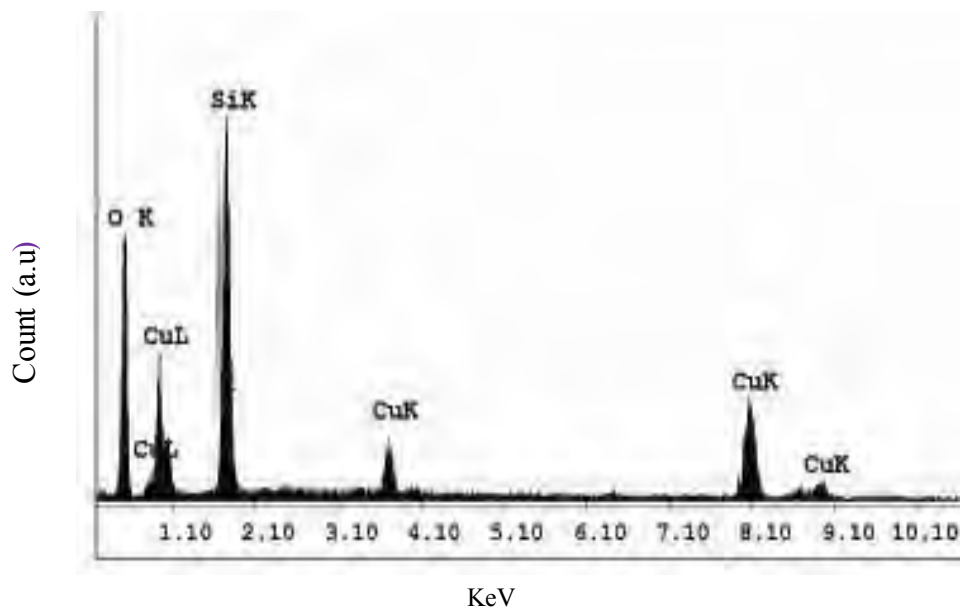


Fig. 4.15 EDX spectra of CuO thin films at T_s of 400 °C (MC = 0.10 M)

4.2.2.2 Structural Analyses

XRD patterns for CuO thin films synthesized at different T_s of 250, 300, 350, 400 and 450 °C from 0.10 M solution are shown in Fig. 4.16. The diffraction peaks observed at 2θ values of 32.2, 35.5, 38.3, 39.1, 48.85 and 52.7° correspond to the diffraction lines produced by (110), (002), (111), (200), (202), and (020) planes of the end-centered monoclinic structured CuO (JCPDS card No. 89-5895). Crystallite size (D) of the prepared CuO thin films was determined from the strongest peak for (111) for every XRD pattern using Debye-Scherrer formula [1]. It is observed from Fig. 4.16 that the diffraction peak positions are identical for all the CuO thin films obtained at different T_s , indicating the formation of monoclinic phase CuO in all the cases. Although (111) and (200) reflections are present, no other planes are present for Cu₂O as the case for different MC. The lattice constants of the CuO thin films deposited at 400 °C for MC of 0.10 M are found to be: $a = 4.6749$ Å, $b = 3.4536$ Å and $c = 5.1207$ Å, and are in good agreement with the standard JCPDS data for monoclinic structured of CuO. For peak (111) the calculated values of D for the CuO thin films are presented in Table 4.2. In Table 4.2, it is observed that the D increases with T_s up to about 400 °C and then decreases. For CuO there are many dangling bonds related to the Cu and/or oxygen defects at the grain boundaries. As a result, these

defects are favorable to the merging process to form larger CuO grains while increasing T_s [12]. It implies that the crystallinity of the CuO thin films is improved at higher T_s . This may be due to gaining enough energy by the crystallites to orient in proper equilibrium sites at high T_s , resulting in the improvement of crystallinity and degree of orientation of the CuO thin films [13-14]. Similar result was reported in ref. [15] as increasing T_s , the size of the crystallites (16.55 to 48.69 nm) for TiO₂ thin film prepared by SPT. These results are in good agreement with the reported observation in refs. [16-17].

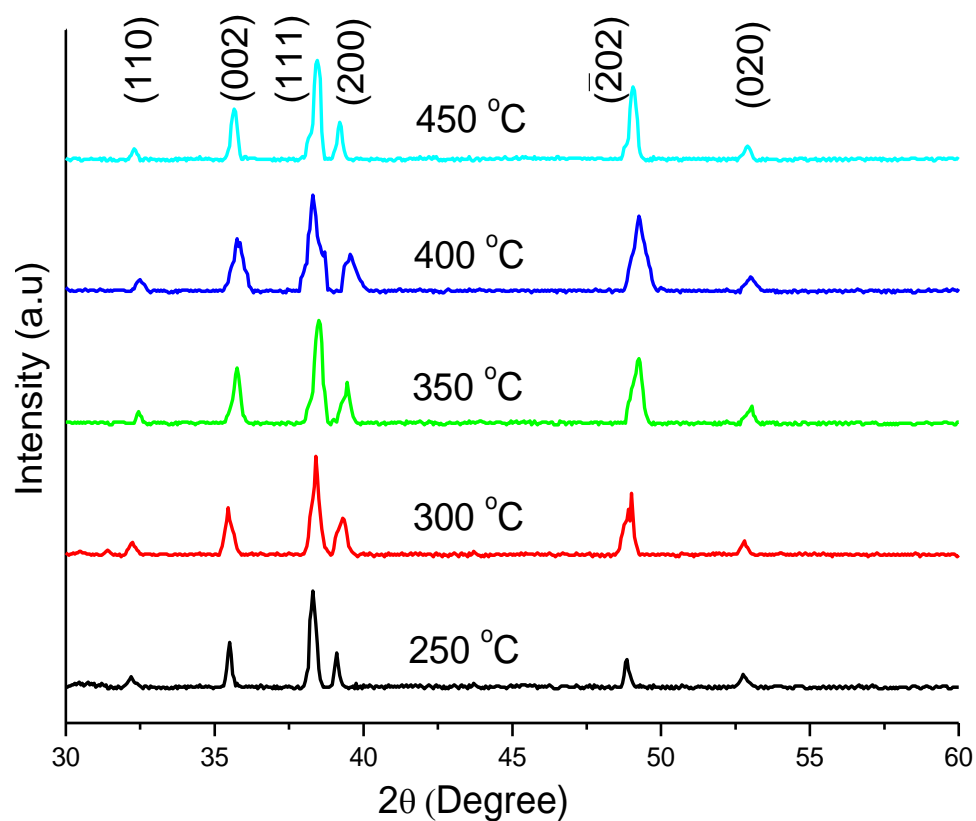


Fig. 4.16 XRD patterns of CuO thin film synthesized at various T_s (MC = 0.10M)

Table 4.2 Crystallite size for the CuO thin films at various T_s (MC= 0.10 M)

T_s (°C)	250	300	350	400	450
D (nm)	8.4784	9.0257	9.5743	9.6545	9.6223

4.2.2.3 Optical Properties

4.2.2.3.1 Transmittance and Optical Band Gap

The optical properties of CuO thin films deposited at various T_s for solution of 0.10 M were investigated by recording of the transmission spectra as shown in Fig.4.17. It is seen that the transmittance is high in the NIR region and minimum at wavelength ~ 300 nm. Average 60 to 80% transmittances are observed in the wavelength range of 800-1100 nm and below 800 nm, T decreases gradually. The transmittance increases from 5 to 10% with T_s , and shows the highest transmittance of about 80 % for the thin films grown at T_s of 350 °C. The increase in transmittance may be due to the transition of the CuO films from amorphous to polycrystalline structure. The transmittance values are decreased for the next higher T_s , it may be due to crystallinity of the film decreases. The E_g of semiconductors is determined using the Tauc model and parabolic bands [5]. Fig. 4.18 shows the absorption coefficient squared $(\alpha h\nu)^2$ as a function of, $h\nu$ for the CuO thin films deposited at various T_s . The E_g of the CuO thin films at various T_s is plotted in Fig. 4.19. It is seen in Fig.4.19 that for the CuO thin films deposited at T_s of 250 °C the E_g is found to be 1.90 eV and then a minimum value 1.60 eV is found for sample obtained at 350 °C. It can be seen that band gap tunes by 0.30 eV due to change of T_s by about 100 °C. The value of the α and E_g decrease as the T_s increases gradually up to 350 °C whereas it starts to increase with further increase of T_s . The decrease of E_g may be due to the removal of defects and disorderness in the as-deposited film by increasing T_s .

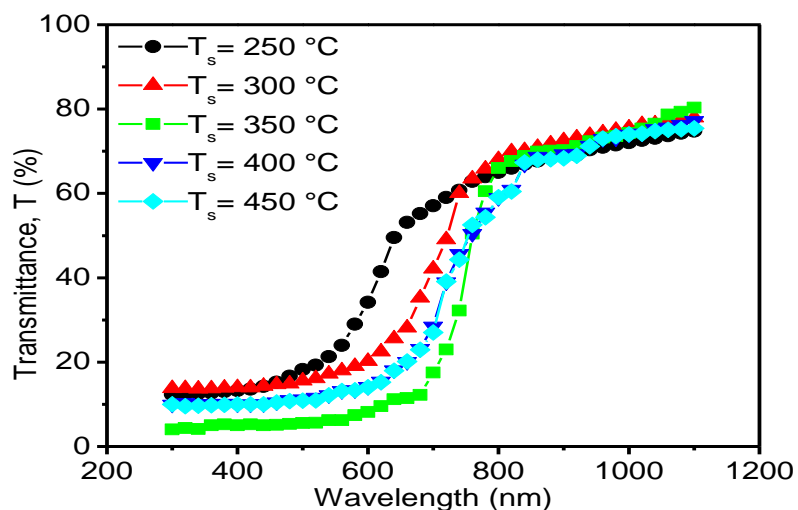


Fig. 4.17 Optical transmittance vs. wavelength for CuO thin films at various T_s (MC = 0.10M)

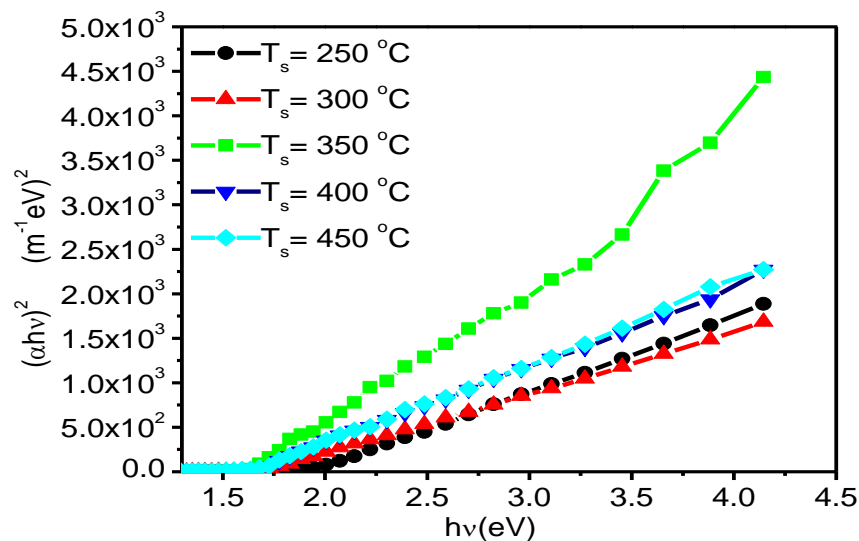


Fig. 4.18 Variation of $(\alpha hv)^2$ with $h\nu$ for CuO thin films at various T_s (MC = 0.10M)

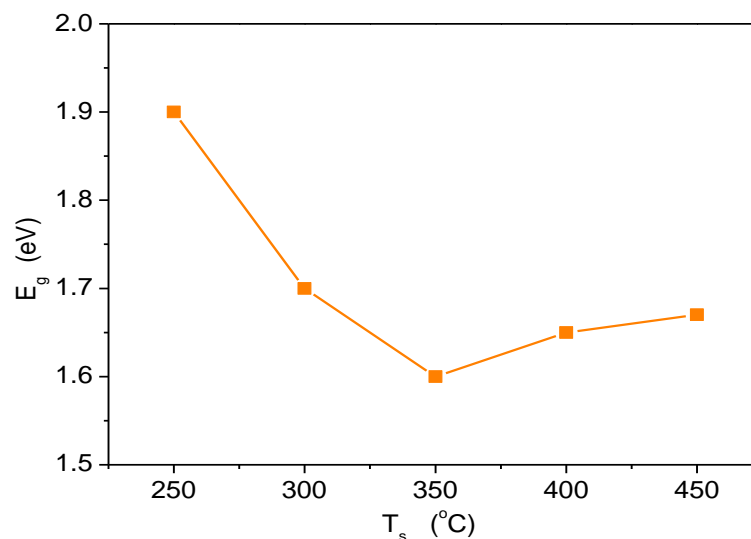


Fig. 4.19 Variation of E_g with T_s for CuO thin films (MC = 0.10M)

4.2.2.3.2 Refractive index and Extinction Coefficient

The variations of refractive index, n for CuO thin films with T_s is shown in Fig. 4.20. The n of CuO thin film has been obtained to be 2.75 at T_s of 250 °C and it becomes lowest, 2.68 at $T_s = 350$ °C. The low value of n may be due less scattering and absorbing by CuO synthesized at T_s of 350 °C. A higher T_s , n is increased which may be due to scattering of phonons dominant with atoms. This value is very close to the reported value 2.65 of CuO thin film prepared by RF magnetron sputtering [6] and it is lower than that of bulk CuO and this low value of refractive index may probably due to the lower density of the films.

The variation of extinction coefficient, k with $h\nu$ is shown in Fig. 4.21. It is observed that the k increases with the increase of T_s . The k about 0.1 in the wavelength range 800-1100 nm (1.6-1.0 eV) is shown in Fig. 4.21, which is lower than that of CuO thin films prepared by RF magnetron sputtering [6] and is very close to the reported value of CuO thin films prepared on to ITO glass substrates from an aqueous electrolytic bath containing CuSO_4 and tartaric acid [18]. The k of CuO thin films increases rapidly for photon energies above 1.6 eV and tends to decrease above 2.3 eV.

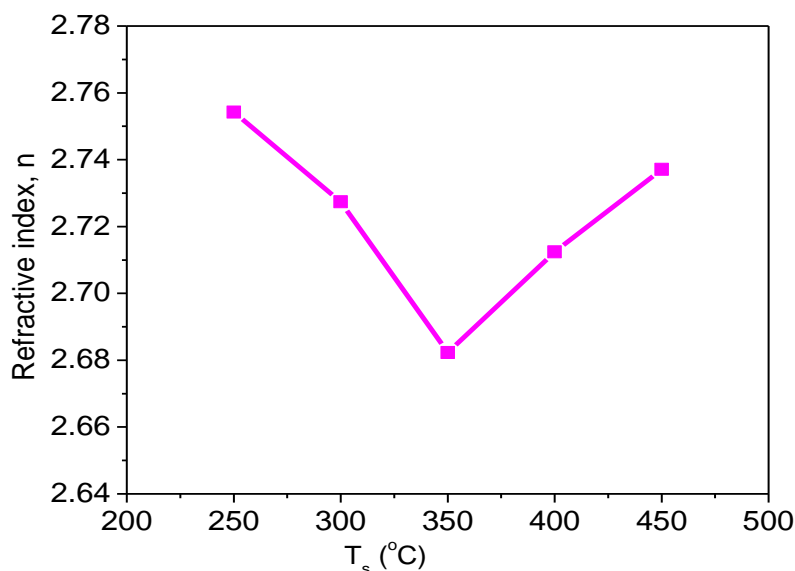


Fig. 4.20 Variation of n for CuO thin films with T_s (MC = 0.10M)

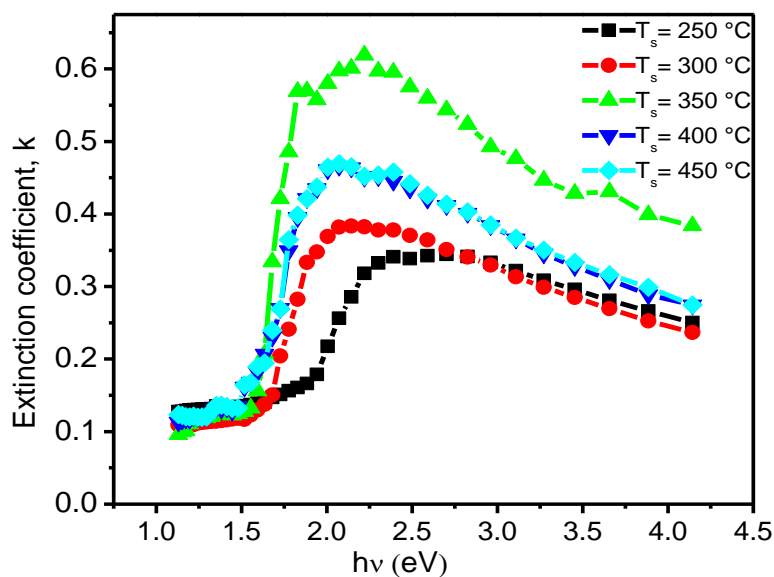


Fig. 4.21 Variation of k for CuO thin films with $h\nu$ at various T_s (MC = 0.10M)

4.2.2.4 Electrical Properties

The ρ of CuO thin films as a function of temperature is shown in Fig. 4.22. It is observed that the ρ of CuO thin films decreases with the increase of temperature, showing semiconducting nature. Dependence of room temperature ρ of CuO thin films on T_s is presented in Fig. 4.23. The ρ of the films varying from 30 to 18 Ω -cm. The minimum ρ is found to be 18 Ω -m for CuO thin film deposited at $T_s = 350$ °C. The decrease in ρ with T_s can be explained in terms of stoichiometric changes induced by oxygen ion vacancies and neutral defects. The formation of these defects depends on the sticking coefficient, nucleation rates and the migration of impinging Cu and oxygen species on the heated substrate during deposition. The reduction in ρ with the increase in T_s is due to the increase of carrier concentrations due to the presence of Cu and lower scattering of excess conduction electrons. It may be due to increase in the free path of carrier concentration.

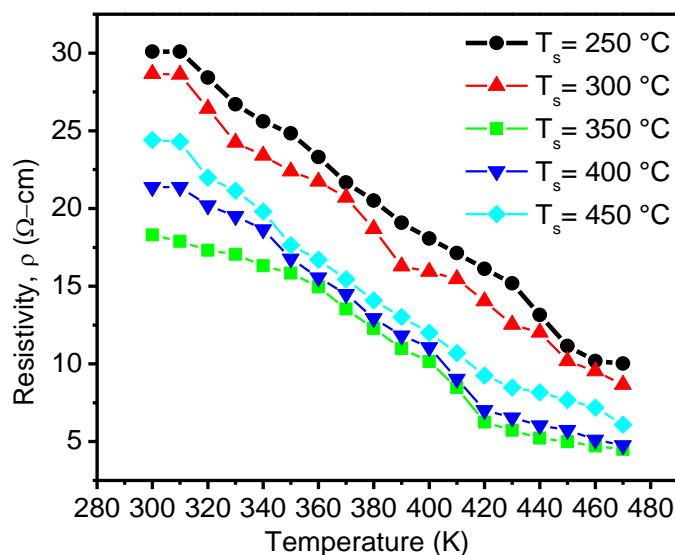


Fig. 4.22 Variation of DC electrical resistivity for CuO thin films with temperature for various T_s (MC = 0.10M)

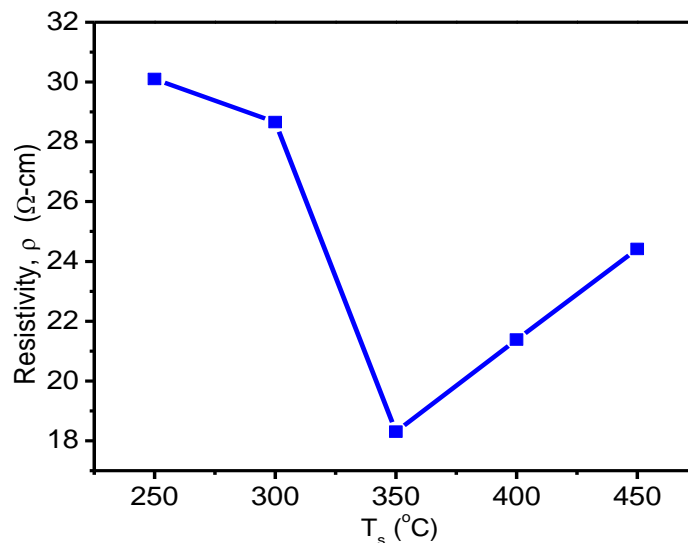


Fig. 4.23 Variation of DC electrical resistivity for CuO thin films at room temperature with various T_s (MC = 0.10M)

The temperature dependence of electrical conductivity ($\ln\sigma$) is shown in Fig.4.24. The variation of E_a with T_s is shown in Fig.4.25. The activation energy E_1 is varying from 0.21 to 0.26 eV at high temperature region and that varies from 0.03 to 0.09 eV at lower temperature region. The maximum value of E_a of CuO thin film is found to be at higher temperature region is 0.30 eV for 0.10 M and T_s of 350 °C. This value of E_a is assumed due to the stoichiometry of the CuO thin films. From SEM and EDX observations, it is also found that CuO thin films are stoichiometric. The low value of E_a referred to be due to lower crystallinity of the thin film [19] prepared by spin coating technique using copper acetate as precursor. The Figure of merit is well-known as an index for evaluating the performance of transparent conducting films. It has been expressed by equation in chapter II. Fig. 4.26 shows the Figure of merit values of CuO thin films deposited at various T_s and it is $0.14 \Omega^{-1}\cdot\text{cm}^{-1}$ at T_s of 350 °C. The increase in the Figure of merit of the CuO thin films is mainly due to the increase in the optical transmittance with increasing T_s up to 350 °C, beyond this T_s it is decreased. This result is comparable with the reports of ref. [20], where CuO thin films were deposited on glass substrates at various growth temperatures by reactive RF magnetron sputtering using Cu target. The maximum value of the Figure of merit, $0.17 \Omega^{-1}\cdot\text{cm}^{-1}$ was obtained for the CuO film deposited at 350 °C. The experimental data suggest that T_s of 350 °C is the best condition for depositing high-quality CuO thin films.

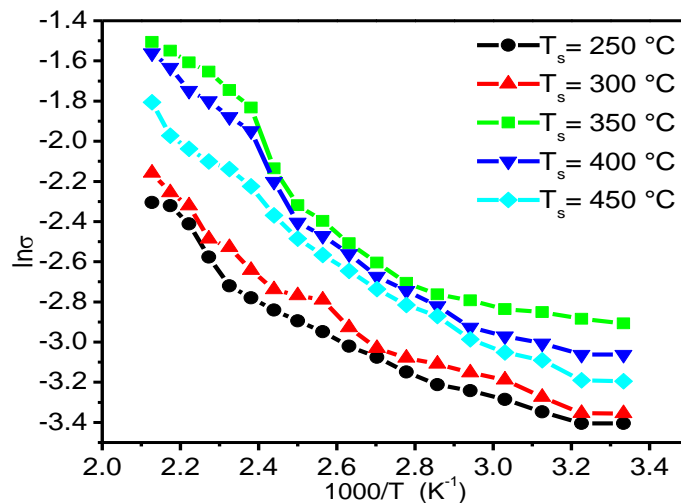


Fig. 4.24 Variation of $\ln\sigma$ for CuO thin films with respect to inverse of temperature at various T_s of CuO thin films (MC = 0.10M)

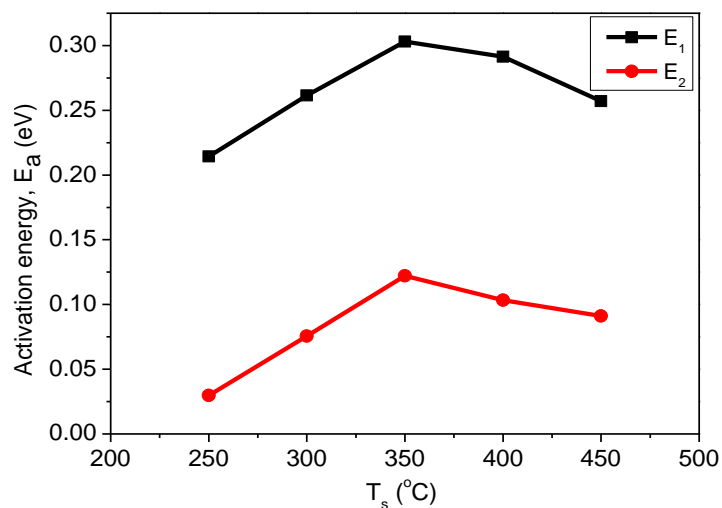


Fig. 4.25 Variation of activation energy with T_s for CuO thin films (MC = 0.10M)

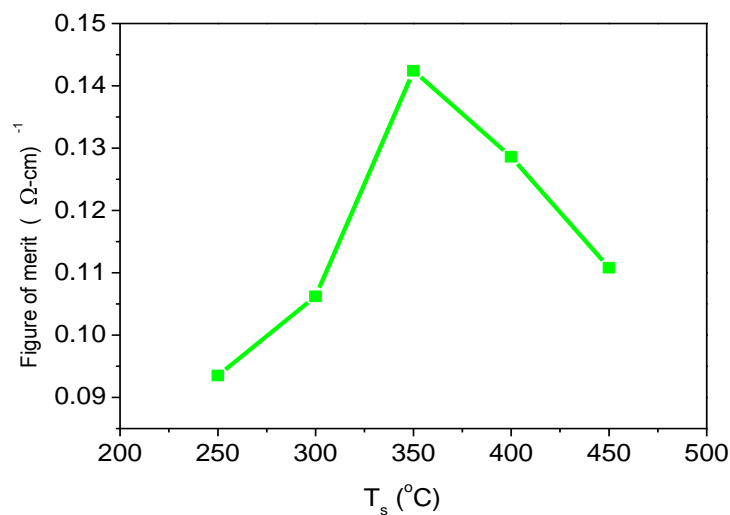


Fig. 4.26 Variation of Figure of merit with T_s for CuO thin films (MC = 0.10M)

4.2.3 Summary of Findings on CuO Thin Films

CuO thin films have been deposited using SPT by variation of MC from 0.05 to 1.5 M different at T_s from 250 to 450 °C. The SEM images and EDX analyses of CuO thin films reveal that deposited films are stoichiometric. Structural analysis confirmed that CuO thin films were monoclinic structure with planes at (110), (002), (111), (200), (202), and (020). It is observed that CuO thin film prepared with 0.10 M at T_s of 350 °C is a good stoichiometric and homogeneous one and is highly oriented along the CuO (111) plane. The average D is about 9.5743 Å and the average T is 75% in the wavelength range of 800-1100 nm for the film deposited at 350 °C. The E_g is 1.6 eV for MC of 0.10 M. The E_g varies from 1.90 to 1.65 eV and the k increases with the increase of T_s . The lowest value of n is 2.68 for thin film prepared with 0.10 M at T_s of 350 °C. The CuO thin film with these E_g values is a good absorber material for solar cell application. The ρ of CuO thin film is 30.09 Ω -cm for T_s of 250 °C and it is reduced as T_s increases so that the minimum ρ is found to be 18 Ω -cm for MC of 0.10 M and T_s of 350 °C. The E_a is varying from 0.21 to 0.26 eV at high temperature region and 0.03 to 0.09 eV at lower temperature region. The maximum value of E_a of CuO thin film is found to be 0.30 eV at higher temperature region for 0.10 M and T_s of 350 °C. The highest Figure of merit is found for the films grown from 0.10 M solution at T_s of 350 °C with an optical transmittance about 76% in the wavelength range of 800-1100 nm. Thus the crystalline phases, morphology, optical, and electrical properties of the prepared CuO thin films are found to be significantly influenced by the change in MC and T_s . The results suggest that high-quality CuO thin film can be produced from MC of 0.10 M solution of $\text{Cu}(\text{CH}_3\text{COO})_2 \cdot \text{H}_2\text{O}$ at T_s of 350 °C. The obtained experimental results compared with others, it can be inferred that prepared CuO thin films are bearing good quality. This synthesized alloy compound could be environmental friendly and suitable as a potential buffer layer in the fabrication of heterojunction solar cells and optoelectronic devices.

4.3 Results and Discussion on TiO₂ Thin Films

4.3.1 TiO₂ Thin Films Synthesized from Aqueous Solutions of Different Molar Concentrations at T_s of 400 °C

4.3.1.1 Surface Morphology and Elemental Analysis

SEM images of the TiO₂ thin film deposited from MC of solutions (0.05 - 0.15M) at T_s of 400 °C on to glass substrates are shown in Fig. 4.27. It is observed that the surface morphology of the thin films is uniform and homogeneous without any crack over a wide area. As the MC increased, the number density and the size of TiO₂ particles increased. TiO₂ thin films for the MC of 0.10M, very fine particles were observed and very densely packed columnar crystals with a prismatic top structure became dominant. These grains correspond to small aggregates of microcrystallites visualized by SEM. These results suggest that the specific surface area increased significantly in the early stage of TiO₂ film growth, however, the specific surface area may have been maintained almost constant after MC of 0.10 M. So, surface studies of TiO₂ thin films by SEM reveals a homogeneous growth on the entire surface with in the field of view.

The wt % of the elements determined by EDX is reported in Table 4.3. Table.4.3 shows the presence of titanium (Ti) and oxygen (O), which confirm that the TiO₂ thin films prepared through the chemical oxidation route are free from impurities.

Table 4.3 Quantitative results of TiO₂ thin films for various MCs (T_s =400 °C)

MC (M)	wt % of element	
	Ti	O
0.05	55.66	44.34
0.075	59.55	40.45
0.10	67.34	32.66
0.15	64.68	35.32

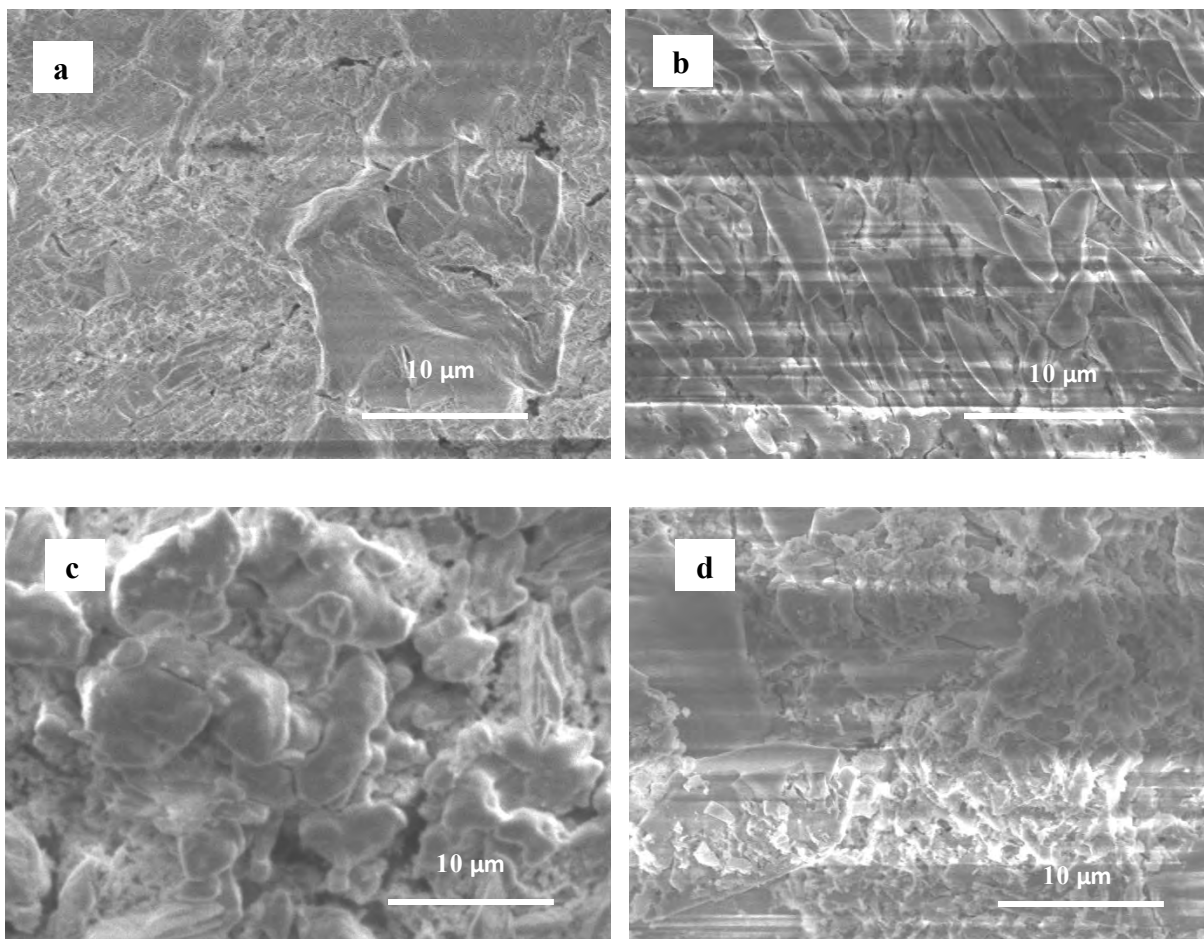


Fig. 4.27 SEM image of TiO_2 thin films deposited at T_s of $400\text{ }^\circ\text{C}$ for MC of (a) 0.05, (b) 0.075 (c) 0.10 and (d) 0.15M

4.3.1.2 Structural Analyses

Fig. 4.28 presents the XRD patterns of the TiO_2 thin films for four different MCs. The diffused XRD pattern of as deposited film grown for 0.05M concentration of solution indicate that the film is amorphous in nature. However, the diffraction peaks observed at 2θ values of 25.25 , 38.05 , and 48.5° correspond to the diffraction lines produced by (101), (004), and (200) planes of the tetragonal structure with anatase phase [21] for $\text{MC} > 0.05\text{ M}$ and the diffraction data are in good agreement with TiO_2 thin films prepared using reactive RF magnetron sputtering [22]. The XRD patterns with higher MC show that the TiO_2 film contains only anatase, which is well known as the most suitable structure for the photocatalysis. It is found that the initiation of the crystalline phase occur at MC of 0.075

M. The lower concentration (0.05 M) was insufficient for the crystallization of TiO₂ thin films. The solution concentration has great impact on the crystallization. The well defined reflection (101) of the TiO₂ thin films could be indexed in terms of the anatase phase lattice as identified for the precursor concentration of 0.10 M. The D was obtained by Debye-Scherrer formula [23]. The D and the lattice constants (a = b, c) are calculated from the peak (101) of the XRD patterns and these values are given in Table 4.4. It can be noticed in Table 4.4 that D increases as MC increases and the crystallinity and homogeneity of the TiO₂ thin films improves progressively with increasing MC. This may be due to gaining enough energy by the crystallites to orient in proper equilibrium sites, resulting in the improvement of crystallinity and degree of orientation of the TiO₂ thin films [24]. The D of TiO₂ thin films is 13.51 nm, which is smaller than the commercially available one (26.7 nm) and smaller than 15.9 nm of TiO₂ thin films prepared by spin coating method from TiCl₄ [25].

Upon increasing the precursor concentration from 0.075 to 0.10 M, the D increases from 11.21 to 13.51 nm due to particle residence time. Similar result was observed by the authors of ref. [26], where TiO₂ thin films were produced from TiCl₄ (as precursor) by diffusion flame technique. These findings are similar to the well defined reflections of TiO₂ anatase phase thin films prepared by SPT from precursor concentration of 0.10 M of titanium tetra isopropoxide [27].

Table 4.4 D and lattice constants of the TiO₂ thin films for various MCs (T_s = 400 °C)

MC (M)	0.05	0.075	0.10	0.15
D (nm)	-	11.2134	13.5138	13.3514
a (Å)	-	3.7870	3.8067	3.7621
c (Å)	-	9.5194	9.1021	8.9745

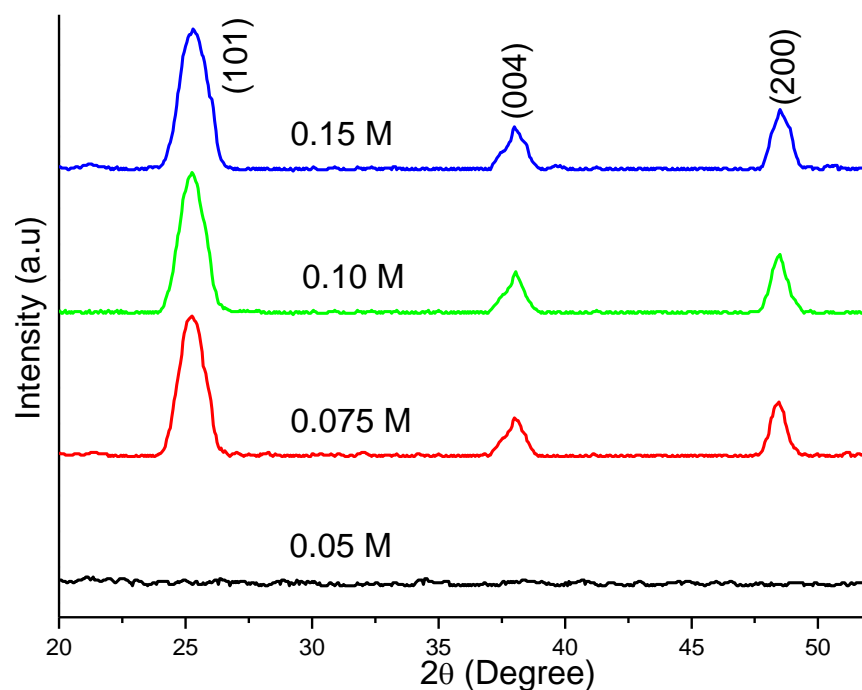


Fig. 4.28 XRD patterns of TiO₂ thin film synthesized from various MCs ($T_s = 400\text{ }^\circ\text{C}$)

4.3.1.3 Optical Properties

4.3.1.3.1 Transmittance and Optical Band Gap

The variation of optical transmission (T) as a function of wavelength was recorded for TiO₂ thin films prepared from MC of 0.05-0.15 M and is presented in Fig. 4.29. It can be noticed that the values of T are high in the visible and NIR regions (600-1100 nm). It is observed that T is greater than 70% in the visible and NIR region for films prepared with solution of 0.10 M. An average of 75 to 80% T is observed in the wavelength range of 800-1100 nm and below 600 nm T decreases gradually. The T increases from 15 to 20% with the increase of MC, and shows the highest T of about 88 % for the thin films grown with MC of 0.10 M. The shift in the fundamental absorption edge is due to the small structural changes as revealed by XRD analysis. The increase in T may be due to the transition of the TiO₂ films from amorphous to polycrystalline structure. A relatively high T value for the thin film deposited with MC of 0.10 M may be attributed to less scattering due to the decrease in the degree of irregularity in the grain size distribution. The T of the films is also influenced by a number of effects, which include surface roughness and optical inhomogeneity in the

direction normal to the film surface [28]. The T values are decreased for the next higher level of MC of 0.15 M. The α vs. wavelength curves of TiO_2 thin films for various MCs are shown in Fig.4.30. It is observed that α first increases slowly in the low energy region and then increases sharply near the absorption edge. So the value of α depends on MC of the solutions. From both the figures it is observed that the α first increases slowly in the low energy region i.e. in the high wavelength region and then increases sharply near the absorption edge so the value of the α depends on MC.

Fig. 4.31 shows the variation of $(\alpha h\nu)^2$ with $h\nu$ for various MCs of the solutions of TiO_2 thin films. The dependence of E_g of the TiO_2 thin films obtained from Fig. 4.1 with MC of solution is plotted in Fig. 4.32. It is seen that E_g of TiO_2 thin film deposited from MC of 0.05 M is 3.65 eV. Then a minimum value of 3.40 eV is observed for TiO_2 thin film deposited from MC of 0.10 M. It can be seen that E_g tuning of 0.25 eV is observed when the MC is changed by about 0.05 M.

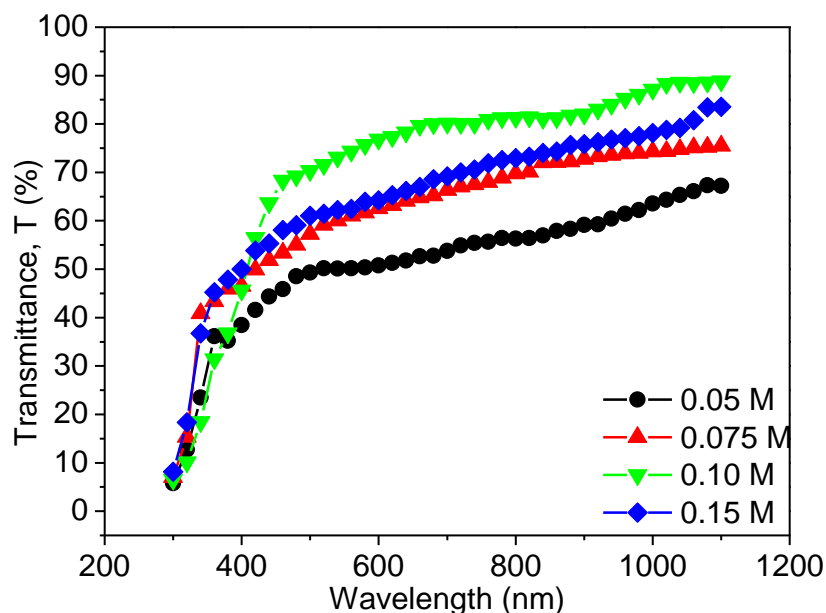


Fig. 4.29 Optical transmittance vs. wavelength TiO_2 thin films for various of MCs ($T_s = 400^\circ\text{C}$)

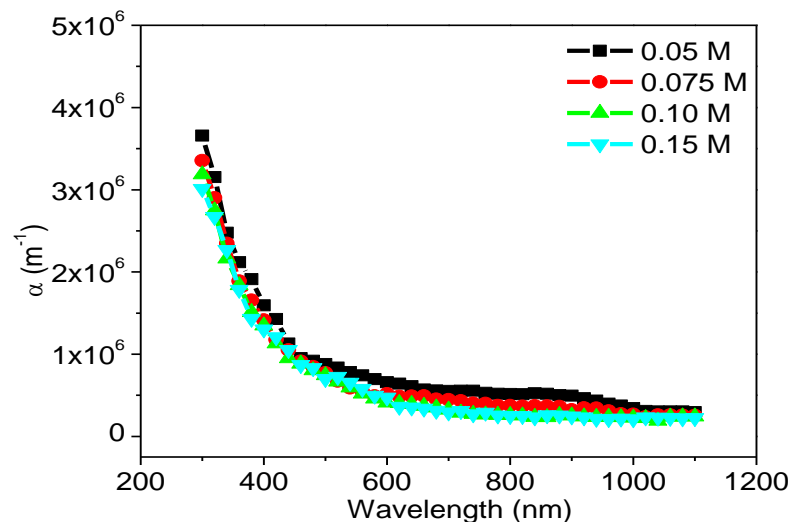


Fig. 4.30 Absorption coefficient vs. wavelength of TiO_2 thin films for various MCs ($T_s = 400^\circ\text{C}$)

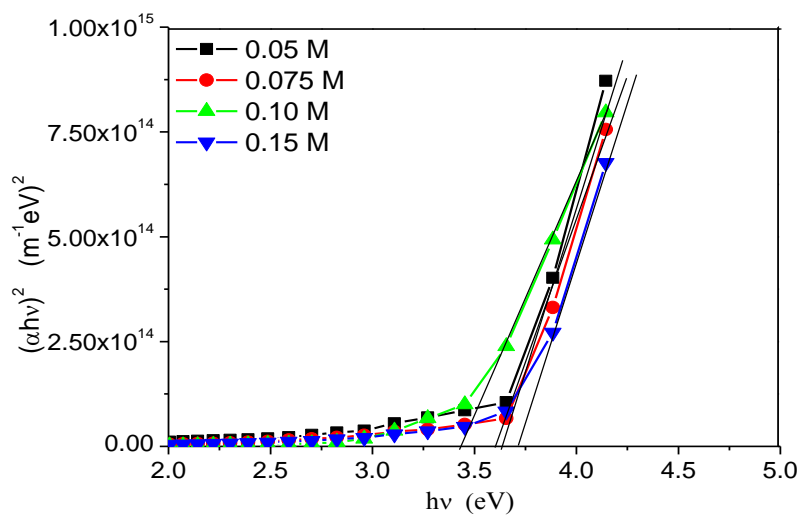


Fig. 4.31 Variation of $(\alpha h\nu)^2$ with $h\nu$ for various MCs of solution of TiO_2 thin films ($T_s = 400^\circ\text{C}$)

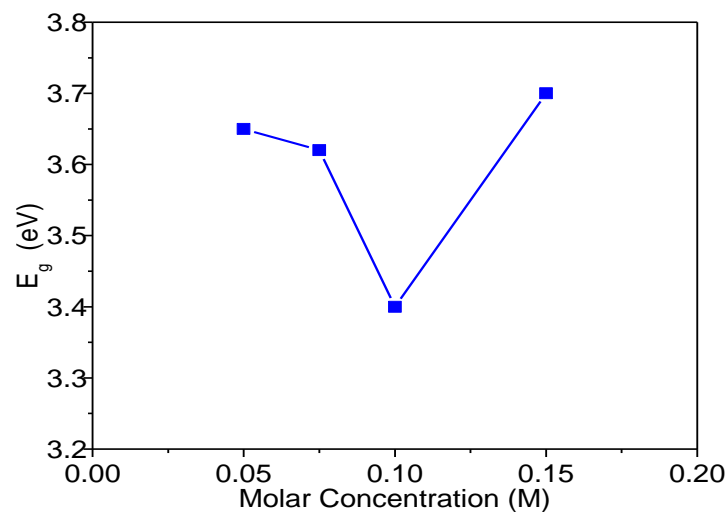


Fig. 4.32 Variation of E_g with MC of TiO_2 thin films ($T_s = 400^\circ\text{C}$)

4.3.1.3.2 Refractive Index and Extinction Coefficient

The refractive index, n of TiO_2 thin films increases with T_s , as shown in Fig. 4.33. The value of n of TiO_2 thin film has been obtained to be 2.76 for MC of 0.05 M and it becomes lowest, 2.55 for MC of 0.10 M. This value is lower than that of the reported value 2.80 of TiO_2 thin film prepared by DC magnetron sputtering [28] and it is lower than that of bulk 2.61 TiO_2 [29]. It is also observed that n increases for MC of 0.15 M, which may be due to the increase of inhomogeneity and surface roughness of the thin films.

The variation of extinction coefficient, k with $h\nu$ is presented in Fig. 4.34. It is observed that k decreases with the increase of MC. The increase and decrease of k directly related to the absorption of light. The k of about 0.04 in the wavelength region of 500-1100 nm is very close to that of the reported value of TiO_2 thin films prepared by DC magnetron sputtering method [28]. The low value of n and k may probably be due to the lower density of the films. T and n in wavelength ranging from 400 to 700 nm and E_g of the TiO_2 thin film for various MC are recorded in Table 4.5.

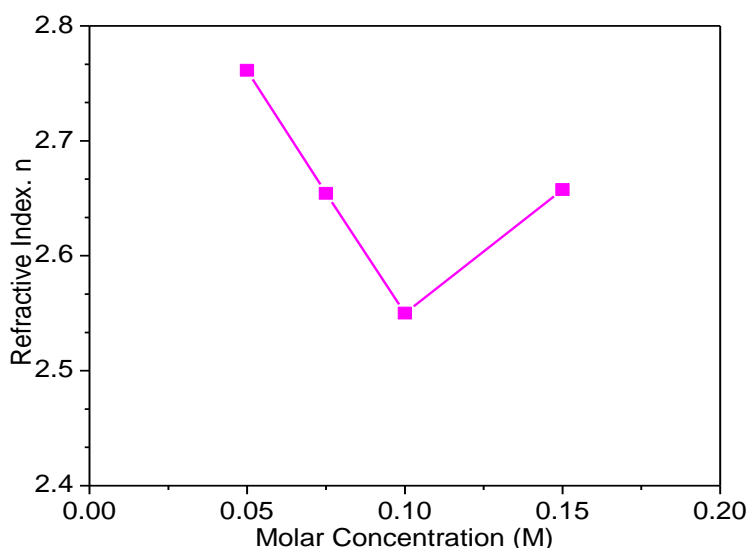


Fig. 4.33 Variation of n with MC of TiO_2 thin films ($T_s = 400\text{ }^\circ\text{C}$)

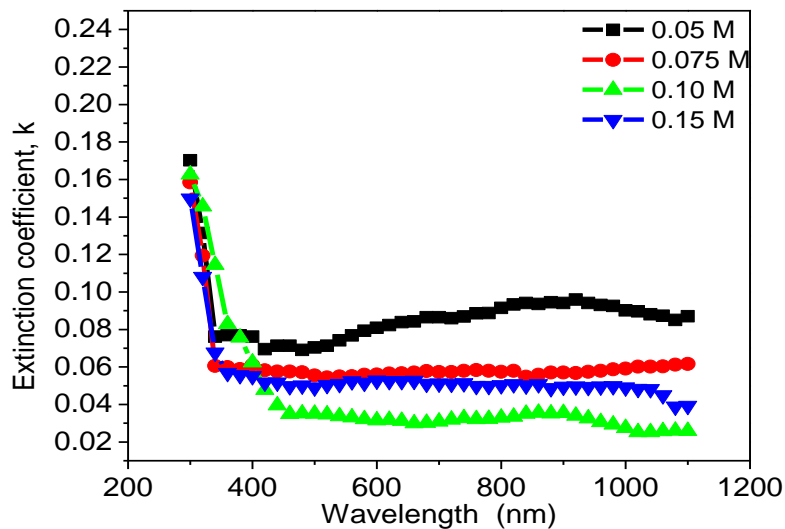


Fig. 4.34 Variation of k with wavelength for various MCs of the solution of TiO_2 thin films ($T_s = 400\text{ }^\circ\text{C}$)

Table. 4.5 Values of maximum $T(\lambda)$, E_g , and n of the TiO_2 thin films for various MCs ($T_s = 400\text{ }^\circ\text{C}$)

MC (M)	0.05	0.075	0.10	0.15
T (%) (800-1100 nm)	0.67	0.75	0.89	0.84
E_g (eV)	3.65	3.62	3.40	3.70
n	2.76	2.65	2.55	2.66

4.3.1.4 Electrical Properties

The electrical characterization of TiO_2 thin films prepared from various MC of precursor solution was done by van der Pauw method [30]. The dependence of the resistivity, ρ of TiO_2 thin films on the absolute temperature and MC are shown in Fig.4.35 and Fig. 4.36 respectively. These studies reveal that MC has a considerable effect on the electrical properties of TiO_2 thin films. Generally, the σ in semiconductor is caused by thermal excitation of electron, impurities and lattice defects such as dislocation, stacking faults microtwines, etc. [8]. The increase of σ with temperature may be due to the increase of carrier mobility or due to increase of carrier concentration from neutral defects and stoichiometric changes of the films. This is clearly understood from Fig. 4.28, where one can see a single phase structure of TiO_2 thin film, the single phase structure enhances the

electron mobility thus improve the conductivity [31-32]. In the present study 0.10 M film has the highest electrical conductivity and lowest electrical resistivity. This may be due to the highest grain size of 0.10 M film. The increase of grain size may be due to the improved crystallinity of 0.10 M film. The growth in grains leads to the reduction of grain boundary scattering which decreases the resistivity for the films and eventually the increase in the conductivity of the films.

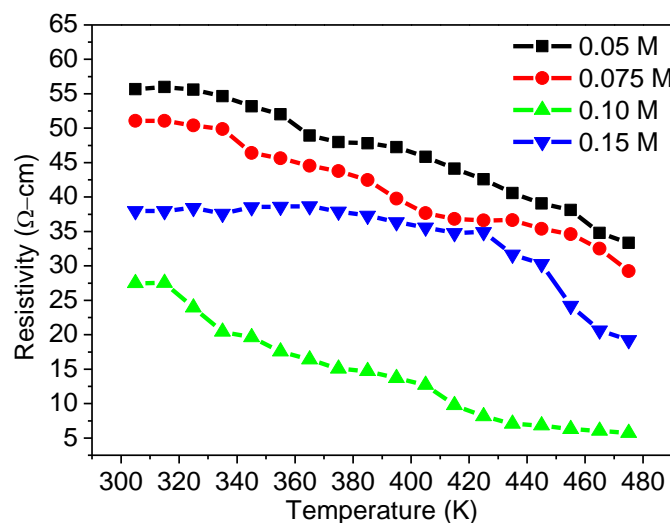


Fig. 4.35 Electrical resistivity vs. absolute temperature TiO₂ thin films ($T_s = 400\text{ }^\circ\text{C}$)

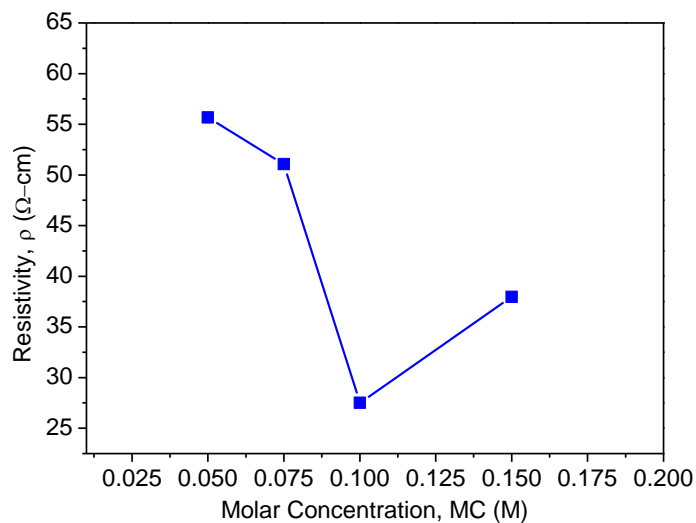


Fig. 4.36 Room temperature electrical resistivity vs. MC of TiO₂ thin films ($T_s = 400\text{ }^\circ\text{C}$)

Fig. 4.37 shows electrical conductivity ($\ln\sigma$) vs. inverse of absolute temperature for various MCs of the solution of TiO₂ thin films. The E_a was calculated from the slopes of $\ln\sigma$ vs

1000/T plots of Fig. 4.37 using the Arrhenius relation [33]. Fig. 4.38 shows the E_a of TiO_2 thin films for various MCs. The conduction mechanism can be explained in terms of hopping through a band of localized states and carriers to the band edges.

Fig. 4.39 shows the Figure of merit values of TiO_2 thin films for various MC. This value is well cumulative with TiO_2 thin films prepared by sputtering [34]. The increase in the Figure of merit of the TiO_2 thin films is mainly due to the increase in the optical transmittance with increasing MC. The experimental data suggest that MC of 0.10 M is the best MC with other conditions for depositing high-quality TiO_2 thin films.

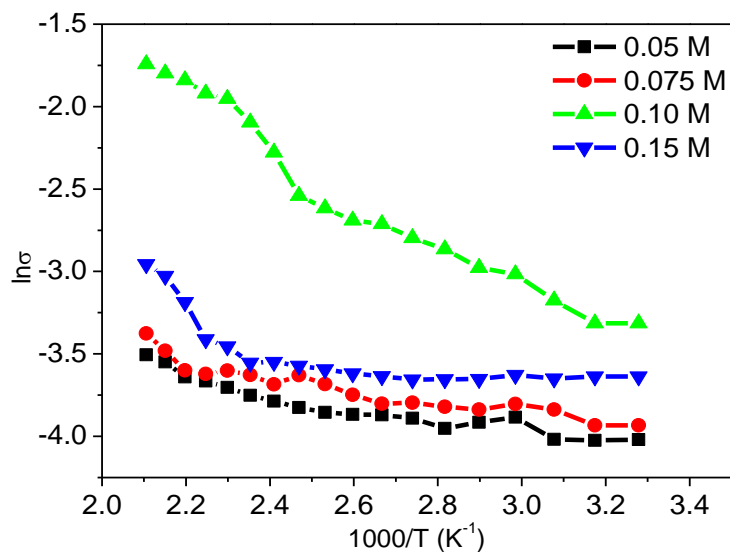


Fig. 4.37 $\ln\sigma$ vs. inverse of absolute temperature for various MCs of TiO_2 thin films ($T_s = 400$ °C)

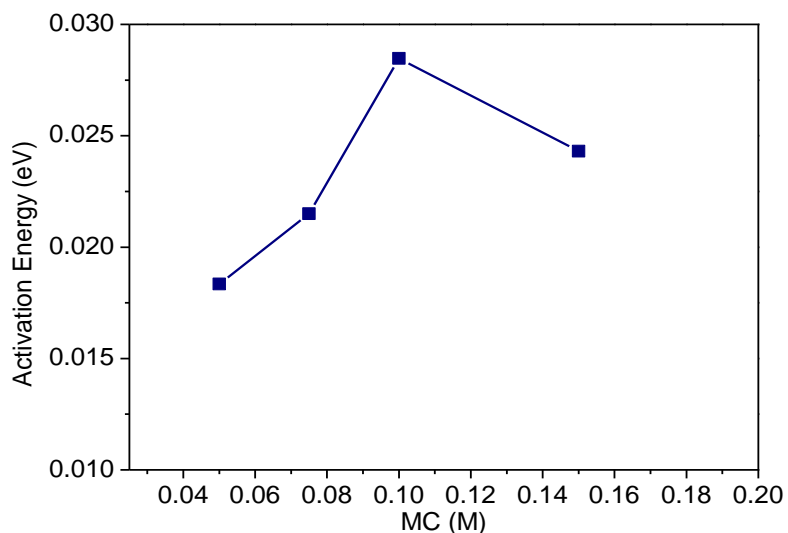


Fig. 4.38 Variation of activation energy vs. MC of TiO_2 thin films ($T_s = 400$ °C)

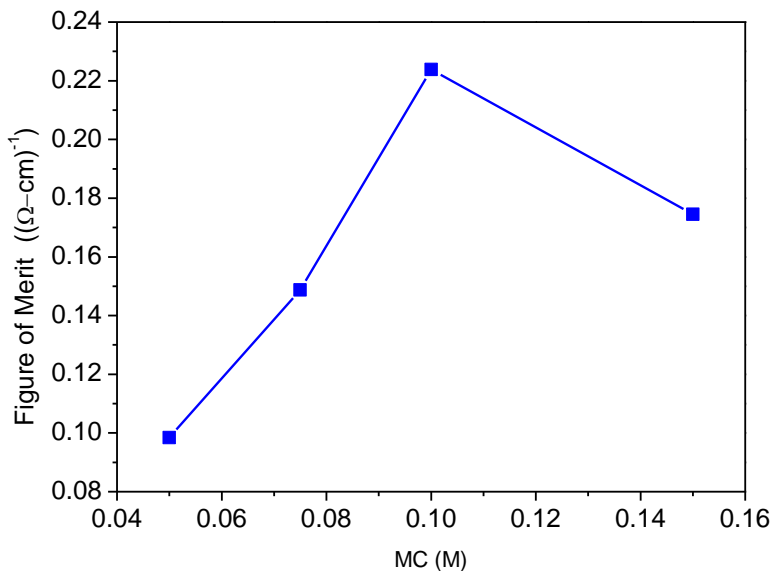


Fig. 4.39 Variation of Figure of merit with MC the solution of TiO₂ thin films ($T_s = 400$ °C)

4.3.2 TiO₂ Thin Films Synthesized Using MC of 0.10 M at Different T_s

4.3.2.1 Surface Morphology and Elemental Analyses

SEM images of the TiO₂ thin films are presented in Fig. 4.40. The surface of the thin films is uniform and homogeneous with grains. SEM images reveal that sprayed particles (atoms) are absorbed onto the glass substrate into clusters as the primary stage of nucleation and finally form grain agglomerate. It is observed that the coating is transparent. From SEM micrographs, it is seen that agglomerates become larger as T_s increases up to 450 °C and D increases. This change corresponds to the change in D, as seen present in Table 4.7. EDX analysis reveals the presence of Ti and O and confirms the formation of TiO₂ thin films through the chemical oxidation route free from impurities (Table.4.6).

Table 4.6 Quantitative results of TiO₂ thin films at various T_s (MC = 0.10 M)

T_s (°C)	wt % of element	
	Ti	O
250	62.63	37.37
300	64.74	35.26
350	66.45	33.55
400	67.34	32.66
450	67.88	32.12

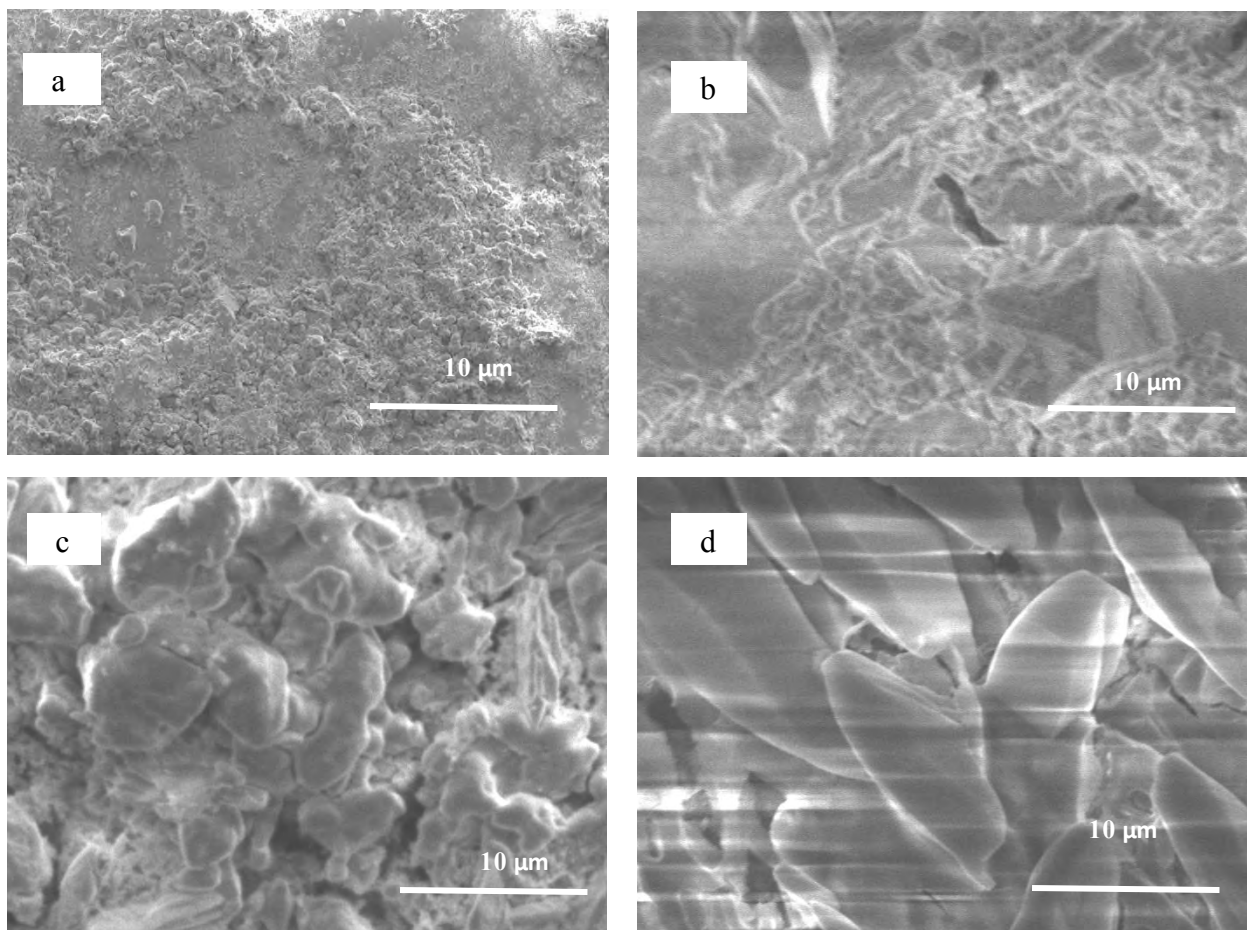


Fig.4.40 SEM images of TiO₂ thin films at T_s of (a) 250 (b) 350 (c) 400 and (d) 450 °C (MC=0.10M)

4.3.2.2 Structural Analyses

XRD patterns of TiO₂ thin films synthesized at different T_s are illustrated in Fig. 4.41. These indicated that TiO₂ thin film prepared at T_s of 250 °C was amorphous whereas those prepared at T_s viz, 300, 350, 400 and 450 °C were crystalline nature and there was no indication of other crystalline by-products. The diffraction peaks observed at 2θ values of 25.25, 38.05, and 48.50° correspond to the diffraction lines produced by (101), (004), and (200) planes of the tetragonal structure with anatase phase (JCPDS card No. 21-1272) and the diffraction data are in good agreement with TiO₂ thin films prepared by sol-gel method [23]. Strong diffraction peaks at 25° and 48° are indicating TiO₂ in the anatase phase [38]. With the increase of T_s there is an increase in intensity and sharpening of this peak, which is caused by improvement of crystallinity of the films. These diffraction patterns show that

the TiO₂ thin film contains only anatase phase, which is well known as the most suitable structure for the photocatalysis. This thin film is better when compared to the TiO₂ thin films prepared by plasma-enhanced atomic layer deposition (PE-ALD) using Ti(NMe₂)₄ [tetrakis(dimethylamido) Ti] and O₂. In that study, film deposited below 200 °C was amorphous, while the films deposited at 300 and 400 °C showed anatase and rutile phases, respectively [36]. It can be noted that prepared TiO₂ thin films by SPT is better than TiO₂ thin film by sol-gel process using dip coating method onto glass substrates from tetra-n-butylorthotitanate as precursor [37]. The (101) surface of TiO₂ thin film is energetically the most stable and the predominant crystal face found in polycrystalline samples. From XRD data of TiO₂ thin films, D and lattice constants (a = b, c) are calculated using equation 2.4 and 2.6 given in chapter II, and these values of D, a and c are depicted in Table 4.7. No trace of rutile phase was found in the TiO₂ thin films regardless of T_s. The increase of T_s increases the intensity of the peaks. It is due to the increases of crystallinity of the TiO₂ progressively with T_s. It is noticed that no additional XRD peaks appear corresponding to T_s > 250 °C. The values of average D is in the range 12.74–13.05 nm for T_s of 300 to 450 °C. This means that the homogeneity of the thin film is improved with substrate heating at higher temperatures during the film deposition. As a result, the defects are in favorable condition for the merging process to form larger TiO₂ grains while increasing T_s. It implies that the crystallinity of the TiO₂ thin films is improved at higher T_s. The coagulation or aggregation of particles leads to the formation of larger particles due to higher chances of collisions among the particles [40]. It was reported that TiO₂ thin films prepared from the solution containing titanium (IV) isopropoxide, acetylacetonate and ethanol onto n-type Si(100) and HD Si(100) wafers at T_s < 500 °C, TiO₂ thin films obtained were amorphous and at 500 °C films were crystalline phase [41]. So it can be mentioned that the TiO₂ thin films synthesized in the present study are better because these are in anatase phase at T_s of 400 °C without annealing.

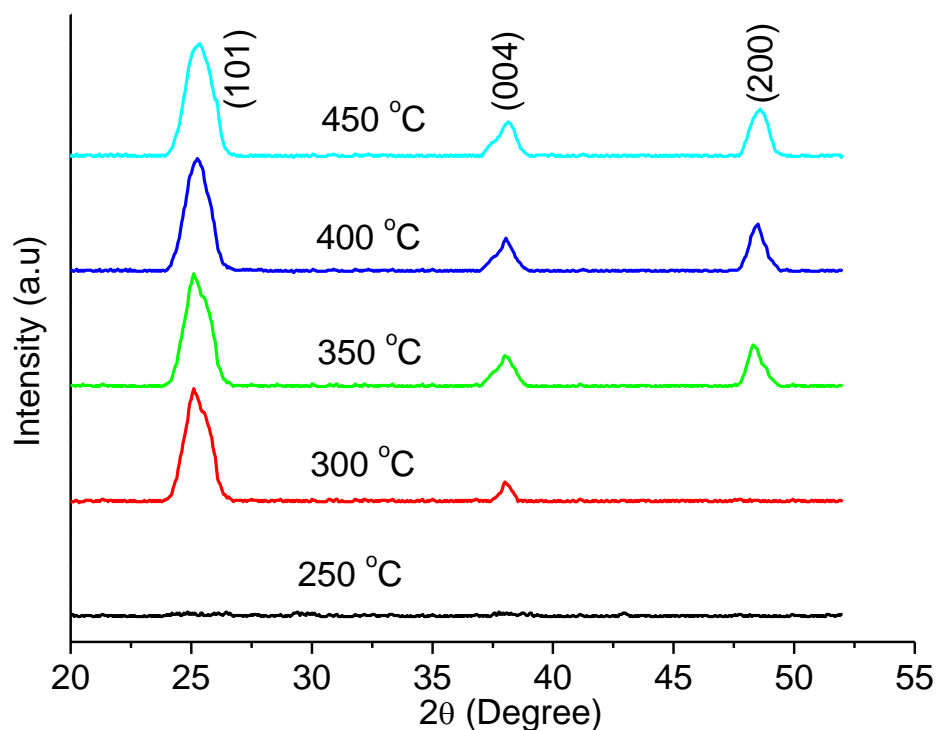


Fig. 4.41 XRD patterns of TiO₂ thin film synthesized at various T_s (MC = 0.10 M)

Table 4.7 Crystallite size and lattice parameters for the TiO₂ thin films synthesized at various T_s (MC= 0.10 M)

T _s (°C)	250	300	350	400	450
D (nm)	-	12.7417	12.8498	13.5138	13.0451
a (Å)	-	3.7870	3.7829	3.8072	3.8035
c (Å)	-	9.5194	9.0856	8.9276	8.9640

4.3.2.3 Optical Properties

4.3.2.3.1 Transmittance and Optical Band Gap

Transmission spectra were taken in the range of 300 to 1100 nm for TiO₂ thin films prepared at T_s of 250 to 450 °C and are shown in Fig. 4.42. It is seen from Fig. 4.42 that the value of T is high in the visible and NIR regions. About 75 to 85% T is observed in the wavelength range of 800-1100 nm and below 600 nm, T decreases gradually. The T increases from 10 to 15% with T_s, and shows the highest T of about 88 % for the thin films grown at T_s of

400 °C. The shift in the fundamental absorption edge may be due to the change in crystallite size as revealed by XRD analysis. The T of the films is also influenced by a number of effects, which include surface roughness and optical inhomogeneity in the direction normal to the film surface. The increase in transmittance may be due to the transition of the TiO_2 films from amorphous to polycrystalline structure and relatively high transmittance may be attributed to less scattering due to the decrease in the degree of irregularity in the grain size distribution [42]. Fig. 4.43 shows the $(\alpha h\nu)^2$ as a function of $h\nu$ for the TiO_2 thin films deposited at various T_s . The α was found in the order of 10^5 m^{-1} which may be suitable for a transparent conducting film. In Fig. 4.43, it is observed that α first increases slowly in the low energy region and then increases sharply near the absorption edge, so the value of the α depends on T_s . The E_g of the TiO_2 thin films decreases when T_s increases. At T_s of 250°C the E_g was found to be 3.62 eV and a minimum value 3.40 eV was observed at T_s of 400 °C, as seen in Fig. 4.44. The value of E_g for T_s of 450 °C is same as those of TiO_2 thin films prepared at T_s of 400 °C. It can be seen that a band gap tuning of 0.22 eV is possible when T_s is changed by about 150 °C by increasing T_s . It may be due to some modification in surface morphology and structure of the TiO_2 thin films. The observed E_g values are in good agreement with the reported values 3.60 to 3.40 eV ($T_s = 375 - 475$ °C) of TiO_2 thin films prepared by SPT [15].

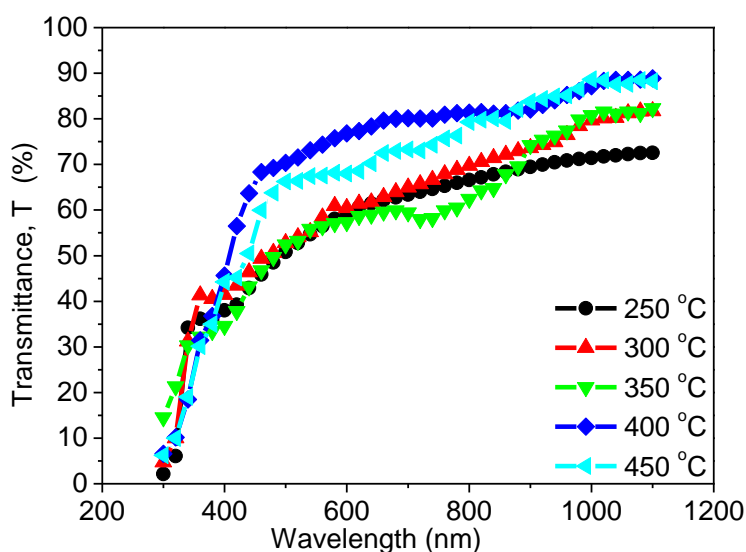


Fig. 4.42 Optical transmittance vs. wavelength for TiO_2 thin films synthesized at various T_s (MC = 0.10 M)

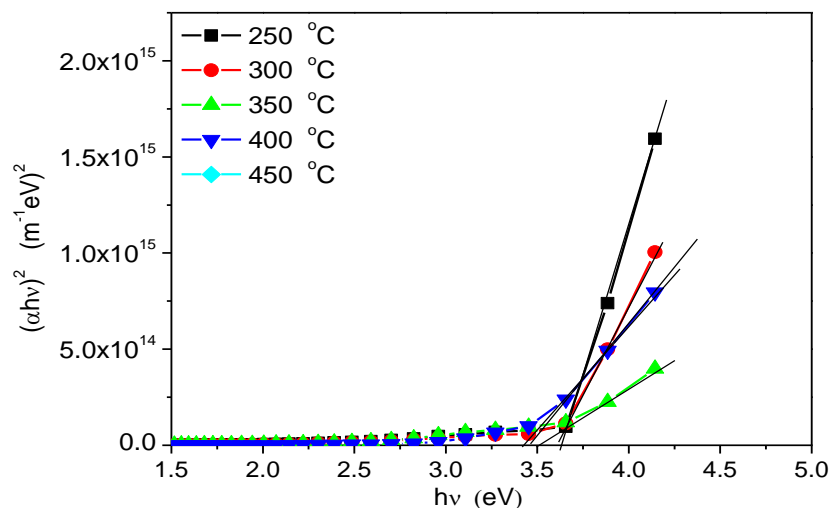


Fig. 4.43 Variation of $(\alpha hv)^2$ with $h\nu$ for TiO_2 thin films synthesized at various T_s (MC = 0.10 M)

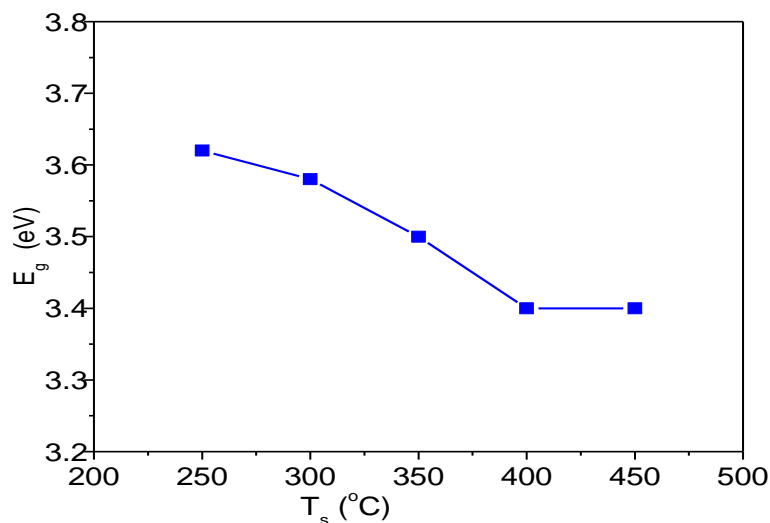


Fig. 4.44 Variation of E_g with T_s of TiO_2 thin films synthesized at various T_s (MC = 0.10 M)

4.3.2.3.2 Refractive Index and Extinction Coefficient

The n for TiO_2 thin films decreases with increasing T_s , as shown in Fig. 4.45. The n of TiO_2 thin film is obtained to be 2.75 at T_s of 250 °C and it becomes lowest 2.55 at T_s of 400° C. This value agreed well with the n values for TiO_2 thin film synthesized using titanium (IV) isoprop-oxide as a precursor by spin coating method [42]. The low value of n may probably be due to the smaller density of the films which is suggested by Arai [43]. The decrease of n with T_s may be due to the decrease of defects in the thin films. The variation of k with wavelength is presented in Fig. 4.46. It is observed that k increases with

the increase of T_s . The k of about 0.05 in the range of wavelength 500-1100 nm is very close to the reported value of TiO_2 thin films prepared by sol-gel dip coating process deposited on glass substrate using titanium isopropoxide in isopropanol alcohol [44].

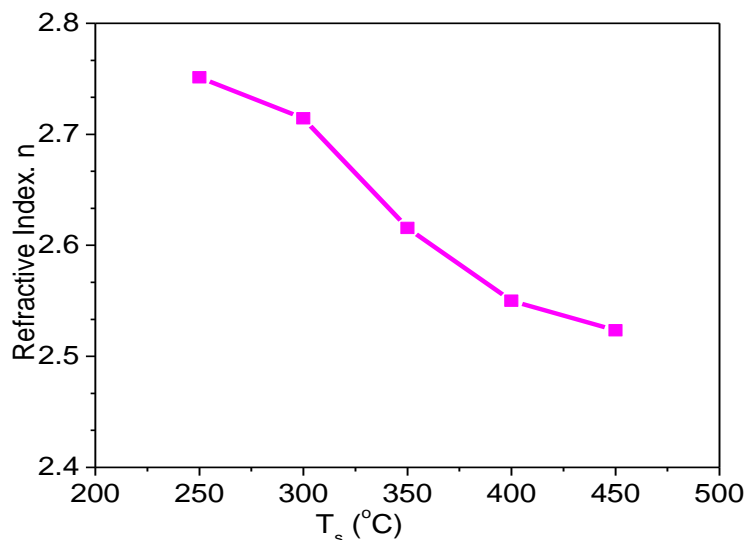


Fig. 4.45 Variation of n with T_s of TiO_2 thin films ($\text{MC} = 0.10 \text{ M}$)

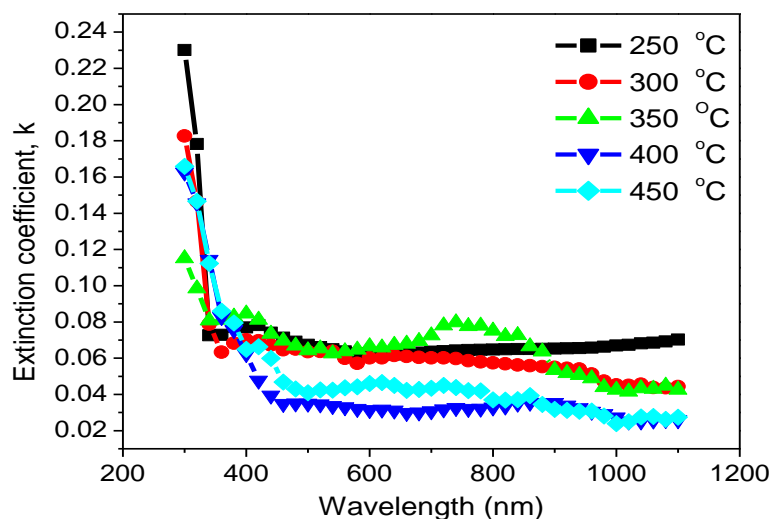


Fig. 4.46 Variation of k with $h\nu$ at various T_s for TiO_2 thin films ($\text{MC} = 0.10 \text{ M}$)

4.3.2.4 Electrical Properties

Variation of ρ of TiO_2 thin films synthesized with 0.10 M solution for different T_s with temperature is shown in Fig. 4.47. This behavior of TiO_2 thin films indicates semiconducting nature. The variation of room temperature ρ of TiO_2 thin films as a function of T_s is shown in Fig.4.48. It is observed that ρ of the TiO_2 thin films is decreased

with increasing T_s . The decrease of ρ means increase of σ with temperature which may be due to the increase of carrier mobility or due to increase of carrier concentration for neutral defects and morphological changes of the films. It may be due to increase in the free path of carrier concentration. The formation of these defects depends on the sticking coefficient, nucleation rates, etc. of the thin films on the hot substrate during deposition.

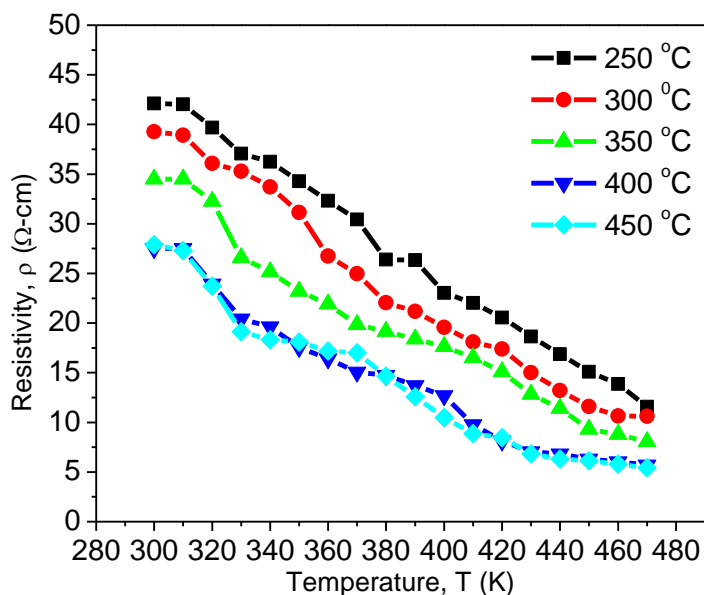


Fig. 4.47 Variation of ρ with room temperature for TiO_2 thin films at various T_s ($\text{MC}=0.10\text{M}$)

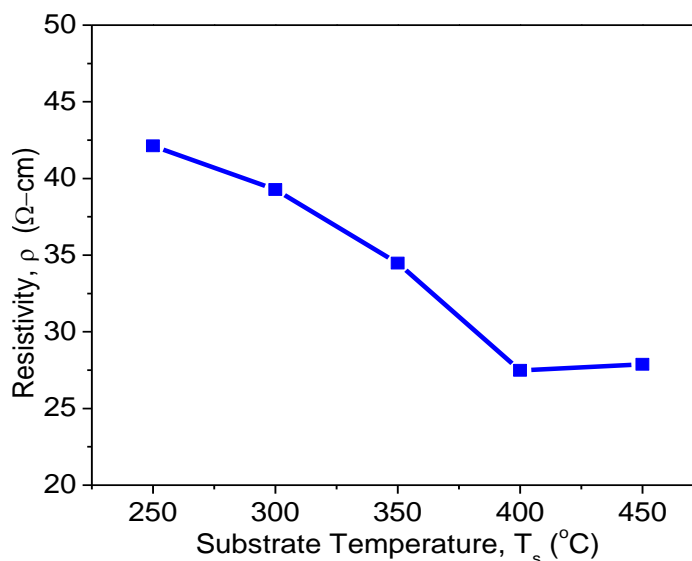


Fig. 4.48 Variation of resistivity at room temperature for TiO_2 thin films at various T_s ($\text{MC}=0.10\text{M}$)

The σ of the prepared TiO_2 thin films increases as T_s increases which is shown in Fig.4.49. At high temperature, the mechanism of impurity thermal activation becomes the dominant

one. TiO₂ thin films deposited at T_s of 400 °C has high electrical conductivity. The increase in σ is due to the increase in the crystalline nature as the T_s increases. Consequently, Ti⁴⁺ ions have more concentration in the films obtained at high T_s. Regarding the O²⁻ ions, which results in an increase of the free electron concentration after there is a decrease in the resistivity of the films [45-46]. On the other hand, the increase in the conductivity with temperature can also be explained as follows: the grain size increases with T_s which leads to a decrease in grain boundaries and so is the case in electrical resistivity [31, 39]. This is clearly understood from XRD patterns of TiO₂ thin films where one can see a single phase structure of TiO₂ thin film (Fig.4.41). It is established that the single phase structure enhances the electron mobility thus improve the conductivity [32]. So the high electrical conductivity has been found for TiO₂ thin films deposited at T_s of 400 °C.

E_a is calculated from the slope of the ln σ vs. (1/T) curves in Fig. 4.49 and the variation of E_a with different T_s is shown in Fig. 4.50. The low value E_a may be associated with the localized levels hopping due to the excitation of carriers from donor band to the conduction band. This low value of activation energy was assumed due to the nonstoichiometry of the TiO₂ thin film but in the present case the higher values of activation energy may suggest that the prepared samples are stoichiometric at higher T_s. From SEM and EDX observations, it is also found that TiO₂ thin films are stoichiometric.

The Figure of merit is well-known as an index for evaluating the performance of transparent conducting films, and it is given by the equation $F = (-\rho \ln T)^{-1}$ where ρ is the electrical resistivity and T is the average transmittance in the wavelength range of 800-1100 nm. Fig. 4.51 shows the Figure of merit values of TiO₂ thin films deposited at various T_s. The Figure of merit for the TiO₂ thin films deposited at T_s of 250 - 400 °C are found to be 0.0666 - 0.2238 $\Omega^{-1} \cdot \text{cm}^{-1}$. The increase in the Figure of merit of the TiO₂ thin films is mainly due to the increase in the optical transmittance with increasing T_s. The experimental data suggest that T_s of 400 °C is the best T_s with other conditions for depositing high-quality TiO₂ thin films.

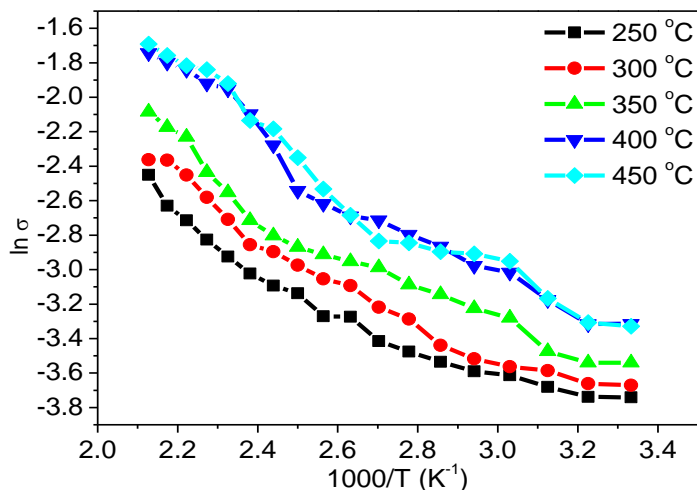


Fig. 4.49 Variation of $\ln \sigma$ with respect to inverse temperature T (K) for TiO_2 thin films at various T_s (MC=0.10 M)

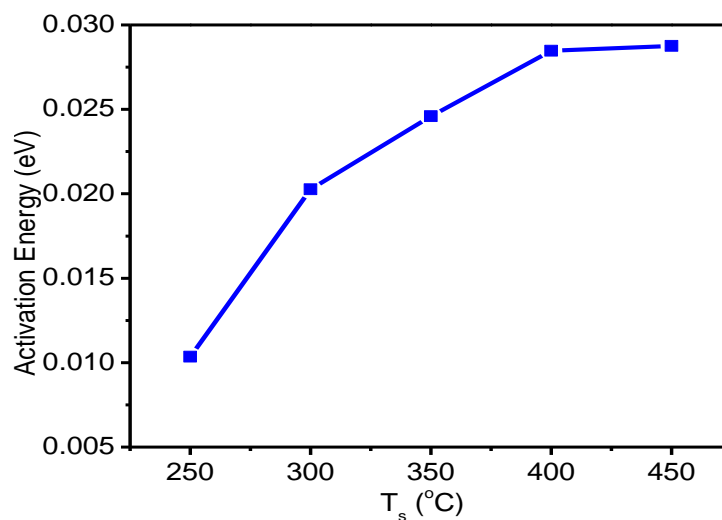


Fig. 4.50 Variation of activation energy with T_s of TiO_2 thin films (MC=0.10 M)

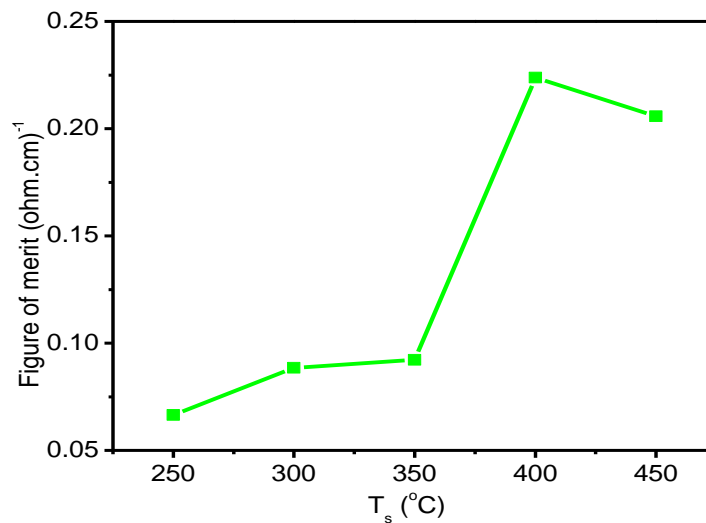


Fig. 4.51 Variation of Figure of merit with T_s of TiO_2 thin films (MC=0.10 M)

4.3.3 Summary of Findings on TiO₂ Thin Films

Transparent and homogeneous TiO₂ thin films have been synthesized using TiCl₄, ethanol and water solution by employing SPT at T_s from 250 to 450 °C and MC variation from 0.05 to 0.15 M. SEM images suggest that homogeneity of TiO₂ thin films improved with T_s and are stoichiometric. Elemental analysis clearly showed that the TiO₂ grains were typically comprised of both Ti and O. XRD data confirmed that the TiO₂ thin films were highly oriented along the plane (101). TiO₂ thin film prepared at T_s of 400 °C with 0.10 M is tetragonal structure. Strong diffraction peaks (101) and (200) at 25° and 48° respectively indicating TiO₂ in the anatase phase. The peaks were found to shift slightly from their standard positions at higher T_s, and there was some deviation in the lattice parameters. The average D was found to vary from 11.21 to 13.51 nm with increasing concentration. D is found to be around 13 nm for TiO₂ thin film deposited at T_s of 400 °C. The average T is 70-85% in the wavelength range of 800-1100 nm and the band gap energy shifts from 3.64 to 3.40 eV with the increase of T_s and MC. The n of the thin films is about 2.76 for MC of 0.05 M and 2.55 for MC of 0.10 M. The lowest value of E_g and n are 3.40 eV and 2.55 respectively for TiO₂ thin films deposited at T_s of 400 °C from solution of 0.10 M. The k values of the grown films indicated that the films are stronger absorbing medium in the lower wavelengths. The room temperature ρ varies from 42 to 27 Ω-cm for the thin films grown at different T_s and 55.67 to 37.96 Ω-cm for variation of MC from 0.05 to 0.15 M. The minimum ρ was found to be 27 Ω-cm for TiO₂ thin film deposited at T_s of 400 °C. E_a of TiO₂ thin films varies in the range of 0.010 to 0.028 eV for different T_s. The highest Figure of merit found for the film grown at 400 °C with an optical transmittance about 85% in the wavelength range of 800-1100 nm. The obtained experimental results compared with others, it can be inferred that prepared TiO₂ thin films are of good quality. The results suggest that high-quality TiO₂ thin film can be produced when deposited at a growth temperature of 400 °C. Finally, it is stated that the SPT could be employed for large-scale synthesis of TiO₂ films. The obtained experimental results also discuss the suitability of homogeneous TiO₂ thin films as transparent and conducting window materials in solar cells, gas sensors etc. applications.

4.4 Results and Discussion on Cu/TiO₂ Thin Films

4.4.1 Cu doped TiO₂ Thin Films Synthesized from Aqueous Solutions of (0 -10%) (Cu(CH₃COO)₂.H₂O) Doped in TiCl₄ of 0.10 M Molar Concentration at T_s of 400 °C

4.4.1.1 Surface Morphology and Elemental Analyses

To examine the surface morphology of the TiO₂ and Cu/ TiO₂ thin films, SEM images were recorded and the images are presented in Fig. 4.52. The surface of the TiO₂ thin films prepared at T_s of 400 °C is homogeneous and there are no clearly visible grains. This is in good agreement with TiO₂ thin films prepared by SPT at T_s of 410 °C using tetraisopropyl titanate as precursors [47]. SEM micrographs reveal the formation of particles with different shapes and sizes, and coalesced grain agglomerates. However, a comparative study shows that the morphology of particles depend on the precursor solution as well as Cu incorporation in TiO₂ matrix. After Cu doping the surface is flat and without any microcrack. This fact is in good agreement with the proposed growth mechanism, nucleation and the subsequent combination of the nuclei lead to a final film microstructure. The thin films consist of near-spherical particles with an average diameter. It is seen the SEM images that agglomerates become larger as Cu doping increases up to 8%. This change corresponds to the change in D as observed in XRD data in Table 4.9. If SEM images of prepared Cu/TiO₂ thin films are compared with the SEM images of hemin doped TiO₂ thin films, it is seen that the films obtained from hemin doped TiO₂ are homogeneous with amorphous background. But when these films were annealed above 400°C, exhibited a uniform distribution of grains with an average grain size of about 50 – 100 nm and shows the compact structure with the segregation of hemin atoms [48].

The presence of Ti and O in TiO₂ thin film and Ti, O and Cu in Cu/TiO₂ thin films was observed by EDX. EDX analysis reveals the presence of Ti, O and Cu in Cu/TiO₂ and confirms the formation of Cu/TiO₂ thin films (Table 4.8).

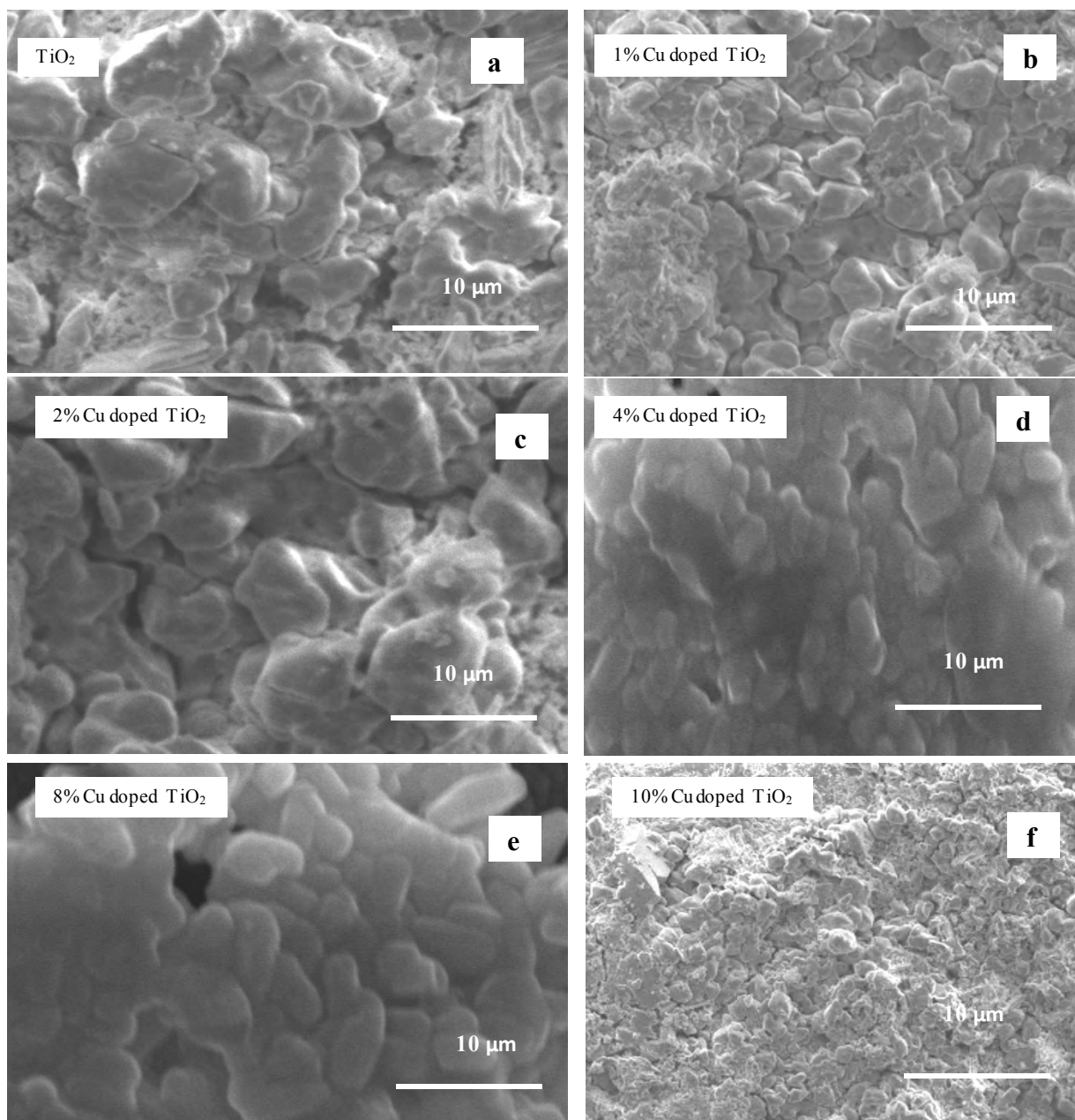


Fig. 4.52 SEM images of Cu/ TiO_2 thin films ($T_s = 400\ ^\circ\text{C}$, $\text{MC} = 0.10\ \text{M}$)

Table 4.8 Elemental analysis of Cu/ TiO_2 thin films ($T_s = 400\ ^\circ\text{C}$, $\text{MC} = 0.10\ \text{M}$)

wt% of Element	Cu (wt%)					
	0	1	2	4	8	10
Ti	67.34	65.51	65.12	63.64	61.40	60.61
Cu	0	0	1.45	3.24	7.32	8.64
O	32.66	34.49	33.43	33.12	31.28	30.75

4.4. 1.2 Structural Analyses

Fig. 4.53 shows XRD patterns of the synthesized Cu/TiO₂ thin films. The prominent diffraction peaks can be identified as a TiO₂ phase with tetragonal crystal structure with characteristic peaks at $2\theta = 25.35^\circ$, 38.05° , and 48.50° correspond to (hkl) values of (101), (004), and (200) respectively. The peaks of Cu/TiO₂ were identified by comparing JCPDS – 84 – 1286 data file which confirmed tetragonal (anatase, $2\theta=25.35^\circ$) structure of Cu/TiO₂ thin films. It is noteworthy to mention that the diffractograms of the samples do not contain any peak assigned to rutile phase ($2\theta=27.36^\circ$). These diffraction data of Cu/TiO₂ thin films are in good agreement with the XRD data of TiO₂ thin films prepared by RF magnetron sputtering [49]. TiO₂ thin films grown by MOCVD showed anatase phase when deposited on to Si (100) substrate and amorphous when deposited on to glass substrate [48]. No plane for Cu or CuO is present in the XRD patterns for Cu/ TiO₂ thin films. This observation is satisfied by comparing with the XRD data reported in ref. [50-52]. It was reported [53] that the Cu/TiO₂ thin films had anatase phase when annealed at 900 °C and some shifts in the Bragg's peaks have been observed in Cu/TiO₂ thin films which might be due to the presence of Cu in the structure. Thus it is seen that the as deposited TiO₂ and M/TiO₂ thin films are amorphous or mixed polycrystalline/amorphous in nature in their work whereas in the present study the TiO₂ and Cu/TiO₂ thin films synthesized by SPT are crystalline in nature with anatase phase tetragonal system. Thus this is an advantage over some of the techniques to synthesize crystalline M/TiO₂ thin films.

From the diffraction peaks (101) of Fig.4.53, D was calculated using Debye-Scherrer's formula [1], and lattice constants a, and c of TiO₂ calculated from the formula for tetragonal crystal structure, and these values of the lattice constants are recorded in Table 4.9. It is seen in the Table 4.9 that lattice parameters a and c increase with Cu doping. The small change in the lattice parameters is mainly due to occupying interstitial positions in the lattice by the dopant. It is evident that the lattice parameters remain almost constant up to 4% of Cu doping, but more change occurs for 8% of Cu doping and above 8% of Cu doping a decreasing trend is observed. For concentrations at or under 8% of Cu, the Cu substitutes into the Ti sites of the lattice, while higher concentrations led to slight change in the formation of the the crystal lattice. This may be due to the lattice disorder and strain induced by Cu⁺² substitution in the host lattice. D varies from 13.51 to 14.76 nm (Table-

4.9) for Cu/TiO₂ thin films, which are smaller than those for the commercially available ones (26.7 nm) and much smaller than 50 nm for TiO₂ thin films prepared by spin coating method from Ti(OC₄H₉)₄ precursor [39-40]. No peak corresponding to either Cu or any of its oxides is observed in any of the diffractograms, which indicates that no additional phase present in the prepared Cu/TiO₂ thin films at least within the limit of 10 wt% of Cu. It is suggested in reference [54] that Pt/TiO₂ nanocomposite thin films prepared by co-sputtering method, maintaining a single phase beyond this level is difficult. The crystallite size increases may be due to the decrease of strain and dislocation density in the film [16].

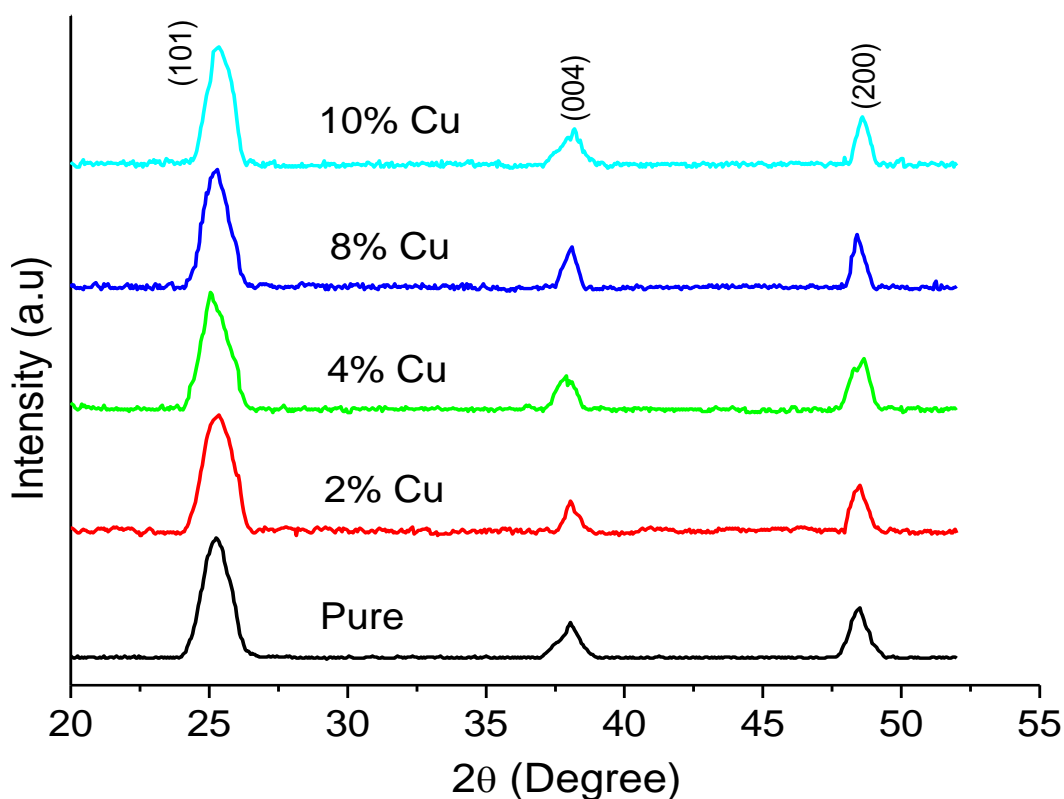


Fig. 4.53 XRD patterns of Cu/TiO₂ thin films ($T_s = 400\text{ }^\circ\text{C}$, $MC = 0.10\text{ M}$)

Table 4.9 XRD data for Cu/TiO₂ thin films ($T_s = 400\text{ }^\circ\text{C}$, $MC = 0.10\text{ M}$)

Cu (wt%)	0	2	4	8	10
D (nm)	13.5138	13.5172	13.6119	14.76	14.56
a (Å)	3.8067	3.8188	3.8246	3.8567	3.8514
c (Å)	9.1021	9.1285	9.1452	9.2132	9.2014

4.4. 1.3 Optical Properties

4.4. 1.3.1 Transmittance and Optical Band Gap

Fig. 4.54 shows the variation of T with wavelength in the wavelength region of 300 to 1100 nm for Cu/TiO₂ thin films synthesized at T_s of 400 °C. It is seen from Fig. 4.54 that the values of T are higher in the visible and NIR regions. TiO₂ thin films prepared at T_s of 400 °C exhibit a T of > 60%, in the visible and NIR regions and that for Cu/TiO₂ thin films is > 70% in the visible and NIR regions, which is greater than that of TiO₂ thin films. An average of 75 to 80% T is observed in the wavelength range of 800-1100 nm and below 600 nm T decreases gradually. A sharp ultraviolet cut-off at $\lambda = 300$ nm, for TiO₂ and Cu/TiO₂ thin films was found. These results in this experiment comply well with the findings in ref. [55]. The T increases from 5 to 10% with Cu doping, and shows the highest T of about 95 % for the thin films grown with 8wt% Cu. The T of the films is also influenced by a number of effects, which include surface roughness and optical inhomogeneity in the direction normal to the film surface. A relatively high T value for the thin film deposited with 8% of Cu may be attributed to less scattering due to the decrease in the degree of irregularity in the grain size distribution. The observed value of T is low compared to the reported values for Li and Nb doped TiO₂ thin films prepared by SPT [55]. The variation of α of Cu/TiO₂ thin films is shown in Fig.4.55. The α in the entire wavelength region is low but it is high at wavelength <400 nm. The value of the α depends on Cu doping. It decreases as the concentration of Cu increases upto 8 wt% but α increases above 8% Cu doping. This reduction of absorbance in Cu/ TiO₂ thin films can be explained as due to the removal of defects and disorder in the TiO₂ thin film by Cu doping. The important optical characteristic of Cu/TiO₂ thin film is that it is transparent in the wavelength ranging from 400 to 1100 nm. At wavelengths shorter than 400 nm, absorption occurs due to the fundamental band gap, and thus light cannot be transmitted due to quantum phenomenon. At longer wavelengths, reflection occurs because of the plasma edge, and light cannot be transmitted due to a classical phenomenon.

The E_g is determined from the plots of $(\alpha h\nu)^2$ vs. $h\nu$ for direct transition of Cu/TiO₂ thin films, as shown in Fig. 4.56. The E_g of the films has been obtained from the intercept on the energy axis after extrapolation of the straight line section of $(\alpha h\nu)^2$ vs. $h\nu$ curve. The

variation of E_g for Cu doping is presented in Fig. 4.57. The E_g of TiO_2 thin films obtained to be 3.40 eV which is in excellent agreement with the value of E_g , 3.40 – 3.65 eV reported by other worker for TiO_2 thin films deposited by SPT [15]. For 8% Cu doping the direct band gap of the film becomes 3.20 eV. So it is clear that for Cu doping the E_g decreases up to 8% Cu doping and increases above 8% Cu doping. These values are lower compared to the reported values of TiO_2 thin films prepared by SPT [55]. The excess of Cu atoms do not occupy the proper lattice positions to contribute to the free carrier concentration while, at the same time, enhance the disorder of the structure leading to an increase in E_g [56]. Beyond 8% Cu doping scattering occurs due to increase of disorder resulting, in E_g increase. As it can be seen, in both cases, the E_g energies obtained by this method are larger than the value in stoichiometric bulk TiO_2 (3.20 eV for anatase phase and 3.11 eV for rutile phase) [47, 57], which is probably due to the polycrystalline nature and to the reduced grain size of the films. After Cu doping the band gap of TiO_2 thin films reduces, such reduction in E_g is reported for Ge/ TiO_2 thin films [57].

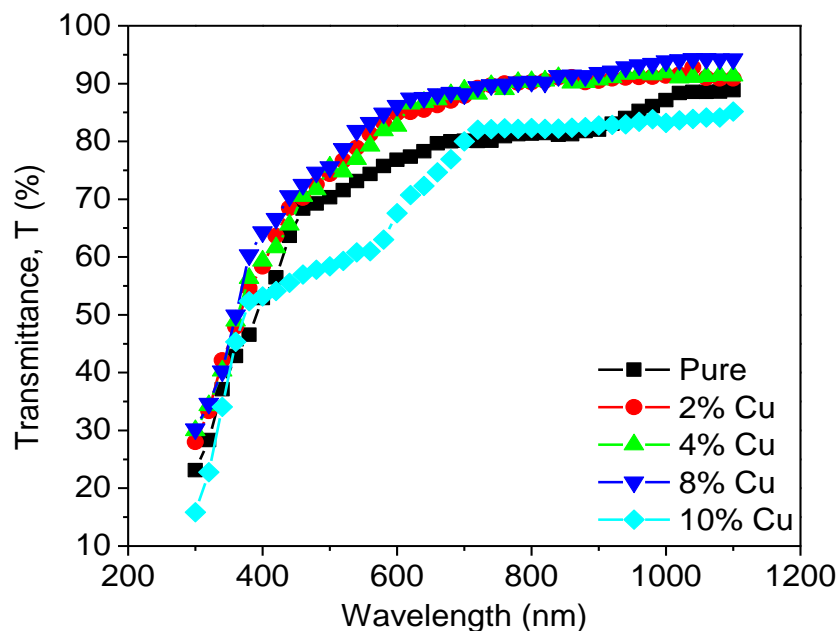


Fig. 4.54 Optical transmittance vs. wavelength of Cu/TiO_2 thin films ($T_s = 400\text{ }^\circ\text{C}$, $\text{MC} = 0.10\text{ M}$)

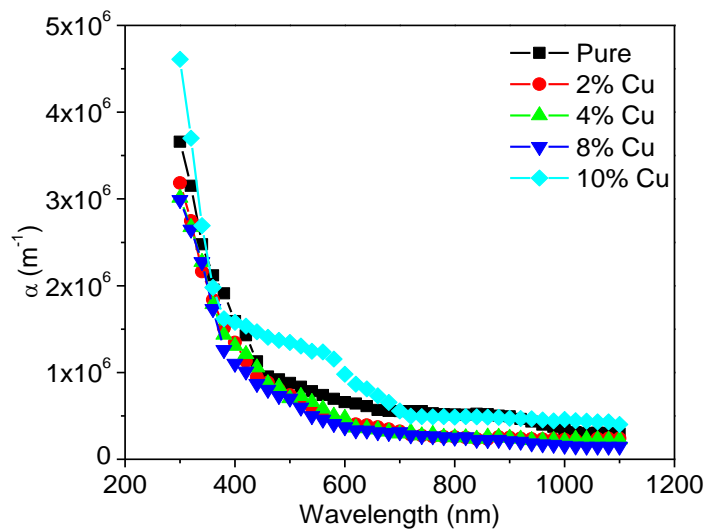


Fig. 4.55 α vs. wavelength of Cu/TiO₂ thin films ($T_s = 400$ °C, MC = 0.10 M)

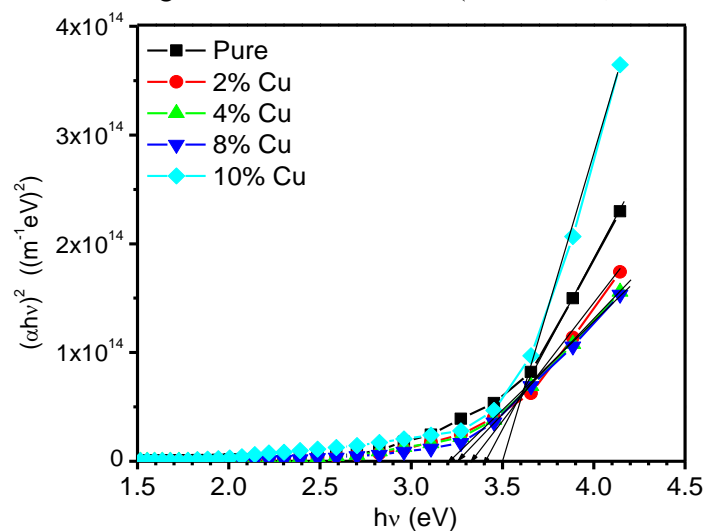


Fig. 4.56 Variation of $(\alpha h\nu)^2$ with $h\nu$ for Cu/TiO₂ thin films ($T_s = 400$ °C, MC = 0.10 M)

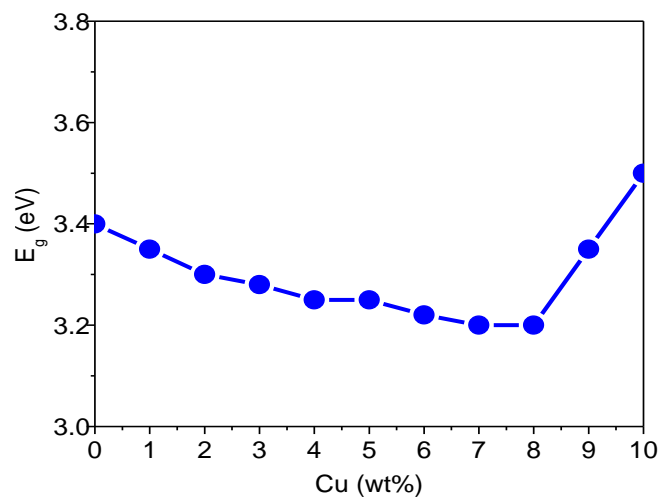


Fig. 4.57 Variation of E_g with Cu for Cu/TiO₂ thin films ($T_s = 400$ °C, MC = 0.10 M)

4.4. 1.3.2 Refractive Index and Extinction Coefficient

The variation of n for Cu/TiO₂ thin films with Cu doping is shown in Fig. 4.58. The n of TiO₂ thin film has been obtained to be 2.55 which is very close to the reported values 2.60 to 2.55 and lowest refractive index become 2.45 for 8% Cu doping. These observed results are well matched with the results of TiO₂ thin films prepared by MOCVD which is close to 2.6 [56]. As suggested by Arai in ref. [58], the low value of refractive index may probably due to the smaller density of the films.

The variation of k with $h\nu$ is presented in Fig. 4.59. It shows that k about 0.04 in the range of wavelength 500 - 1100 nm. The plotted curves of n and k are very similar to that described for TiO₂ thin film prepared by sol-gel dip coating and the bulk TiO₂ [44, 59]. This low value of k may probably be due to the smaller density of the films. It is observed that the k decreases with the increase of Cu doping (2-8%) in the range of wavelength 500 - 1100 nm. It is also observed that k of Cu/TiO₂ thin film increases of for doping by 10 wt% Cu, which may be due to the increase of inhomogeneity and surface roughness of the films so that, the defect in the film increases. This is expected as the periodicity of Ti matrix is disturbed in the film in presence of Cu atoms which might enhance the scattering of the conduction electrons. On increasing the concentration of Cu the band gap of the Cu/TiO₂ decreases and above 8% Cu doping increases the band gap of the Cu/ TiO₂ thin film which may be due to the decrease in the atomic density of these films. This process leads to the movement of Ti⁴⁺ ions in the interstitial sites and also an increase in the amorphous phase and disorder in Cu/TiO₂. This behavior appears to be a consequence of valence fluctuation in Ti between the 2⁺ and 4⁺ states. It attribute that Ti interstitials rather than oxygen vacancies alone present as Ti²⁺.

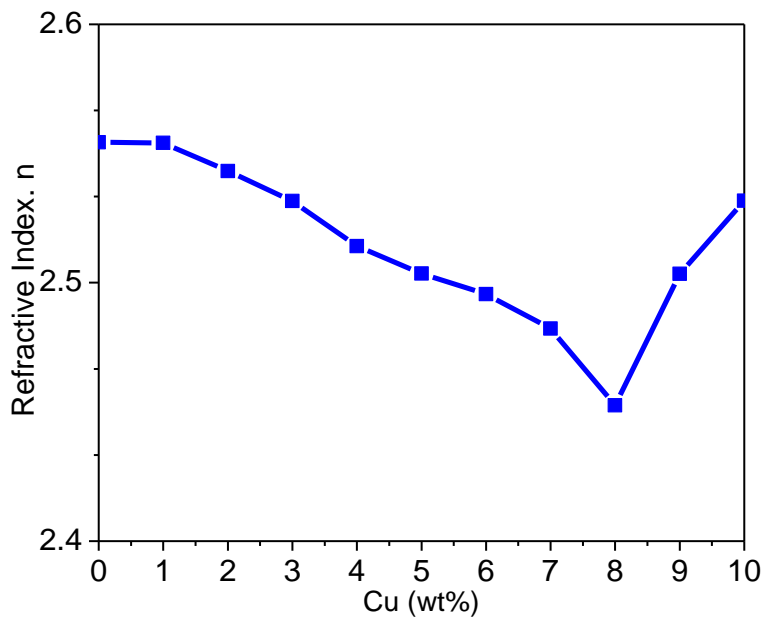


Fig. 4.58 Variation of refractive index with Cu for Cu/TiO₂ thin films ($T_s = 400\text{ }^\circ\text{C}$, $MC = 0.10\text{ M}$)

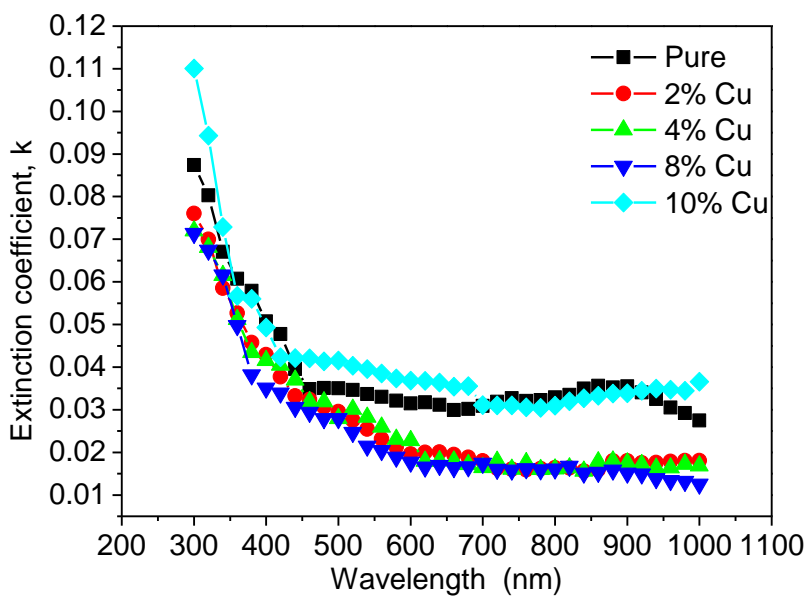


Fig. 4.59 Variation of extinction coefficient with wavelength for Cu/TiO₂ thin films ($T_s = 400\text{ }^\circ\text{C}$, $MC = 0.10\text{ M}$)

4.4. 1.4 Electrical Properties

The variation of ρ with temperature 300 to 470 K is presented in Fig. 4.60. It is observed that ρ of the Cu/TiO₂ thin films is decreased with increasing Cu doping. The decrease of ρ with temperature which may be due to the increase of carrier mobility or due to increase of carrier concentration for neutral defects and morphological changes of the films. Whereas the decrease in ρ with Cu doping can be explained in terms of stoichiometric changes induced by Cu introduction in the lattice vacancies and neutral defects in Cu/TiO₂ thin films. The formation of these defects depends on the sticking coefficient, nucleation rates and migration of impinging copper and oxygen species on the substrate during deposition. Fig. 4.61 also shows that ρ decreases with increasing concentration of Cu. This observed reduction in resistivity upon doping is understandable, as some Ti atoms are replaced with Cu, where the shell is not full and has states near the bottom of the conduction band. This addition of conduction band states will accommodate more conduction electrons and therefore lower the resistivity. This kind of behavior has been observed in previous Ni/ZnO thin films studies [60]. The room temperature ρ of the films decreases with increase of Cu doping (0 -10%) and is found to be 27.50-23.57 Ω -cm. The obtained results indicate that ρ of the thin films reaches to a minimum value of 23.19 Ω -cm with 8% of Cu doping. This resistivity behavior is due, on the one hand, to the increase of the Ti atoms in the regular sites in the films network. The concentration of Ti⁴⁺ in Cu/TiO₂ thin films forms a donor level in the band gap of TiO₂ which results in the reduction of recombination of electrons and holes [39, 46]. Consequently, Ti⁴⁺ ions have more concentration in thin films obtained with high Cu doping. Regarding the O²⁻ ions, which results in an increase in the free electron concentration; thereafter there is a decrease in film's resistivity [46]. The electrical conductivity obtained for the synthesized TiO₂ thin films for Cu doping (0 – 8%) varying from 4×10^{-2} to $5 \times 10^{-2} \Omega^{-1}\text{-cm}^{-1}$ which are much smaller than $1.42 \times 10^2 \Omega^{-1}\text{-cm}^{-1}$ (on glass substrate) and $3.46 \times 10^5 \Omega^{-1}\text{-cm}^{-1}$ (on ITO substrate), reported for TiO₂ thin films prepared by spin coating method from TiCl₄ precursor [61].

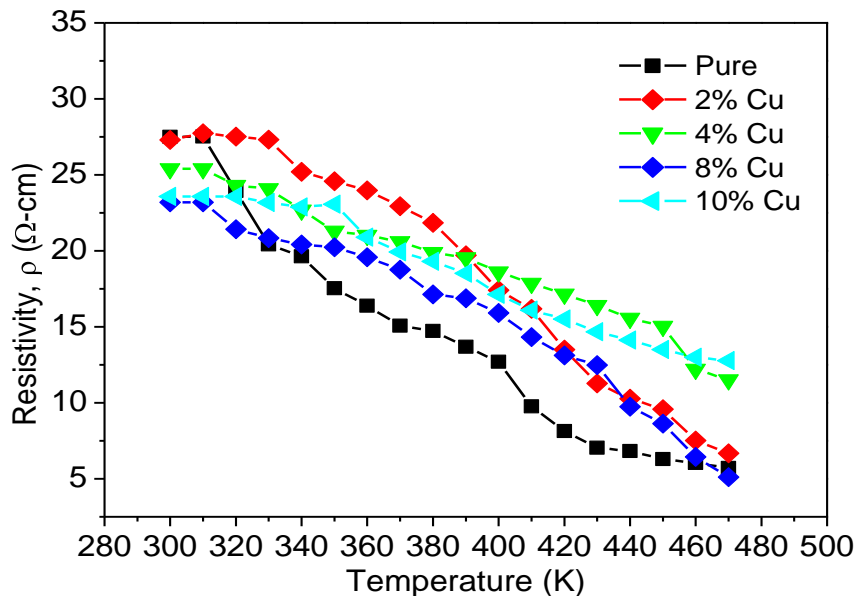


Fig. 4.60 Variation of resistivity with temperature for Cu/TiO₂ thin films ($T_s = 400\text{ }^\circ\text{C}$, $MC = 0.10\text{ M}$)

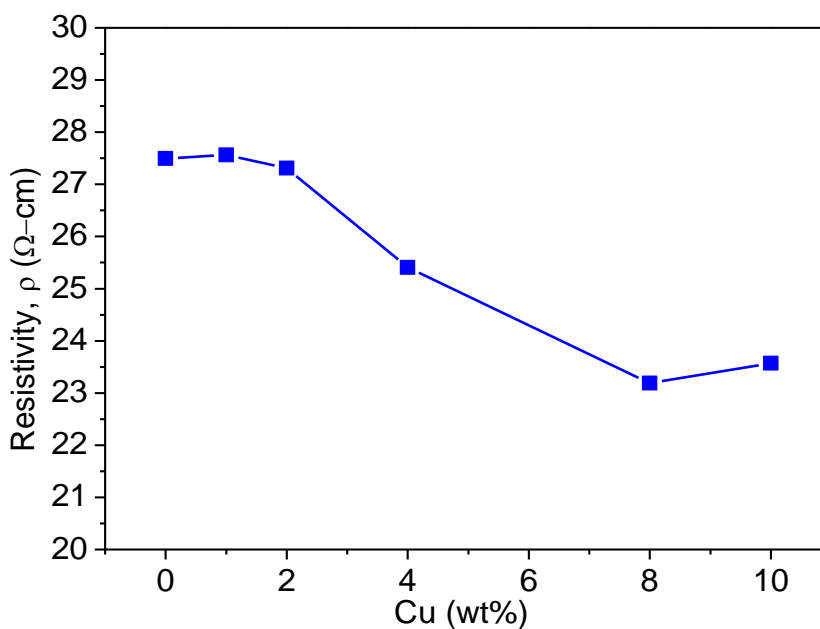


Fig. 4.61 Variation of resistivity with Cu for Cu/TiO₂ thin films ($T_s = 400\text{ }^\circ\text{C}$, $MC = 0.10\text{ M}$)

The σ of the prepared thin films is increased with Cu doping and increase of temperature as shown in Fig. 4.62, because of concentration of carrier increase and may also be due to increase in the free path of carries. The conductivity of the Cu/TiO₂ thin films increases with Cu doping because of light scattering, reduced internal resistance, enhanced adsorption and surface chemistry changes. The electrical conductivity of TiO₂ thin films

prepared by DC magnetron sputtering (at temperature = 310-468K) have been found to be $2.42-0.12 \Omega^{-1}\text{-cm}^{-1}$ [62], which is well agreed with the result observed in the present study. The E_a is calculated from the slope of the curves $\ln\sigma$ vs. $(1/T)$ and the variation of E_a with Cu (0- 10 wt %) is presented in Fig. 4.63. The E_a is maximum, 0.0311 eV for 8% Cu doped thin films. It is observed that for Cu doping the E_a increases. The low value E_a may be associated with the localized levels hopping due to the excitation of carriers from donor band to the conduction band. This low value of E_a was assumed due to the nonstoichiometry of the TiO_2 thin film but in the present case the higher values of E_a of Cu/TiO_2 thin films may suggest that the prepared samples become more stoichiometric with Cu doping.

Variation of Figure of merit vs. Cu (0-10%) TiO_2 thin films is presented in Fig. 4.64. It is seen that due to Cu doping the Figure of merit is increased. The Figure of merit of Cu/TiO_2 thin films is varied from 0.2238 to 0.0.2334 $\Omega^{-1}\text{-cm}^{-1}$ for Cu doping from 1 to 8 wt% and it become reduced for more than 8 wt% Cu doping. The increase in the Figure of merit of the Cu/TiO_2 thin films is mainly due to the increase in the optical transmittance with increasing Cu doping. The increase of resistivity can be explained by more carrier concentration and disordering of crystal structures of thin films. It may be stated that the optical and electrical characterization of TiO_2 thin films has been modified with Cu doping in thin films.

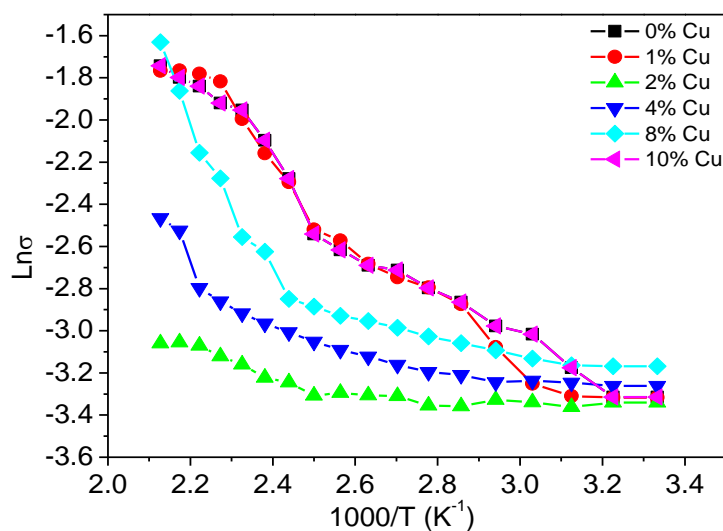


Fig. 4.62 Variation of $\ln\sigma$ with inverse of temperature T (K) for Cu/TiO_2 thin films ($T_s = 400 \text{ }^\circ\text{C}$, $MC = 0.10 \text{ M}$)

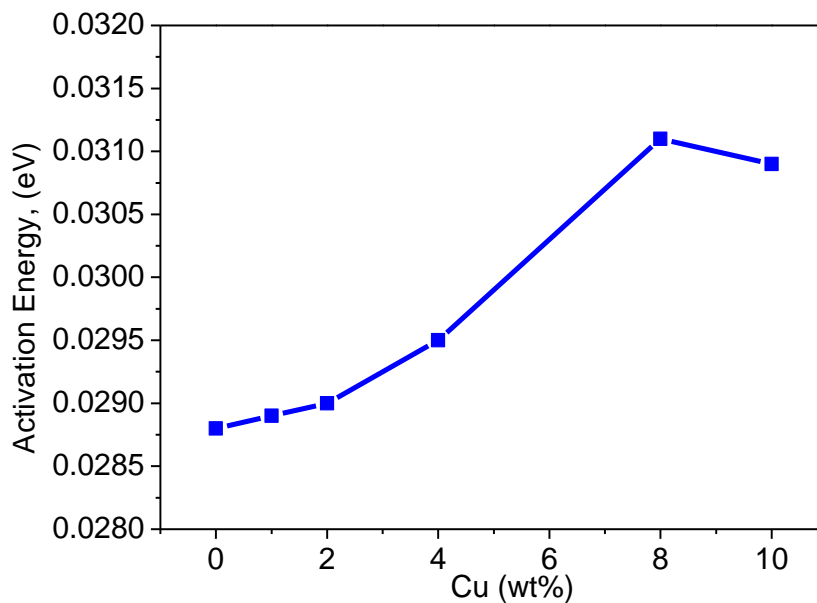


Fig. 4.63 Variation of activation energy with Cu for Cu/TiO₂ thin films ($T_s = 400\text{ }^\circ\text{C}$, $MC = 0.10\text{ M}$)

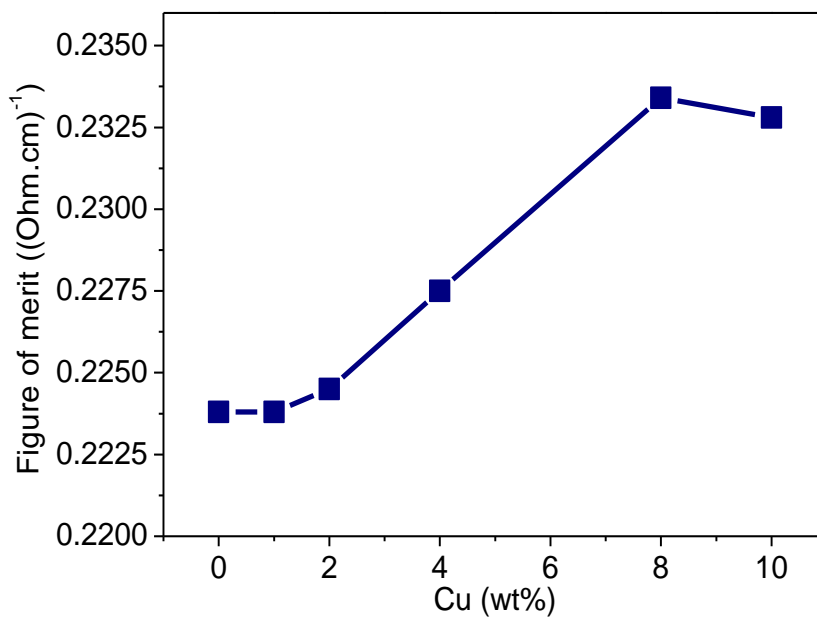


Fig. 4.64 Variation of Figure of merit with Cu for Cu/TiO₂ thin films ($T_s = 400\text{ }^\circ\text{C}$, $MC = 0.10\text{ M}$)

4.4.2 Summary of Findings on Cu/TiO₂ Thin Films

The doping concentration of Cu was varied from 1-10 wt.%. The average thickness of the film is found to be 200 nm. SEM images of Cu/TiO₂ thin film show good and homogeneous surface. EDX data reveal that Ti, Cu, and O are present in Cu/TiO thin films. TiO₂ thin film made up of tetragonal structure with anatase phase. Cu/TiO₂ films showed good crystallinity, suggesting the substitution of Ti ion by Cu ion as evident from XRD. XRD results indicated that the Cu ions replaced the Ti ions without changing the tetragonal structure. The optical transmission of the thin films was found to increase from 88 % to 94 % with the addition of Cu up to 8 wt% and, beyond 8 wt% of Cu doping transmission decreases. The optical band gap for TiO₂ thin film is found to be 3.40 eV. Due to Cu doping, the band gap is shifted to lower energies and then increases further with increasing concentration of Cu. The refractive index of the thin films is found to be 2.58 and the variation of refractive index is observed due to Cu doping and that for 8 w% of Cu doped TiO₂ thin film is 2.45, which is minimum. The room temperature resistivity of the films decreases with increasing Cu doping and is found to be 27.50- 23.19 Ω-cm. TiO₂ thin film shows resistivity, 27.50 Ω-cm, after Cu doping it reduces to 23.19 Ω-cm for 8 wt% of Cu doping in thin films. Again resistivity of the Cu/TiO₂ thin films increases when Cu doping is increased above 8 wt%. The maximum value of E_a and Figure of merit for Cu/TiO₂ thin film is 0.0311 eV and 0.2334 Ω⁻¹-cm⁻¹ for Cu doping of 8wt%.

It is evident from the present study that the Cu doping promoted the thin film morphology. These results demonstrate the ability of tuning band gap of TiO₂ thin films by Cu doping. By doping Cu the TiO₂ thin film becomes conductive so it can be used as transparent conducting electrodes. It may also be used in sensors. Finally, the results found in the present study and the reported ones are summarized in the following Table 4.5 for comparison.

4.5 Summary of Results of the Prepared Thin Films and the Reported TiO₂ Thin Films

Table 4.10 Comparison of results of all prepared TiO₂ thin films with the reported results of TiO₂ thin films

Technique, Salt	Variation	Structure	E _g (eV)	ρ (Ω-cm)	E _a (eV)	Ref. No.
SPT, TiCl ₄	M = 0.05-0.10, 0.15	Anatase	3.65-3.4, 3.7	55.67-27.5, 37.96	0.0183-0.0285	Present sample
	T _s = 250- 450 °C	Amorphous-Anatase	3.62 -3.4	42.12-27.90	0.0105-0.0285	
	Cu(0-8%, 10 wt%)	Anatase	3.4 -3.2, 3.5	27.50- 23.57	0.0289-0.0319	
SPT, Ti(OC ₃ H ₇) ₄	MC 0.05 -0.125	Amorphous, Anatase	3.60-3.45		Thickn ess, t = 480-735 nm	[15]
	T _s = 375 -475 °C		3.60-3.40			
	SR = 1-4 ml/min		3.65-3.50			
RF mag. sputtering. Ge-TiO ₂	Ge (9 – 33%)	Anatase, Rutile, Ge	0.70 -2.2		t = 1-0.5 μm	[57]
Spin coating, TiCl ₃	Substrate	Rutile		10.69 Ω/sq σ = 3.46 × 10 ⁵ Ω ⁻¹ .cm ⁻¹		[25]
SPT, Ti(OC ₃ H ₇) ₄	T _s = 315 -500 °C	Anatase at T _s = 500 °C	n = 2.1 – 2.4	dielectric cons. 75		[41]
DC mag. sputt., TiO ₂	Temperature 310-468 K			σ = 2.42-0.12 Ω ⁻¹ .cm ⁻¹		[62]
Solgel, Ti [OC ₃ H ₇] ₄	T _a = 400-700 °C a= annealing	Anatase – Ana. + Rutile	3.13-3.0			[50]
Solgel, Ti [OC ₃ H ₇] ₄	T _a = 0 – 400 °C	Amophous - Anatase	3.42 - 3.04	0.14 – 0.08	t = 232 – 177 nm	[39]
Solgel	Cu (1-10 wt%) T _s = 450 °C	Anatase				[64]
RF magnetron sputtering, TiO ₂	TiO ₂ T _a = 200 – 400 °C	Amophous-Anatase	3.64 - 3.78			[63]
	TiO ₂ +2%ZnFe ₂ O ₄ T _a = 200 – 400 °C	Anatase-Composite	3.14 - 3.56			
RF, TiO ₂ , Cu	As deposited	Amorphous				[53]
	T _a = 300 -900 C	Anatase-Anatase+Rutile	3.2 -3			

References

- [1] Debye P., "Zur Theorie der spezifischen Waerme", *Annalen der Physik*, 344, pp. 789 – 839, 1912.
- [2] Saravanakannan V., Radhakrishnan T., "Structural, electrical and optical characterization of CuO thin films prepared by spray pyrolysis technique", *Int. J. Chem. Tech Res.*, 6, 1, pp. 306-310, 2014.
- [3] Das C. R., Alexander D., Christy A. J., Jeyadheepan L., Raz A. M. E., Raza C. S., "Preparation and characreization of CuO thin films prepared by spray pyrolysis technique for ethanol gas sensing application", *Asian J. Appl. Sci*, 7, pp. 671-684, 2014.
- [4] Ghosh M., Rao C.N.R., "Solvothormal synthesis of CdO and CuO nanocrystals", *Chem. Phys. Lett.*, 393, 4-6, pp. 493-497, 2004.
- [5] Tauc J., Optical properties and electronic structure of amorphous Ge and Si, *Mater. Res. Bull.*, 3, pp. 37–46, 1968.
- [6] Parretta A., Jayaraj M. K., Nocera A. D., Loreti S, Quercia L., and Agati A, "Electrical and optical properties of copper oxide films prepared by reactive RF magnetron sputtering", *Phys. Stat. Sol.*, 155, pp. 399-404, 1996.
- [7] Revathi N., Prathap P. Reddy K. T. R., "Synthesis and physical behavior of In₂S₃ films", *Appl. Surf. Sci.* 254, pp. 5291-5298, 2008.
- [8] Revathi N., Prathap P., Subbaiah Y. P. V., Ramakrishna R. K. T., "Substrate temperature dependent physical properties of In₂S₃ films", *J. Phys. D: Appl. Phys.*, 41, 1, pp. 155-404, 2008.
- [9] Revathi N., Prathap P. Reddy K. T. R., "Thickness dependent physical properties of close space evaporated In₂S₃ films" *Solid State Sci.*, 11, 1288-1296, 2009.
- [10] Drobny V. F., Pulfrey L., "Properties of reactively-sputtered copper oxide thin films", *Thin Solid Films*, 61, 1, pp. 89-98, 1979.
- [11] Cho S., "Structural, Optical and electrical properties of RF- sputtered indium oxide thin films", *J. Korean Phys. Soc.*, 60,12, pp. 2058-2062, 2012.

- [12] Akkari F. C., Kanzaria M., Rezig B., "Preparation and characterization of obliquely deposited copper oxide thin films", *Eur. Phys. J. Appl. Phys.* 40, pp. 49–54, 2007.
- [13] Sanal K.C., Vikas L.S., Jayaraj M.K., "Room temperature deposited transparent p-channel CuO thin film transistors", *Appl. Surf. Sci.*, 297, pp. 153–157, 2014.
- [14] Saravanan V., Shankar P., Mani G. K., Rayappan J. B. B., "Growth and characterization of spray pyrolysis deposited copper oxide thin films: Influence of substrate and annealing temperatures", *J. Analyt. Appl. Pyro.*, 111, pp. 272–277, 2015.
- [15] Manohari A. G., Dhanapandian S., Kumar S., Mahalingam T., "Optimization of deposition parameters on the physical properties of TiO₂ thin films by spray pyrolysis technique", *Int. J. Thin Fil. Sci. Tec.*, 3, 1, pp. 1-6, 2014.
- [16] Edelestein A.S., Camarata R.C., "Nanomaterials synthesis properties and applications", Institute of Physics Publishing, Bristol, 1998.
- [17] Aseel M. A. M., Ahmed N. A., Ali A. H., Nadir F. H., "Fabrication and characterization of copper oxide nanoparticles/si heterodiode", *International Letters of Chemistry, Physics and Astronomy*, 57, pp. 25-35, 2015
- [18] Dhanasekaran V., Mahalingam T., "Electrochemical and physical properties of electroplated CuO thin Films", *J. Nanosci. Nanotechnol.*, 13, 1, pp. 250-259, 2013.
- [19] Kumar D. A., Francis P. X., Shyla J. M. "Investigation on the variation of conductivity and photoconductivity of CuO thin films as a function of layers of coating", *Arch. Appl. Sci. Res.*, 4, 5, pp. 2174-2183, 2012
- [20] Shinho Cho, "Optical and electrical properties of CuO thin films deposited at several growth temperatures by reactive RF magnetron sputtering", *Met. Mater. Int.*, 19, 6, pp. 1327-1331, 2013.
- [21] Ba-Abbad M, Kadhum A. H, Mohamad A, Takriff M. S, Sopian K., "Synthesis and catalytic activity of TiO₂ nanoparticles for photochemical oxidation of concentrated chlorophenols under direct solar radiation", *Int. J. Electrochem. Sci.*, 7, pp. 4871-4888, 2012.

- [22] Jeong S-H., Kim B-S., Lee B-T., "Structural and optical properties of TiO₂ films prepared using reactive RF magnetron sputtering", *J. Korean Phys. Soc*, 41, 1, pp. 67-72, 2002.
- [23] Vijayalakshmi R., Rajendran V., "Synthesis and characterization of nano-TiO₂ via different methods", *Arch. Appl. Sci. Res.*, 4, 2, pp. 1183-1190, 2012.
- [24] Mahdi E. M., M. Hamdi , Meor Yusoff M. S., Wilfred P., "XRD and EDXRF analysis of anatase nano-TiO₂ synthesized from mineral precursors", *Adv. Mater. Res.*, 620, pp. 179-185, 2013.
- [25] Daniyan A. A., Umoru L. E., Fasasi A. Y., Borode J. O., Oluwasegun K. M., Olusunle S. O., "Electrical properties of Nano-TiO₂ thin film using spin coating method", *J. Miner. Mater. Charact. Engn.*, 2, pp. 15-20. 2014.
- [26] Karan N.S., Agarwal A., Pandey P.K., Smitha P., Sharma S.J., Mishra D.P. Gajbhiye N.S., "Diffusion flame synthesis of hollow, anatase TiO₂ nanoparticles", *Mater. Sci. Eng., B*, 163, 128 – 133, 2009.
- [27] Manohari A. G., Dhanapandian S., Santhosh K., Mahalingam T., "Optimization of deposition parameters on the physical properties of TiO₂ thin films by spray pyrolysis technique", *Int. J. Thin Film Sci. Technol.*, 3, 1, pp1-6, 2014.
- [28] Stamate M., Vascan I., Lazar I., Lazar G., Caraman I., Caraman M., "Optical and surface properties of TiO₂ thin films deposited by DC magnetron sputtering method", *JOAM*, 7, 2, pp. 771 – 774, 2005.
- [29] Devore J. R., "Refractive indices of rutile and sphalerite", *J. Opt. Soc. Am.* 41, pp. 416-419, 1951,
- [30] van der Pauw L. J., "A method of measuring specific resistivity and hall effect of discs of arbitrary shape", *Philips Res. Rep.* 13, pp. 1-3, 1958.
- [31] Biju K. P., Jain M. K., "Effect of crystallization on humidity sensing properties of sol-gel derived nanocrystalline TiO₂ thin films", *Thin Solid Films*, 516, pp. 2175–2180, 2008.
- [32] Nowotny J., Bak T., Burg T., "Electrical properties of polycrystalline TiO₂. Prolonged Oxidation Kinetics", *J. Ionics*, 13, pp. 79-82, 2007.
- [33] Arrhenius, "Chemical kinetics and dynamics", *Chem 1 Virtual Text Book*, 2011.

- [34] Dhar A., Alford T. L., “High quality transparent TiO₂/Ag/TiO₂ composite electrode films deposited on flexible substrate at room temperature by sputtering”, *APL Mater.*, 1, 012102-1, 2013.
- [35] Okuya M., Shiozaki K., Horikawa N., Kosugi T., Kumara G.R. A., Madarasz J., Kaneko S., Pokol G., “Porous TiO₂ thin films prepared by spray pyrolysis deposition (SPD) technique and their application to UV sensors”, *Solid State Ionics*, 172, pp. 527–531, 2004.
- [36] Lee C-S, Kim J., Son J. Y., Maeng W. J., Jo D-H, Choi W., Kim H., “Plasma-enhanced ALD of TiO₂ thin films on SUS 304 stainless steel for photocatalytic application”, *J. Electrochem. Soc.*, 156, 5, pp. 188-192, 2009.
- [37] Paez L. R., Matousek J., “Preparation of TiO₂ solgel layers on glass”, *Ceramcs-Silikaty.*, 47, 1, pp. 28-31, 2003.
- [38] Thamaphat K., Limsuwan P., Ngotawornchai B., “Phase characterization of TiO₂ powder by XRD and TEM”, *Kasetsart. J. (Nat. Sci.)*. 42, pp. 357-361, 2008.
- [39] Hanini F., Bouabellou A., Bouachiba Y., Kermiche F., Taabouche A., Hemissi M., Lakhdari D., “Structural, optical and electrical properties of TiO₂ thin films synthesized by sol-gel technique”, *IOSRJEN*, 3, 11, pp. 21-28, 2013.
- [40] Karan N.S., Agarwal A., Pandey P.K., Smitha P., Sharma S.J., Mishra D.P. Gajbhiye N.S., “Diffusion flame synthesis of hollow, anatase TiO₂ nanoparticles”, *Mater. Sci. Eng., B*, 163, pp. 128 – 133, 2009.
- [41] Oja I., Mere A., Krunk M., Solterbeck C-H., Es-Souni M., Properties of TiO₂ films prepared by the spray pyrolysis method, *Solid State Phenomena*, 99-100, pp 259-264, 2004.
- [42] Sta I., Jlassi M., Hajji M., Boujmil M. F., Jerbi R., Kandyla M., Kompitsas M., Ezzaou H., “Structural and optical properties of TiO₂ thin films prepared by spin coating”, *J. Sol-Gel Sci. Technol.*, 72, pp. 421-427, 2014.
- [43] Arai K., Wu G., Takahashi M., Inaba H., Minoshima K., “Extremely high-accuracy correction of air refractive index using two-colour optical frequency combs”, *Sci. Rep.*, 3, 1894, 2013.

- [44] Bouachiba Y., Bouabellou A., Hanini F., Kermiche F, Taabouche A., Boukheddaden K., “Structural and optical properties of TiO₂ thin films grown by sol-gel dip coating process”, *Mater. Sci.-Poland*, 32, 1, pp. 1-6, 2014.
- [45] Malati M. A., Wong W. K., “Doping TiO₂ for solar energy applications”, *Surf. Tech.*, 22, pp. 305-322, 1984.
- [46] Zhao X., Zhao Q., Yu J., Liu B., “Development of multifunctional photoactive self-cleaning glasses”, *J. Non-Crys. Solids*, 354, pp. 1424–1430, 2008.
- [47] Ayouchi R., Casteleiro C., Schwarz R., Barrado J. R., Martin F., “Optical properties of TiO₂ thin films prepared by chemical spray pyrolysis from aqueous solutions”, *Phys. Stat. Sol. C*, 7, pp. 933–936, 2010.
- [48] Begum N. S., Ahmed H. M. F., “Synthesis of nanocrystalline TiO₂ thin films by liquid phase deposition technique and its application for photocatalytic degradation studies”, *Bull. Mater. Sci.*, 31, 1, pp. 43–48, 2008.
- [49] Mardare D. , Tasca M. , Delibas M. , Rusu G. I. , “On the structural properties and optical transmittance of TiO₂ R.F. sputtered thin films”, *Appl. Surf. Sci.*, 156, 1–4, pp. 200–206, 2000.
- [50] Hai H., Wen-jun X., Jian Y., Jian-wei S., Ming-xia C., Wen-feng S. G., “Preparations of TiO₂ film coated on foam nickel substrate by sol-gel processes and its photocatalytic activity for degradation of acetaldehyde”, *J. Environ. Sci.*, 19, pp. 80–85, 2007.
- [51] Li D., Haneda H., Hishita S., Ohashi N., Labhsetwar N. K., “Fluorine-doped TiO₂ powders prepared by spray pyrolysis and their improved photocatalytic activity for decomposition of gas-phase acetaldehyde”, *J. Fluorine Chem.*, 126, pp. 69–77, 2005.
- [52] Jung S-C., Kim S-J., Imaishi N., Cho Y-I., “Effect of TiO₂ thin film thickness and specific surface area by low-pressure metal–organic chemical vapor deposition on photocatalytic activities”, *Appl. Catal. B: Environ.*, 55, pp. 253–257, 2005.
- [53] Ryu S. W., Kim E. J., Ko S. K., Hahn S. H., “Effect of calcination on the structural and optical properties of M/TiO₂ thin films by RF magnetron co-sputtering”, *Mater. Lett.*, 58, pp. 582–587, 2004.

- [54] Sasaki T., Koshizaki N., Terauchi S., Umehara H., Matsumoto Y., Koinuma M., "Preparation of Pt/TiO₂ nanocomposite films using co-sputtered method", *Nanostruct. Mater.*, 8, 8, pp. 1077-1083, 1997.
- [55] Golego N., Studenikin S. A., Cocivera M., "Spray pyrolysis preparation of porous polycrystalline thin films of titanium dioxide containing Li and Nb", *J. Mater. Res.*, 14, 3, pp. 698-707, 1999.
- [56] Bernardi M. I. B., Lee E. J. H., Lisboa-Filho P. N., Leite E. R., Longoa E., Varela J. A., "TiO₂ thin film growth using the MOCVD method", *Mater. Res.*, 4, 3, pp. 223-227, 2001.
- [57] Chatterjee S., "Titania-germanium nanocomposite as a photovoltaic material", *Sol. Energy*, 82, pp. 95-99, 2008.
- [58] Arai T., "The study of the optical properties of conducting tin oxide films and their interpretation in terms of a tentative band scheme", *J. Phys. Soc. Jpn.* 15, pp. 916-927, 1960.
- [59] Ribalski M. W., *Handbook of Optical Constants of Solids I*, Academic Press, San Diego, 1998.
- [60] Das S. C., Green J. R., Podder J., Regier T. Z., Chang G. S., Moewes A., "Band gap tuning in ZnO through Ni doping via spray pyrolysis", *J. Phys. Chem. C*, 117, pp. 12745-12753, 2013.
- [61] Tang Z. L., Zhang J. Y., Cheng Z., Zhang Z. T., "Synthesis of rutile TiO₂ at low temperature," *Mater. Chem. Phys.*, 77, 2, pp. 314- 317, 2001.
- [62] Yildiz A., Lisesivdin S.B., Kasap M., Mardare D. "Electrical properties of TiO₂ thin films, *J. Non-Crystalline Solids*, 354, pp. 4944-4947, 2008.
- [63] Li G.H., Yang L., Jin Y.X., Zhang L.D., Structural and optical properties of TiO₂ thin film and TiO₂ + 2 wt.% ZnFe₂O₄ composite film prepared by r.f. sputtering, *Thin Solid Films*, 368, pp. 163-167, 2000.
- [64] Ying X., Jing-an L., Li-fu Y., Lin-hua L., Ping Y., Nan H., "Preparation and characterization of Cu-doped TiO₂ thin films and effects on platelet adhesion", *Surface and Coatings Technology*, 261, 15, pp. 436-44, 2015.

CHAPTER- V

CONCLUSIONS

5.1 Conclusions

5.2 Suggestions for Further Research

CHAPTER- V

CONCLUSIONS

5.1 Conclusions

The purpose of this chapter is to summarize the results obtained in this study. As demonstrated, the low-cost spray pyrolysis technique (SPT) can be used to obtain uniform conductive layers of CuO, TiO₂ and Cu/TiO₂ thin films with good repeatability. The effects of varying the concentration and T_s on the structural, optical and electrical properties were investigated on the above mentioned compounds synthesized by SPT in thin film form. The results of the present study are summarized below and the noteworthy conclusions are described as follows:

The CuO and TiO₂ thin films were deposited on to glass substrates at various T_s from 250 to 450 °C and various MCs from 0.05 to 0.15 M and Cu/TiO₂ thin films were prepared by varying Cu doping concentration (1-10 wt%) at T_s = 400 °C and MC = 0.10 M by SPT.

Good stoichiometric and homogeneous CuO thin films with monoclinic structure have been obtained at T_s = 350 °C and MC = 0.10 M. The lattice constants of the CuO thin films for solution of 0.10M and T_s of 350 °C are found to be: a = 4.6623 Å, b = 3.4431 Å and c = 5.1345 Å and are in good agreement with the standard JCPDS data for monoclinic structure of CuO. The crystallite size is about 9.5743 Å for the CuO thin film synthesized at the optimized condition. The E_g varies from 1.90 to 1.65 eV. The lowest value of E_g and n are 1.65 eV and 2.52, respectively, at T_s of 350 °C and MC = 0.10 M. The minimum ρ of about 18 Ω-cm for the CuO thin films is observed for T_s = 350 °C and MC = 0.10 M. The electrical measurement reveals the semiconducting behavior of the CuO thin films. The activation energy in the high temperature region, E₁ is found to be 0.30 eV and that in the low temperature region, E₂ is found to be 0.12 eV for CuO thin film deposited at T_s of 350 °C from solution of 0.10 M.

The highest value of Figure of merit occurs for the film grown at T_s = 350 °C and MC = 0.10 M with an optical transmittance about 76% in the wavelength range of 800-1100 nm. The crystalline phases, surface morphology, optical and electrical properties of the prepared CuO thin films are found to be significantly influenced by the variation of MC and T_s. From the obtained experimental results as compared to others, it can be inferred

that CuO thin films prepared from 0.10 M solution of $\text{Cu}(\text{CH}_3\text{COO})_2 \cdot \text{H}_2\text{O}$ at T_s of 350 °C bears good quality. The synthesized CuO thin films could be environmental friendly and suitable as a potential buffer layer in the fabrication of heterojunction solar cells, optoelectronic devices etc.

Roughness of TiO_2 thin film decreases with increasing MC and T_s and optimum surface condition is observed at $T_s = 400$ °C for MC = 0.10 M. Elemental analysis clearly shows that the grains in TiO_2 thin films typically comprise of both Ti and O. At $T_s < 300$ °C, the TiO_2 thin film is amorphous in nature. At $T_s \geq 300$ °C, strong diffraction peaks corresponding to (101) and (200) planes at 25° and 48° respectively indicating TiO_2 thin films have tetragonal structure with anatase phase. The peaks are found to shift slightly from their standard positions at higher T_s , and there is some deviation in the lattice parameters. The lattice constants of the TiO_2 thin films are found to be: $a = b = 3.8067$ Å, and $c = 9.1021$ Å, and the D is found to be around 13.51 nm for MC of 0.10 M and T_s of 400 °C. TiO_2 thin film prepared with 0.10 M at $T_s = 400$ °C is homogeneous and having good stoichiometry with tetragonal structure. The optical transmission of TiO_2 thin films is found to increase from 73 to 89 % and the E_g shifts from 3.64 to 3.40 eV with the increase of T_s . The lowest E_g is 3.4 eV, and the lowest value of n is 2.55 for the film obtained at T_s of 400 °C from solution of 0.10 M. The k values of TiO_2 thin film indicated that the films are stronger absorbing medium in the lower wavelengths. The n of TiO_2 thin film is 2.55 for MC of 0.10 M and T_s of 400 °C. The best surface structure and transparent TiO_2 thin film is obtained for 0.10 M and T_s of 400 °C. The minimum ρ and maximum value of Figure of merit of TiO_2 thin film deposited at T_s of 400 °C from solution of 0.10 M are found to be 27 $\Omega\text{-cm}$ and 23 $\Omega^{-1}\text{-cm}^{-1}$, respectively. The room temperature ρ varies from 42 to 27 $\Omega\text{-cm}$ for TiO_2 thin films grown for T_s varying from 250 to 450 °C. The ρ of TiO_2 thin film decreases as T_s increases. The minimum ρ is found to be 27 $\Omega\text{-cm}$ for TiO_2 thin film deposited at T_s of 400 °C from solution of 0.10 M. The E_a of TiO_2 thin films varies in the range of 0.010 to 0.028 eV for different MC and T_s . E_a is found to be 0.28 eV for TiO_2 thin film obtained at T_s of 400 °C from solution of 0.10 M. The highest Figure of merit is found for the film grown at 400 °C with an optical transmittance about of 85% in the wavelength range of 800-1100 nm.

It can be attributed that synthesized TiO₂ thin films have better structural, optical and electrical properties when deposited at T_s of 400 °C from solution of 0.10 M. The observed experimental results indicate the suitability of this material as transparent and conducting window material in thin film solar cells, gas sensor devices, etc.

The Cu/TiO₂ thin film surface is homogeneous and Ti, Cu, and O are present in Cu/TiO₂ thin film in stoichiometric ratio. Cu/TiO₂ thin films grown by SPT shows good crystallinity and tetragonal structure with anatase phase, suggesting the substitution of Ti ion by Cu ion as evident from XRD analysis. The value of D increases with Cu doping. Lowest value of 13.52 nm and highest value of 14.76 nm are observed for 2 and 8 wt% Cu doped TiO₂ thin films respectively. The values of a and c of Cu/TiO₂ thin film increase with Cu doping. The optical transmission of Cu/TiO₂ thin films is found to increase from 88 % to 94 % with the addition of Cu up to 8 wt% and decreases for higher percentage of Cu doping. Due to Cu doping, the E_g is shifted to lower energy, 3.20 eV, for 8 wt% of Cu/TiO₂ thin film and increases further with increasing the concentration of Cu doping. The variation of n is observed due to Cu doping and it has lowest value of 2.45 for 8 wt% of Cu/TiO₂ thin film. The room temperature ρ of Cu/TiO₂ thin film decreases with increasing Cu doping and is found between 27.50 and 23.19 Ω-cm. It is reduced to 23.19 Ω-cm for 8% of Cu doping in thin films. Again, ρ of the Cu/TiO₂ thin films increases when Cu doping is increased above 8 wt% Cu. The E_a varies with Cu (0-10 wt%) from 0.029 to 0.031 eV. The E_a is maximum, 0.0311 eV, for 8 wt% Cu doped TiO₂ thin films. Figure of merit for the Cu/TiO₂ thin films deposited at T_s of 400 °C varies from 0.2238 to 0.2328 Ω⁻¹.cm⁻¹ for Cu doping (1 – 10 wt%) and it is maximum, 0.2334 Ω⁻¹.cm⁻¹, for 8 wt% Cu doping TiO₂ thin films.

Notably, the XRD studies indicate that the prepared Cu/TiO₂ thin films are polycrystalline in nature with preferred grain orientation along (111) plane, exhibiting tetragonal crystal structure with anatase phase. It is also observed that Cu doping tunes the E_g of TiO₂ thin films. The conductivity increases with increasing Cu concentration. By doping Cu, the TiO₂ thin film becomes conductive. So it can be used in transparent conducting electrodes, optoelectronic devices, sensors, etc. The structure, optical transmittance and electrical resistivity of Cu/TiO₂ thin films depend on the concentration of the dopant, which are optimized in the present work.

The substrate temperature is the most important parameter that should be controlled when spraying. Before spraying, the temperature distribution contributes to the non-uniformity of the deposited thin films on the substrate. In conclusion, it can be stated that the SPT could be employed for large-scale and large area synthesis of CuO, TiO₂ and Cu/TiO₂ thin films because of its high yield, simplicity and relatively low cost. So SPT is a suitable and very good technique for the production of quality CuO, TiO₂ and Cu/TiO thin films.

In this research work, the results obtained from morphological, structural, optical and electrical studies on CuO, TiO₂ and Cu/TiO₂ thin films deposited by SPT are found to be in good agreement with the results obtained by other techniques.

5.2 Suggestions for Further Research

CuO, and TiO₂ thin films have been deposited varying MC and T_s, and Cu/TiO₂ thin films for MC of 0.10 M at T_s of 400 °C on glass substrate by SPT and have been studied some of their structural, optical and electrical properties. To understand further these films and details characterization are necessary. Hence to get better performance from the as deposited thin films by spray pyrolysis technique, the following research work may be extended:

1. Characterization and analysis of prepared sample after annealing.
2. Characterization and analysis of thin films prepared of more than 10% Cu doped.
3. Investigation of the magnetic properties.
4. Optimization of film growth condition like as thickness and deposition time.
5. More structural study like as AFM.
6. Measurements of Hall Effect and temperature dependence of Hall Effect, etc.

APPENDIX

Publications

(I) Journals

- [1] **Roy S. S.**, Bhuiyan A. H., Podder J., “Optical and Electrical Properties of Copper Oxide Thin Films Synthesized by Spray Pyrolysis Technique”, *Sensors & Transducers*, 191, 8, pp. 21-27, 2015.
- [2] **Roy S. S.**, Bhuiyan A. H., “Optical Characterization of Synthesized Pure and Copper Doped Titanium Oxide Thin Films”, *ARN J. Sci. Tech.* 5, 8, 2015.
- [3] **Roy S. S.**, Bhuiyan A. H., “Surface Morphology, Compositional, Optical and Electrical Properties of TiO₂ Thin Films”, *Sensors & Transducers*, 192, 9, pp. 66-73, 2015.
- [4] **Roy S. S.**, Bhuiyan A. H., “TiO₂ and Cu/TiO₂ Thin Films Prepared by SPT”, *Sensors & Transducers*, 195, 12, pp. 18-24, 2015.
- [5] **Roy S. S.**, Bhuiyan A. H., “Optimization of Molar Concentration of Titanium Oxide Thin Films Deposited on Glass Substrate”, (Communicated to the “Surface Review and Letters”, 2016).

(II) Contributed Research Presentation in the Conferences

(Published in the Abstract Book)

- [1] **Roy S. S.**, Bhuiyan A. H., “Effect of molar concentration on the structural, optical and electrical properties of copper oxide thin films”, International Conference on Physics, BPS, Atomic Energy Center, Dhaka, Bangladesh, 2016.
- [2] **Roy S. S.**, Bhuiyan A. H., “Effect of Molar Concentration on the Structural and Optical Properties of Titanium Oxide Thin Films Prepared by SPT”, 2nd International Bose Conference, Nabab Nawab Ali Chowdhury, Cenate Bhaban, Dhaka University, Dhaka, Bangladesh, 2015.
- [3] **Roy S. S.**, Bhuiyan A. H., ”Study on the optical and electrical properties of CuO thin films synthesized by spray pyrolysis method”, 23rd Bangladesh Science Conference, BSMRAU, Gazipur, Bangladesh, 2015.

- [4] **Roy S. S.**, Bhuiyan A. H., Podder J., Saha D.K, Gafur M. A., “A Study of Surface Morphology, Optical and Electrical Properties of Titanium Oxide Thin Films Deposited by SPT”, International Conference on Advances in Physics, University of Rajshahi, Rajshahi, Bangladesh, 2015.
- [5] **Roy S. S.**, Bhuiyan A. H., Podder J., “Different techniques for preparation of thin films”, International Conference on Physics for Energy and Environment, BPS, Atomic Energy Center, Dhaka, Bangladesh, 2014.
- [6] **Roy S. S.**, Bhuiyan A. H., Podder J., Saha D. K., “Synthesis and electrical properties of pure and copper doped titanium oxide thin films by spray pyrolysis”, International Conference on Physics for Energy and Environment, BPS, Atomic Energy Center, Dhaka, Bangladesh, 2014.